UNIVERSITY OF SOUTHAMPTON

MODELLING THE THERMOHALINE CIRCULATION

by

Mark Shawn Bean

A dissertation submitted in candidature for the degree of
Doctor of Philosophy at the University of Southampton.

March 1997

UNIVERSITY OF SOUTHAMPTON

ABSTRACT

FACULTY OF SCIENCE

OCEANOGRAPHY

Doctor of Philosophy

MODELLING THE THERMOHALINE CIRCULATION

by Mark Shawn Bean

A coarse resolution, single hemisphere, single basin ocean general circulation model (OGCM) showed multiple modes of the thermohaline circulation. During the integration the thermohaline circulation underwent an initial adjustment phase, 2 different haline dominated modes, 2 strengths of thermal flushes, deep decoupled oscillations (DDOs) and salt loop oscillations. For each mode of circulation the stability and longevity were related to the strength of the stabilising and destabilising feedbacks.

The OGCM domain was divided into 4 boxes and parameterisations of the heat and salt fluxes between the boxes were derived. Fluxes of heat and salt due to advection were reasonably modelled by a 'Stommel type' parameterisation where the tracer flux was linearly dependent on the mean velocity and tracer gradient. In accordance with this parameterisation the strength of the meridional overturning cell was highly correlated with the meridional deep water density gradient. A coupled convection and surface boundary condition scheme was developed which provided a direct connection between the surface forcing and deep water.

The parameterisations derived from the OGCM data were incorporated into a number of box models. Sensitivity studies of these box models showed that the stability and strength of the thermohaline circulation was strongly dependent on the parameterisation of the strength of the meridional overturning cell. A quantitative comparison of the box model and OGCM results suggested that the box model could be used predictively over a limited range of thermohaline circulation modes.

Contents

Chapter V - The reduced box model

Chapter VI - The full box model

Chapter VII - Discussion and future work

List of tables

List of figures

Acknowledgements

I would like to thank both my supervisors Dr Neil Wells and Dr Richard Wood for their help and guidance during the period of research leading to this thesis. Their comments and corrections on this manuscript are also greatly appreciated. My thanks also go to my office mates Helene and Lisa for our discussions however light hearted and for their help and support over the last couple of years. Amanda Tyler and Duncan Baldwin for their help and advice on the computer system.

For their help and advice on the Met. Office's ocean model and computer system I would like to thank David Wright, Dave Sexton and all the others at the Hadley centre who answered my never ending stream of questions.

For general moral support and livening up the department my thanks go to Richard, Pete, Matt, Mai, and Greg. I would also like to thank Steve Chamberlain and Seb Larsson for our discussions of numerical methods and other mathematical techniques. Special thanks go to Jae and my parents for their support and encouragement.

I would also like to acknowledge the financial support from NERC in the form of a grant and the Hadley Centre for the CASE award.

Definitions

Abbreviations

AABW	Antarctic bottom water.
BP	Before present.
DDO	Deep decoupled oscillation.
EBM	Energy balance model (of the atmosphere).
FBM	Full box model.
Myr	Million years.
NADW	North Atlantic deep water.
NCON	The convection scheme used in the OGCM.
O-AGCM	Coupled ocean and atmosphere general circulation model.
OGCM	Ocean general circulation model.
P - E	Precipitation minus evaporation, the net surface freshwater flux.
SA	Haline driven mode of the thermohaline circulation found in the Stommel (1961) box model.
Sv	Sverdrup. One Sv = 10^6 m^3/s.
TF1	The first thermal flush of the OGCM results.
TF2	The second thermal flush of the OGCM results.
TF3	The third thermal flush of the OGCM results.
TH	Thermally driven mode of the thermohaline circulation found in the Stommel (1961) box model.
WC1	The first haline driven mode of the OGCM results.
WC2	The second haline driven mode of the OGCM results.
WC3	The third haline driven mode of the OGCM results.

Symbols

a	Radius of the Earth.
A_{ij}	The area of a face between boxes i and j in a box model.
A_{MH}	Horizontal eddy viscosity used in the OGCM.
A_{MV}	Vertical eddy viscosity used in the OGCM.
A_{TH}	Horizontal eddy diffusivity.
A_{TV}	Vertical eddy diffusivity.
c_p	The specific heat capacity for sea water.
D	A diffusivity.
dz	The vertical separation of 2 boxes in a box model.
f	The Coriolis parameter.
F	Viscosity.
g	Acceleration due to gravity.

h_i The depth of box i in a box model.

k^a_b A non dimensionalised diffusivity in a box model, with the sub and superscripts indicating T or S and position.

m Volume flux of water in a box model.

p The ratio of the thermal diffusivity for the deep water to the haline diffusivity for the surface waters.

p Pressure.

q The density ratio, which is the ratio of the haline density difference between the surface and deep water and the thermal density difference between the surface and deep water.

Q A flux of water or tracer.

q The strength of the meridional overturning cell in a box model.

q^a_b A heat or salt flux in a box model, with the sub and superscripts indicating T or S and position.

Q_i A heat flux in the coupled convection and surface boundary conditions scheme.

q_i A salt flux in the coupled convection and surface boundary conditions scheme.

R The relative density ratio, which is the ratio between the haline and thermal contributions to the net surface buoyancy flux.

r The ratio of the haline to thermal density forcing for a box model.

S_i Salinity of box i in a box model.

T Temperature.

t Time.

T^* The effective atmospheric temperature in a relaxation surface boundary condition.

T_i Temperature of box i in a box model.

u Velocity along the x-axis.

v Velocity.

Velocity along the y-axis.

Vol_i Volume of box i in a box model.

x A linear dimension in the zonal direction.

y A linear dimension in the meridional direction.

Y_0 Separation of boxes in a box model in the meridional direction.

z Linear depth.

α The thermal expansion coefficient.

The Haney relaxation time in the Haney (1971) surface boundary condition.

A parameter used by the distorted physics scheme in the spin up of the OGCM.

γ The ratio of the depth of the surface to deep boxes in a box model.

A parameter used in the distorted physics scheme during the spin up of the OGCM.

ϕ Latitude.

κ^a_b A diffusivity in a box model, with the sub and superscripts indicating T or S and

	position.
λ	The ratio of the relaxation time for the temperature surface forcing to the advective flushing time.
	Longitude.
	The strength of the coupling between the density gradient and the meridional overturning cell in the Stommel model.
μ	The ratio of the thermal to haline restoring time scales.
ν_0	Constant of proportionality between the deep water density difference and the strength of the meridional overturning cell in the FBM.
ν_{offset}	Zero offset of the strength of the meridional overturning cell in the FBM.
ρ_0	The reference density for sea water.
τ	A time scale.
τ_S	Non dimensional time scale associated with the convective mixing of salinity in the FBM.
τ_T	Non dimensional time scale associated with the convective mixing of temperature in the FBM.
Δt_T	The time step used for the tracer equations in the OGCM.
Δt_V	The time step used for the momentum equation in the OGCM.
ΔS	A salinity difference.
ΔT	A temperature difference.
$\Delta\rho$	A density difference.
$\Delta\rho_c$	The critical density difference at which convection starts to occur.
Γ	The proportion of a box convecting.
	The advective operator in the OGCM equations.
Γ^a_b	An enhanced diffusivity used in a box model convection scheme, with the sub and superscripts indicating T or S and position.

Chapter I

Introduction

1.0 The climate system.

The Earth's climate system consists of the atmosphere, hydrosphere, cryosphere, the surface lithosphere and biomass all of which are driven by the sun. The annual mean radiation budget for the Earth shows greater solar heating near the equator than the poles and yet the surface temperatures are comparatively even. To maintain this even distribution of surface temperatures the climate system has to transport the excess heat from the equator towards the poles. This poleward heat transport is accomplished by the mobile components of the climate system, the atmosphere and the ocean. It is estimated that the ocean is responsible for up to 40% of the total heat transport (Oort 1973, Trenberth 1979 and Carissimo et. al. 1985). The transport of heat poleward in the oceans is not zonalLy uniform and varies from ocean to ocean and across ocean basins. Variations in either the total or the spatial distribution of the oceanic heat transport impact on the other components of the climate system. The large thermal mass of the oceans compared to the atmosphere enable the oceans to store large amounts of thermal energy. Through the storing and release of thermal energy the oceans can either act to damp or drive climatic change. To understand and predict changes in the climate an understanding of the ocean circulation and heat transport is required.

1.0.1 Ocean circulation.

The large scale ocean circulation is driven entirely by the forcing acting on the ocean surface. Although the ocean circulation is a non linear response to the total forcing it is convenient to separate the circulation into 2 components, the wind driven circulation and the thermohaline circulation.

The surface winds drive the surface gyre circulations. This wind driven circulation is mainly confined to above the thermocline. The response of these surface currents to changes in the forcing wind stress occurs on time scales from weeks to months. Longer time scale responses to the wind driven circulation are caused by the advection of water masses around the surface gyres which takes approximately a decade (Dickson et al. 1988). Thus the wind driven ocean circulation is near surface and has associated time scales of a decade or shorter.

The thermohaline circulation is the response of the ocean to the spatial variation in surface buoyancy forcing. Heating and cooling change the sea surface temperature while evaporation and precipitation alter the sea surface salinity. Both of these effects change the density of the surface waters and create horizontal density gradients. As surface heating and precipitation vary more strongly with latitude than longitude the thermohaline circulation is predominantly in the meridional - vertical plane. Fluctuations in the thermohaline circulation are caused by changes in the surface forcing or natural variability. These fluctuations can cause dramatic

changes in the strength of the thermohaline circulation over a few decades (see chapter II). Similar to the wind driven circulation advection of anomalous water masses by the thermohaline circulation can lead to variations in the ocean circulation. The low velocities of the deep ocean and the long path length make the advective time scale of the thermohaline circulation much longer than that of the wind driven circulation (centuries compared to decades).

Oceanic poleward heat transport in the Atlantic is mainly due to the thermohaline circulation. The wind driven gyres dictate the path of the surface flows but the thermohaline forcing controls the net mass transport by the deep waters and the return flow in the surface layers. Changes in the thermohaline circulation will alter the poleward heat transport and so will affect the rest of the climate system.

1.1 Motivation and aims.

To answer the question "How variable is the oceanic heat transport and what influences will it have on the Earth's climate?" it is necessary to understand and be able to predict the ocean circulation. When trying to predict the climate change for centuries into the future the affects of the thermohaline circulation must be considered. This thesis attempts to broaden the understanding of the processes controlling the thermohaline circulation and to incorporate these processes into an ocean model. The aim was to produce a conceptual model of the thermohaline circulation that could be used to study the response of the thermohaline circulation to a large set of parameters and surface forcings. To make a comprehensive parameter study possible the model had to be simple and so computationally efficient. For the model to be useful as a predictive tool it had to include all the relevant physical processes. In constructing the simple model the quantitative errors in the parameters used were assessed to give an indication of the validity of any quantitative predictions made by the model.

1.1.1 Overview.

An Ocean General Circulation Model (OGCM) was used to generate a long time series of data that included multiple modes of the thermohaline circulation (chapter III). These results were examined in some detail and the controlling processes and feedback mechanisms were identified. Guided by these observations a set of parameterisations was developed (chapter IV). The parameterisations of tracer fluxes, strength of convection and the strength of the meridional overturning cell were matched to the OGCM results to give the correct heat and salt fluxes for each process. Through comparison with the OGCM data an estimate of the uncertainty in the parameterised heat and salt fluxes was obtained. A simple box model was developed using these parameterisations (chapters IV and VI). The box model was used to study the sensitivity of the thermohaline circulation to the parameterisations and the surface forcing conditions (chapters V and VI).

Although the box model developed had significant improvements over those in current literature (chapter II) it still fell short of being able to make reliable quantitative predictions. The sensitivity of the box model to some of the parameterisations developed has implications for any model

that attempts to predict the changes in the thermohaline circulation. These results act as pointers to which processes it is important to model accurately and which can be approximated when developing an ocean model for climate prediction (chapter VII).

1.2 Past and present thermohaline circulation.

In discussing the thermohaline circulation this section will concentrate on the circulation of the deep oceans as it is this circulation that is dominated by the surface buoyancy forcing. For a more comprehensive review of the past and present thermohaline circulation see Weaver and Hughes (1992). Any net flow in the deep ocean is balanced by a return flow in the surface layers. The path of the surface return flow is dominated by the surface wind stress and not by the surface buoyancy fluxes. The abyssal circulation is driven by the formation of dense, deep water by convection. This deep water is formed intermittently over small areas (Killworth 1983). Known sites for deep water formation are the Mediterranean, the Greenland, Iceland, Labrador and Norwegian seas and the Antarctic continental shelf (Weaver and Hughes 1992). The dense salty water formed in the Mediterranean gains buoyancy as it exits into the Atlantic through mixing with lighter waters. This water spreads out at mid depth rather than sinking to the bottom and does not drive the abyssal circulation (Warren 1981).

Antarctic bottom water (AABW) is formed mainly in the Weddell Sea (Foldviik and Gammelsrød 1988). The coldest and densest AABW can not escape over the sill of the Weddell sea basin. By mixing with the lighter surrounding waters the AABW that fills many of the deepest valleys of oceans is created (Mantyla and Reid 1983). The rate of flow of bottom water out of the Weddell Sea is estimated at 5 Sv (Weppernig 1996).

The Greenland sea is a major site of deep water formation (Killworth 1979 and Warren 1981). This deep water flows over the Greenland - Scotland ridge with about 1 Sv passing either side of the Faeroe islands. These overflows entrain Atlantic water to give a total flux of 3 to 5 Sv (Dickson & Brown 1994). The bottom water then passes through the Gibbs fracture zone into the Labrador basin. Through mixing with deep water from the Denmark strait and Labrador sea the flux of North Atlantic Deep Water (NADW) increases to 13 - 15 Sv (Warren 1981, McCartney and Talley 1984). The NADW flows south into the South Atlantic and then around the Antarctic continent, branching out into the Indian and Pacific Oceans as the *Conveyor Belt* (Gordon 1986, Broecker 1987 and 1991). This meridional overturning cell driven by the NADW has a strength of 18 Sv and carries approximately 1.2 PW of heat poleward at 24°N (Hall and Bryden 82). The return path of the Conveyor belt in the North Atlantic is via the surface waters through the Gulf Stream and North Atlantic Drift.

1.2.1 Variability of the thermohaline circulation.

The present day conveyor belt circulation of the thermohaline circulation is driven by the formation of cold dense NADW. This is caused by the meridional differential in the forcing of the sea surface temperature. During the late Cretaceous Period (135 Myr BP) it is thought that the warmer climate reduced the relative effect of the thermal forcing in comparison with the haline

forcing. This led to deep saline bottom water being formed in the subtropical waters of the Cretaceous ocean (Brass et al. 1982 and Crowley 1983).

There is also evidence for fluctuations in the thermohaline circulation during the last glaciation (2 - 3 Myr BP): Ice core records indicate that the climate system had 2 quasi - stable states between which the system oscillated in the transition from glacial to postglacial times (Oeschger et al. 1984, Crowley 1983 and Weaver 1990). This oscillation was characterised by the presence or absence of NADW formation (Oeschger et al. 1984, Boyel and Keigwin 1987). During the Younger Dryas cold event (10,000 - 11,000 Yr BP) and 3 other times since the last glaciation the production of NADW has been substantially reduced or eliminated. This supports the idea that the thermohaline circulation may have more than one mode of circulation (Keigwin et al. 1991).

1.3 Controlling processes of the thermohaline circulation.

The thermohaline circulation is driven by the formation of deep water by convection. This deep convection occurs when the surface buoyancy forcing causes the surface waters to become denser than the underlying waters. The surface buoyancy forcing has 2 components, the surface heat flux that determines the sea surface temperature and the surface fresh water flux that alters the sea surface salinity. The surface heat flux into the ocean is the downward flux of solar radiation minus the upwards fluxes of black body radiation, sensible and latent heat (Gill 1982). The solar radiation is fairly constant in time and the upwards heat fluxes are strongly coupled to the sea surface temperature (Haney 1971). Thus the surface heat flux is strongly coupled to the sea surface temperature. In contrast the surface fresh water flux is the precipitation minus the net evaporation. Neither the rate of evaporation nor the quantity of rain fall depends on the sea surface salinity, making the coupling between the sea surface salinity and the surface fresh water flux very weak if there is any coupling at all.

The solar radiation is unequally distributed giving a higher heat flux near the equator than at the poles (Ghil 1982). Thus the surface heat flux driving the oceans promotes a thermohaline circulation similar to the present day conveyor belt with bottom water formation at the poles and weak upwelling elsewhere (Weaver & Hughes 1992). This thermally driven mode is characterised by cold, fresh deep water. Conversely the fresh water flux is acting to drive the thermohaline circulation in the opposite direction. There is strong evaporation in the tropics and an excess of precipitation in the subpolar regions. This leads to a gradient in the sea surface salinity with the most saline water near the equator and the fresher water towards the pole. If the salting of the subtropical water were sufficiently strong, warm salty deep water could form in the subtropics as is suggested for the Cretaceous Period (Brass et al. 1982 and Crowley 1983). This haline mode is characterised by a reversed thermohaline circulation with warm salty deep water. With the 2 components of the surface buoyancy forcing acting against one another any process that changes the strength of the surface heat or salt flux can alter the state of the thermohaline circulation. The differences between the coupling of the surface heat and salt

fluxes to the sea surface temperature and sea surface salinity fields lead to a number of feedback mechanisms that control the thermohaline circulation.

1.3.1 The haline advective feedback.

The haline advective feedback mechanism is driven by the competing effects of the surface salinity forcing and surface temperature forcing (Rooth 1982, Walin 1985, Bryan 1986). In a thermally driven mode the thermohaline circulation is driven by the net pole to equator surface density gradient caused by the meridional variation in the surface heat flux. The surface temperature forcing acts to accelerate a positive overturning cell, with the surface waters flowing poleward and the deep waters flowing towards the equator. The salinity forcing encourages a negative overturning cell, with the surface flow being towards the equator and the deep flow being poleward. Thus in a thermally driven mode the salinity forcing acts as a braking mechanism to the thermally driven positive overturning cell. Adding a positive salinity anomaly at high latitudes reduces the braking and hence the rate of meridional overturning is increased. The increased rate of meridional overturning brings surface warm, salty water (from the sub tropical gyre) more rapidly poleward. This acts to increase the surface salinity at high latitudes. Hence this is a positive feedback mechanism. If a freshwater anomaly is introduced at high latitudes the opposite occurs and the mechanism acts to slow the meridional overturning. The same arguments apply in reverse if the thermohaline circulation is in a haline dominated mode when the process still acts as a positive feedback. A typical overturning time scale for a salinity anomaly to be advected around the ocean basin is of the order of one century (based on an overturning cell of 12 Sv).

The haline advective feedback is reliant on the longevity of sea surface salinity anomalies. As the fresh water flux is not coupled to the sea surface salinity it is possible for these salinity anomalies to persist for a decade or longer (Dickson et al. 1988).

1.3.2 The thermal advective feedback.

The thermal advective feedback employs a similar mechanism to the haline advective feedback (Greatbatch 1994 and 1995). Similar to the haline advective feedback this mechanism relies on the advection of sea surface temperature anomalies. This is only possible if the life time of local sea surface temperature anomalies is greater than the typical advective time scale of the surface waters (Cai 1996). Hence the thermal advective feedback is only possible if the local coupling between the sea surface temperature and the surface heat flux is sufficiently weak. This point is discussed further in chapter 2. Here I will detail the feedback mechanism assuming a sufficiently weak boundary condition on the sea surface temperature.

If the thermohaline circulation is in a thermally dominated mode then an anomalously cool water mass near the pole exaggerates the strength of the thermal forcing. This would increase the strength of meridional overturning bringing the warm subtropical waters poleward more quickly. With these warmer surface waters brought more rapidly poleward the polar sea surface temperature increases, reducing the surface thermal forcing. Hence reducing the strength of the

meridional overturning cell (Greatbatch and Zhang 1995). This is a negative feedback mechanism. As with the haline advective feedback mechanism the thermal advective feedback mechanism has an advective time scale of about a century.

1.3.3 The convective feedback mechanism or polar halocline catastrophe.

The convective feedback mechanism operates over a much shorter time scale than the advective feedback mechanisms (decades rather than centuries) (Rahmstorf 1994). This mechanism is triggered by a negative surface salinity anomaly at high latitudes. The reduction of the surface salinity at high latitudes increases the vertical stratification and so inhibits convection. This reduces the rate of deep water formation and decreases the strength of the meridional overturning cell. The weakened meridional overturning decreases the poleward surface transport of warm salty water (from lower latitudes). This reduces the high latitude surface salinity some more. If the initial perturbation was sufficiently large deep water formation can stop completely and a cap of cold fresh water form over the surface of the sub polar gyre resulting in a polar halocline catastrophe (Bryan 1986 and Marotzke 1990). The convective feedback mechanism is a positive feedback. If a positive salinity anomaly is introduced at high latitudes the opposite happens and the convective feedback mechanism acts to increase the rate of overturning.

1.3.4 Atmosphere - ocean feedbacks.

Fluctuations in the strength of the thermohaline circulation change the oceanic poleward heat transport and the sea surface temperature. Variations in the sea surface temperature affect the atmospheric circulation and give rise to coupled ocean - atmosphere feedbacks (Lohmann et al. pre print).

If the thermohaline driven meridional overturning weakens then the oceanic poleward heat transport decreases. This leads to cooler surface waters in the subpolar gyre and warmer surface waters in the tropics. The increase in meridional sea surface temperature gradient drives a stronger atmospheric circulation with stronger winds and increased cyclonic activity (Schiller et al. 1996). Strengthening the atmospheric circulation affects the ocean through changes in surface wind stress and the hydrological cycle.

The strengthened winds increase the Ekman suction in the subpolar regions (Schiller et al. 1996). With increased upwelling the vertical stratification at high latitudes is decreased and the surface waters are cooled by the vertical advection of heat. Cooling the surface waters increases the thermal forcing of the thermohaline circulation making the Ekman suction a negative feedback. Decreasing the vertical stability at high latitudes promotes the formation of deep water by convection, so is a negative feedback mechanism. Both of these mechanisms are negative feedbacks acting to stabilise the thermohaline circulation.

The enhanced atmospheric circulation leads to a stronger hydrological cycle increasing the fresh water flux into the polar regions (Schiller et al. 1996). This strengthens the surface haline

forcing of the thermohaline circulation. Stronger haline forcing weakens the meridional over turning making this a positive feedback.

1.3.5 Cryosphere - ocean feedback.

The interaction of the thermohaline circulation and the Laurentide ice sheet is a possible explanation for the climate oscillations during the last glacial period (Heinrich events) (Paillard and Labeyrie 1994). These Heinrich events were identified in climate records from Greenland ice cores (Bond et al. 1993, Johnsen et al. 1992 and Dansgaard et al. 1993). The collapse of the Laurentide ice sheet would result in a massive discharge of icebergs into the North Atlantic. This would decrease the surface salinity of the polar waters, reducing the strength of the thermohaline circulation. With a weaker meridional overturning the oceanic poleward transport of heat would decrease. Reducing the poleward heat transport may slow the melting of the ice sheet and reduce the flux of icebergs (Bond et al. 1993). Results from a box model show that the coupling between the thermohaline circulation and the ice sheet can model climate oscillations similar to Heinrich events (Paillard and Labeyrie 1994).

1.4 Modes of the thermohaline circulation.

There are multiple modes of the thermohaline circulation, some steady states and some oscillatory. The existence and stability of any given state is dependent on the relative strengths of the feedback mechanisms that control it. Described below are the major circulation modes and mechanisms for oscillations of the thermohaline circulation.

1.4.1 The thermally dominated mode or conveyor belt.

The present day, conveyor belt, thermohaline circulation is thermally dominated (section 1.2) as the dominant forcing is the meridional gradient in the surface heat fluxes. The thermally dominated mode is characterised by the formation of cold, fresh, deep water in the polar regions (Winton and Sarachik 1993). There is a strong meridional overturning cell with the deep waters flowing from pole to equator and a surface return flow (Figure 1 - 1). In single hemisphere models the sinking in the polar regions is balanced by upwelling throughout the rest of the ocean basin. For larger model domains the circulation is more "conveyor belt" like with the upwelling further from the sites of deep water formation.

1.4.2 The haline dominated thermohaline circulation.

When the surface fresh water fluxes are sufficiently strong that the haline surface forcing dominates the surface thermal forcing a polar halocline catastrophe can occur (section 1.3.3) stopping the formation of deep water (Winton 1993 and Zhang et al. 1993). The haline dominated mode of the thermohaline circulation is characterised by a cold fresh water cap over the surface of the sub polar gyre and warm salty deep waters. There is no deep convection though warm salty intermediate water may be formed at mid latitudes by convection to intermediate depths (chapter III and Winton and Sarachik 1993). Any meridional circulation is weak and confined to the surface layers (Figure 1 - 2).

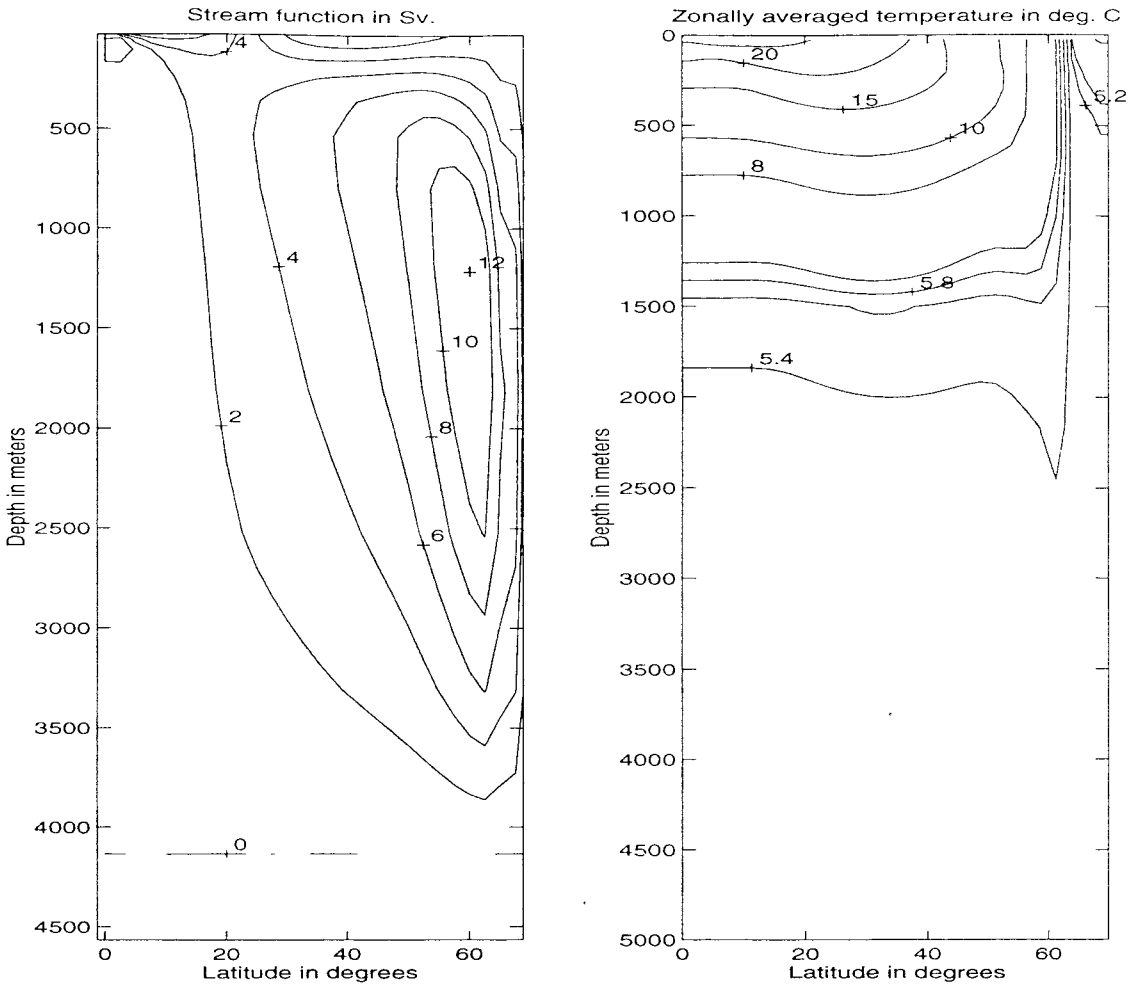

Figure 1 - 1: A typical meridional stream function and zonally averaged temperature profile for a thermally dominated mode of the thermohaline circulation. The meridional overturning cell has sinking at high latitudes upwelling elsewhere. The non zero stream function at the surface is due to the contouring algorithm not the underlying data.

1.4.3 The salt loop oscillator.

The advection of a salinity anomaly around the conveyor belt circulation can lead to centennial oscillations in the thermohaline circulation (Winton and Sarachik 1993). This "salt loop oscillator" is dependent on the haline advective feedback mechanism. A salinity anomaly that is advected around the meridional circulation will pass through the region of deep water formation. The presence of the salinity anomaly will alter the strength of the surface haline forcing. This will change the strength of the thermohaline circulation. In states with a very strong meridional cell (the thermal flushes obtained by Winton and Sarachik (1993) and chapter III) the advective time scale is greatly reduced. In this case the salt loop oscillator can give oscillations with periods of a few decades. The oscillations are sustained by the advection of the salinity anomalies around the meridional overturning cell so that the anomalies keep returning to the sites of deep water formation. The amplitude of the salinity anomalies is gradually reduced by mixing, convection and surface fluxes.

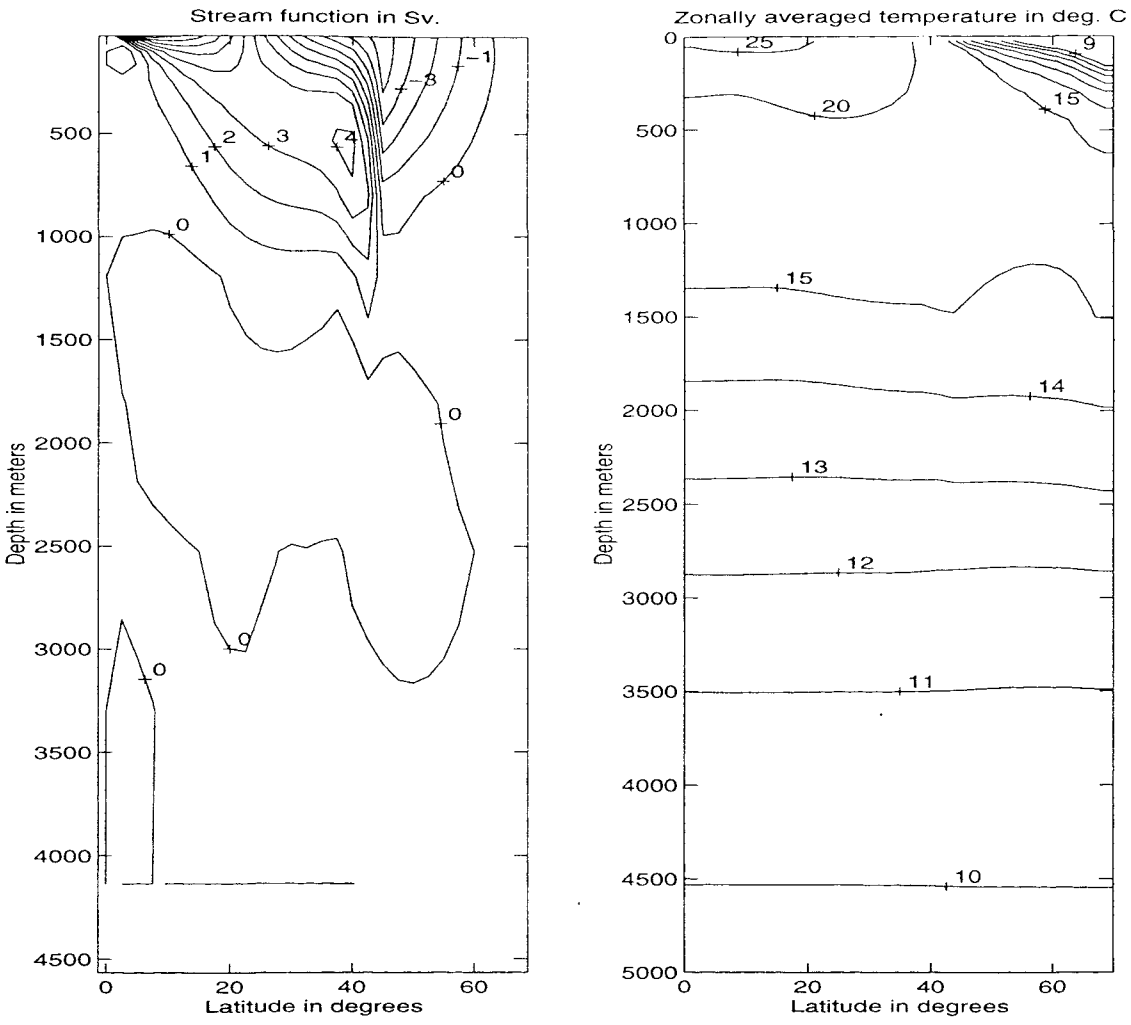

Figure 1 - 2: A typical meridional stream function and zonally averaged temperature profile for a haline dominated mode of the thermohaline circulation. The non zero stream function at the surface is due to the contouring algorithm not the underlying data.

1.4.4 Deep decoupled oscillations.

Deep decoupled oscillations (DDOs) of the thermohaline circulation have periods of 300 to 1000's of years (Winton and Sarachik 1993 and Huang 1994). DDOs involve long periods of weak haline driven circulation terminated by rapid, strongly overturning, thermally driven flushes. When the surface temperature forcing is not dominant a halocline catastrophe can occur (Bryan 1986) giving a haline dominated thermohaline circulation (section 1.4.2). Throughout this weak, haline driven mode the abyssal ocean becomes warmer and more saline. The warming of the deep ocean decreases the vertical stratification of the high latitude waters. This eventually reaches a point where a small perturbation in the surface density field is sufficient to overcome the stabilising effect of the polar fresh water cap. The density perturbation causes convection to start in a small area of the subpolar gyre. The convective mixing brings the warm salty deep water to the surface, which is then cooled driving further convection. The initial density perturbation is amplified and the surface currents spread the region of convection via the "Domino effect" (Lenderink and Haarsma 1994). Once the convective process has started

forming deep water a strong meridional overturning cell rapidly develops. During this thermally driven flush the deep ocean rapidly losses the heat that was gained during the weak circulation mode. As the deep water cools convection is inhibited and the rate of formation of deep water drops. This allows the polar fresh water cap to reform and the process to repeat itself. During a period of deep decoupled oscillations the thermohaline circulation fluctuates between a weak haline driven mode and a strong, thermally driven flush.

1.4.5 Decadal oscillations.

Decadal oscillations are 3 dimensional, unlike salt loop oscillations and DDOs that are 2 dimensional (McWilliams and Ghil 1994). Decadal oscillations are caused by the propagation of a jet like disturbance along the polar boundary. The variability involves a baroclinic jet forming in the north eastern corner of the basin when the surface forcing creates a lobe of cold water in this region (Winton 1996 and Döscher et al. 1994). When a warm boundary disturbance, from the western boundary current, is advected into the region of the jet, the jet becomes intensified. The presence of the warm disturbance increases the density gradient across the baroclinic jet and causes the jet to propagate westwards along the boundary. As the jet propagates westwards it leaves behind warmer more stratified water (Winton 1996). These fluctuations in the surface circulation and density fields cause variations in the strength of the thermohaline circulation. These oscillations are reliant on the surface forcing producing thermal wind currents normal to weakly stratified coasts and weak damping of propagating boundary waves. It is probable that numerical ocean models over estimate the variability of the thermohaline circulation due to decadal oscillations. Numerical models tend to exaggerate the available potential energy in large scale baroclinicity as they under estimate the dissipative affects of baroclinic eddies (Winton 1996).

Chapter II

Models of the thermohaline circulation

2.0 Parameters affecting the thermohaline circulation.

Numerical ocean models show that there are a large number of parameters that can influence the state and stability of the thermohaline circulation (Weaver and Hughes 1992). These parameters can either be representations of processes that are unresolved by the numerical model or the parameters can determine the external forcing of the ocean. This chapter collects these results together to indicate which processes have a significant controlling influence on the thermohaline circulation and what effects the surface forcing has on the large scale ocean circulation. The aim was to identify those processes that should be incorporated in a model of the thermohaline circulation for the model to be of use for climate prediction. The view taken was that if numerical models indicate that the thermohaline circulation is sensitive to a parameterisation then the physical process that the parameterisation represents has an important influence on the thermohaline circulation. If the thermohaline circulation is insensitive to the parameterisation used for a physical process then it is unnecessary for an ocean climate model to resolve that process with a high degree of accuracy. All this assumes that the parameterisation is in some sense physically correct.

The results from numerical models that are reviewed in this chapter are segregated by the type of model used. This first half of the chapter concentrates on results obtained from Ocean General Circulation Models (OGCMs) and the second half on box models. The results are divided in this way as the 2 sets of models represent the ocean circulation in different manners. OGCMs attempt to model the ocean circulation on the gyre scale (or better) and include the spatial variation in currents and water mass characteristics on scales of hundreds of kilometres (or better). The surface wind driven gyres (when wind stress is present) and boundary currents (to some extent) are explicitly included in OGCMs. Box models do not attempt to capture all the detail of the state of the ocean, rather they model the overall state of the ocean using a small number of variables. As box models do not explicitly resolve the surface circulation and boundary currents the effects of these parts of the circulation included through parameterisations.

2.1 OGCM response to surface buoyancy forcing.

The primary driving mechanism for the thermohaline circulation is the meridional gradient in the surface buoyancy fluxes. Any process or parameter that changes the strength, time scale or spatial distribution of the thermal or haline components of the surface buoyancy flux is likely to influence the mode or stability of the thermohaline circulation.

If the thermal surface buoyancy forcing is sufficiently strong then only the thermally dominated mode is possible (chapter I). As the strength of the thermal forcing decreases DDOs and

multiple equilibria may be possible. Multiple equilibria are possible when the balance between the thermal and haline surface forcing is sufficiently close that both the thermally and haline dominated modes are possible and stable. If both circulation modes are possible but unstable then DDOs are observed (Huang 1994 and Winton and Sarachik 1993). When the strength of the thermal forcing is significantly weaker than the haline surface forcing only the haline dominated mode is stable. If the surface forcing is such that DDOs exist then the period of the DDOs is related to the relative strength of the thermal and haline surface buoyancy forcing. The oscillation period of DDOs is dependent on a number of model parameters but there is a tendency for the period to increase as the relative strength of the salinity forcing increases in the presence of a surface wind stress (Huang 1994 and Winton and Sarachik 1993).

2.1.1 The surface heat flux.

There are a number of ways of determining the surface heat flux for an OGCM. The choice is dependent on what assumptions are made about the heat capacity of the atmosphere. Changing the heat capacity of the atmosphere need not alter the relative magnitudes of the thermal and haline surface buoyancy fluxes but it does change the strength of the coupling between the sea surface temperature and the surface heat flux. The higher the heat capacity of the atmosphere, the stronger the damping of sea surface temperature anomalies. As the thermal advective feedback mechanism relies on the advection of sea surface temperature anomalies, changing the damping of these anomalies alters the strength of the feedback. When the sea surface temperature anomalies are weakly damped the thermal advective feedback acts to stabilise the thermohaline circulation. For stronger damping the stabilising effect of the thermal advective feedback was reduced (Zhang et al. 1993 and Cai 1993).

Using a Haney (1971) relaxation term for the surface heat fluxes ignores the influence of the surface heat fluxes on the temperature of the atmosphere. This gives a very strong coupling between the sea surface temperature and the surface heat flux and is equivalent to assuming that the atmosphere has an infinite heat capacity. Under mixed boundary conditions (a fixed surface salt or fresh water flux and the surface heat flux given by a Haney term) the thermohaline circulation was very sensitive to small perturbations in the sea surface salinity (Marotzke 1988). This sensitivity was somewhat dependent on the relaxation time scale (an e-folding time for the sea surface temperature if there are no other heat fluxes other than the surface heat flux) chosen for the surface temperature forcing. For short relaxation times (<200 days) the thermally dominated circulation mode was either unstable or highly sensitive to high latitude salinity perturbations (Cai 1996 and Zhang et al. 1993). Using a longer relaxation time stabilised the thermal mode. When a seasonal variation was added to the surface heat fluxes of a 3 layer model the thermohaline circulation showed multiple thermally dominated modes (Lendrink and Haarsma 1994). These thermally dominated modes differed in the sites of deep water formation and small changes in the strength of the meridional overturning cell. The

response to the seasonally varying forcing showed a hysteresis in the state of the thermohaline circulation which was associated with the non linearity of convection (Lendrink and Haarsma 1994).

Forcing the ocean with a prescribed heat flux made the thermally dominated mode more stable than if the ocean model were forced with mixed boundary conditions by enhancing the thermal advective feedback (Zhang et al. 1993 and Capotondi and Saravanan 1996). Using a constant heat flux implies that the atmosphere has zero heat capacity and only acts to transport heat. DDOs were not observed when an ocean model was forced with constant surface heat flux but decadal oscillations were possible (Greatbatch and Zhang 1995).

Some of the atmospheric responses to the changes in ocean circulation can be included into the surface heat fluxes by adding an extra diffusion term to the standard Haney boundary condition (Rahmstorf 1994). Increasing the local response of the atmosphere stabilised the thermally dominated thermohaline circulation. Similar to using the prescribed heat flux boundary condition, with the extra diffusion term the thermal mode splits into a number of different thermally driven modes distinguished by the differing locations of deep water formation (Rahmstorf 1994). A similar increase in stability of the thermally dominated mode was found when an Energy Balance atmosphere Model (EBM) was used to determine the surface heat flux driving the thermohaline circulation (Capotondi and Saravana 1996, Pierce et al. 1996 and Fanning and Weaver 1996). As with the previous 2 boundary conditions there were multiple states of the thermal mode with differing sites of deep water formation. The extra stability of the thermal mode was due to the increased effect of the thermal advective feedback as the damping on the sea surface temperature was less than for the Haney boundary condition. Using an EBM that had a scale variant coupling between the sea surface temperature and surface heat flux produced a sea surface temperature response to a given change in meridional overturning 4 times greater than when restoring (Haney) boundary conditions were imposed (Pierce et al. 1996). This increase in the sea surface temperature response was possible as the large scale coupling was weak (2 $W/°Cm^2$). Damping of anomalies in the sea surface temperature was controlled by the small scale (determined by atmospheric length scales) coupling which remained strong (40 $W/°Cm^2$) (Pierce et al. 1996). Reducing the small scale thermal coupling (to 20 $W/°Cm^2$) stopped oscillations of the thermohaline circulation that were present with the stronger coupling, implying that the strengths of both the large and small scale thermal couplings were important for determining the stability of the thermohaline circulation. The strength of the small scale thermal coupling controls the size of the sea surface temperature anomalies. The local sea surface temperature anomalies can cause local convection by changing the vertical density profile. Thus the strength of the small scale thermal coupling impacts on the local convection possibly explaining the impact of the small scale thermal coupling on the stability of the thermohaline circulation.

Coupled ocean - atmosphere general circulation models (O-AGCMs) confirm that restoring (Haney) boundary conditions under estimate the stability of the thermohaline circulation

(Lohmann et al. 1996). The results from O-AGCMs suggest that the stability of the thermohaline circulation falls between that predicted by the Haney boundary conditions (unstable) and that predicted by fixed flux conditions (overly stable) (Shiller et al. 1996 and Lohmann et al. 1996). As mixed boundary conditions employ a relaxation term for the surface temperature forcing (as in Haney boundary conditions) they probably under estimate the stability of the thermohaline circulation. This sensitivity of the thermohaline circulation to the surface boundary conditions makes inter-comparisons of model results difficult. Small differences in the surface forcing between models can cause significant differences in the model results.

2.1.2 Surface fresh water forcing and the hydrological cycle.

The relative strength of the surface fresh water flux compared to the surface heat flux determines both the stability of the various circulation modes and the oscillation period of DDOs if they are possible. As the coupling between the sea surface salinity and the surface fresh water flux is weak or non existent OGCMs usually represent the haline forcing by prescribing a surface salt flux equivalent to the surface fresh water flux. This salt flux has either been prescribed as a function of position or diagnosed from a spin up run. To diagnose the surface salt flux the OGCM is 'spun up' using a restoring boundary condition for the sea surface salinity with the reference salinity being prescribed (chapter IV). Once the OGCM has reached a steady state the salt fluxes from the restoring boundary condition are diagnosed and then used as the fixed fluxes for the actual model run. Frequently swapping from restoring (Haney for both temperature and salinity) to mixed (fixed salt flux and a Haney condition for temperature) boundary conditions makes the circulation unstable and the model enters an adjustment phase (Marotzke 1988, Winton and Sarachik 1993). The strength of the fresh water forcing influences the duration and strength of the meridional overturning cell of the adjustment period (Winton and Sarachik 1993). The stronger the fresh water forcing the longer and more energetic the adjustment phase. If DDOs were possible then increasing the strength of the surface haline forcing increased the period of oscillation. When the fresh water flux became sufficiently strong the DDOs were no longer periodic and the time between flushing events became chaotic (Winton and Sarachik 1993).

Spatial distribution of the surface fresh water flux influences the thermohaline circulation. The stability of the thermohaline circulation seems to be especially sensitive to the distribution of the surface fresh water flux at high latitudes e.g.:

- DDOs were seen only when the strength of the surface haline forcing decreased near to the polar boundary of the OGCM (Winton and Sarachik 1993);
- A region of strong evaporation in the Greenland Sea promoted oscillations with a decadal time scale. These oscillations were driven by the advection of sea surface salinity and sea surface temperature anomalies created in the region of strong evaporation, to the sites of deep water formation (Weaver et al. 1991).

- The stability of the thermohaline circulation (under mixed boundary conditions) was increased by lengthening the time period of the spin up run that the diagnosed salt flux was averaged over (Tziperman et al. 1994). The longer averaging period produced a spatially smoother distribution of surface salt fluxes (especially at high latitudes) suggesting that the noisy forcing field (the forcing field with the short averaging period possibly contained 2 grid point noise) enhanced instability of the thermohaline circulation (Rahmstorf 1996).

Including a seasonal component in the fresh water forcing gave a thermohaline circulation that had decadal variability and DDOs with centennial periods (Myers and Weaver 1992). The seasonal forcing reduced the strength of the thermal flushes during the DDOs compared to those obtained with steady boundary conditions. The strength of the meridional overturning cell did not show any seasonal variation where as the number of convection events did (Myers and Weaver 1992). Adding a time varying stochastic component to the surface salt flux had some influence on the stability of the thermohaline circulation depending on the strength and spatial coherence of the perturbation. Strong perturbations caused the thermohaline circulation to flip between different modes more often than weaker perturbations (Weaver and Hughes 1994, Osborn 1996). The greater the spatial coherence the stronger destabilising affect the perturbation had on the thermohaline circulation (Osborn 1996).

Although the coupling between the surface fresh water flux and the sea surface salinity is weak the rate of evaporation is related to the sea surface temperature. Using a fixed flux for precipitation and a linear relation between the rate of evaporation and the sea surface temperature adds an extra positive feed back to the system. Though this extra coupling acts to destabilise the thermohaline circulation the inclusion of the extra coupling did not significantly alter the evolution of an OGCM compared to mixed boundary conditions (Hughes and Weaver 1996).

Most OGCMs use a surface salt flux to emulate the effects of a surface fresh water flux. This approximation simplifies the numerics but can cause long term climate drift (Wadley et al. 1996). This long term climate change is caused by a drift in the total salt content of the OGCM. This drift in total salt content arises from small imbalances in the surface salt flux diagnosed from: a) Spin up runs using accelerated physics (section 3.0.3); b) rounding errors in the calculated surface salt flux (Wadley et al. 1996). The effect of rounding errors is strongest in areas of deep convection (Weaver and Sarachik 1991). It is possible to avoid these problems by including the surface fresh water flux directly into an OGCM using a model like Huang (1993).

2.1.3 Surface wind stress.

The surface wind stress determines the tracks of the surface currents that act as the return pathway for the thermohaline circulation. By changing the surface circulation the surface buoyancy forcing that the water is subjected to is altered, thus affecting the thermohaline circulation. The presence of surface wind forcing has a stabilising effect on the thermal mode of the thermohaline circulation and inhibits DDOs (Winton and Sarachik 1993). An OGCM that exhibited DDOs without wind forcing showed a stable circulation when a surface wind stress was

applied (Marotzke 1990). Similarly adding a surface wind stress to an OGCM caused the period of the DDOs to increase by up to a factor of 8 (Huang 1994). In a global OGCM the wind stress biased the model towards conveyor belt type circulations and against symmetric modes of the thermohaline circulation (Weaver and Hughes 1992). Adding a spatially varying component to the surface wind fields dramatically increased (up to an order of magnitude) the mean kinetic energy and eddy kinetic energy of the ocean (Miliff et al. 1996). These increases would probably impact on the thermohaline circulation.

2.2 Parameterisation of sub grid scale processes.

Any process that has a length scale smaller than the grid scale used or a time scale shorter than the time step employed by an OGCM will not be resolved by that model. The affects of these sub grid scale processes are included in OGCMs by parameterising them in terms of the variables calculated by the model. The parameterisations relate the influence of the sub grid scale processes to the large scale gradients and values of the tracer fields. There is a choice as to which sub grid scale processes to include in an OGCM and how to parameterise them. The choice of parameterisations can influence the strength and stability of the thermohaline circulation.

2.2.1 Diffusion.

At the resolution of current OGCMs (order 1°) the tracer transport due to molecular diffusion is negligible compared to the tracer transport due to sub grid scale mixing processes like turbulent mixing and eddy stirring. These mixing processes can be included in an OGCM through eddy diffusion (see appendix A - The OGCM equations). The size of the temperature and salinity eddy diffusivities has a strong affect on the stability and strength of the thermohaline circulation.

For a single hemisphere, rectangular and flat bottomed, ocean basin the depth of the thermocline and the strength of the meridional overturning cell (in a thermally dominated mode) increased as $(A_{TV})^{1/3}$ (Where A_{TV} was the vertical diffusivity of heat) (Bryan 1987). Varying the vertical diffusivity of heat over a range valid for the oceans in the same simple geometry OGCM caused the poleward heat flux to vary by a factor of 5 (Bryan 1987). Large values of A_{TV} favoured the thermally dominated modes of thermohaline circulation and inhibited DDOs (Winton and Sarachik 1993, Winton 1995). The simple relationship between the strength of meridional overturning and the thermal vertical diffusivity did not hold for an OGCM that included realistic topography (Hirst and Cai 1994). There was a general trend for the strength of the meridional overturning cell to increase as the thermal vertical diffusivity was increased (Hirst and Cai 1994). A_{TV} controlled the stability of the modes of thermohaline circulation in a zonally averaged model. For high A_{TV} only the 2 cell haline dominated mode was possible, for small A_{TV} only the single cell thermal mode was stable and for intermediate values of A_{TV} both modes of the thermohaline circulation were obtained (Schmidt and Mysak 1996).

The horizontal diffusivity of heat A_{TH} had the opposite affect to A_{TV} on the thermohaline circulation. Large values of A_{TH} favoured the haline dominated mode of circulation (Winton and

Sarachik 1993). Increasing the horizontal thermal diffusivity decreased the strength of the meridional overturning cell in a thermally dominant mode (Hirst and Cai 1994).

Altering the ratio of the vertical haline and thermal diffusivities had a strong influence on the strength of the meridional overturning cell. With the vertical diffusivity of salinity being 1.25 times the vertical diffusivity of temperature the strength of the meridional overturning cell was 40% smaller than when the 2 diffusivities were equal (Gargett and Holloway 1992).

The transport of tracers between the 2 surface gyres in an eddy permitting model was due to 3 processes (Figueroa and Olson 1994):

- Sub grid scale diffusion was responsible for less than 1% of the total meridional transport;
- Rings did not significantly contribute to the transport of tracers, though the associated stirring did affect tracer transport;
- Meandering of streamlines relative to the tracer front was the most significant mechanism for meridional tracer transport.

To mimic these processes in a coarse resolution OGCM required a spatially varying eddy diffusivity (Figueroa and Olson 1994). Considering the sensitivity of the thermohaline circulation to changes in diffusivity this spatial dependence of the eddy diffusivity could have a strong influence on the thermohaline circulation.

2.2.2 Convection.

The current generation of OGCMs used for long time scale climate studies are unable to explicitly resolve the small scale convective chimneys responsible for the formation of deep water. Regions where deep convection occurs have a typical scale of 10 Km (Killworth 1979 and 1983) compared to OGCM grid scales of 40 Km (1° resolution at 70°N). The parameterisation of convection affects the stability of the thermohaline circulation. An OGCM that showed a polar halocline catastrophe when using the NCON scheme(Bryan 1986a and 1986b and appendix A) had a stable thermally dominated mode when using a complete mixing parameterisation (Marotzke 1991, Weaver and Sarachik 1991a). Changing the parameterisation of convection only effected the stability of the thermohaline circulation if the surface buoyancy forcing was close to the critical limit (Weaver et al. 1993 and Weaver & Sarachik 1991a).

2.3 OGCM resolution.

It is hoped that the higher the resolution used in an OGCM the more accurately the ocean is represented. As sub grid scale parameterisations are not perfect increasing the resolution of an OGCM can affect the modelled thermohaline circulation (Greatbatch and Zhang 1995). High resolution OGCMs that were eddy permitting had increased variability compared to their lower resolution counter parts (Beckmann et al. 1995). Decreasing the grid spacing of an OGCM allowed for a more realistic representation of the North Atlantic overturning cell by reducing

spurious upwelling of deep water near the Gulf Stream found in coarse resolution OGCM results (Boning et al. 1996).

The resolution of an OGCM influences the wave speed of propagating waves (Döscher et al. 1994). An OGCM responded to changes in high latitude surface buoyancy forcing through the propagation of fast waves along the western boundary. These waves lead to changes in the deep western boundary current so influencing the strength of the meridional overturning cell. Adjustment to a dynamic quasi equilibrium was through the propagation of Kelvin waves along the equator and Rossby waves in the interior. The speed of the fast waves along the western boundary was dependent on the model resolution with the propagation speed being higher for finer resolutions. This implies that coarse resolution OGCMs over estimate the time lag in the response of the thermohaline circulation to changes in high latitude surface buoyancy forcing (Dösher et al. 1994).

I believe that to accurately model the thermohaline circulation it is necessary to force the model with physically realistic surface boundary conditions. This is especially important in regions where deep convection can occur. Given the significance of deep convection in setting the characteristics of deep water I think that the parameterisation of convection has a large effect on the models results. Diffusion, the advective coupling, surface wind stress and the basin also influence the thermohaline circulation and should be included in a complete model of the thermohaline circulation.

2.4 Box models of the thermohaline circulation.

A box model is a highly truncated finite element model. The ocean is split into a small number of interconnecting boxes with the state of the water in each box represented by a set of characteristic values. These values are usually the mean temperature and salinity of the boxes. All other relevant quantities (density, strength of meridional overturning, heat and salt fluxes) are calculated from the characteristic values.

The relative simplicity of box models lends them to analytic investigation and numerical sensitivity studies. The finite element formulation enables box models to represent various basin topographies without changing the form or complexity of the model, though the parameterisations of the heat and salt fluxes are dependent on the topography. With suitable parameterisations the finite element formulation enables conserved quantities to remain conserved making box models suitable for integration over long time periods.

Box models represent the ocean by a small set of variables and can not hope to contain all the small scale details seen in OGCMs. The effects of the small scale structure are averaged to give a mean state and the unresolved processes are accounted for by the parameterisations of heat and salt fluxes between the boxes. This lack of resolution in box models makes their results limited by the validity of the parameterisations used.

The computational efficiency and ease of use of box models have lead to them being widely used to help explain and investigate phenomena seen in OGCMs (Stommel 1961 and Lohmann

et al. 1995). Box models are also used as part of simple climate models to examine the role of the thermohaline circulation in the climate system (Birchfield et al. 1990).

2.4.1 Nomenclature of box models.

Box models will be named following the convention of Huang et al. (1992) where a model consisting of *m* horizontal boxes split into *n* vertical boxes is referred to as *m*×*n*. When the number of surface and deep boxes differs then *m*/*n* indicates *m* surface boxes and *n* deep boxes (Figure 2 - 1). An *m*-*n* model has *m* vertically stacked boxes attached to *n* stacked boxes (Figure 2 - 1).

2.5 Stommel type box models.

As in OGCMs the 2 main states of the thermohaline circulation found in box models are the thermally driven mode (TH) with sinking at the pole, cold fresh deep water and a strong overturning cell, and the haline driven mode (SA) with sinking in the tropics, warm salty deep water and weak overturning. The existence and stability of these 2 modes is dependent on the relative strengths of the thermal and haline surface buoyancy forcing and the strength of the advective transport.

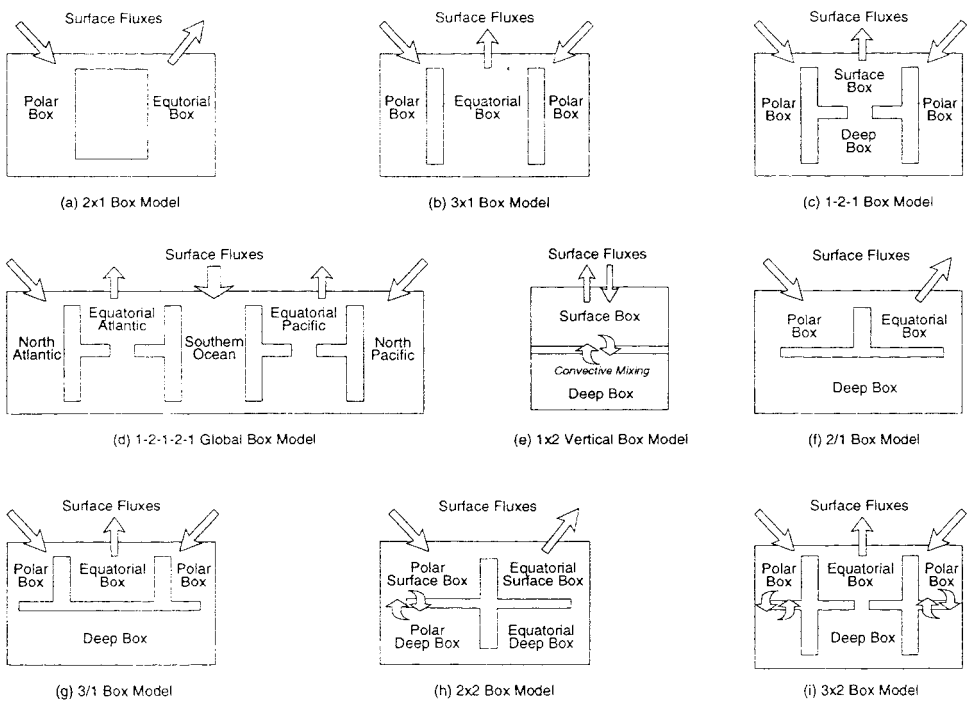

Figure 2 - 1: The nomenclature of ocean box models.

Both the SA and TH modes were found in the 2x1 Stommel model of a single ocean basin. The model was subjected to heating and salting of the tropics' box and cooling and freshening of the polar box. The 2 boxes were considered to be connected by capillary tubes so the strength of

the advective exchange between the boxes was given by a linear friction law. Under a linear friction law the flow was proportional to the density difference between the boxes (Stommel 1961, Huang et al. 1992, Marotzke 1990). For Haney boundary conditions the system was controlled by 3 non-dimensional parameters (Equations 2 - 1 to 2 - 3).

I. The relative density ratio, R, the ratio between the haline and thermal contribution to the net buoyancy flux;

II. μ the ratio of the thermal to haline restoring time scales;

III. λ the ratio of the relaxation time for the temperature forcing and the advective flushing time.

$$R = \frac{\beta k_S \Delta S}{\alpha k_T \Delta T} \qquad \textbf{Equation 2 - 1}$$

$$\mu = \frac{k_S}{k_T} \qquad \textbf{Equation 2 - 2}$$

$$\lambda = \frac{2 q_0 \rho_0 \alpha \Delta T}{k_T} \qquad \textbf{Equation 2 - 3}$$

Where ΔS and ΔT were the differences in the reference salinities and temperatures for the two boxes used in the Haney boundary conditions (see appendix B - The Stommel box model).

For a given set of values for R, μ and λ the Stommel model had either two stable equilibria and one unstable equilibrium or a single stable equilibrium (Weaver and Hughes 1992). The number and type of equilibria was primarily controlled by the relative density ratio (R). If the haline density flux was greater than the thermal density flux ($R>1$) then there was a stable haline dominated equilibrium (SA) independent of the values of μ and λ. When the relaxation time for the temperature forcing was sufficiently longer than that for the salinity forcing ($\mu>R$) and the advective flushing time sufficiently shorter than the temperature relaxation time (λ large) then in addition to the SA equilibrium the model had 2 thermally dominant equilibria, one stable and one unstable. Conversely if the thermal buoyancy flux was largest ($R<1$) then there was always a stable thermally dominant equilibrium (TH). Two extra haline dominant equilibria occurred if the salinity forcing relaxation time was sufficiently longer than the temperature forcing relaxation time ($\mu<R$) and the advective flushing time was sufficiently short compared to the temperature forcing relaxation time (λ large) (see appendix B - The Stommel box model).

2.5.1 Alternative surface forcings.

Mixed boundary conditions were obtained by taking the limit where the salinity relaxation time tended to infinity ($\mu=0$) while the relative buoyancy flux (R) remained finite. Under mixed boundary conditions the model always had a stable haline dominant equilibrium (SA). Two thermally dominant equilibria were possible only if the thermal buoyancy flux exceeded the

salinity buoyancy flux (R<1) and the advective flushing time was sufficiently short (see appendix B -The Stommel box model).

Adding a small stochastic component to the fresh water flux of the 2×1 box model caused the model to 'rattle' around the steady state solution. If the model was in a region of parameter space that permitted multiple equilibria then the stochastic surface forcing could induce the model to flip from one state to the other (Cessi 1994). There was a critical amplitude of the stochastic forcing below which no state flip could be induced in the model. If the strength of the random forcing was increased beyond this critical limit then the residence time for a given state decreased as the strength of the forcing increased (Cessi 1994).

2.5.2 Global box models.

Adding an extra box to the 2×1 model to form a 3×1 box model either increases the horizontal resolution or allows a larger domain to be covered. If, as before, the flow between boxes is governed by a linear friction law then the steady states of these multiple-box models are a superposition of the 2×1 box model steady states (Welander 1986). The 3×1 box model can be used as a simplified global ocean model with the boxes representing the North Pacific, North Atlantic and Southern Ocean (Staffer and Bendtsen 1994, Weaver and Hughes 1992, Welander 1986). From the superposition principle this system has 4 stable equilibria (see Table 2 - 1).

Circulation Mode	Description
Halocline Catastrophe	No deep water formation in the North Atlantic and Pacific boxes, two SA modes.
Conveyor Belt	Deep water formation in the North Atlantic box and upwelling in the North Pacific Box. A pole-to-pole mode i.e. a TH and a SA mode.
Reverse Conveyor Belt	Deep water formation in the North Pacific box and upwelling in the North Atlantic box. A pole-to-pole mode i.e. a SA and a TH mode.
Twin polar convection	Deep water formed in both the North Atlantic and Pacific. Two TH modes.

Table 2 - 1: The steady states of the 3×1 box model.

The equilibrium solutions of a global ocean 3×1 Stommel type box model and their relations to the equilibria of the Stommel 2×1 box model. These 4 equilibria apply equally well if the 3×1 box model was of a 2 hemisphere single ocean basin. In this case the boxes represent the Northern, equatorial and Southern regions of the ocean basin.

The 3×1 box model behaved as the combination of two 2×1 box models where the possible equilibrium states for the Pacific and Atlantic were determined by the relative buoyancy flux ratio for each ocean independently. Under mixed boundary conditions this model was controlled by the relative strength of the fresh water flux and how this fresh water flux was split between the North Atlantic and North Pacific. With a very strong fresh water flux only the halocline

catastrophe mode was stable unless there was a strong bias in the fresh water flux to the North Pacific when the conveyor belt mode was stable (if the bias was to the North Atlantic then the reverse conveyor belt mode was stable). For intermediate and weak fresh water fluxes all 4 modes became possible (Staffer and Bendsten 1994). The affect of the Bering strait on the thermohaline circulation was included by adding an extra connection from the North Pacific box to the North Atlantic box. For high fresh water flux opening the Bering strait made the conveyor belt mode more difficult to obtain as it required a larger split in the fresh water flux between the North Atlantic and the North Pacific. At intermediate strengths of the haline forcing the halocline catastrophe and twin polar convection were the only possible modes for reasonably even splitting of the freshwater flux. If there was a bias towards the North Pacific in the fresh water flux then the conveyor belt mode also becomes possible. As in the case with the Bering strait closed, for weak freshwater flux all four modes were possible (Staffer and Bendtsen 1994).

The results of the Stommel type box models suggest that the type and strength of the surface boundary conditions play a significant role in determining the possible modes of thermohaline circulation. Despite the simplicity of the box models they capture the 2 main thermohaline circulation modes, TH and SA, exhibited in OGCMs. Using the superposition principle the more complicated circulation patterns of multiple box models can be interpreted in terms of combinations of the 2×1 box model equilibria. The sensitivity of the more complex models to the surface buoyancy forcing is dependent on the arrangement of pipe connections between the boxes.

2.6 Vertical resolution and convection in box models.

Splitting the equatorial box of the 3x1 box model into an equatorial deep water and an equatorial surface water box gave a 1-2-1 box model that could distinguish between positive and negative overturning cells. With this extra vertical resolution the symmetric halocline catastrophe and twin polar convection modes became unstable to asymmetric perturbations (under Haney boundary conditions) but remained stable to symmetric perturbations. The instability of the symmetric modes agrees closely with the results from 2D Boussinesq models in which the symmetric circulation modes were not observed (Thual and McWilliams 1992). Under mixed boundary conditions the symmetric states were stable but the probability of a perturbed symmetric state flipping to an asymmetric state increased as the size of the salinity anomaly applied increased (Marotzke 1990). This preference for asymmetric circulation even under symmetric surface boundary conditions matches results from 2 hemisphere OGCMs that also show a preference for asymmetric thermohaline circulation (Bryan 1986). These results suggest that for the box model results to qualitatively match those of the OGCMs a separate representation of the surface and deep waters is necessary.

If the Indian ocean is considered to be passive then a global ocean box model can be obtained by coupling two 1-2-1 models to give a 1-2-1-2-1 model. The boxes in the 1-2-1-2-1 global model represent the North Atlantic, Equatorial Atlantic, Southern Ocean, Equatorial Pacific and North Pacific respectively. As with the 1-2-1 model the asymmetric, pole-to-pole, equilibria were

preferred and of these the states where the circulation in the Pacific and Atlantic were in the same direction were favoured (Marotzke 1990). When a small imbalance was introduced between fresh water forcing of the North Atlantic and Pacific one ocean was selected over the other for deep water formation and the dominance of the states where flow in both oceans was in the same direction stopped. With an imbalance in the fresh water flux global conveyor belt type circulations were the most likely to occur with the circulation in the 2 oceans in opposite directions.

2.6.1 Oscillations driven by convection.

The simplest model to explicitly include convection is a 1 box model where the temperature and salinity of the box is subject to surface buoyancy forcing and vertical diffusion with a deep water box of fixed temperature and salinity. Convection was included by dramatically increasing the vertical diffusivity (of both temperature and salinity) when the density of the surface box became greater than the density of the deep water box. If the surface buoyancy forcing was represented by Haney type terms for both temperature and salinity and convection was considered to occur when the vertical density gradient became slightly statically unstable then the model had 2 possible equilibrium states one with and one without convection (Welander 1982). When the relaxation time for the salinity forcing was greater than that for the temperature forcing it was always possible to find a value for the relative density flux ratio such that neither of the equilibria existed and the model oscillated between a convecting and non convecting state in a limit cycle (Weaver and Hughes 1992). If an equilibrium solution did exist then dependent on the strength of the surface buoyancy forcing in relation to the strength of the convective mixing either one or both equilibria could occur. Thus it was possible for the model to have multiple equilibria, a convecting equilibrium, a non convecting equilibrium and limit cycles for differing values of the surface buoyancy forcing (Lendrink and Haarsma 1994). The existence of limit cycles was not exclusive to this set of parameterisations and also existed when mixed boundary conditions were used. In order for a limit cycle to occur the forcing had to be such that the density of the active box could decrease or increase depending on the temperature and salinity of the box. The parameterisation of convection was critical to the existence of limit cycles in that the mixing had to change strength rapidly at a finite density difference (Stommel 1986, Ruddick and Zhang 1989). If convection were assumed to occur when the system became neutrally stable rather than slightly unstable then the system always decayed towards a pseudo-steady state characterised by a vibration of the system about the neutrally stable point with decreasing amplitude and increasing frequency.

The 1 box model was extended by allowing the temperature of the deep water to vary, so that the model consisted of 2 vertically stacked boxes with the surface forcing applied to the top box and the effects of horizontal exchange included by diffusion terms: a salt diffusion for the top box and a temperature diffusion for the deep water box. Under mixed boundary conditions the system oscillated if:

$$p < q < 1$$ **Equation 4 - 1**

Where p was the ratio of the thermal diffusivity for the deep water and the haline diffusivity for the surface water, and q was the density ratio i.e. the ratio of the haline density difference between the surface and deep water and the thermal density difference between the surface and deep water (Yin 1995).

The period and amplitude of the oscillations increased as q increased and p decreased (Yin 1995). The results of this vertical 2 box model extend those of the 1 box convection model by showing that oscillations can be driven by both the surface buoyancy forcing and warming of the deep water. Assuming that the relaxation time of the surface salinity is greater than that of the surface temperature then for surface buoyancy driven oscillations to occur the surface box must be being made warm and salty. OGCM results show that this warm salty water is not sufficiently dense to form deep water and tends to form intermediate water (chapter III). As this warm salty water is probably intermediate water it does not drive a significant thermohaline circulation overturning cell. When the oscillations are due to the warming of the deep water by horizontal advection and diffusion the surface water is cold and salty. This cold salty water can become dense enough to form bottom water (as seen in the formation of North Atlantic deep water in the current thermohaline circulation). The destabilising effect of surface cooling and sub surface warming can be enhanced by the equation of state's non-linear dependence on temperature (Winton 1993). As the box models discussed so far used a linear equation of state to make the analysis of the models tractable the results have a tendency to under estimate the destabilising effect of the thermal forcing when the surface is being cooled and the deep waters warmed. This destabilising effect of the non-linearity in the equation of state was shown in the results of Winton (1993) where a simplified primitive equation model had a stable state when using a linear equation of state but underwent DDOs with a non linear equation of state for the same surface boundary conditions.

To include the convective process in a box model explicitly the deep and surface polar waters must be resolved. This can be achieved by splitting the polar box in a 1-2 box model in half to give a 2×2 box model of a single hemisphere ocean basin. The response of the 2×2 box model to mixed boundary conditions was very similar to that of the simpler 2×1 box model. The 2×2 box model had 2 equilibrium solutions that corresponded to the TH and SA modes, with cool fresh and warm salty deep water respectively. The probability of the model reaching one of these equilibria from a random initial condition was determined by the relative strengths of the surface buoyancy forcing as in the simpler models (Huang et al. 1992). If the fresh water flux was small then the model was more likely to find the TH equilibrium. As the strength of the fresh water flux increased so did the probability of the model reaching the SA equilibrium. If the strength of the fresh water flux was higher than a critical value then only the SA equilibrium was possible (Huang et al. 1992). When diffusion was added to the 2×2 box model it was possible for no stable equilibria to exist over a small range of surface buoyancy forcing. In this small range the model would oscillate in a similar manner to the convective box models. The addition

of diffusion also changed the qualitative nature of the TH and SA equilibria, without diffusion the model only contained 2 types of water. Without diffusion the deep and convecting boxes were filled with dense water and the remaining box with lighter water. When diffusion was included the dense water was confined to the 2 convecting boxes while the other 2 boxes were stably stratified with light water in the surface box and the bottom box containing intermediate water (Gargett et al. 1995). If the ratio of the thermal and haline vertical diffusivities was allowed to vary from 1 and the horizontal diffusion was sufficiently strong then the range of surface buoyancy forcing over which multiple equilibria existed was increased and additional intermediate modes were possible. These additional intermediate modes had no convection as they were stably stratified and had weak advective transports. As the coupling between the surface and deep boxes was weak in the intermediate modes the effects of the surface buoyancy forcing were confined to the surface boxes making the surface temperatures and salinities markedly different from those seen in the TH and SA modes (Gargett et al. 1995).

2.6.2 Two hemisphere box models that include convection.

The 2×2 single hemisphere box model can be extended to a 3×2 two hemisphere model in a similar manner to the 2×1 to 3×1 transformation. As in the 3×1 box model the 3×2 model had asymmetric pole-to-pole modes as well as the symmetric circulations. For symmetric surface buoyancy forcing with weak salinity forcing only the twin polar convection and pole-to-pole modes were possible. The twin polar convection mode was more likely to occur than the asymmetric modes if the system was started from a random set of initial conditions. As the strength of the salinity surface forcing increased the probability of the pole-to-pole modes being found increased and the halocline catastrophe mode became possible but unlikely. When the salinity forcing reached a critical strength the twin polar convection mode was no longer stable leaving only the pole-to-pole and halocline catastrophe modes. At this critical strength of fresh water forcing the pole-to-pole modes were the most probable when starting the model from random initial conditions. Increasing the strength of the salinity forcing further increased the chance of the halocline catastrophe mode being obtained until a critical value of the fresh water flux, above which only the halocline catastrophe mode was stable (Huang et al. 1992, Thual and McWilliams 1992). The 3×2 box model behaved very similarly to the simpler models in that the relative strengths of the thermal and haline surface buoyancy forcing controlled the possible equilibria and the asymmetric modes were possible under symmetric boundary conditions. The position of the different circulation modes in parameter space differed between the 3×2 and simpler models with the 3×2 model having a closer agreement with the results from simplified primitive equation models (Thual and McWilliams 1992).

By changing the pattern of the fresh water flux into the surface boxes of the 3×2 box model the model could be viewed as representing a single hemisphere of an ocean basin where the sub polar, mid latitudes and equatorial regions were all resolved. As with the 2×2 box model, under a weak fresh water flux the TH mode dominated and for very strong haline forcing only the SA

mode was stable. For intermediate strengths of haline forcing the response of the model was very dependent on the spatial distribution of the fresh water fluxes. Under certain distributions of fresh water flux intermediate modes became possible where the main circulation was confined to either the sub polar and mid latitude boxes or the equatorial and mid latitude boxes. Depending on the nature of the surface forcing these intermediate modes could either replace or coexist with the multiple equilibria states seen in the simpler models.

2.7 Coupled ocean-atmosphere box models.

The effect of multiple equilibria and possible fluctuations in the ocean circulation on the climate system can be examined by coupling a simple atmosphere model to an ocean box model. The use of an atmosphere model rather than Newtonian or mixed boundary conditions allows for extra feedback mechanisms. The extra feedback mechanisms are coupled to the thermohaline circulation through the surface temperature forcing and the hydrological cycle. An energy balance atmosphere model coupled to a 2/1 box model gave a more realistic atmosphere-sea surface temperature interaction than the traditional mixed boundary conditions (Birchfield 1989). If the fresh water flux was prescribed then this coupled atmosphere-ocean model had the same equilibrium solutions as the uncoupled 2/1 ocean box model. For weak freshwater forcing there was 1 stable equilibria with cold fresh deep water corresponding to the TH mode and for strong haline forcing the SA mode with warm salty deep water was the only stable equilibrium. At intermediate strengths of fresh water forcing both the TH and SA modes were stable and the final equilibrium solution of the model was dependent on the starting conditions (Birchfield 1989). Replacing the fixed fresh water flux with a hydrological cycle that was part of the atmosphere model altered the stability of the TH mode (Lohmann et al. 1995). This model with a simple hydrological cycle and atmosphere model was more stable to infinitesimal high latitude salinity perturbations in the TH mode than the models with mixed boundary conditions. Increased stability of the TH mode made it less likely for a polar halocline catastrophe to occur when a fresh water perturbation was applied. The TH mode became less stable as the atmospheric heat and fresh water transports increased. As mixed boundary conditions are equivalent to an atmosphere with heat transport so effective that the atmospheric temperature remains unchanged, using mixed boundary conditions under estimates the stability of the TH mode. The 2/1 coupled ocean-atmosphere model was extended to a 2 hemisphere, single ocean basin model by the addition of a box to give a 3/1 ocean box model coupled to an energy balance atmosphere model (Birchfield 1990). If the surface fresh water flux was fixed then the response of the 3/1 model behaved as 2 2/1 models back to back.

2.7.1 Global ocean atmosphere box models.

The coupled ocean-atmosphere box model can be extended further to give a global ocean atmosphere model as in Wang and Birchfield (1992). Both the Atlantic and the Pacific were represented by 3/1 ocean models, with the Southern ocean box being common to both basins. The Indian ocean was also included as a 2/1 box model. Similar to the previous models the atmosphere was represented by an energy balance model and fixed fresh water fluxes. As with

the simpler models the stable equilibrium solutions of the model were very dependent on the magnitude and distribution of the surface fresh water flux. The strength and distribution of the fresh water fluxes was determined by the magnitudes the North Atlantic hydrological cycle and the Atlantic to Pacific fresh water flux. For a weak North Atlantic hydrological cycle the deep water was mainly formed in the North Atlantic and Southern Ocean. As the strength of the hydrological cycle increased the rate of deep water production decreased. At intermediate strengths of the intra basin water vapour transport the ocean model had multiple equilibria solutions. Increasing the North Atlantic hydrological cycle further encouraged deep water formation in the North Pacific and the Southern Ocean, with the rate of deep water production increasing as the strength of the North Atlantic hydrological cycle increased. When the inter basin water vapour transport was increased the range of values of the North Atlantic hydrological cycle for which multiple steady states were possible increased. Increasing the fresh water flux from the Atlantic to the Pacific also enhanced the rate of deep water production in the North Atlantic while decreasing the tendency to form deep water in the North Pacific (Wang and Birchfield 1992).

When a low order atmospheric "general circulation" model was coupled to the 2/1 ocean model (Lorenz 1984 and 1990) the high frequency noise in the atmosphere model drove low frequency quasi periodic oscillations in the ocean model. Even after very long periods of integration the ocean model did not reach a steady state, but fluctuated with periods between 50 and 800 years (Roebber 1995).

2.8 The effects of surface gyres and ice sheets.

The affect of a surface wind driven gyre on the thermohaline circulation was investigated using a 2×2×2 box model, where a single hemisphere ocean basin had been split horizontally and vertically as in the 2×2 box model and then again into east and west sections (Huang and Stommel 1992). The introduction of surface wind stress caused the catastrophic transition between the TH and SA modes to split into a number of smaller separate transitions and had the affect of stabilising the thermally driven modes. As with the simpler models the possible equilibria of the system were controlled by the relative strengths of the thermal and haline surface forcing. The presence of the surface gyre acted selectively to enhance the stability of circulation modes with surface flow in the same direction as the wind driven circulation. This corresponded to increasing the stability of the thermally driven modes in the North Atlantic. If a strong surface gyre was imposed then the multiplicity of the equilibria was suppressed making the TH mode dominant for all but exceedingly large surface salinity forcing. Similar to the less complicated box models the 2×2×2 box model showed a hysterysis when the strength of the fresh water forcing was cycled from low to high to low but the 2×2×2 model made the transition from the TH to SA to TH mode through a series of several small smooth steps rather than 1 large catastrophic transition (Huang and Stommel 1992).

2.8.1 Coupled ocean - ice box models.

Coupling an ice sheet model to a 2-1 box model introduced an extra feedback mechanism into the system that could drive long time scale oscillations (Paillard and Labeyrie 1994). The ice model did not change the equilibrium solutions of the ocean model rather it caused both the SA and TH circulation modes to become unstable. This model showed the ocean circulation flipping between the TH and SA with a period of approximately 12,000 years. Associated with these fluctuations of the thermohaline circulation the ice model had periods of massive iceberg discharge similar to those in a Heinrich event (Paillard and Labeyrie 1994).

2.9 Sensitivity of the thermohaline circulation to model parameters.

In all the models presented the possible modes of the thermohaline circulation are primarily controlled by the relative strengths and distributions of the thermal and haline surface buoyancy forcing. The exact parameterisations of the surface buoyancy forcing have a strong influence on the stability of the thermohaline circulation. These parameteristions control the strength of the feedback between sea surface properties and the surface buoyancy fluxes. Diffusivities have a strong impact on the strength of the thermohaline circulation though the ratio of the thermal to haline diffusivity can be more important than the absolute values. Choice of convection scheme has little effect on the model results unless the model is already in an marginally stable state. Any form of external stochastic forcing increases the variability of the thermohaline circulation. The magnitude of the thermohaline circulations response to external forcing is dependent on both the magnitude and intrinsic time scale of the external forcing.

Box model and OGCM results both agree that the relative magnitude of the thermal to haline surface buoyancy forcing is the main control of the thermohaline circulation. Similarly both types of model are sensitive to the parameterisation of convection when the surface forcing is near the critical value. A smooth relation between the strength of convective mixing and the vertical density gradient tends to stabilise the thermal mode in comparison to the same model using a more step like relationship between the vertical density gradient and the convective mixing. I believe that modelling these two processes accurately is fundamental to improving the quantitative predictions of the thermohaline circulation. Detailed comparison of the differing model results has been avoided as the sensitivity of each model to the surface forcing suggests that the differences in the responses of the various models may well be controlled by the surface forcing used rather than the parameterisations used with in the model. As the surface forcing is not independent of the model configuration it is exceedingly difficult to ensure that 2 distinct models are being forced in exactly the same manner.

Chapter III

Results from the OGCM

3.0 Description of the OGCM.

The results presented in this chapter were all generated using the Hadley Centre's version of the Bryan - Cox code (Cox 1984). This code is based on the primitive equation model described by Bryan (1969). The model solves the Navier - Stokes equations under the hydrostatic and Boussinesq approximations (see appendix A - The OGCM equations). The local pressure is derived from the hydrostatic relation, with a rigid lid approximation. The system is closed by a turbulent viscosity hypothesis. Convective mixing is included using the standard NCON scheme (Bryan 1969 and appendix A).

3.0.1 Model configuration.

The model was configured with a highly idealised topography of a rectangular, flat bottomed, single hemisphere ocean basin. The model dimensions were chosen to represent the North Atlantic. Thus the model covered 0° to 70° North and 60° of Longitude. The ocean basin had a uniform depth of 5 km. A course resolution grid of 2.5° latitude by 3.75° Longitude with 13 vertical levels of varying thickness was used (see appendix C - The OGCM parameters).

3.0.2 Boundary conditions.

Boundary conditions were defined at the lateral walls on the velocity and tracer fields. There was no flow through the boundaries and the gradient of the tracer fields normal to the boundary was set to zero. A symmetry boundary condition was used at the equator for the tracers. The bottom was assumed to be impermeable and insulating. A free slip boundary condition was applied to the velocity fields at the ocean bottom and walls. At the surface a wind stress was specified that had only a zonal component which was a function of latitude (Figure 3 - 1). This surface wind stress was only applied to the surface layer. The values of the wind stress were taken from the idealised profile used by Winton and Sarachik (1993).

The sea surface temperature was forced using a Haney term (Haney 1971). For the spin up of the model a Haney term was also used to force the sea surface salinity. The zonally uniform effective atmospheric temperatures and salinities used in the Haney terms were obtained by averaging the Atlantic sea surface data of Levitus (1982) (Figure 3 - 2). For the main experiment mixed boundary conditions were used. The mixed boundary conditions consisted of a fixed surface salt flux and a Haney term forcing the surface temperature. Using a Haney condition for the surface fresh water flux introduces an unrealistically strong coupling between the sea surface salinity and the surface fresh water flux. Mixed boundary conditions uncouple the surface fresh water flux from the properties of the surface waters. This weakening in the feedback allows for the prolonged existence of surface salinity anomalies such as that observed during the "Great Salinity Anomaly of 1968 - 1982" (Dickson et al. 1988).

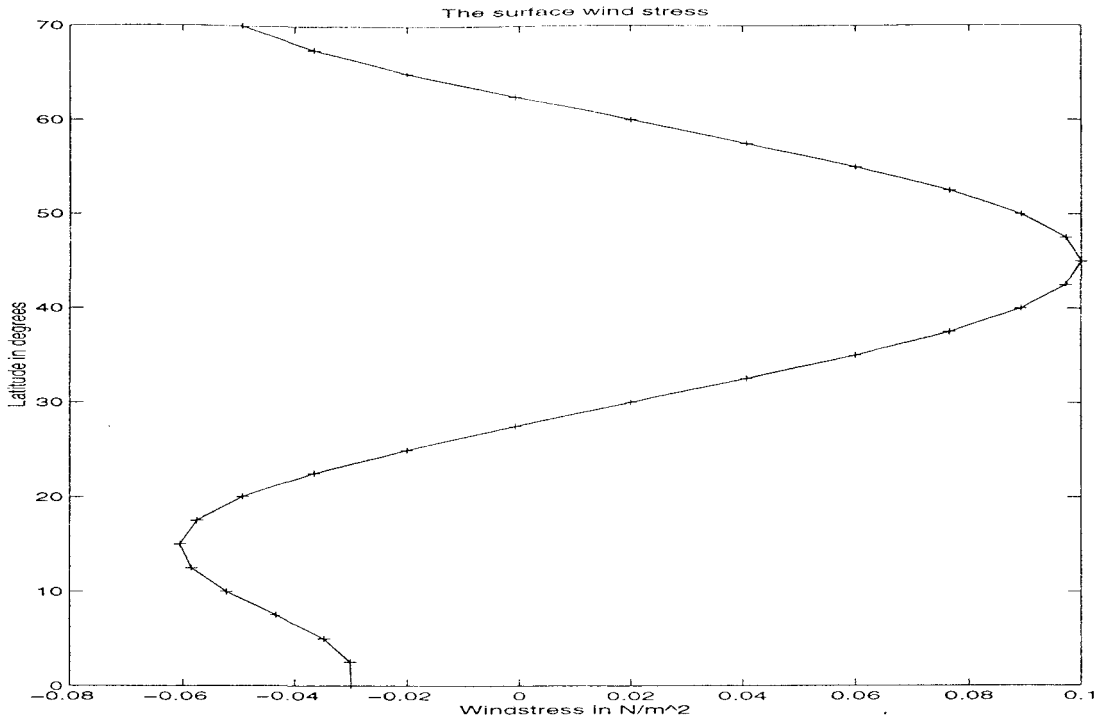

Figure 3 - 1: The surface wind stress as a function of Latitude.

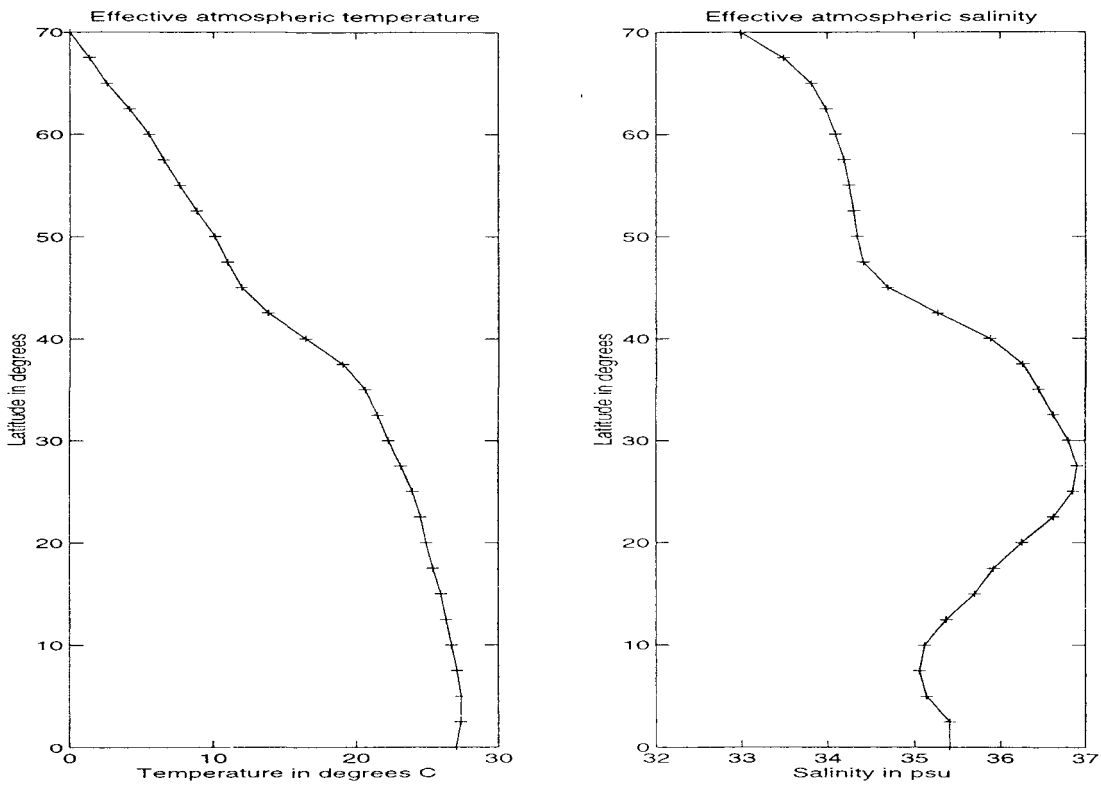

Figure 3 - 2: The effective atmospheric temperature and salinity used in the Haney surface forcing terms.

3.0.3 Discussion of the numerics used in the OGCM.

To improve the computational efficiency of the model, high speed, external gravity waves were eliminated through the use of the "rigid lid" approximation. The half pendulum day constraint associated with internal gravity waves was overcome by using a semi-implicit treatment of the Coriolis term. To enhance the computational efficiency yet further (making the extended integration periods used in this study feasible) the distorted physics of Bryan (1984) was introduced into the equations of motion.

The distorted physics has the affect of reducing the frequency and phase speed of internal gravity waves by a factor of $1/\alpha$ (Bryan 1984) and increasing the pace at which the tracer equations for the deep ocean are evolved relative to the surface by a factor $\gamma_{deep}/\gamma_{surface}$. Bryan (1984) has shown that for steady boundary conditions (as used in this study) the influence of the distorted physics on the equilibrium state approached by the model is negligible. For the main model run γ was set to 1 (independent of depth) ensuring that both energy and tracers were conserved. The conservation of energy and tracers was required when studying the transient properties of the circulation. During the main experiment α remained unchanged from the spinup configuration. The effect of α was to reduce the velocity of the fast waves in the system. Introducing α also reduces the frequencies of the high frequency processes in the model (Killworth 1984). Long time scale (decadal and longer) changes in the ocean circulation are not affected by the distortion of the fast, high frequency processes.

The finite difference scheme used was the same as Bryan (1969) and Cox (1984). The equation of state used was a polynomial fit to the Knudsen formula (Bryan and Cox 1972). The numerical stability of the OGCM is discussed in more detail in appendix (appendix D - The stability of the OGCM).

3.1 Spinup procedure.

During the spinup procedure relaxation boundary conditions were used for both the temperature and salinity surface forcings. The model was started from a resting homogeneous state with a uniform temperature of 5°C and a uniform salinity of 32.5 psu. The model was then integrated forwards in time with a time step of Δt_V=5 hours for the momentum equations and a time step of Δt_T=5 days at the surface (increasing to Δt_T=20 days at depth) for the tracer equations. After an initial period of intense convection the model converged to an approximate equilibrium state with a single overturning cell of magnitude 12 Sv (Figure 3 - 3). This equilibrium state, reached after 1800 years of integration (7200 years at depth), had a temperature field that for a given model level had changed by less than 0.001°C in 500 years.

3.1.1 The surface fresh water flux.

A diagnosed surface salt flux was obtained from the mean surface salt flux of the equilibrium state by taking the time mean of the surface salt fluxes for the final 100 years of the spinup run.

From this surface salt flux the implied fresh water flux (Precipitation minus Evaporation, *P-E*) was calculated according to (Weaver and Hughes 1992).

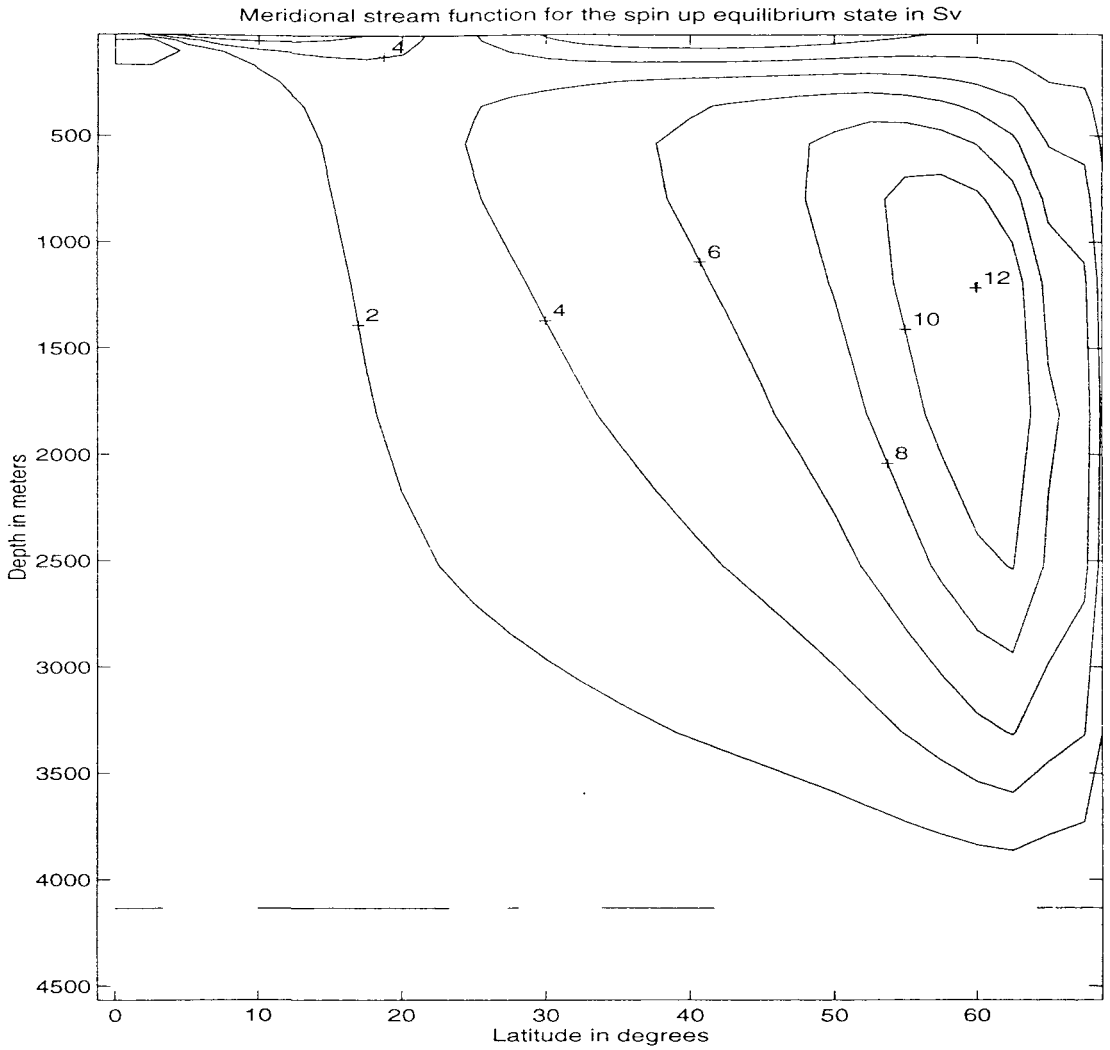

Figure 3 - 3: The meridional stream function of the equilibrium state obtained at the end of the 1800 year spin up run of the OGCM. The non zero stream function at the surface is due to the contouring algorithm and not the data.

By using this technique to calculate the surface fresh water flux, it was hoped to obtain a climatological forcing field which partially compensated for some of the physics missing from the model (Weaver and Hughes 1992). The forcing field may partially compensate for the coarse resolution of the convection scheme and the lack of small scale processes. The diagnosed salt flux was then used as the fixed surface salt flux for forcing the sea surface salinity as part of the mixed boundary conditions.

Qualitatively the diagnosed surface fresh water flux agrees with the expected precipitation minus the evaporation (*P-E*) field for the North Atlantic. As expected there was net evaporation at low latitudes and net precipitation at high latitude. There was an area of strong evaporation associated with the western boundary current of the sub tropical gyre (Figure 3 - 4) and a region

of strong precipitation associated with the jet at 40°N that separates the sub polar and sub tropical gyres.

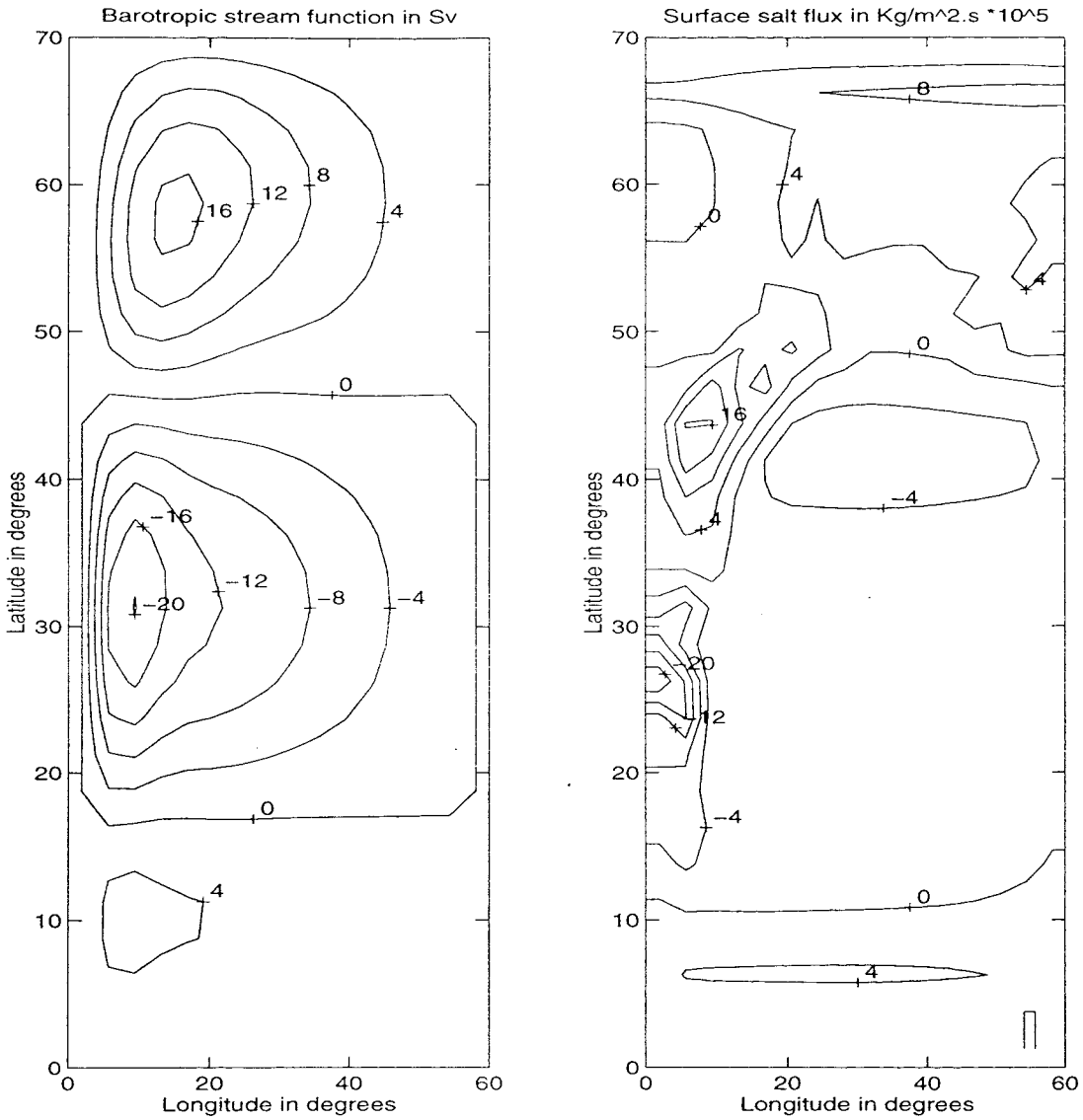

Figure 3 - 4: (a) The barotropic stream function showing the sub polar and sub tropical gyres. (b) The diagnosed surface salt flux used as the fixed forcing field for the mixed boundary conditions. A positive salt flux is out of the ocean.

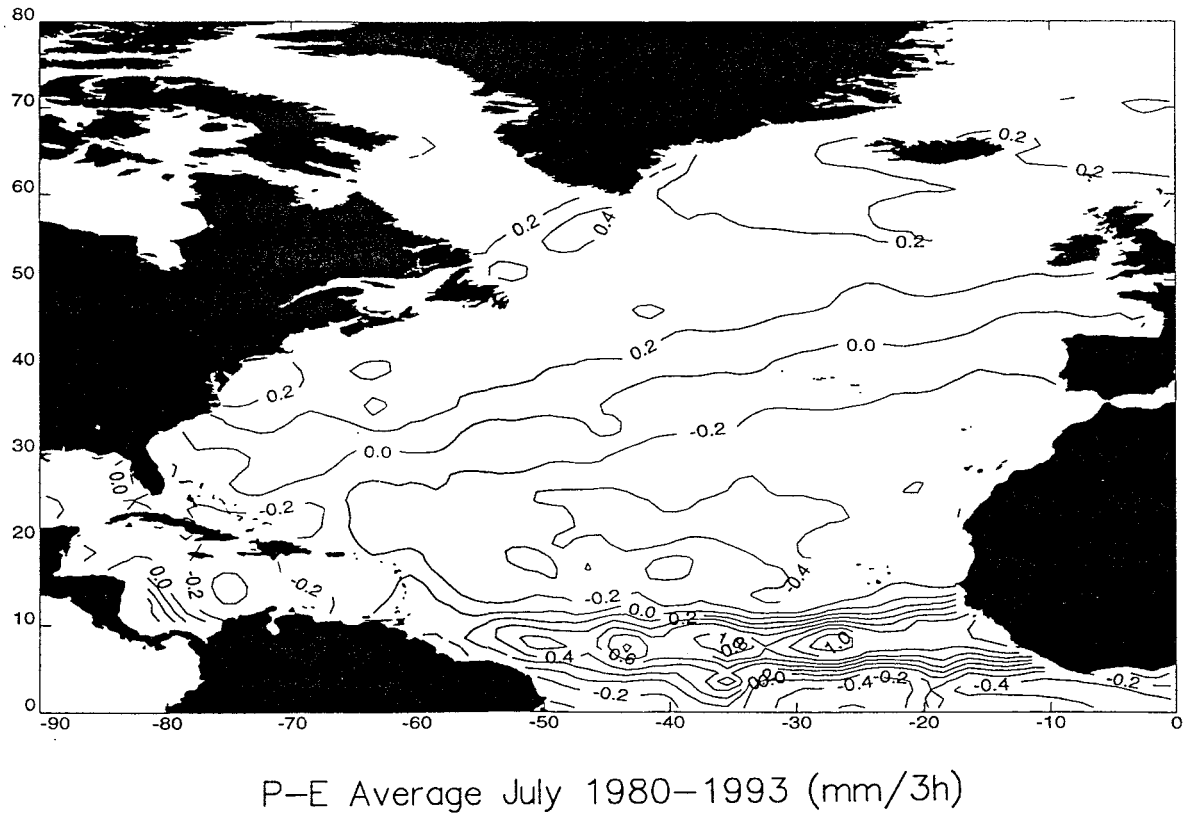

Figure 3 - 5: The observed monthly mean P - E fields for the North Atlantic for January and July taken from Josey et. al. 1996.

Comparing the diagnosed salt flux with the observed P-E fields for the North Atlantic highlights some of the short comings of the OGCM (Figure 3 - 4 and Figure 3 - 5). The general pattern of the salt flux is similar to the observations with excess precipitation at mid latitudes and evaporation at low latitudes. The largest discrepancies occur along the western boundary where the model shows strong maxima and minima in the P-E field which do not occur in the observational data. The western boundary current in the OGCM is rather broad and diffuse in comparison to those observed due to the inability of the OGCM to resolve features with length scales smaller than the grid spacing. These discrepancies in the salt flux are a manifestation of the OGCM's inability to represent the western boundary current. This effect is probably compounded by the lack of topography in the OGCM which results in the surface currents not following the same routes as those observed.

Applying a 1mm/3h P-E flux to a mid latitude surface box in the OGCM with a salinity of 35 psu is equivalent to surface salt flux forcing of $3*10^{5}$ Kg/m^{2}s. Thus the OGCM surface fluxes are 4 to 6 times stronger than those observed. As the stability of the thermohaline circulation is strongly dependent on the strength of the surface buoyancy forcing the stability of the thermohaline circulation in this OGCM is not a fair indication of the stability of the present day ocean circulaiton.

3.2 The OGCM results.

The OGCM was initialised with the equilibrium state obtained from the spinup procedure. Mixed boundary conditions were applied to the surface buoyancy forcing using the same effective atmospheric temperatures as for the spin up and the diagnosed surface salt flux. The depth dependant parameter ($\gamma(z)$) introduced into the tracer equations by the distorted physics (section 3.0.3) was removed. This restored the conservation equation to its original form. The removal of $\gamma(z)$ from the tracer equations was required so that both tracers and energy were conserved. Since the purpose of this study was to examine the transient properties of the thermohaline circulation it was necessary that the dynamics obeyed the fundamental conservation laws. α remained unchanged as it has little effect on the long time scale (decadal and longer) results and considerably improves the computational efficiency (section 3.0.3).

The time step was reduced to 1.25 hours for the momentum equations and 1.25 days for the tracer equations. This reduction in time step was required so that the model remained stable with the large velocities obtained during the strong overturning exhibited during the thermal flushes that were observed during the model run. Due to the large amount of data generated it was not possible to store instantaneous values for all time steps. Since the aim of the study was to examine the long time scale (decadal and longer) variability of the thermohaline circulation, time averaged data was stored. The time period over which the averaging was performed was dependent on the state of the model. For the slowly varying weak, haline driven circulations the data was averaged over 100 years. Close to and during the rapidly varying thermal flushes the averaging period was reduced to 10 years. This provided approximately equal numbers of data

points in the thermal and haline dominated modes. All the results presented are based on this time averaged data.

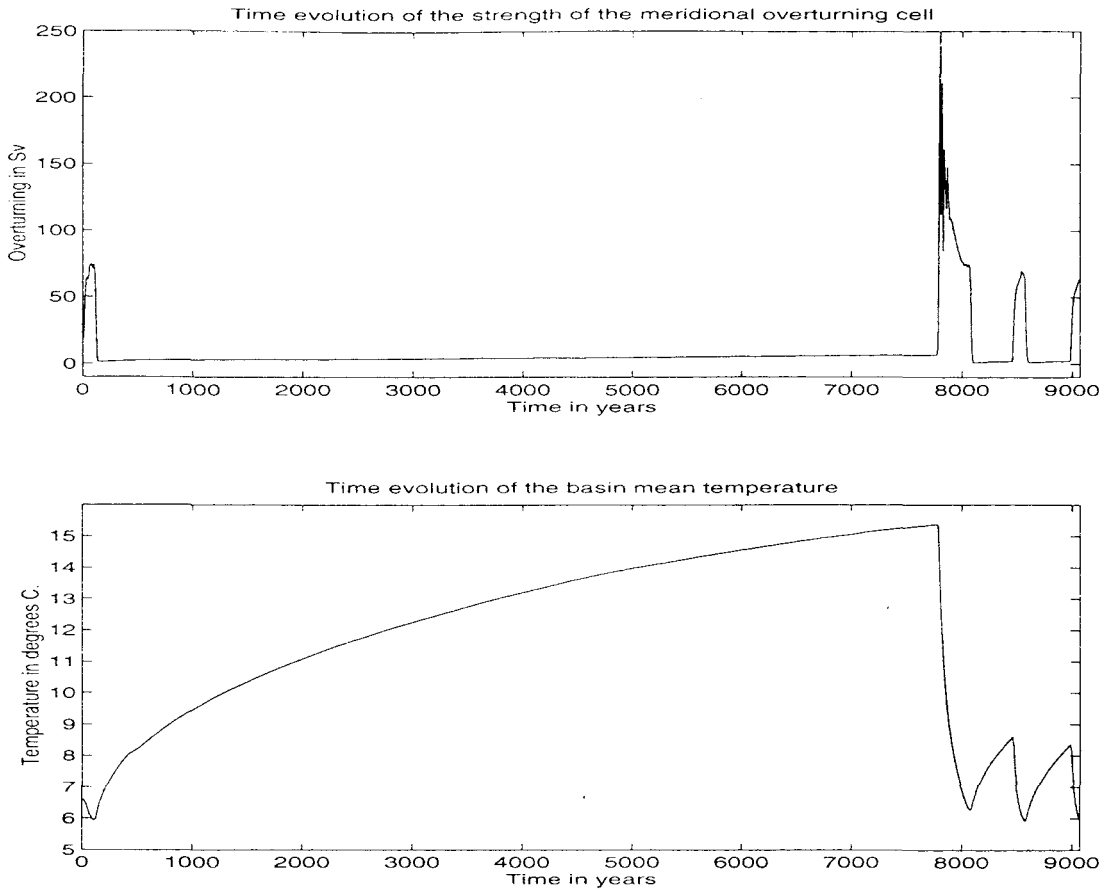

Figure 3 - 6: The strength of the meridional overturning cell and the basin mean temperature as functions of time for the OGCM model run.

The model was integrated forward in time for just over 9000 years. DDOs and salt loop oscillations were observed in the OGCM run. It was convenient to divide the model run into the various circulation modes (Table 3 - 1) and examine each mode individually. After an initial adjustment to the change in surface boundary conditions there was a period when the model was in a haline dominated mode. This was terminated by a strong thermal flush. Following the strong thermal flush the model exhibited DDOs with a period of ≈600 years.

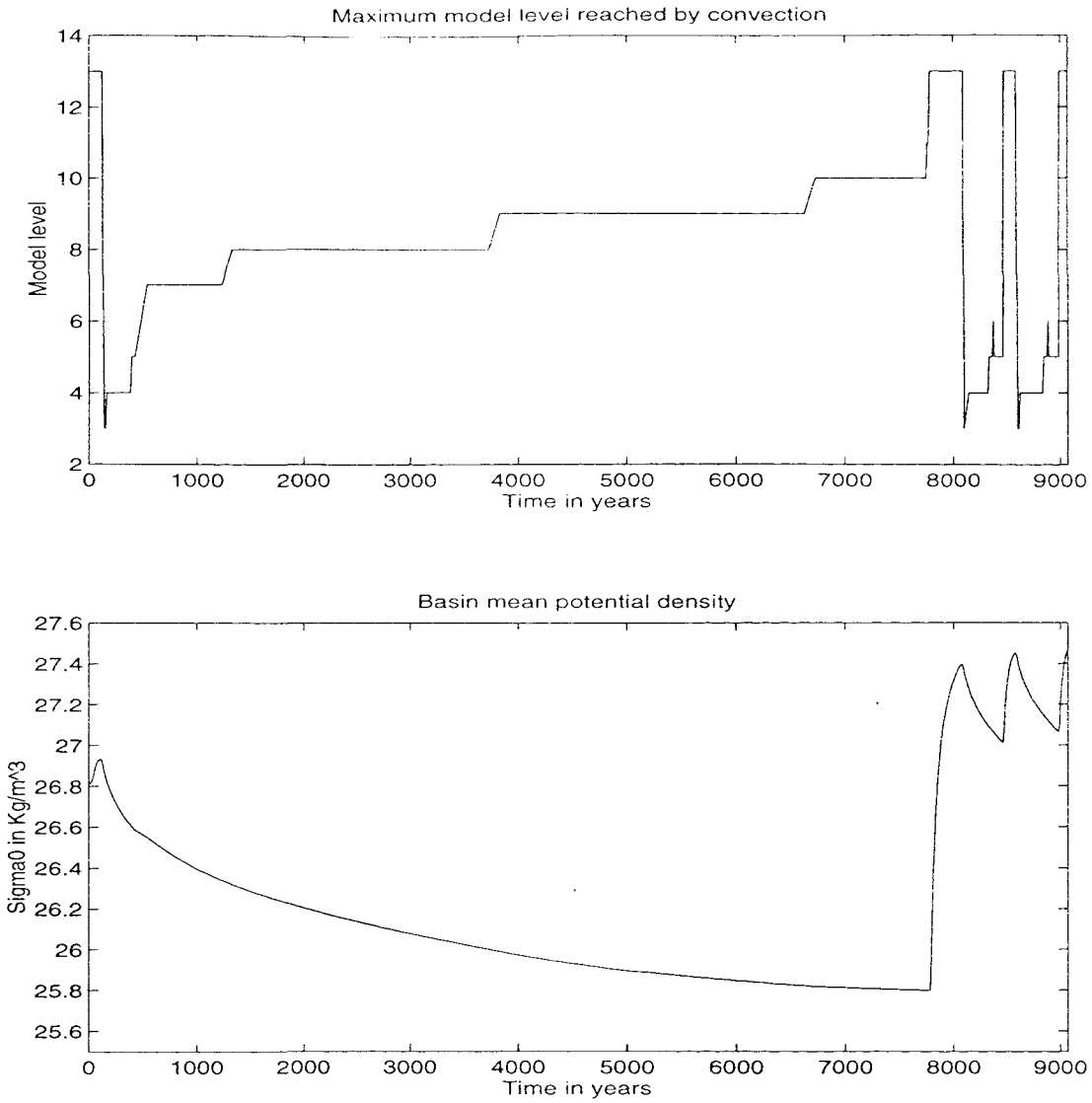

Figure 3 - 7: The maximum depth reached by convection and the basin mean potential density as functions of time for the OGCM model run.

Time Period (in years)	Description	Name
0 to 110	Initial adjustment to change in surface boundary conditions.	Initial adjustment phase
111 to 7780	Weakly overturning with no convection, haline driven circulation.	WC1
7781 to 8100	Strong thermal flush with strong overturning and vigorous convection.	TF1
8101 to 8460	Weakly overturning with no convection, haline driven circulation.	WC2
8461 to 8580	Thermal flush with strong overturning and deep convection.	TF2
8581 to 8980	Weakly overturning with no convection, haline driven circulation.	WC3
8981 to end of run	Thermal flush with strong overturning and deep convection.	TF3

Table 3 - 1: The modes of circulation observed in the OGCM run.

3.3 Initial adjustment phase (years 0 to 110).

The first 110 years of the model run (after switching to mixed boundary conditions) show a peak in the mean kinetic energy and the strength of the meridional overturning cell (Figure 3 - 6). This strong, thermally driven, overturning cell was due to the deep convection along the polar boundary of the model domain. The transition from the stable equilibrium under the Haney forcing to the strong overturning cell under mixed boundary conditions was caused by the intermittence of the convective process (Winton and Sarachik 1993). Under Haney boundary conditions there was a feedback between the sea surface salinity and the surface salt flux, thus the sea surface salinity could not stray far from the reference salinity. With the surface salinity constrained the convective feedback mechanism was damped, so limiting the strength of the meridional overturning cell. Using mixed boundary conditions removed the feedback between the sea surface salinity and the surface salt flux and so removed the damping on the convective feed back mechanism. This allowed a strong overturning cell to develop. The strong overturning cell had the effect of cooling the deep ocean (Figure 3 - 6).

3.4 The weak circulation of years 111 to 7780 (WC1).

Once the cooling of the deep ocean had increased the vertical stratification sufficiently to inhibit the convective process the meridional overturning cell rapidly weakened. The overturning rate dropped from 70 Sv to 2 Sv in 30 years (Figure 3 - 6). This reduction in meridional overturning marked the onset of a halocline catastrophe (Bryan 1986). During the halocline catastrophe a

fresh water cap formed at high latitudes inhibiting convection (Figure 3 - 7). For the next 7670 years a weak, salinity dominated, circulation persisted. This weak circulation mode was similar too that found by Winton and Sarachik (1993). The meridional overturning associated with the thermohaline circulation for this mode was less than 7 Sv and was confined to above the pycnocline. During WC1 the deep ocean was decoupled from the surface circulation as there was no convection penetrating to below the pycnocline (Figure 3 - 7). Below the pycnocline the deep ocean had a uniform temperature and salinity. Throughout the 7670 years of the weak circulation the deep ocean warmed by 10°C and its salinity increased from 33.0 psu to 35.0 psu. There was a strong thermocline separating the cold polar surface waters from the warmer waters associated with the sub tropical gyre (Figure 3 - 8). The strong thermocline stretched from the surface at 45°N (approximately the boundary between the two surface gyres) to a depth of 300 meters at the polar boundary. Despite the warming of the deep waters the surface polar waters (above the thermocline) remained at a constant temperature of 1.5°C.

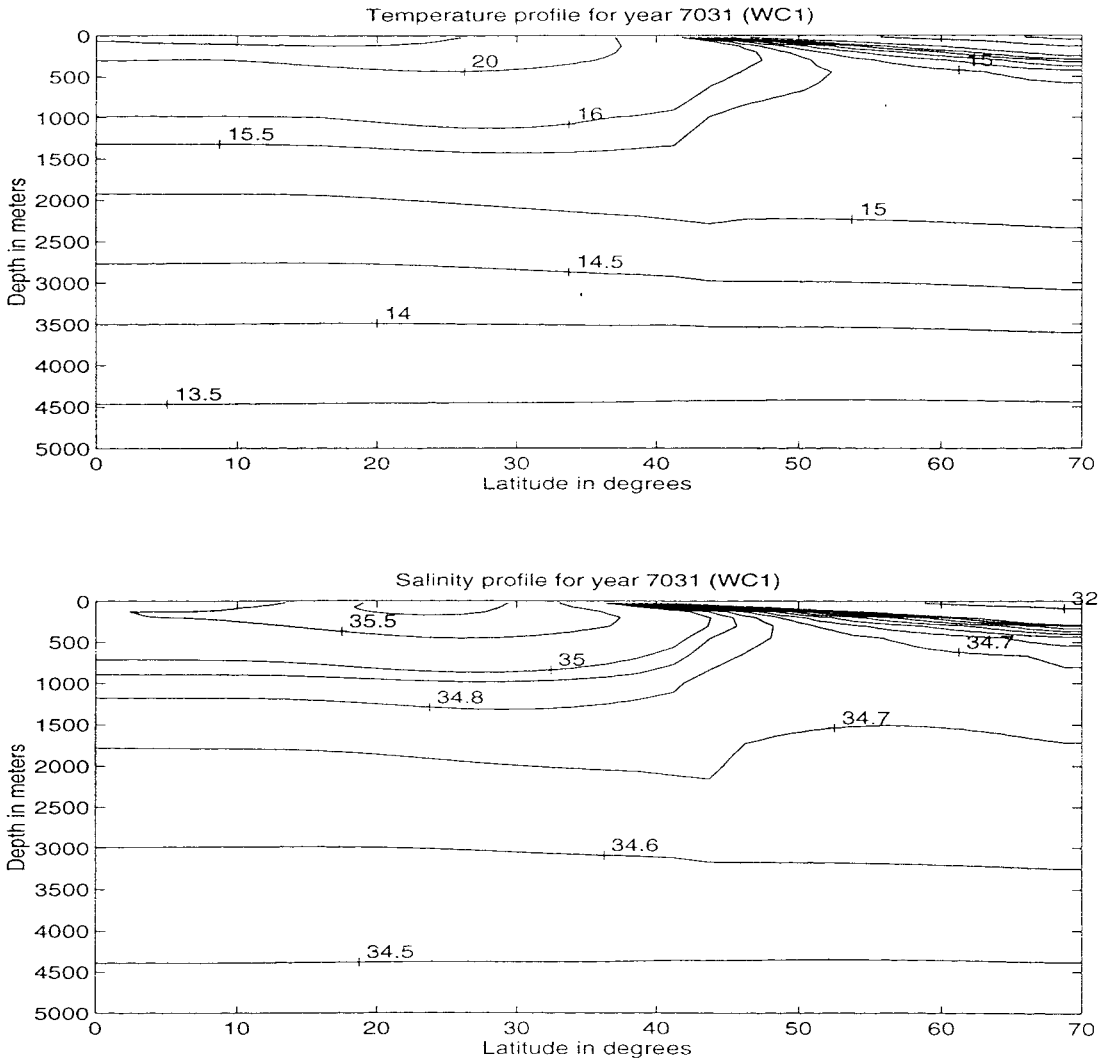

Figure 3 - 8: The zonally averaged temperature and salinity profiles for year 7031. These profiles are characteristic of those found throughout WC1.

There was a strong halocline, that mirrored the thermocline, that separated the polar fresh water cap from the rest of the ocean. While the deep waters were becoming saltier the polar fresh water cap increased in salinity from 31.0 psu to 31.3 psu (Figure 3 - 8).

The density profile closely followed the temperature profile except above the polar thermocline/halocline. The salinity of the polar fresh water cap was sufficiently low to overcome the effect of temperature, causing the fresh water cap to be less dense than the surrounding waters. This made the polar surface water less dense than the warmer, saltier deep waters. Over the length of WC1 the density of the deep water decreased by 1 kg/m^3, while the density of the surface polar waters increased from 1024.8 kg/m^3 to 1025.5 kg/m^3. There was a weak pycnocline that descended from 1000 meters at the start of WC1 to 3000 metes just before the strong thermal flush. This pycnocline weakened throughout the length of WC1. The pycnocline can be linked to the weak temperature gradient that was seen at these depths.

3.4.1 The circulation pattern of WC1.

The general circulation pattern of WC1 remained constant over the entire 7670 years. The surface velocity fields of WC1 were dominated by the wind driven circulation (Figure 3 - 9). The gyre circulation penetrated to a depth of 500 m at the start of WC1 and gradually deepened to 800 m just before the strong thermal flush. The deep ocean was decoupled from the wind driven surface circulation with the velocities below the weak pycnocline (the velocities of the deep waters) being 2 orders of magnitude smaller than the surface velocities. There was upwelling over the majority of the sub polar gyre and downwelling in the sub tropical gyre (Figure 3 - 9). Along the equatorial boundary there was net upwelling while near the northern boundary was a region of downwelling. The small area of strong downwelling stretching westwards from the eastern boundary at 45°N was associated with the formation of intermediate water (section 3.4.3).

3.4.2 Transport of tracers.

Advection was the dominant mechanism for transporting heat and salt downwards for the top 200 meters of the ocean during WC1. Between 200 meters and 700 meters both advection and diffusion were similar orders of magnitude and equally important for the vertical transport of tracers. From 700 meters downwards diffusion was the most significant mechanism for the downwards transport of heat and salt. The convection was acting against both advection and diffusion by cooling the intermediate waters.

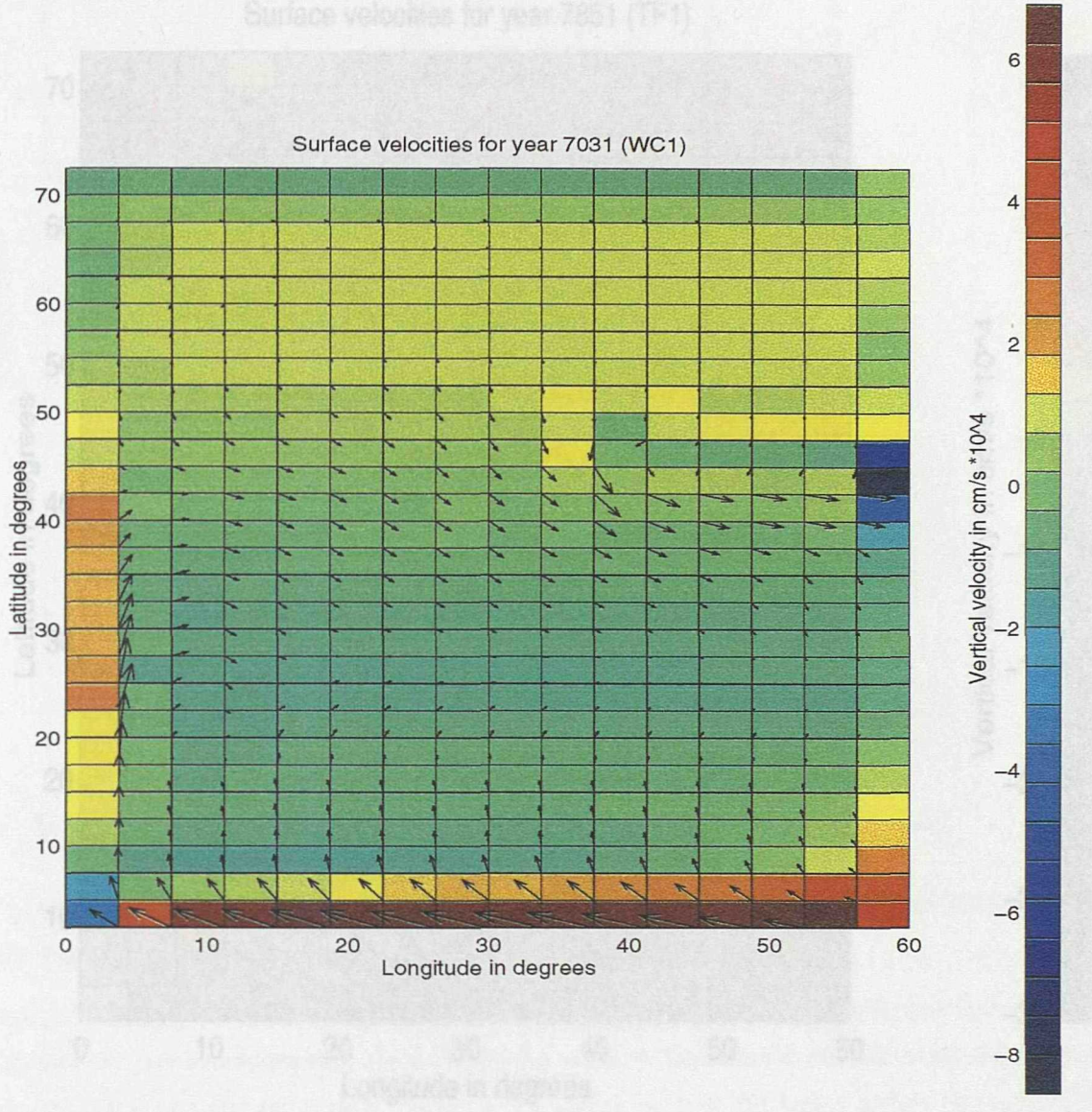

Figure 3 - 9: The surface velocity fields for year 7031 when the weak circulation of WC1 was well developed. The velocity arrows indicate the horizontal surface velocities (with a maximum of 15 cm/s). Vertical velocity is indicated by the shading.

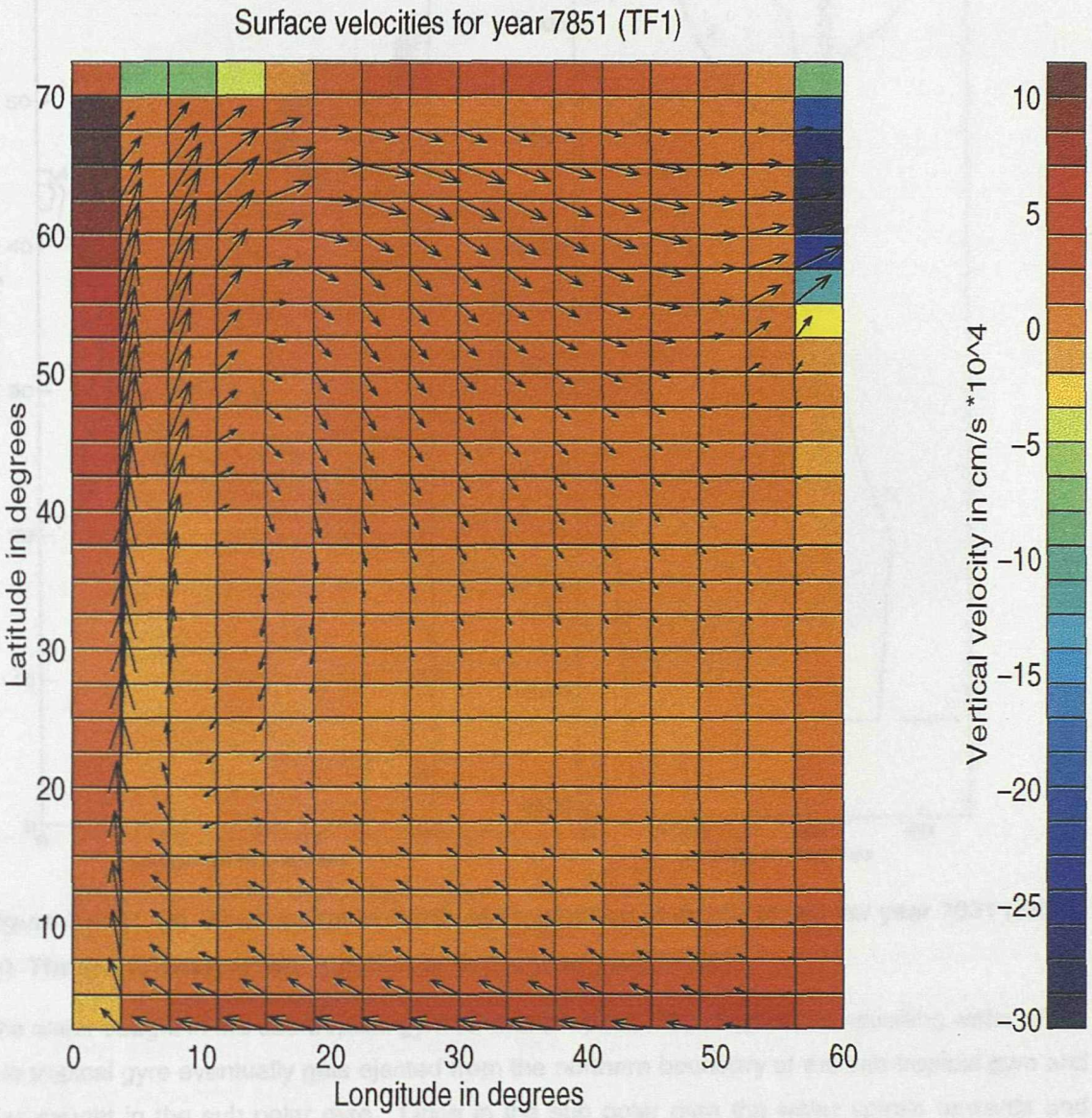

Figure 3 - 10: The surface velocity fields for year 7581 when the thermal flush TF1 had its highest velocities. The arrows indicate the horizontal surface velocities (with a maximum of 17 cm/s). Vertical velocity is indicated by the shading.

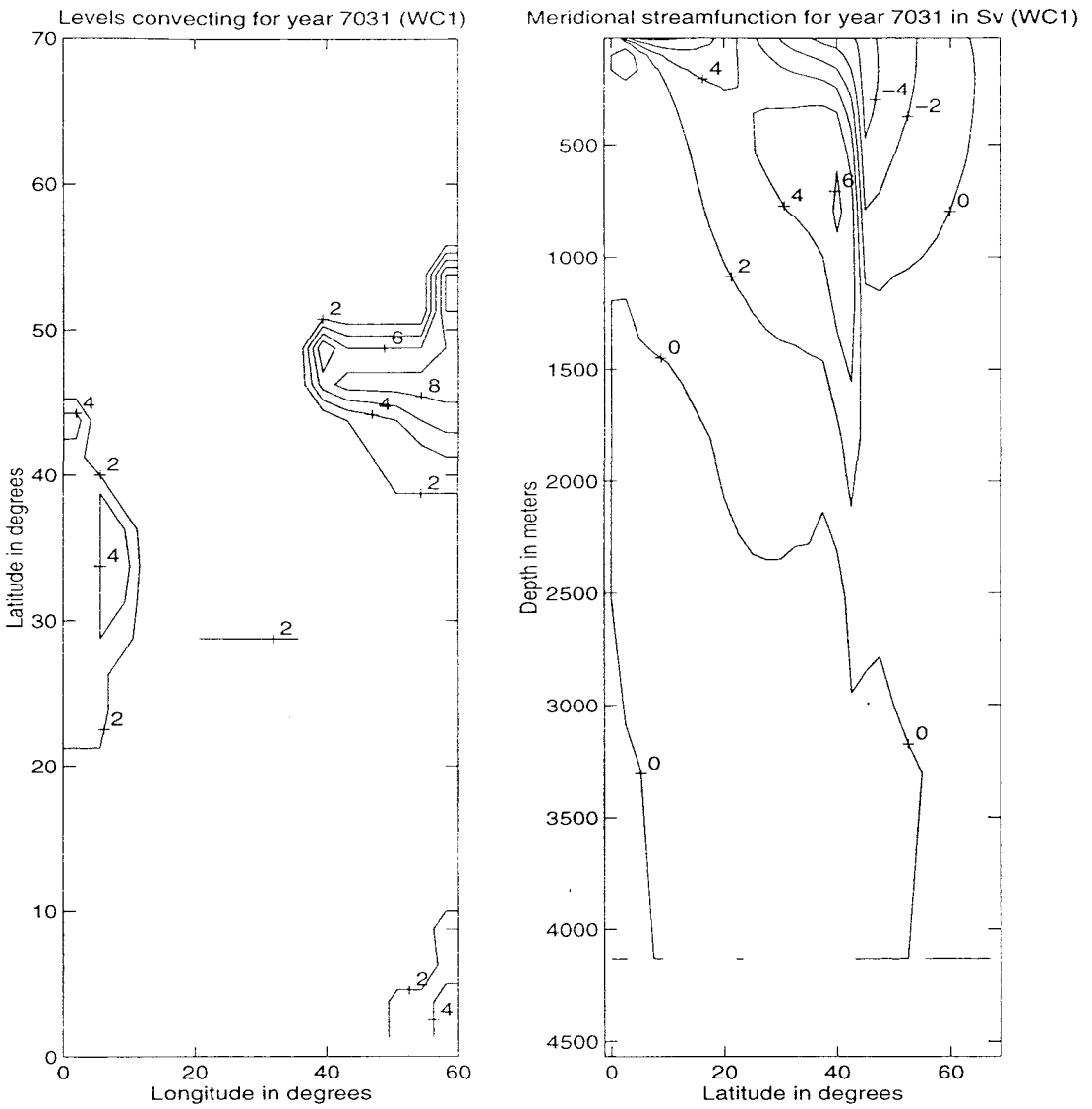

Figure 3 - 11: (a) The maximum depth of convection in model levels for year 7031 (WC1). (b) The meridional stream function in Sv for year 7031 (WC1).

The water caught in the sub tropical gyre tended to spiral. The downwards spiralling water of the sub tropical gyre eventually gets ejected from the northern boundary of the sub tropical gyre and was caught in the sub polar gyre. Once in the sub polar gyre the water spirals upwards and cools. This exchange of water between the 2 gyres occurred mainly between 100 meters and the weak pycnocline. There was a return of water from the sub polar gyre to the sub tropical gyre in the top 100 meters of the ocean. The downwards spiralling water of the sub tropical gyre was responsible for the downwards transport of heat and salt to the top of the pycnocline. From the pycnocline downwards diffusion was the major mechanism for the vertical transport of both heat and salt. Having lost some of its heat and salt, through vertical diffusion, the warm salty water of the sub tropical gyre was returned to the surface via the sub polar gyre.

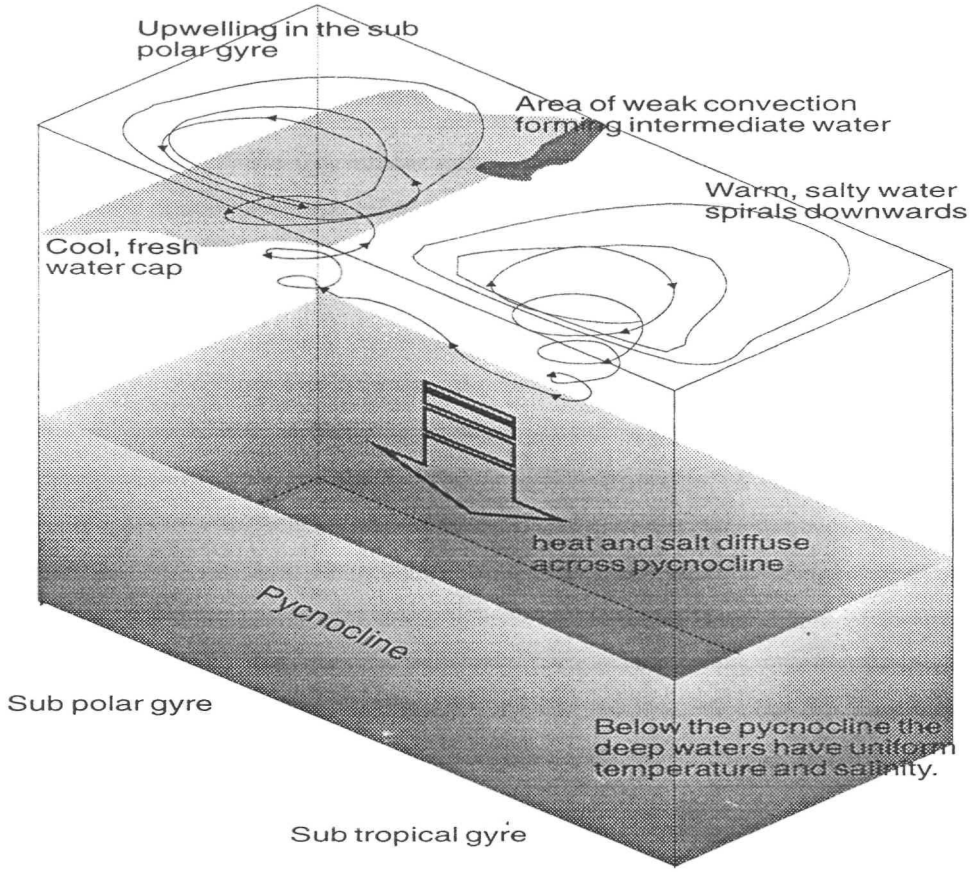

Figure 3 - 12: A summary of the circulation and main features of WC1.

3.4.3 The regions of convective activity.

The western boundary current of the sub tropical gyre was subject to strong evaporation (Figure 3 - 4). This evaporation increased the surface salinity enough to cause convection down to 500 m, forming warm salty intermediate water. This warm, saline water in the western boundary current was advected across the basin to the eastern boundary by the strong jet at 45° North. Near the eastern boundary the depth of the jet decreased bringing the warm salty water towards the surface (Figure 3 - 9). As the warm saline water was brought to the surface (at 45°N between 30°E to 60°E) it was subjected to intense surface cooling. The intense cooling produced a region of cold dense water, driving the convection that penetrated down to the pycnocline. This region of convection (at 45°N and 30°E to 60°E) was also an area of strong downwelling. The downwelling persisted down to the top of the pycnocline where the cold, saline, intermediate water spread out and mixed with the water from the sub tropical gyre. The formation of the intermediate water drove the weak thermohaline circulation of 2 meridional overturning cells. Throughout WC1 the thermohaline circulation gradually strengthened from 2 Sv to 7 Sv as the intermediate water penetrated to greater and greater depths. There was a

small area of weak convection (down to 500 meters) along the equatorial boundary. This area of weak convection was caused by the upwelling of warm salty water that was then cooled by the surface forcing (Figure 3 - 12).

3.5 The strong thermal flush of years 7781 to 8100 (TF1).

The weak circulation of WC1 was broken abruptly at year 7781 when a small area of the sub polar gyre started deep convection, forming cold, fresh deep water. This area of convection was then advected around the sub polar gyre. The deep convection marked the start of the strong thermal flush TF1. Once the convective process had been started a strong meridional overturning cell rapidly developed. The overturning cell reached a magnitude of 290 Sv in the space of 20 years. This result is similar to that of Marotzke (1990). During TF1 the strength of the meridional overturning cell oscillated with a period of 20 years. These oscillations can probably be associated with the salt loop oscillator mechanism (Winton and Sarachik 1993) which operates on an advective time scale (order 20 years for a 290 Sv overturning cell). There was a rapid loss of heat from the deep ocean and a corresponding increase in density of the deep ocean during the thermal flush (Figure 3 - 6). Once the temperature of the deep ocean had cooled to 7°C (4 to 5°C warmer than the present day North Atlantic Deep Water) the convection rapidly shut off, stopping the formation of deep water. As the formation of deep water stopped the strong meridional overturning cell collapsed.

3.5.1 The tracer fields of TF1.

The shape of the vertical temperature profile remains constant throughout TF1. North of 60°N the temperature had no vertical gradient as the water was well mixed by convection. This region of well mixed, cold water was subject to intense surface cooling. There was a strong front (at 60°N) in the temperature separating the cold, well mixed, polar waters from the warmer waters of the rest of the ocean. A small warm water core was trapped in the centre of the sub tropical gyre. Towards the end of TF1 (years 8041 to 8101) the region of cold, well mixed, water retreated northwards and westwards. As the region of cold, polar water retreated the temperature profile of the deep ocean became more stratified.

The salinity showed similar features to the temperature profile. The water north of 60°N was the freshest and the coldest water in the basin. There was a strong front in the salinity that separated the fresh polar waters from the more saline water of the rest of the ocean. This strong salinity front corresponded to the strong front in temperature. Towards the end of TF1 (years 8041 to 8101) a fresh water cap formed on the eastern boundary at 60°N and then spread northwards and westwards inhibiting deep water formation.

The density field was dominated by temperature rather than salinity. The cold polar waters were the densest in the ocean basin. This dense water was separated from the less dense waters of the rest of the ocean by a strong density front. Towards the end of TF1 (years 8041 - 8101) the density front retreated northward and westward. As the density front retreated the vertical

stratification of the ocean increased. During the 320 years of TF1 the potential density of the deep ocean increased by 1.5 kg/m^3.

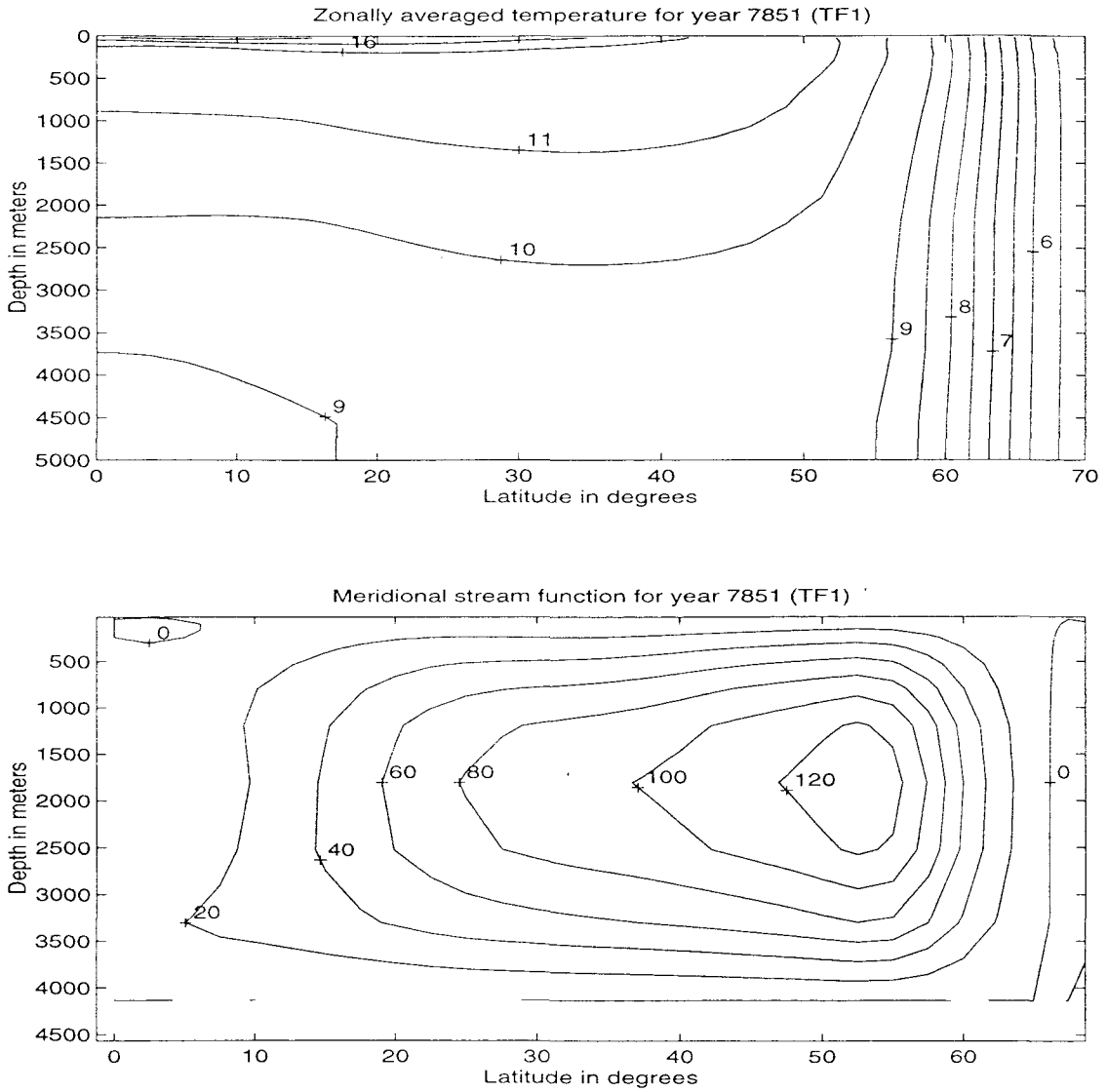

Figure 3 - 13: (a) The zonally averaged temperature profile for year 7851 (TF1) in °C. (b) The meridional stream function for year 7851 (TF1) in Sv.

3.5.2 The circulation pattern of TF1.

The surface velocity field was dominated by a strong eastward drift north of 60°N. This eastward flow completely masked the wind driven circulation of the sub polar gyre. Feeding the strong easterly current was an area of upwelling along the western boundary and a strong western boundary current flowing polewards. There was a weak recirculation in the eastern part of the sub tropical gyre and some upwelling along the equatorial boundary. The upwelling along the equatorial boundary was confined to the top 200 meters of the ocean. Along the eastern boundary, north of 60°N, was a region of strong downwelling. This region of strong downwelling was fed by the net eastward flow of the waters north of 60°N. This pattern of surface flow was repeated down to 3000 m with the magnitude of the velocities decreasing with depth. Below

3000 m the circulation was reversed. In the deep ocean the waters north of 60°N were flowing westwards from the area of downwelling (on the eastern boundary) to the area of upwelling (on the western boundary). On meeting the western boundary some of the current turned towards the equator becoming a deep western boundary current. There was a weak recirculation of the deep waters along the equatorial boundary. This mode of circulation shows up as a strong overturning cell in the meridional stream function (Figure 3 - 13). Towards the end of TF1 (years 8041 - 8101) the strength of the overturning cell decreased from 100 Sv to 3 Sv as the circulation collapsed.

3.5.3 Regions of convective activity during TF1.

The area north of 60°N, where the cold, fresh, deep water was being formed was a region of strong convection. The convection, in this region, mixed the whole water column and lasted for the majority of TF1. Towards the end of TF1 (years 8041 to 8101) the deep convection stopped, starting at the western boundary and moving eastwards. The north eastern corner of the basin was the last to stop the formation of deep water.

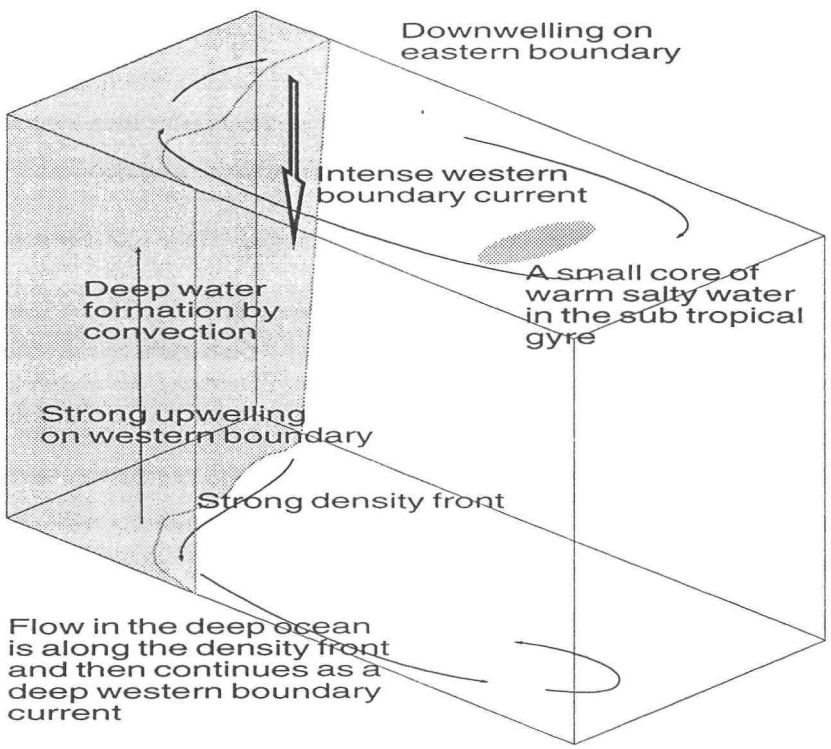

Figure 3 - 14: A summary of the circulation pattern of TF1.

The thermal flush of TF1 was probably triggered by a finite perturbation in the surface salinity of 0.1 psu. This perturbation in the surface salinity was probably formed in the area of strong

evaporation associated with the western boundary current of the sub tropical gyre. Once a volume of anomalously salty water had been created it was advected from the sub tropical gyre to the site of convection in the sub polar gyre. On reaching the region of convection the anomalously salty water was brought to the surface by the upwelling in this area. On reaching the surface the anomalously salty water was cooled. The cooling of the anomalously salty water increased the surface density sufficiently to start the convective process. The convective process was self sustaining as the convection brought the warm, saline, deep water to the surface. Once at the surface the warm, saline water was rapidly cooled, increasing the surface density. The increase in surface density reduced the vertical stratification, so sustaining the convective process. The region of convection was (on an advective time scale of 10 years) spread as it was advected around the sub polar gyre. Once the convection had started and the formation of cold, saline deep water had created a strong meridional density gradient, the meridional overturning cell characteristic of TF1 developed.

The strength of the meridional overturning shows oscillations that had a period of approximately 20 years. These oscillations were probably caused by the advection of salinity anomalies around the meridional overturning cell as in the standard salt loop oscillator (Winton and Sarachik 1993).

The circulation of TF1 was sustained by the formation of cold, dense, deep water by convection. When the deep ocean had cooled sufficiently that the vertical stratification inhibited convection the circulation collapsed. The collapse of TF1 was hastened by a halocline catastrophe (the formation of a fresh water cap at high latitudes which further inhibited the convection).

3.6 WC2 (years 8101 to 8460) and WC3 (years 8581 to 8980).

Modes WC2 and WC3 have almost exactly the same circulation and distribution of tracers. So both WC2 and WC3 are discussed in this section.

3.6.1 Similarities of WC1, WC2 and WC3.

The overall circulation pattern and distribution of tracers in WC2 and WC3 (WC2/3) were similar to that of WC1. The same as WC1 the temperature and salinity of the deep water of WC2/3 were uniform (Figure 3 - 8). WC2/3 had a weak pycnocline, at 1000 meters, through which both heat and salt diffused downwards. The surface velocity fields were dominated by the 2 wind driven gyres as were the surface velocity fields of WC1. Similar to WC1, warm, salty, water spiralled down the sub tropical gyre and then returned to the surface via the sub polar gyre . At 45°N stretching westwards from the eastern boundary was a region of convection associated with the formation of saline intermediate water. The western boundary current of the sub tropical gyre, subjected to strong evaporation, convected to a depth of 500 m. This distribution of convecting sites in WC2/3 matches that of WC1 to within a grid point.

3.6.2 Differences between WC1, WC2 and WC3.

Despite the similarities between all 3 of the weak circulation modes there were some significant differences that caused the variation in life times. The entire ocean basin of WC2/3 was more saline than that of WC1 due to a small imbalance in the surface salinity flux. However the sub surface water in the eastern part of the sub polar gyre, just prior to the thermal flush, was relatively less saline and 1 to 2 °C warmer than the corresponding water mass in WC1. These differences in the sub surface temperature and salinity fields between WC2/3 and WC1 created a difference in the sub surface density fields. This difference in the densities near the eastern boundary of the sub polar gyre weakened the vertical stratification in this region for WC2/3 compared to WC1. The reduction in the vertical stratification allowed deep convection to occur in WC2/3 when it was not possible in WC1. For all 3 weak circulation modes the deep convection that initiated the thermal flushes started in the region of weakest vertical stratification. In all cases the salinity perturbation required to overcome the vertical stratification was approximately 0.1 psu. The area that first convected for WC1 was the south western corner of the sub polar gyre, where as it was further east in both WC2 and WC3.

3.7 TF2 (years 8461 to 8580) and TF3 (years 8991 onwards).

The thermal flushes TF2 and TF3 (TF2/3) were weaker versions of TF1. The circulation patterns of TF2/3 were similar to that of TF1, with the magnitudes of the velocities reduced. TF2/3 had downwelling along the northern part of the eastern boundary and upwelling along the western boundary, as in TF1. The major difference between TF2/3 and TF1 was that the deep convection was confined to the northern boundary for the weaker flushes and so covered a smaller area than in TF1. At the onset of TF2/3 the temperature of the deep ocean was much lower than the temperature of the deep ocean just before TF1 (Figure 3 - 3). To overcome the vertical stratification and start convection the surface water had to be much cooler to allow deep convection in TF2/3 than in TF1. As the surface temperature was set by the atmospheric reference temperature (section 3.0.2) the low surface temperatures required for deep convection in TF2/3 were only possible near the northern boundary. So the deep convection could only occur close to the northern boundary for TF2/3. In TF1 where the deep ocean was warmer than that of TF2/3 the surface temperature did not need to be as cold to allow deep convection. Hence deep convection could occur further south in TF1 than was possible in TF2/3. As the convection was confined to the polar boundary for TF2/3 the formation of cold fresh, deep water was also confined to the polar boundary. This caused the strong temperature, salinity and density fronts to occur much further north in TF2/3 than in TF1. As in TF1 there was a geostrophic eastward surface current and a westward deep current in TF2/3. Though in TF2/3 these currents were confined to high latitudes where the strong meridional density gradient was.

Between years 8511 and 8561 for TF2 (The run ends before the corresponding time period for TF3) there was a region of convection (to 3000 m) along the eastern boundary. This region of

convection was not associated with a strong surface heat flux. Thus this convective activity had little effect on the tracer or velocity fields.

As for TF1, TF2 collapsed when the action of the convection had cooled the deep ocean to the point where the surface cooling could no longer overcome the vertical stratification. This reduced the rate deep water formation and so the meridional overturning cell collapsed. As the meridional overturning collapsed a freshwater cap formed at high latitudes. The formation of the fresh water cap further inhibited the convection, hastening the collapse of the overturning cell.

3.8 Comparison with other OGCM results.

The tracer distributions and meridional stream function of the thermal and haline dominated modes are very similar to those of Winton and Sarachik (1992), Marotzke (1990). The major difference between these results and the results from other OGCMs is the longevity of the initial haline mode. This longevity of the initial weak circulation leads to an exceptionally strong (250 Sv) meridional overturning cell in comparison to those observed in other OGCMs undergoing thermal flushes (Winton and Sarachik 1992). The DDOs in this set of OGCM resutls are similar in character to those of Winton (1995), however the 600 year period is towards the upper bounds of the DDO periods seen in the literature.

Chapter IV

Constructing a box model of the thermohaline circulation

4.0 Why use a box model?

The aim of this study was to produce a simple model of the thermohaline circulation that included the essential physical processes that control the ocean climate. In order for a comprehensive parameter study to be feasible the simple model had to be computationally efficient. Thus in constructing the model there was a balance between the simplicity required to make the model computationally efficient and the natural complexity of the mechanisms controlling the thermohaline circulation. A box model was chosen because:

- The box model could explicitly resolve the advective, diffusive and convective heat and salt transports. This allowed for each mechanism to be parameterised separately;
- A box model represents the state of the ocean by a set of variables that are directly related to quantities calculable from the OGCM. This was necessary so that the 2 models could be compared quantitatively;
- A box model was capable of exhibiting the modes of thermohaline circulation seen in the OGCM (i.e. DDOs, salt loop oscillations, thermal and haline dominated modes);
- The box model could represent the major water masses observed in the OGCM data (i.e. decoupled deep water in the haline mode and the dense convecting water in the thermal mode).

It was hoped that by quantitatively comparing the results of a box model to those of an OGCM the reliability of box model results could be determined. The results from box models with domains larger than a single hemisphere, single ocean basin are mainly combinations of the smaller domain box model results (chapter II). By determining the validity of a single hemisphere, single ocean basin box model an indication of the accuracy of larger domain box models may be obtained.

4.1 Constructing a box model.

The results from the OGCM in chapter III and the box models discussed in chapter II suggested that a 2×2 box model would reproduce the modes and oscillations of the thermohaline circulation seen in the OGCM. As convection was a controlling process of the thermohaline circulation it had to be parameterised explicitly in the box model, which was possible in a 2×2 model. As convection was explicitly parameterised in the box model the sensitivity of the thermohaline circulation to the form of the convection scheme could be examined. With the inclusion of diffusion in the 2×2 box model the model could represent the vertical and horizontal gradients in temperature and salinity seen in the OGCM. The OGCM results presented in chapter III were

used to guide the choice of boxes and to obtain the parameterisations used in the box model. Since the OGCM showed both the SA and TH modes with varying strengths of overturning cell the OGCM results provided a suitable set of test data for the box model without a bias towards either mode of circulation.

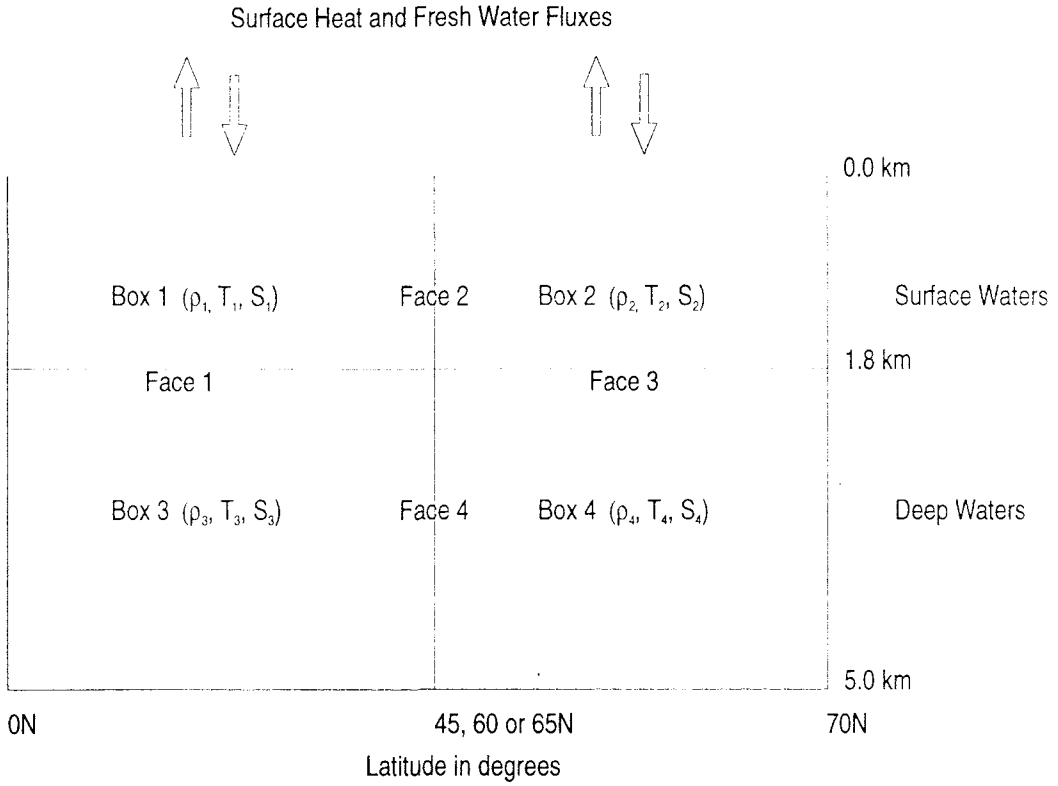

Figure 4 - 1: The layout of the boxes used in the 2×2 box model and their relation to the dimensions of the ocean basin used in the OGCM.

4.1.1 Dimensions of the box model.

The OGCM results suggested splitting the basin horizontally at a depth of 1800 meters. This level was approximately the centre of the overturning cell in the TH mode and was the maximum depth of convection in the SA mode. By splitting the basin at 1800 meters the box model distinguished between the deep waters and surface waters but could not resolve the warm saline intermediate water formed in the SA mode. There were 3 possibilities for the placement of the meridional split.

I. A vertical split at 45°N that would divide the basin between the subpolar and subtropical gyres. This would minimise the exchange between the surface boxes due to the surface wind forcing ensuring that the circulation in the box model was mainly the thermohaline circulation;

II. Splitting the basin at 60°N ensured that in the strongly convecting TH mode the region of deep water formation was completely contained in the polar boxes;

III. By placing the vertical split at 65°N the entire polar box underwent convection during the TH modes irrespective of the strength of the overturning.

4.1.2 The method for obtaining the parameterisations from the OGCM data.

The OGCM data was used to guide the parameterisations of the heat and salt fluxes used in the box model. To obtain the parameterisations the OGCM data was binned into the regions that correspond to the 4 boxes in the box model (Figure 4 - 1). The mean temperature and salinity was calculated for each region along with the heat and salt fluxes into each region. Heat and salt fluxes due to advection, diffusion, convection and the surface boundary conditions were calculated separately. Parameterisations of the heat and salt fluxes for each mechanism were found in terms of the mean temperatures and salinities. Since the box model represented the state of the ocean by the mean temperatures and salinities of the 4 boxes these parameterisations could be used to give the heat and salt fluxes between the boxes. This allowed the box model to be time marched forward with its time evolution being that of the OGCM (given the correct initial conditions) to an accuracy determined by the reliability of the parameterisations.

The parameterisations attempt to capture the averaged effect of these perturbations on the large scale evolution of the ocean. This stochastic approach is only valid if the averaging takes place over a suitably large number of perturbations and that a single small scale event can not dramatically change the mean state of the ocean.

The rest of this chapter discusses the choices made in parameterising the heat and salt fluxes for use in the box model. An estimate of the errors in each of the fluxes was derived through comparing the parameterisation with the OGCM data.

4.2 Advection.

The parameterisation of the heat and salt fluxes due to advection was done in 2 stages. First the flux across a given face was related to the temperatures (or salinities) of the adjoining boxes given the volume flux of water between the 2 boxes. Second the volume flux of water between the boxes is parameterised in terms of the dynamic variables in the box model. As the face between 2 boxes do not completely dissect the ocean basin the heat and salt fluxes across a given face have an associated mass flux.

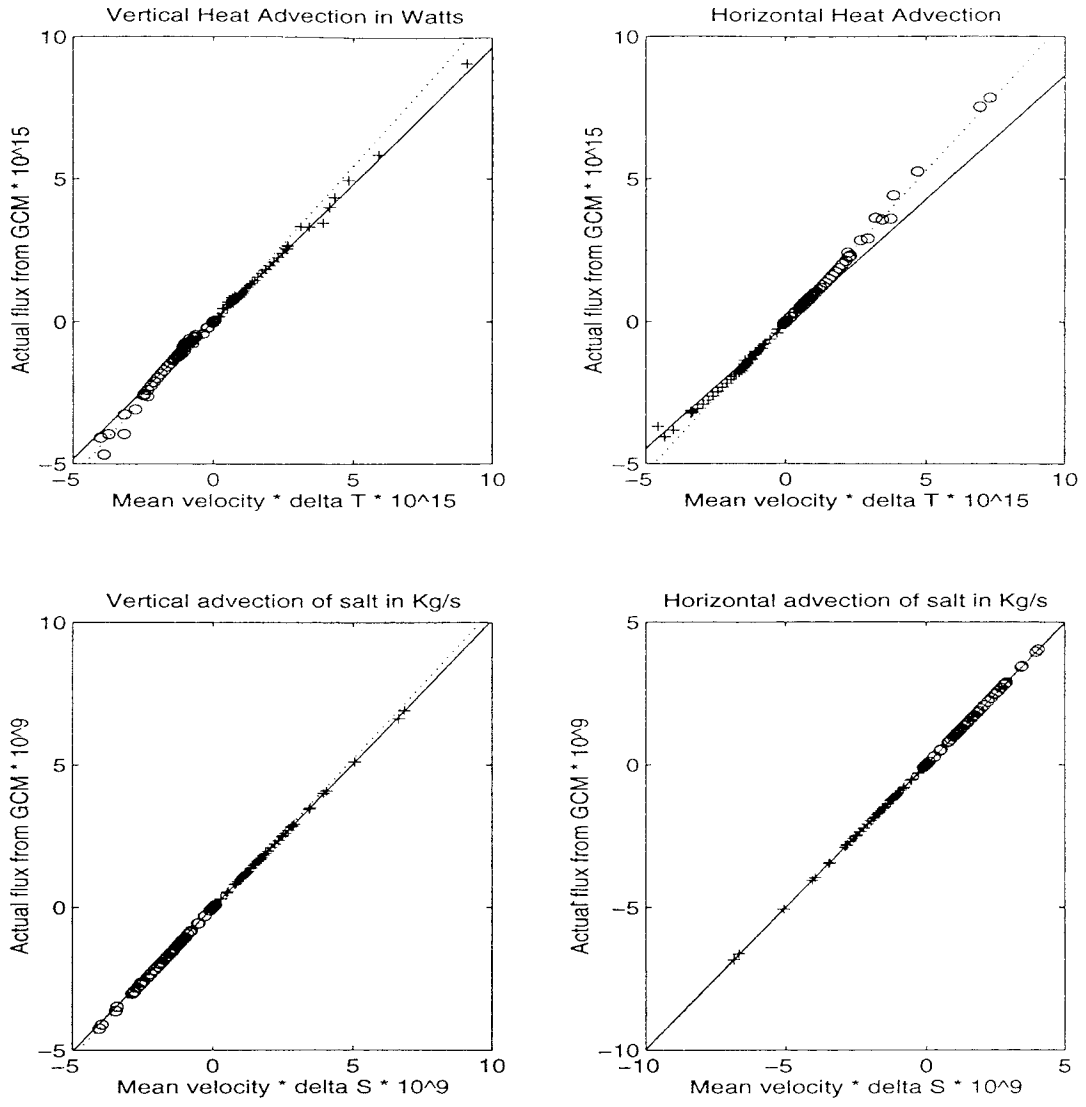

Figure 4 - 2: The correlation between the advective fluxes in the OGCM and $\bar{v}.\bar{T}$. For the vertical fluxes the crosses and solid line indicate data for the 2 polar boxes while the circles and dotted line are for the 2 tropical boxes. For the horizontal fluxes the crosses and solid line give the data for the 2 surface boxes while the circles and the dotted line are for the 2 deep boxes. The x-axes have been scaled by $c_p\rho_0$ for temperature and ρ_0/1000 for salinity. Hence a perfect fit would have a gradient of 1. In all cases the lines are the lines of best fit calculated using a least squares method.

Results from the OGCM showed that the advective fluxes could be predicted using the mean velocity across the face and a centred scheme for the temperatures and salinities of the 2 boxes (Equation 4 - 1 and Figure 4 - 2):

$$Advective\ flux \propto area_{ab} \times v \times \left(\frac{T_a + T_b}{2} \right) \qquad \textbf{Equation 4 - 1}$$

Where v was the mean velocity across the face with area A_{ab} and T_a and T_b were the temperatures or salinities either side of the face. The constant of proportionality was $c_p \times \rho_0$ for temperature and $\rho_0/1000$ for salinity.

The relationship given in Equation 4 - 1 held equally well for all 3 choices of meridional split.

4.2.1 Parameterisation of the strength of the meridional overturning cell.

To employ Equation 4 - 1 in the box model the mean velocity across the face (v) needed to be parameterised in terms of the variables in the box model. From continuity the volume flux was constant across each of the 4 faces in the box model and was a measure of the strength of the thermohaline overturning cell in the box model. To keep the box model simple it was assumed that the relationship between the strength of the overturning cell and the temperature and salinities of the boxes could be modelled using a Taylor expansion to first order (Equation 4 - 2):

$$Q = \sum_{i=1}^{i=4} a_i T_i + \sum_{i=1}^{i=4} b_i S_i + c \qquad \textbf{Equation 4 - 2}$$

Where Q was the volume flux of the overturning cell, a, b and c are parameters to be determined, T and S were the temperatures and salinities of the boxes.

The parameters *a*, *b* and *c* were determined by minimising the least squares error function between the *Q* calculated from Equation 4 - 2 and the actual values from the OGCM using a simplex search method. The best fit was obtained when the values of the parameters were such that the right hand side of Equation 4 - 2 corresponded to calculating the deep water pressure gradient using a linear equation of state. This result supports that of Hughes and Weaver (1994), who found a linear relationship between the North Atlantic overturning and the meridional gradient of the depth-integrated steric height. Using this parameterisation in the box model made the strength of the overturning cell proportional to the deep water pressure gradient and thus dependent on the temperatures and salinities of all 4 boxes. This relationship was simplified as the deep water pressure gradient was mainly dependent on the deep water density gradient with the density gradient of the surface waters acting as a minor correction. By making this assumption the strength of the overturning cell in the box model was made proportional to the density difference between deep polar and deep equatorial boxes. Using the deep water density gradient rather than the deep water pressure gradient reduced the correlation coefficient between the calculated volume flux and the actual volume flux in the OGCM, from 0.86 to 0.8 (for the 45°N split). By accepting this small decrease in accuracy the simplicity of the box model was greatly increased making the model more tractable to analysis.

The approximation that the strength of the overturning cell was proportional to the deep water density gradients held best for the 45°N split and was less accurate for the 60°N and 65°N splits. The correlation between the parameterisation and the OGCM data was unacceptably poor for the 65°N split. The parameterisation had a maximum difference between the calculated and actual fluxes of 2×10^{15} W in the heat flux and 3×10^{9} kg/s in the salt flux. Typically the errors in the heat and salt fluxes were ≈10% though the relative errors were much larger when the advective fluxes were small.

The line of best fit for the strength of the meridional overturning cell vs. the deep water density had a small zero offset. This offset gave a positive meridional overturning cell of 3.5 Sv when the deep water density difference was zero (Figure 4 - 3).

4.2.2 The parameterisation of heat and salt fluxes due to advection.

Using Equation 4 - 1 with the parameterisation in section 4.2.1 meant that the advective fluxes in the box model were given by a centred scheme where the velocity was proportional to the difference in density between boxes 4 and 3 (Equation 4 - 3):

$$Advective\ Flux \propto \Delta\rho_{deep} \times \frac{T_i + T_j}{2} \qquad \textbf{Equation 4 - 3}$$

$$\Delta\rho_{deep} = \rho_4 - \rho_3$$

Where ρ_i was the density of box i and T_i was the temperature or salinity of box i. The constants of proportionality were chosen such that equal volume fluxes of water flowed through each of the faces of the boxes.

The main error associated with the parameterisation given in Equation 4 - 3 was due to the approximation that flow was proportional to the deep water density difference and not due to the centred scheme for the tracer. As the error was not in the centred scheme the affect applied to all 4 boxes equally and did not cause advective heat or salt transport against the tracer gradient.

4.2.3 Comparison with parameterisations used in other box models.

The parameterisation described by Equation 4 - 3 is the same as that used by Stommel (1961) and most of the other box models described in chapter II. Using this relation implies that the strength of the overturning cell is governed by a linear friction law and that a predominantly meridional flow is being driven by a meridional density gradient, contrary to geostrophy. This linear friction parameterisation is the relationship obtained if the flow is assumed to take place in a non rotating basin in the limit of infinite Prandlt number (Maas 1994). In this infinite Prandlt number limit in a non rotating frame the buoyancy torque is balanced by the torque provided by friction.

4.2.4 Physical justification for the parameterisation.

In a simplified view of the TH mode the ocean basin, excluding the western boundary, is split into 2 sections. The water within each section is assumed to be zonally uniform but the density is allowed to vary with depth. The polar section represents the cold dense water that is convecting and the other section represents the rest of the ocean. Each of the sections is subject to a surface pressure and the width of the interface is assumed to be finite. Away from the western boundary the circulation is in geostrophic balance. Using geostrophy the zonal velocity along the interface can be expressed in terms of the difference in surface pressures and the depth integral of the density difference between the 2 sections (see Appendix E - Relation between the strength of the meridional overturning cell and the deep water density gradient). By assuming that there is a depth at which the interface velocity goes to zero, as found in the OGCM, the surface pressure can be eliminated from the relationship and the strength of the zonal overturning cell is given by (Equation 4 - 4):

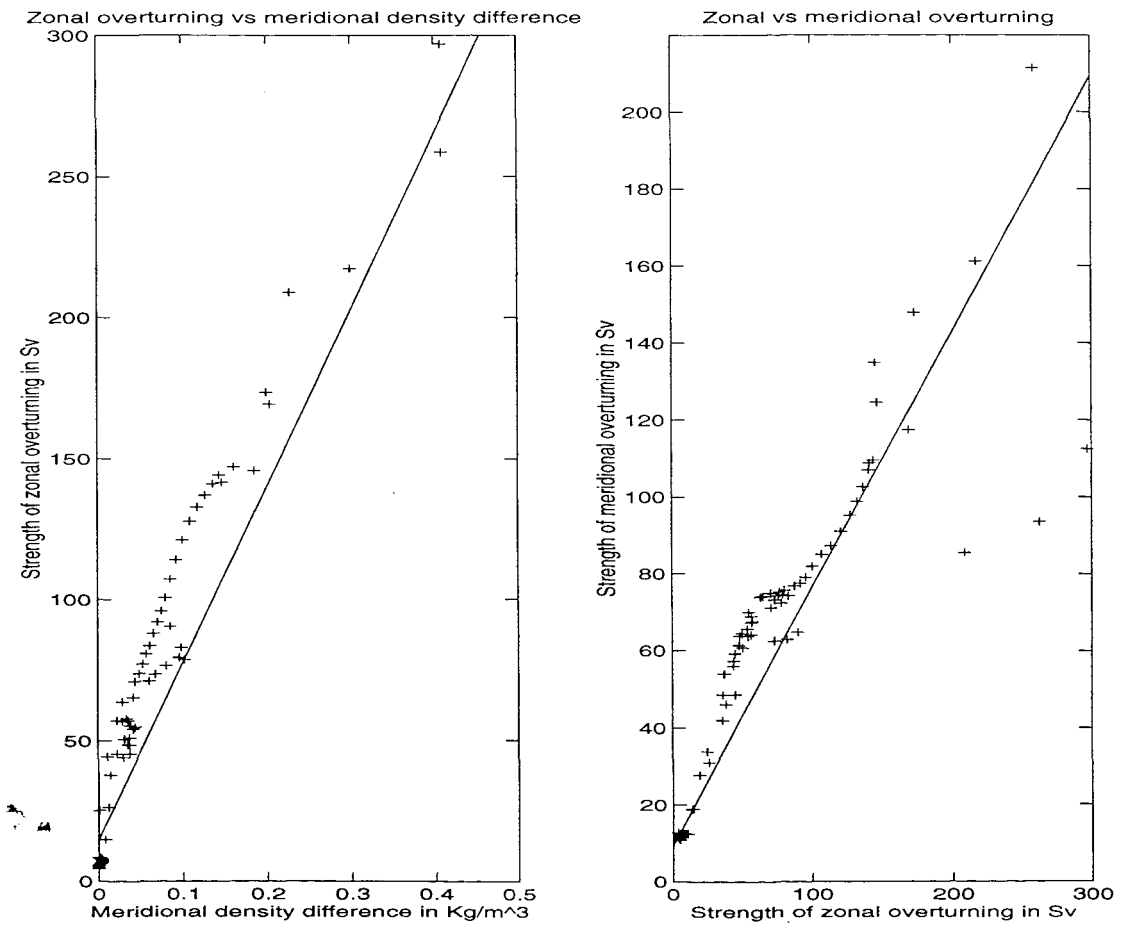

Figure 4 - 3: The correlation between the meridional density gradient and the strength of the zonal overturning and the correlation between the strength of the zonal and meridional overturning. The lines of best fit are also shown. All the data is taken from the OGCM run.

$$Q = \frac{g.\Delta\rho.D^2}{f.\rho_0}\left\{\frac{\alpha^2}{2} - \frac{\alpha}{2} - \alpha\left(\overline{S(D)} - \overline{S(\alpha D)}\right)\right\}$$ **Equation 4 - 4**

Where Q is the volume flux of the zonal overturning cell, g the acceleration due to gravity, D the depth of the ocean basin, f the Coriolis parameter, $\Delta\rho$ the density difference between the 2 sections, ρ_0 the reference density, and the function inside the brackets a correction factor dependent on the vertical density profiles (see Appendix E - Relation between the strength of the meridional overturning cell and the deep water density gradient).

As expected from geostrophy, the strength of the zonal overturning cell is proportional to the meridional density difference. The constant of proportionality is dependent on the basin dimensions and the vertical density profiles (Equation 4 - 4). This relationship was consistent with the OGCM results with the constant of proportionality equal to 0.25. The constant of proportionality represents the effects of the vertical density profiles. A value of 0.125 corresponds to the case where the density in both boxes is uniform (Figure 4 - 3).

At the western boundary the geostrophic assumption no longer holds as the non linear and friction terms become important in the momentum equations. On reaching the western boundary the deep branch of the zonal overturning cell split into 2 with the majority of the water becoming a deep western boundary current and the remainder upwelling. This deep western boundary current formed the lower half of the meridional overturning cell that was completed by the surface return flow in a western boundary current. The fraction of water from the zonal cell that entered the meridional cell via the deep western boundary current remained constant (Figure 4 - 3). The strength of the meridional overturning cell was 0.666±0.004 of the zonal overturning cell.

4.3 Diffusion.

The OGCM results showed that the heat and salt transport due to diffusion was small compared to that of advection and convection. Diffusion only played a significant role during the SA mode when the advective transports were small. The box model needed to include diffusion so that heat and salt could be transported to the deep water during the SA mode but the parameterisation did not need to be accurate during the TH mode when the error in the advective transport was a similar magnitude to the total diffusive transport.

There was no simple relationship between the diffusive fluxes of heat and salt between boxes and the temperatures and salinities of the boxes in the averaged OGCM data (Figure 4 - 4). The affects of the 2 different circulation modes could be seen in the diffusive fluxes for the OGCM (Figure 4 - 4). Differences in the relationship between the diffusive fluxes and the circulation modes were due to the small scale differences in the tracer fields between the circulations modes. The thermal diffusivities distinguished between the TH and SA modes with the diffusivity for the TH mode being smaller than the SA mode for a given temperature gradient. Each of the SA modes had a different relationship between the mean salinity gradients and the

diffusive fluxes of salt. The box model does not take the differences in diffusivity caused by changes in the mode of circulation into account.

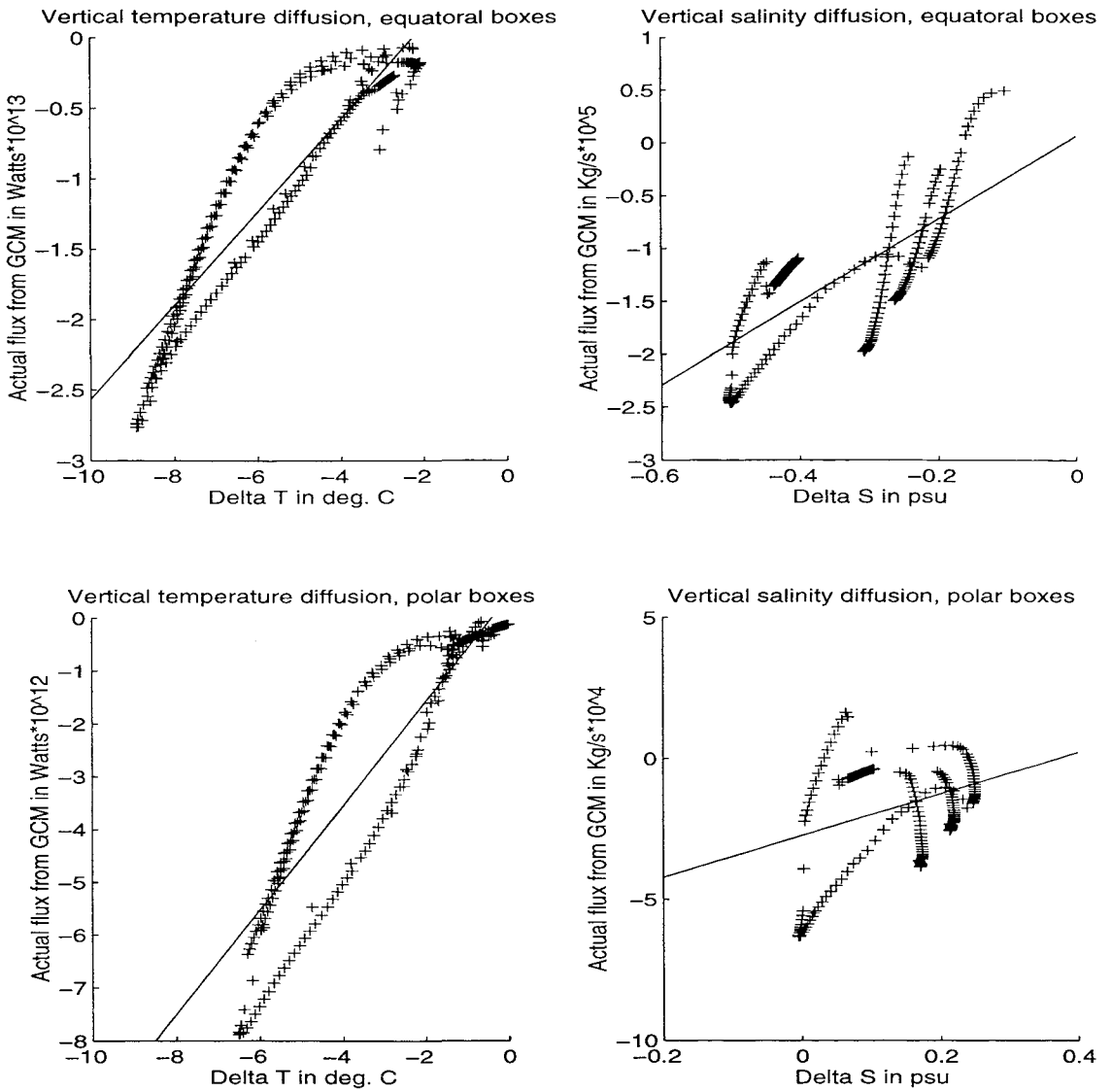

Figure 4 - 4: The relationship between the diffusive fluxes of heat and salt and the differences between the temperatures and salinities of the binned OGCM data. The lines of best fit are shown. The graphs only show the points where the diffusive flux was more than 1% of the total flux.

If only the points where the diffusive flux was more than 1% of the total flux were considered then there was a positive correlation between the difference in temperature (salinity) of 2 boxes and the diffusive heat (salt) transport between those 2 boxes. The diffusive fluxes were modelled in terms of diffusivities between the boxes (Equation 4 - 5). This gave reasonable results when the diffusive transport was significant. This parameterisation worked equally well for the 45°N, 60°N and 65°N splits.

$$Diffusive\ Flux = A_{ij}(T_i - T_j) \qquad \textbf{Equation 4 - 5}$$

for temperature:

$$A_{ij} = \frac{c_p \cdot \rho_0 \cdot D.area_{ij}}{dz_{ij}}$$

and for salinity:

$$A_{ij} = \frac{\rho_0 \cdot D.area_{ij}}{dz_{ij}.1000}$$

Where D was the diffusivity, $area_{ij}$ the area of the common face between boxes i and j, dz_{ij} the separation of boxes i and j, T_i the temperature or salinity of box i.

4.3.1 The magnitude of the diffusivities used in the box model.

The diffusivities for the box model obtained from the linear fits to the OGCM data were similar to the diffusivities used in the OGCM. The box model diffusivities were insensitive to the choice of meridional split and the diffusivities for heat and salt were similar but not equal (Table 4 - 1).

	45°N Split.	60°N Split.	65°N Split.
Vertical Diffusivities of Temperature in cm^2/s			
Equatorial Boxes	0.64	0.66	0.65
Polar Boxes	0.70	0.69	0.70
OGCM	0.50	0.50	0.50
Vertical Diffusivities of Salt in cm^2/s			
Equatorial Boxes	0.39	0.40	0.41
Polar Boxes	0.45	0.46	0.40
OGCM	0.50	0.50	0.50
Horizontal Diffusivities of Temperature in $cm^2/s \times 10^7$			
Surface Boxes	2.7	1.7	1.5
Deep Boxes	3.6	2.0	1.7
OGCM	2.0	2.0	2.0
Horizontal Diffusivities of Salt in $cm^2/s \times 10^7$			
Surface Boxes	2.6	2.7	2.5
Deep Boxes	3.8	2.6	2.3
OGCM	2.0	2.0	2.0

Table 4 - 1

The diffusivities are quoted to 2 significant figures. The errors in the diffusivities were not estimated since they were calculated using a subset of the total data. The data points used were those where the diffusive flux was greater than 1% of the total heat or salt flux.

4.4 Convection.

It was assumed that deep convection only occurs between the 2 polar boxes in the box model. This assumption excludes the possibility of forming deep water in the tropics. Formation of intermediate water occurs entirely within the surface boxes and is not explicitly resolved within the box model. The assumption worked best for the 45°N split where the heat and salt transport for the equatorial boxes due to convection was at most 2% of the total heat and salt transports. Moving the meridional split poleward increased the amount of convective mixing that occurred between the equatorial boxes. For the 60°N split convection accounted for less than 6% of the total flux and for the 65°N split the transport was less than 25% of the total heat and salt fluxes between the equatorial boxes.

The convective transport of heat and salt was a highly non linear process. In the OGCM convection was a local small scale process only taking place when a column of water became hydrostatically unstable. In the box model the convective scheme represented the large scale effect of convective mixing on the surface and deep waters and did not try to describe the local, small scale, convective chimneys. The convective fluxes between the 2 polar boxes could not be accurately modelled by a smooth polynomial function of the temperatures and salinities of the boxes. This is in keeping with the view that convection is a highly non linear process. The strength of the convective fluxes was highly correlated to the proportion of the deep polar box that was convecting (Figure 4 - 5).

Assuming that convection mixed the given proportion of the 2 polar boxes then the convective heat and salt fluxes were given by (Equation 4 - 6):

$$Q = \frac{\Gamma . h_4 . c_p . \rho_0 . Vol_2}{(h_2 + h_4).\tau} \Delta T \qquad \textbf{Equation 4 - 6}$$

Where Q was the heat flux between the 2 polar boxes, Γ the proportion of the deep box convecting, h_2 and h_4 the depths of the surface and polar boxes respectively, Vol_2 the volume of the surface box, τ a time scale and ΔT the temperature difference between the 2 polar boxes. The equation took a similar form for the salt flux in terms of the salinity difference between the 2 polar boxes.

In this parameterisation of the convective fluxes the heat and salt transports were governed by a diffusion equation where the strength of the diffusion increased as the proportion of the deep polar box that was convecting increased. The time scales in Equation 4 - 6 were free parameters that were determined using a least squares fit to the OGCM data. The least squares fits gave:

$$\tau = \begin{cases} 2.44 \pm 0.05 yrs & \text{for temperature} \\ 0.0612 \pm 0.0005 yrs & \text{for salinity} \end{cases}$$

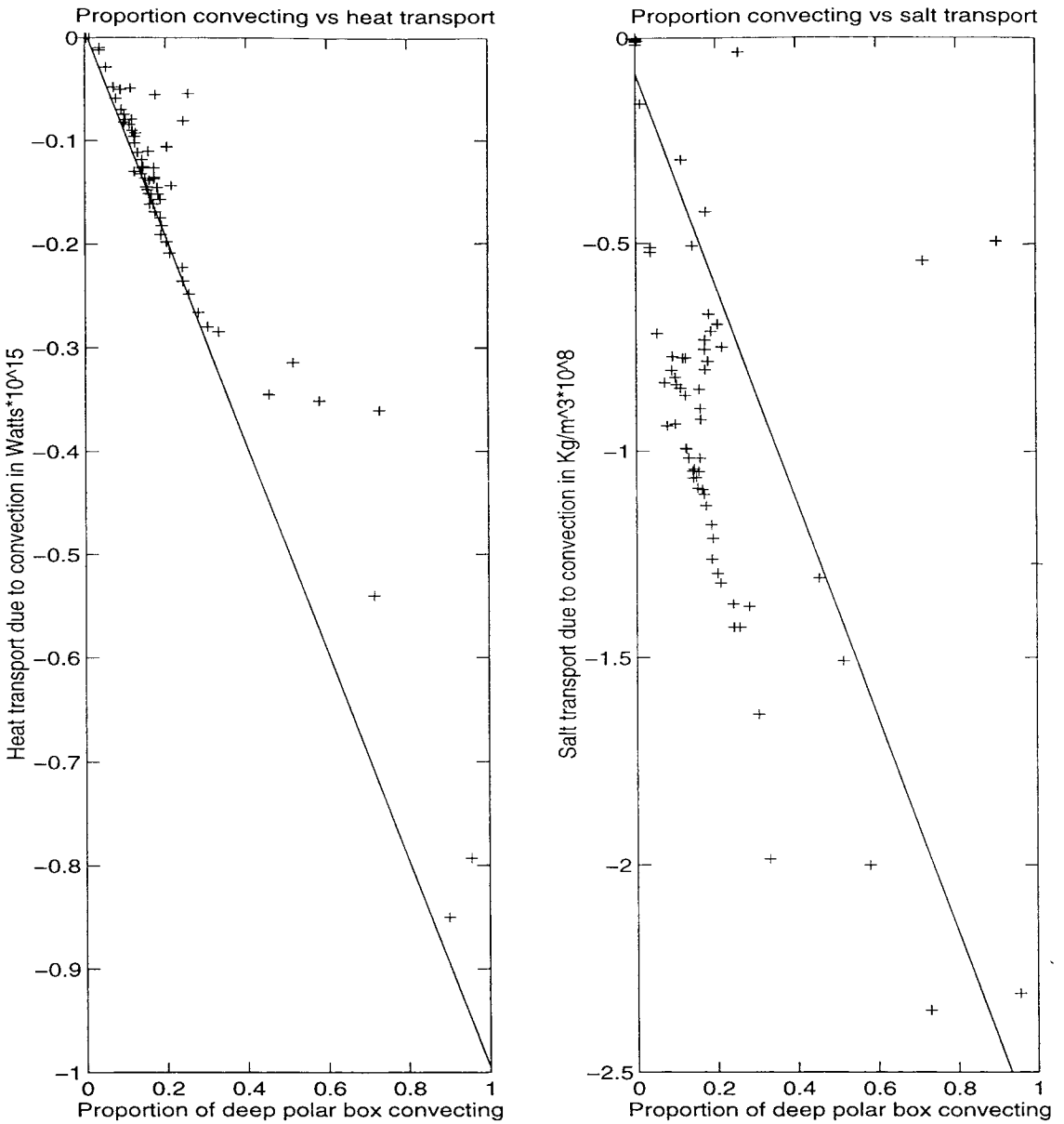

Figure 4 - 5: The correlation between the proportion of the deep polar box convecting and the vertical heat and salt transports due to convection for the binned OGCM data. Lines of best fit are indicated.

The least squares fits had correlation coefficients of 0.37 and 0.67 for the heat and salt fluxes respectively (for the 45°N split). Agreement between the parmeterisation and the OGCM data got significantly worse as the meridional split was moved poleward. The poor correlation and the large difference in the two time scales suggested that this enhanced diffusion parameterisation was an over simplification of the convective process. To improve on this enhanced diffusion parameterisation of convection the affects of convection had to be considered in conjunction with the surface boundary conditions (see section 4.6).

4.4.1 Parameterisation of the proportion of the polar boxes convecting.

To include the proportion of the deep polar box that was convecting in any convection scheme for the box model it had to be prescribed as a function of the variables in the box model. The convection scheme in the OGCM mixed a water column if the density profile was unstable. As the convection scheme in the box model represented a large scale average of the OGCM scheme the strength of the convection was dependent on the polar vertical density gradient (Figure 4 - 6).

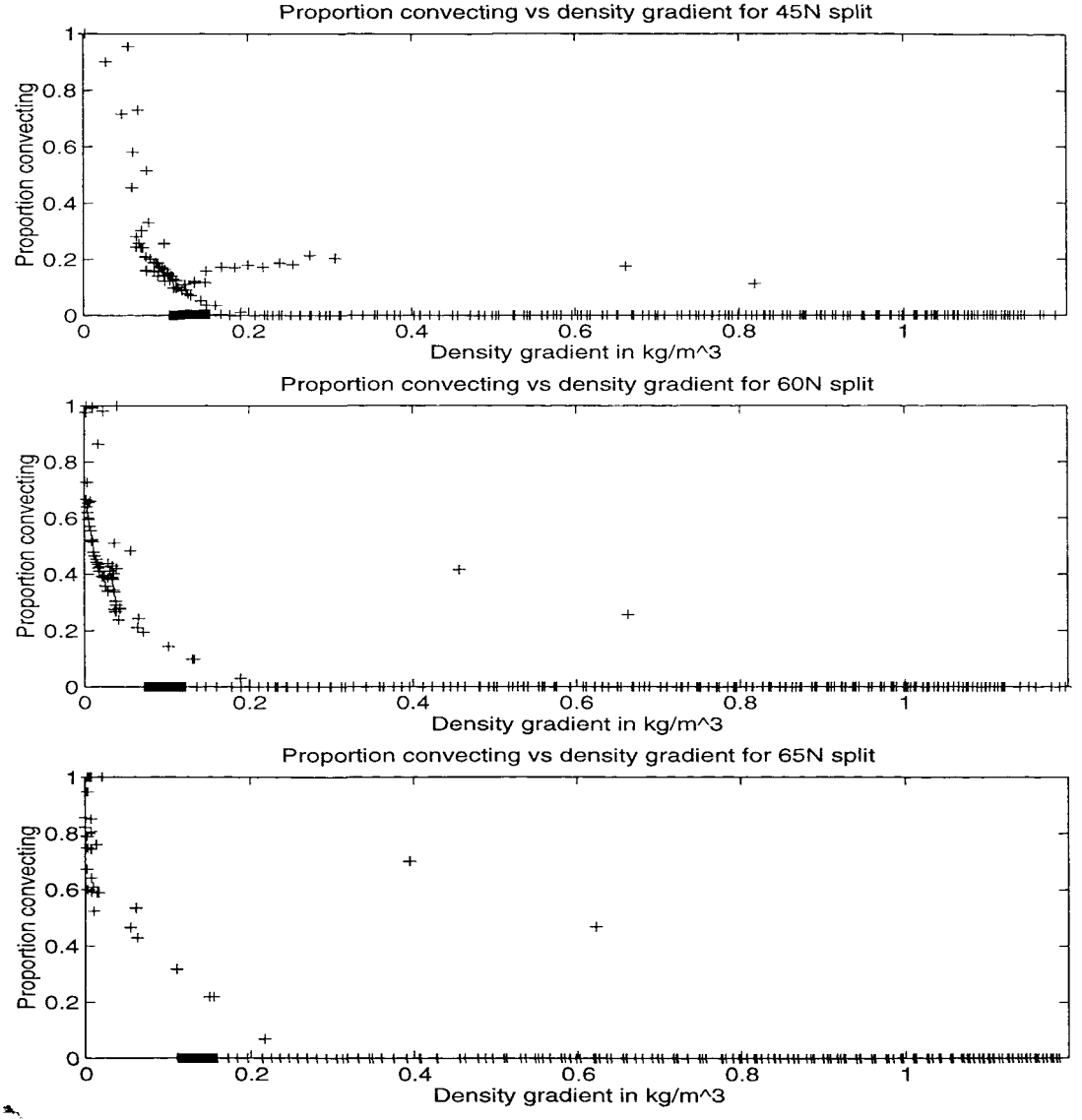

Figure 4 - 6: The proportion of the deep polar box convecting as a function of the density difference between the surface and deep polar boxes from the OGCM data. The relationship is shown for all 3 meridional splits. The density difference was defined such that a positive value indicates stable stratification.

Contrary to some of the convection schemes used in previous box models (see chapter II) the density difference did not have to be unstable for convection to occur. The relationship between the proportion convecting and the vertical density gradient in Figure 4 - 6 showed little or no

convection for large (stable) density differences. There was little change in the strength of convection until the density difference reached a critical lower limit when the proportion convecting increased rapidly as the stratification became less stable. If the polar boxes were neutraly stratified then the entire box underwent convective mixing ensuring that the system never reached an unstable state. The proportion convecting was a highly non linear function of the density difference for all 3 meridional splits and was nearest to being monotonic for the 65°N split. The relationship became less monotonic as the split moved nearer the equator. As a first approximation this relationship was modelled by a linear function below a critical density difference above which no convection occurred (Equation 4 - 7):

$$\Gamma(\Delta\rho) = \begin{cases} 0 & \text{for } \Delta\rho > \Delta\rho_c \\ 1 - \dfrac{\Delta\rho}{\Delta\rho_c} & \text{for } \Delta\rho \le \Delta\rho_c \end{cases} \qquad \textbf{Equation 4 - 7}$$

Where $\Gamma(\Delta\rho)$ was the proportion of the deep polar box convecting, $\Delta\rho$ the polar vertical density difference and $\Delta\rho_c$ the critical density difference

4.5 Surface boundary conditions.

The surface boundary conditions for salinity translated directly from those used in the OGCM. The salt flux into both of the surface boxes in the box model was equal to the total salt flux over the corresponding surface area in the OGCM. Using this formulation ensured that the total salt content of the box model was conserved to the same accuracy as the total salt content of the OGCM.

4.5.1 Surface heat fluxes.

The surface heat flux into the equatorial box could be modelled using a Haney (1971) boundary condition for the TH and SA modes separately (Figure 4 - 7):

The Haney boundary condition provided a reasonable fit to the TH mode data for all 3 meridional splits with the agreement improving as the equatorial box was made larger. In the SA mode the surface heat fluxes were accurately parameterised by the Haney condition for high temperatures but the strength of the surface warming was under estimated for low sea surface temperatures. The relaxation times and effective atmospheric temperatures obtained from these fits to the binned OGCM data were dependent on both the mode of circulation and the choice of meridional split (Table 4 - 2). For the 45°N meridional split the difference between the parameters for the TH and SA modes was least pronounced and the surface heat flux could be reasonably modelled using a Haney condition with a time constant of 208±2 years and an atmospheric temperature of 19.9±0.2 °C for both modes. The large differences between the relaxation times for the box model and the OGCM are discussed in sections 4.5.2 and 4.6.

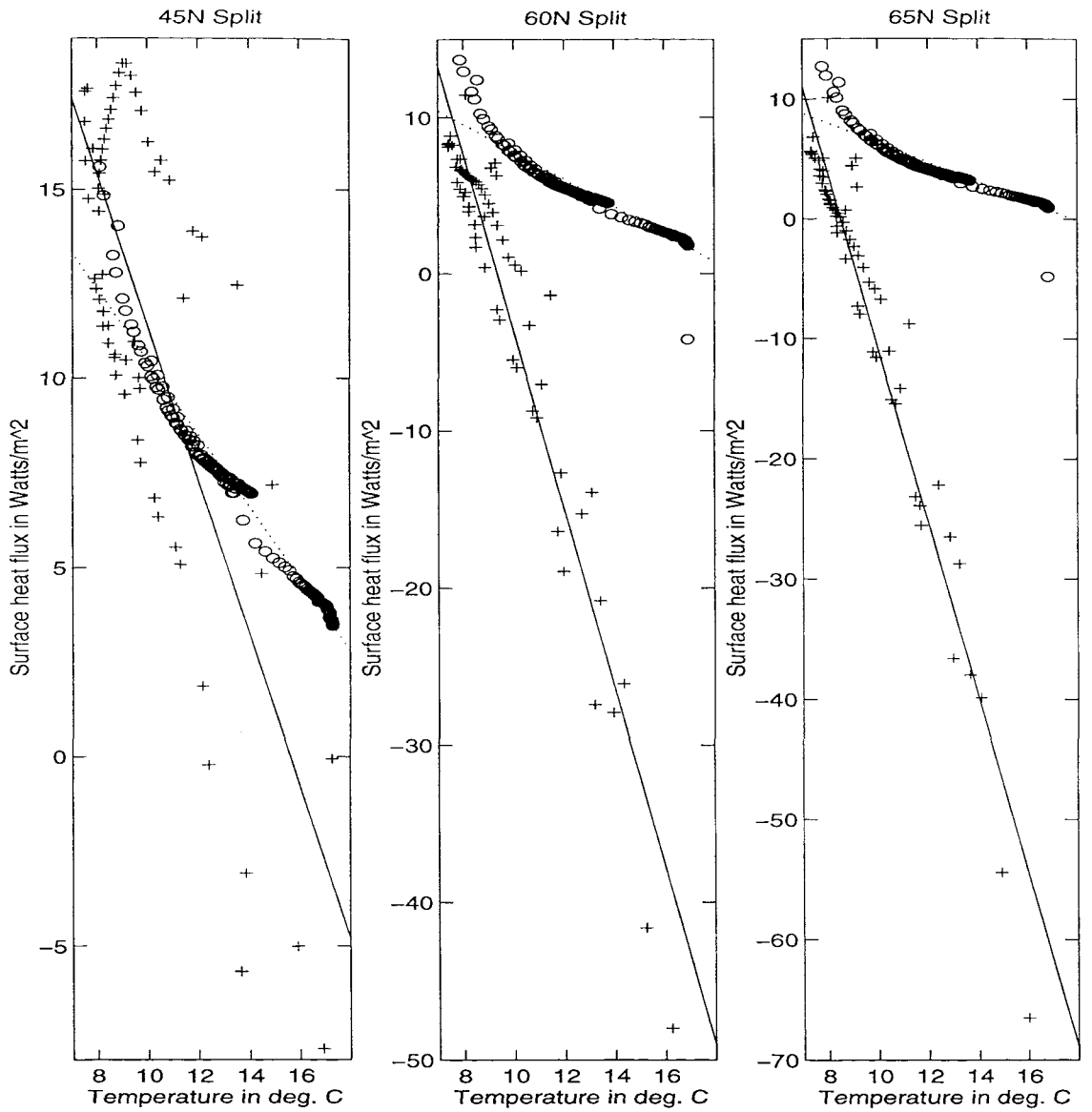

Figure 4 - 7: The surface heat flux for the surface of the OGCM region corresponding to box 1 of the 2×2 box model as a function of the temperature of the binned OGCM data for box 1. The crosses and solid line represent data from the TH modes and the circles and dotted line data from the SA modes.

Circulation mode	Effective atmospheric temperature in °C	Relaxation time in years
45°N meridional split		
TH mode	19.5 ± 0.6	188 ± 3
SA mode	21.0 ± 0.3	247 ± 3
60°N meridional split		
TH mode	9.3 ± 0.3	42 ± 2
SA mode	18.9 ± 0.2	280 ± 2
65°N meridional split		
TH mode	8.5 ± 0.3	32 ± 1
SA mode	17.8 ± 0.2	307 ± 3

Table 4 - 2: The effective atmospheric temperatures and time scales for the parameterisation of the surface heat flux into the sub tropical surface box (box 1).

Where the errors were estimated from the errors in the least squares fit to the binned OGCM data.

4.5.2 The strength of the coupling between the sea surface temperature and the surface heat flux.

The differences in the parameters between the TH and SA modes can be explained by the different couplings between the sea surface temperature and the mean temperature of box 1 in each mode. In the OGCM the surface heat flux was given by a Haney condition for each surface grid cell. The surface heat flux into the volume of water in the OGCM, corresponding box 1 of the box model, was the sum of the individual surface heat fluxes. Thus summing the heat flux over the surface of box 1 and relating this to the temperature change of box 1 gives (Equation 4 - 8):

$$\frac{dT_B}{dt} = \frac{\alpha z_G}{z_B}\left(\overline{T_G^*} - \overline{T_G}\right)$$ **Equation 4 - 8**

where

$$\overline{T_G^*} = \frac{\Sigma T_G^*}{area}$$

$$\overline{T_G} = \frac{\Sigma T_G}{area}$$

Where T_B is the mean temperature of the box, t is time, α the Haney coefficient used in the OGCM surface boundary condition, T^*_G and T_G the atmospheric and sea surface temperatures of the OGCM, z_B and z_G the depths of the box and surface layer of the OGCM, area the surface area of the box. The summations are taken over the surface of the box.

By assuming that $\overline{T_G}$ (the mean sea surface temperature) is linearly related to T_B (the mean temperature of the box) the surface boundary condition for box 1 becomes a Haney term with an altered relaxation time and effective atmospheric temperature (Equation 4 - 9):

Assuming that **Equation 4 - 9**

$$\overline{T_G} = m.T_B + c$$

then

$$\frac{dT_B}{dt} = \frac{\alpha.z_G.m}{z_B}\left(\frac{\overline{T_G^*} - c}{m} - T_B\right)$$

If the average sea surface temperature were equal to the mean temperature of the box then the relaxation time for box 1 would be 3 years and the effective atmospheric temperatures would be 22.9, 19.4 and 18.2 °C for the 45°N, 60°N and 65°N meridional splits respectively.

Using Equation 4 - 9 the strength of the coupling between the sea surface temperature and the surface heat flux was inferred for the TH and SA modes. The coupling between the sea surface temperature and the temperature of box 1 was strongest in the TH mode as the box was relatively well mixed by the strong overturning cell. In the SA mode the coupling was weaker as the mixing within box 1 was weaker.

4.6 Coupling the convection scheme and the surface boundary conditions

A Haney boundary condition did not provide a reasonable fit to the OGCM data for the polar surface heat flux. The surface heat flux for the surface polar box had a strong correlation to the proportion of the box convecting. This was be incorporated into the parameterisation by considering the polar boxes to be split into the convecting and non convecting regions (Figure 4 - 8).

In the OGCM a convecting column of water provided a link between the surface boundary conditions and the deep waters and acted as a channel for the formation of dense deep water without a large affect on the surface waters. By coupling the surface boundary conditions and the convection scheme in the box model this effect of bypassing the surface waters was included in the simpler model.

The polar half of the box model was broken into 3 regions (Figure 4 - 8) so that the surface heat flux into the convecting and non convecting areas (regions *a* and *b*) could be parameterised separately. By splitting the polar region this way the effects of convection on the surface heat flux can be included in the box model. This makes the formulation of the surface forcing consistent with the convection scheme that allows for a fraction of the box to under go convection while the rest of the box does not.

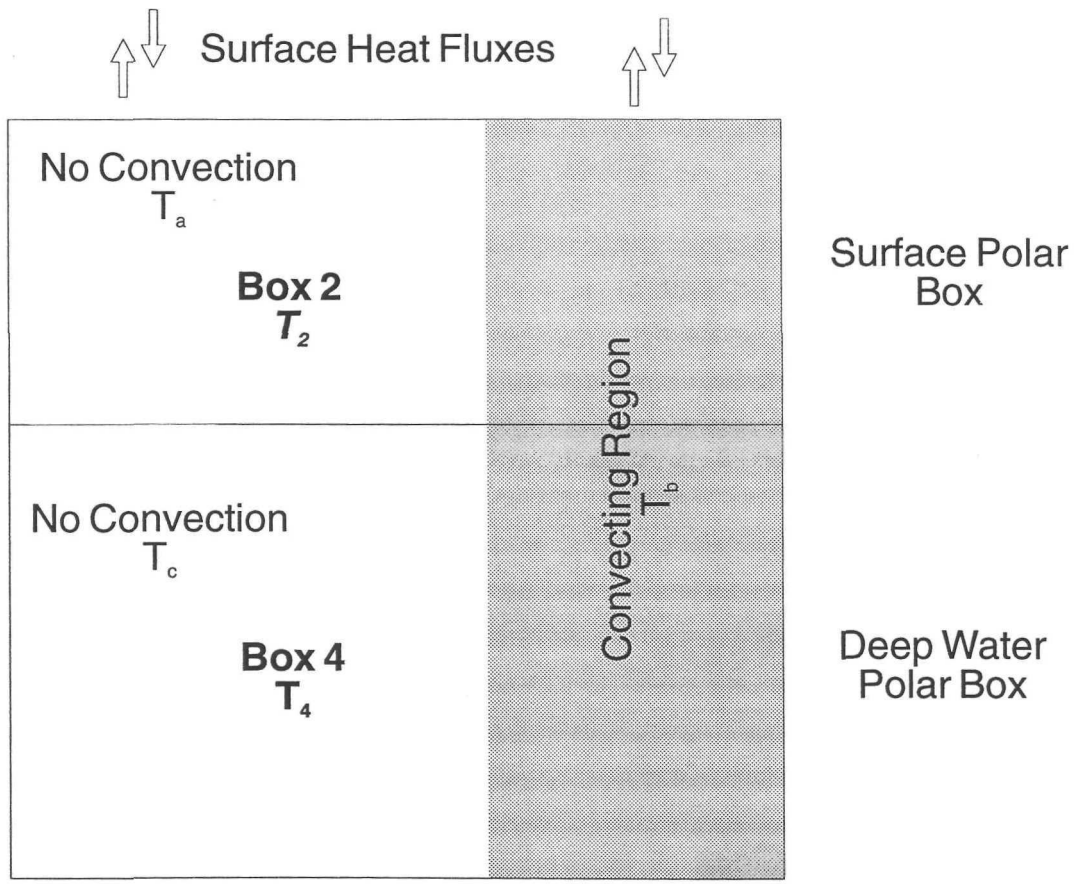

Figure 4 - 8: Splitting the polar boxes into the convecting and non convecting regions. The temperatures of boxes 2 and 4 were T_2 and T_4 respectively while T_a, T_b and T_c were the temperatures of the non convecting surface waters, convecting region and non convecting deep water.

4.6.1 The polar surface heat flux.

The surface heat flux out of the convecting region (region b) was proportional to the surface area of the region (Figure 4 - 9) and was equivalent to a heat loss of 238±2 Watts/m^2 over the entire surface of the region. Variations in the temperature of region *b* had negligible effect on the surface heat flux per unit area. This implies that when averaged over a large scale the rate at which the ocean can loose heat through convective mixing was governed by the rate that warm water could be mixed to the surface and then cooled. A possible explanation of this result is that in the OGCM the rate of heat transfer from the deep ocean to the surface by convection was limited. The maximum possible mixing due to convection (in the OGCM) was the water column being homogenised each time step. Thus the maximum heat transfer was limited by the size of the time step. As the time step was a parameter of the model this raises the question of whether this limiting of the vertical heat transport was a numerical artefact?

The non convecting surface region was subject to a surface heating that was the integral of the Haney term over the region's surface. This heat flux was parameterised using a Haney term where the effective atmospheric temperature and the relaxation time were dependent on the size of the region (Equation 4 - 10):

$$Q_a = c_p \rho_0 Vol_2 (1-\Gamma).\alpha(\Gamma).\left(T^*(\Gamma) - T_a\right) \qquad \textbf{Equation 4 - 10}$$

Where Q_a was the surface heat flux for region a, Vol_2 the volume of box 2, Γ the proportion of the box convecting, T^* the effective atmospheric temperature and T_a the temperature of region a (see below for descriptions of $\alpha(\Gamma)$ and $T(\Gamma)$).

The dependence of the heat flux on (1-Γ) was the effect of the variation of the surface area of region due to changes in the proportion of box 2 that was convecting. As the size of region *a* changed so the effective atmospheric temperature changed as the effective atmospheric temperature used in the OGCM varied with the latitude. In the OGCM the effective atmospheric temperature dropped from 12°C at 45°N to 0°C at 70°N. The relaxation time was strongly dependent on the size of the region. This was caused by the relationship between the size of region *a* and the dominant mode of circulation. In the TH mode when strong advection couples the sea surface temperature and the interior temperature there was some convective activity reducing the size of region *a*. Thus in the TH mode Γ was non zero and there was a high correlation between the sea surface temperature and the mean temperature of box *a*. This high correlation gave a short relaxation time. Conversely in the SA mode there was no convection (making Γ zero) and the relaxation time was long as there was weak correlation between the sea surface temperature and the mean temperature. The dependence of T^* and α on Γ was modelled using linear relationships (Equation 4 - 11):

$$\alpha(\Gamma) = \alpha_1(1 + \alpha_2 . \Gamma)$$
$$T^*(\Gamma) = T_1^* + T_2^* . \Gamma$$

Equation 4 - 11

The 4 unknown parameters were found using a simplex search method to minimise a least squares error function between the calculated flux and the flux in the OGCM. The fit was insensitive to the value of α_2 as long as the value was above 180. The surface of the least squares error function was flat near to the minimum point giving a range of parameters that gave equally good fits to the data. A typical set of parameters that gave a good fit to the binned OGCM data were:

$$\alpha_1 = 4.64 \pm 0.04 * 10^{-11} \text{ s}^{-1} m^{-2}$$
$$\alpha_2 = 200 \text{ no units}$$
$$T_1^* = 0°\text{C}$$
$$T_2^* = 7°\text{C}$$

These values of α_1 and α_2 correspond to a relaxation time scale of 690 years when there is no convection and 3.5 years if the entire polar region is undergoing convection. T_a is not calculated in the box model but it can be approximated using the value of T_2. This approximation worked well for all but the strongest convecting states when the heat flux into region a was small compared with the total polar surface heat flux. As the convecting region (region *b*) was in both the surface and deep boxes of the box model the relevant fraction of the surface heat flux into this region was applied to both of the boxes. This provided the direct link between the surface boundary conditions and the deep waters as in the OGCM.

The convective flux (Q_c) was parameterised by an enhanced diffusion parameterisation (as per Equation 4 - 6). Using this parameterisation was consistent with convection mixing a proportion of the 2 polar boxes. The poor correlation of the enhanced diffusion scheme and the OGCM data (section 4.4) was not relevant to the coupled convection surface boundary conditions scheme as the total convective flux into box 4 was a combination of Q_c *and* Q_b.

The total convective and surface flux into box 2 was the surface flux into region *a* plus the convective flux and a fraction of the surface flux into region *b*. The flux into box 4 was the convective flux plus a fraction of the flux into region *b* (Equation 4 - 12):

$$Q_2 = Q_c + Q_a + \frac{h_2}{h_2 + h_4} Q_b$$
$$Q_4 = -Q_c + \frac{h_4}{h_2 + h_4} Q_b$$

Equation 4 - 12

Where Q_n denoted the heat flux into region n and h_m was the depth of region m.

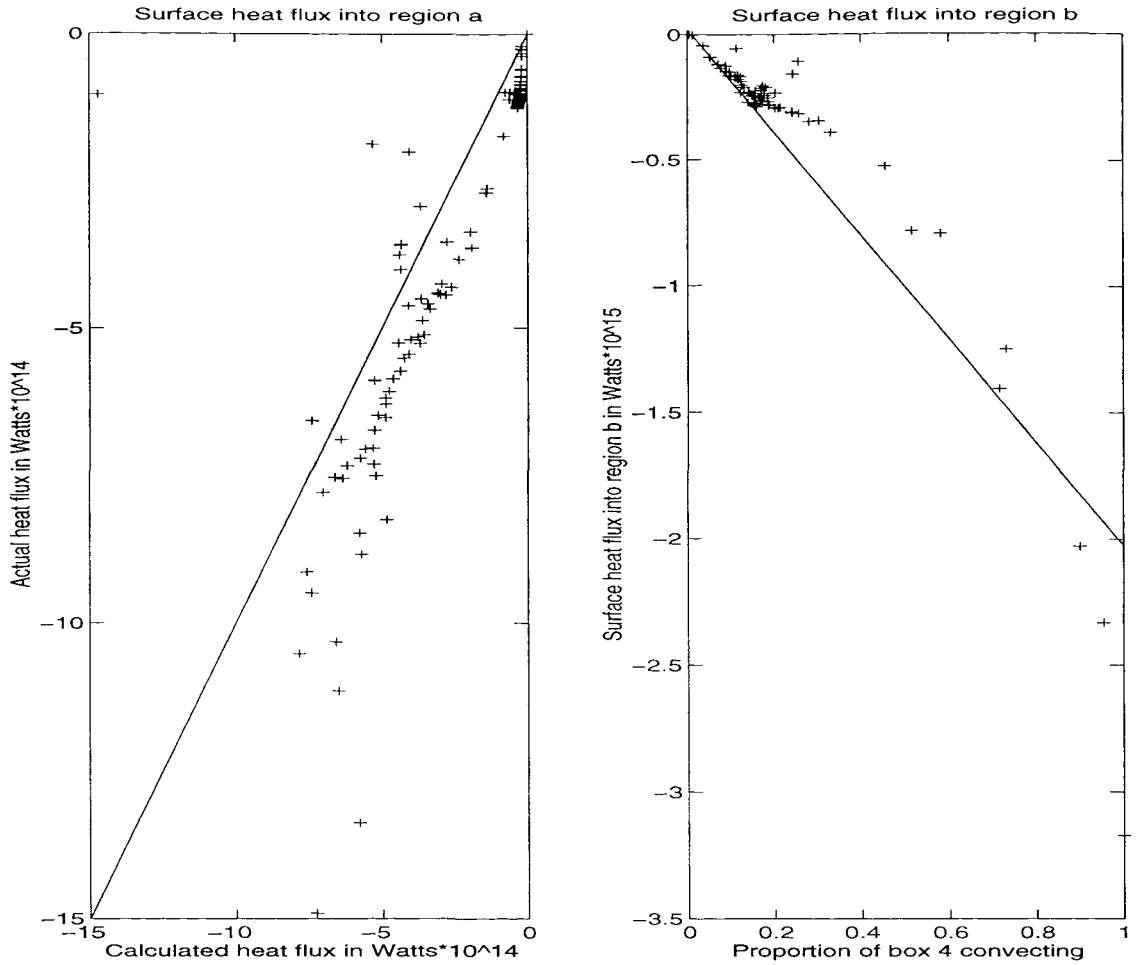

Figure 4 - 9: The calculated surface heat fluxes into regions *a* and *b* compared to the actual heat fluxes for the non convecting and convecting regions of the OGCM. The calculated heat fluxes were obtained using the parameterisations discussed in section 4.6.

Substituting the parameterisations for the surface heat fluxes (Equation 4 - 10 and Equation 4 - 11) into Equation 4 - 12 gave the heat fluxes into the polar boxes in terms of the variables in the box model. This combined convection and surface boundary conditions scheme gave a higher correlation to the OGCM heat fluxes than the combined affects of separate schemes (Figure 4 - 10). The major improvement was seen in the heat fluxes into the deep box as the combined scheme allows for the deep water to be forced to a colder temperature than the surface. This caused convection to drive the polar vertical density difference towards a hydrostatically stable state. There were still some discrepancies between the parameterisation and the OGCM data. Specifically when the temperature difference was small and negative when there was little convection. In this instance the enhanced diffusion produced a weak heat flux in the opposite direction to that seen in the OGCM.

To keep the model consistent the surface boundary conditions and convection scheme for salinity were coupled using the same assumptions as used in the coupled scheme for heat

fluxes. The surface boundary condition on salinity in the OGCM was a constant salt flux for each surface grid point. To split this salt flux between the convecting (region *b*) and non convecting (region a) regions (Figure 4 - 8) knowledge of the detailed distribution of salt flux and the shape of the 2 regions was required. To keep the box model simple the surface salt flux was assumed to be constant over the region so that the flux into a given region was proportional to its surface area. As with temperature the affect of convective mixing was modelled by an enhanced diffusion scheme with a time scale determined by a least squares fit to the OGCM data (similar to Equation 4 - 6). This gave a coupled convection and surface boundary conditions parameterisation where the salt flux into the surface box was the sum of the convective flux q_c, the surface flux into the non convecting region q_a, and part of the surface flux into the convecting region q_b. The salt flux into the deep box was the convective flux and the remainder of the surface flux into the convecting region (Equation 4 - 13):

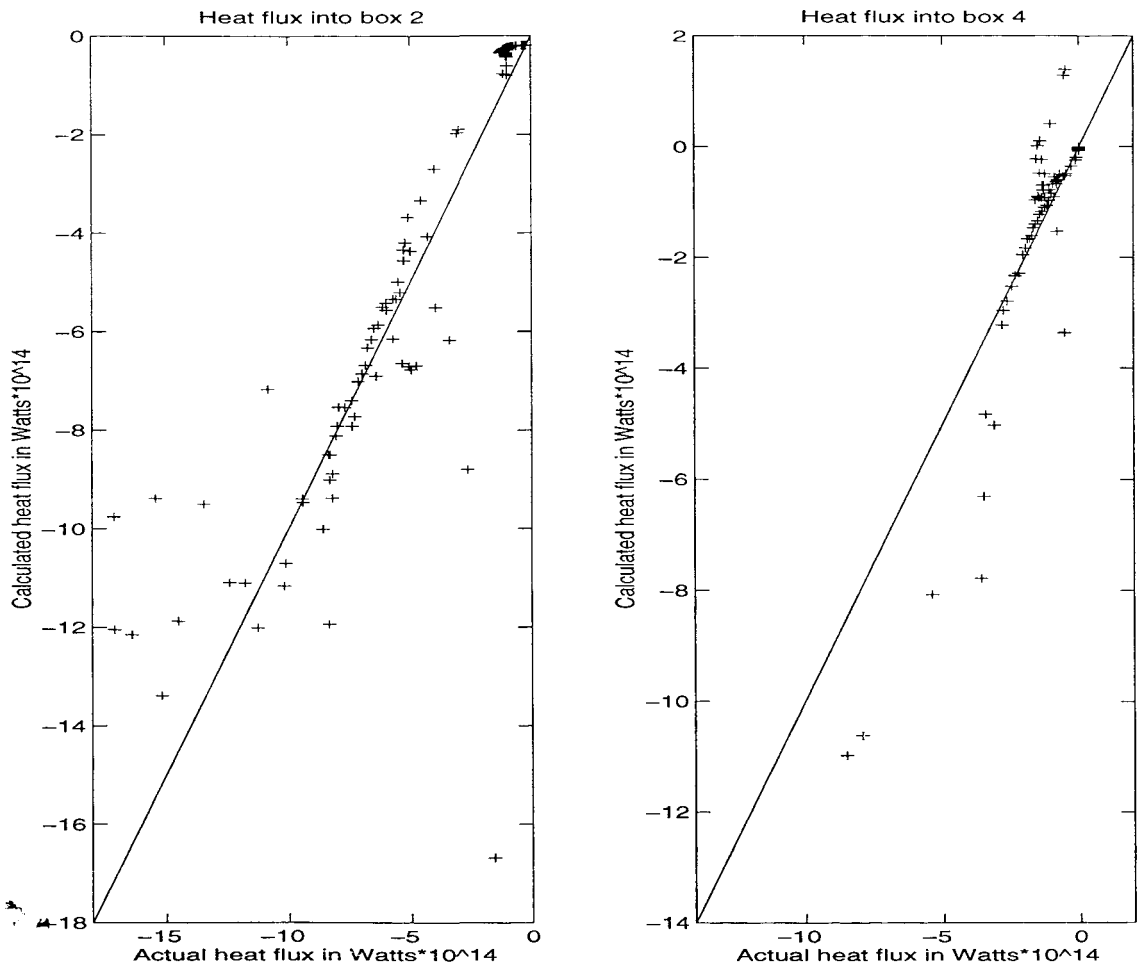

Figure 4 - 10: The correlation between the calculated heat fluxes using the combined convection and surface boundary condition parameterisation described in this section and the corresponding heat fluxes from the binned OGCM data.

$$q_2 = q_c + q_a + \frac{h_2}{h_2 + h_4} q_b$$ **Equation 4 - 13**

$$q_4 = -q_c + \frac{h_4}{h_2 + h_4} q_b$$

Where

$$q_c = \frac{\rho_0 . Vol_2 . h_2}{1000.(h_2 + h_4).t_s} \Delta S$$

$$q_a = (1 - \Gamma).q_{total}$$

$$q_b = \Gamma . q_{total}$$

Where q_n was the salt flux into region n and h_m was the depth of box m, ΔS the salinity difference between the 2 polar boxes and q_{total} the total surface salt flux into the surface of box 2.

As the convective salt flux was at least an order of magnitude bigger than the surface flux for all but the weakest of convecting states the accuracy of this parameterisation was the same as the enhanced diffusion scheme (section 4.4). The correlation between the salt fluxes predicted and the actual salt fluxes in the OGCM was 0.67 for the 45°N split. This correlation dropped rapidly as the meridional divide was moved poleward.

4.7 The implied equation of state.

The parameterisations of the meridional overturning and the strength of convection were dependent on density gradients. In the parameterisations the density gradients were calculated assuming a linear equation of state where the density of a given box was related to the box's temperature and salinity through (Equation 4 - 14):

$$\rho = \rho_0 - \alpha T + \beta S$$ **Equation 4 - 14**

Where ρ was the density of the box, ρ_0 a reference density, T and S the temperature and salinity of the box and α and β the thermal and haline expansion coefficients.

This linear equation of state under estimates the low densities and over estimates the high densities. The discrepancy between the linear equation of state and the binned OGCM data was no larger than 0.15 Kg/m^3. This discrepancy was mainly due to using the average values of temperature and salinity to infer the mean density and not the linear approximation to the non linear equation of state. If a fully non linear equation of state was used then the error in estimating the mean density of a given box from the mean temperature and salinity was the same as that for using the linear equation of state. This suggests that the extra complexity of using a non linear equation of state would not improve the accuracy of the box model.

4.8 Choice of meridional split.

The correlation between the OGCM data and the parameterisations of the advective, convective and surface fluxes were all influenced by the choice of meridional split. For all but the simplest convection scheme (where the fluxes were proportional to the strength of convection) the best agreement with the OGCM data was for the 45° split. Similarly the advection scheme increased in accuracy as the split was moved towards lower latitudes. Thus the discrepancies between the parameterisations and the OGCM results were smallest for the 45° divide. Splitting the basin here between the 2 wind driven gyres also reduced the effects of the wind driven circulation on the box model and the convective fluxes in the tropical boxes. Hence the 45° split was chosen to maximise the agreement between the variables in the box model and the corresponding quantities in the OGCM. The complete box model equations are given in chapter VI.

Chapter V

The reduced box model

5.0 Motivation for using a reduced box model.

The parameterisations developed in chapter IV lead to a box model with 8 independent variables and multiple feedback mechanisms. This full box model is examined in chapter VI. The full box model was unnecessarily complicated for examining the affects of the convection scheme. To isolate the affects of the convection scheme and reduce the complexity of the problem a reduced box model was derived. This reduced model had 4 independent variables and fewer feedback mechanisms. In constructing the reduced model some of the advective and diffusive processes present in the full model were removed and treated as parameters. By removing these feedbacks the model was made more tractable to analysis allowing a more thorough investigation of the parameter space. The insight gained from the reduced box model helped to explain the responses of the full box model to changes in parameters. The reduced model was designed to highlight the affects of the convection scheme while keeping the number of independent variables to a minimum.

5.1 The reduced box model.

The reduced model consisted of 2 polar boxes each with variable temperature and salinity. The sub tropical boxes had fixed temperatures and salinities (Figure 5 - 1). Advection and diffusion were included using the schemes derived in chapter IV, a centred scheme for advection (Equation 4 - 3) and the scheme given in Equation 4 - 5 for diffusion. The strength of the meridional overturning that drove the advective fluxes was considered to be a parameter of the problem and was not coupled to the deep water density gradient. By removing the connection between the deep water density gradient and the strength of the meridional overturning the model was greatly simplified.

The temperatures and salinities of the tropical boxes were parameters of the reduced box model. The processes affecting the polar boxes were the same in the reduced and full box models. Some of the feedback mechanisms in the full box model were removed in constructing the reduced box model. Some steady states found in the reduced box model were not possible in the full box model. The equilibrium states of the full box model were a sub set of the equilibrium states of the reduced box model. This was due to the extra feed backs in the full box model destabilising the some of the equilibrium solutions found in the reduced box model.

Two types of convection scheme were considered, an enhanced diffusion scheme and a coupled scheme (as discussed in sections 4.4 and 4.6). In the enhanced diffuison scheme convection was included by making the vertical diffusivities a function of the vertical density difference. For the coupled scheme the convection was included in the same way as the enhanced diffusion scheme but the surface fluxes were also dependent on the strength of the

convection (see chapter IV). The enhanced diffusion scheme was included in the reduced box model as a benchmark for comparison with the coupled scheme. The 2 types of convection scheme were treated separately as they required different non dimensionalisations of the model's equations. In both cases the affects of the parameters on the number and type of equilibria were examined. If no equilibria existed then the sensitivity of the time dependent behaviour of the reduced model to the parameters was investigated.

To find the equilibria of the reduced model the temperatures and salinities of the 2 boxes were calculated as functions of the strength of convection. From these temperatures and salinities an implied vertical density difference was found using the equation of state. This implied density difference was then used to obtain an implied strength of convection using one of the convection schemes. An equilibrium solution was only realised when the implied strength of convection was equal to the strength of convection used to start the calculation. This method is an extension of that used by Welander (1986). Having found the number and character of equilibria a linear stability analysis was performed (where possible) to determine the stability of each equilibrium.

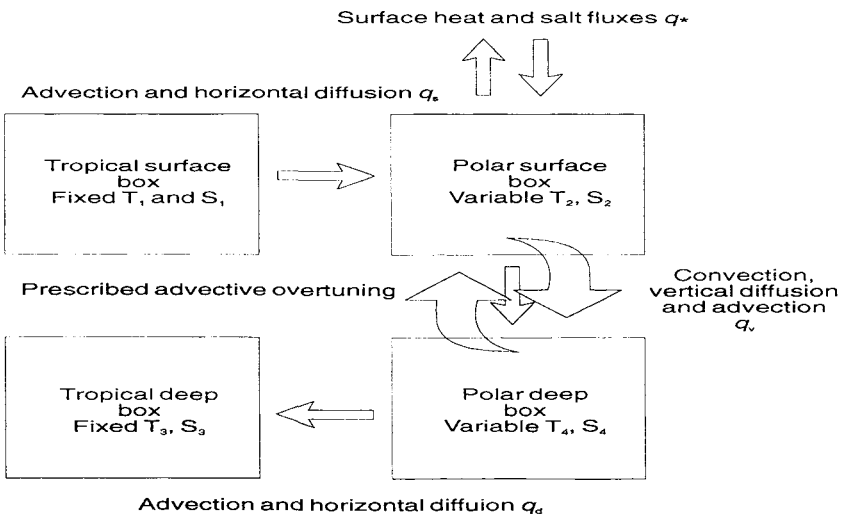

Figure 5 - 1: The layout of the reduced box model. The variables T_n and S_n were the temperature and salinity of box n, q_s was the heat or salt flux between boxes 1 and 2, q_v the heat or salt flux between boxes 2 and 4 and q_d the heat or salt flux between boxes 4 and 3.

5.1.1 The reduced box model equations.

The reduced box model had only 2 active boxes representing the polar, surface and deep waters. The basic model was derived in flux form so that the various parameterisations for convection surface boundary conditions could be implemented without changing the structure of the model. The time evolution equations for the reduced model in flux form are given in Equation 5 - 1.

The horizontal fluxes were a combination of the advective and diffusive fluxes and were independent of the choice of convection scheme and surface boundary conditions. A centred

differencing scheme was used for the advection with the volume flux being prescribed as a parameter. Heat and salt fluxes due to diffusion were proportional to the tracer gradient (Equation 4 - 9). Using these parameterisations the horizontal fluxes (q_s and q_d) are given by Equation 5 - 2:

$$\frac{dT_2}{dt} = \frac{q_s^T - q_v^T + q*^T}{x.y.h_2.c_p\,\rho_0}$$

$$\frac{dT_4}{dt} = \frac{q_v^T - q_d^T}{x.y.h_4.c_p.\rho_0}$$

$$\frac{dS_2}{dt} = \frac{q_s^S - q_v^S + q*^S}{x.y.h_2.1000\,\rho_0}$$

$$\frac{dS_4}{dt} = \frac{q_v^S - q_d^S}{x.y.h_4.1000.\rho_0}$$

Equation 5 - 1

Where T_n and S_n were the temperature and salinity of box n, t time, $q\cdot^S$ and $q\cdot^T$ are the surface salt and heat fluxes, the surface dimensions are x (east - west) and y (north - south), h_2 and h_4 the depths of boxes 2 and 4 respectively, c_p the specific heat capacity of sea water, ρ_0 the reference density and q_i^j a heat or salt flux. i was either S or T indicating a salt or heat flux and j referred to the definitions in Figure 5 - 1.

The fluxes referred to in Equation 5 - 1 are given by (Equation 5 - 2):

$$q_s^T = \left\{\frac{\kappa_s^T}{Y_0}(T_1 - T_2).x.h_2 + m.\frac{T_1 + T_2}{2}\right\}.c_p.\rho_0$$

$$q_d^T = \left\{\frac{\kappa_d^T}{Y_0}(T_4 - T_3).x.h_4 + m.\frac{T_3 + T_4}{2}\right\}.c_p.\rho_0$$

$$q_s^S = \left\{\frac{\kappa_s^S}{Y_0}(S_1 - S_2).x.h_2 + m.\frac{S_1 + S_2}{2}\right\}.\frac{\rho_0}{1000}$$

$$q_d^S = \left\{\frac{\kappa_d^S}{Y_0}(S_4 - S_3).x.h_4 + m.\frac{S_3 + S_4}{2}\right\}.\frac{\rho_0}{1000}$$

Equation 5 - 2

Where all variables were as in Equation 5 - 1 and κ denoted a diffusivity for heat or salt as indicated by the superscript. Y_0 was the meridional distance between the centre of box 1 and the centre of box 2 and m was the advective volume flux.

5.2 The enhanced diffusion convection schemes.

In the enhanced diffusion convection scheme the surface boundary conditions were independent of the strength of convection. The heat and salt fluxes due to convection were proportional to the relevant tracer gradient with the constant of proportionality (the effective diffusivity) being dependent on the vertical density gradient (Equation 4 - 10). Three different enhanced diffusion schemes were investigated. The convection schemes differed in how the effective diffusivity was related to the vertical density gradient. The schemes considered were:

I. A step scheme where the enhanced diffusivity was a Heavyside step function of the vertical density gradient. The jump in the diffusivity occurred at a finite critical density gradient (Equation 5 - 3).

$$D = \begin{cases} 0 \text{ for } \Delta\rho > \Delta\rho_c \\ D_0 \text{ for } \Delta\rho < \Delta\rho_c \end{cases} \qquad \textbf{Equation 5 - 3}$$

Where D was the enhanced diffusivity, $\Delta\rho$ the vertical density gradient (positive was stably stratified), $\Delta\rho_c$ the critical density gradient and D_0 the value of the enhanced diffusivity in the fully convecting state.

II. A piece wise linear scheme where below the critical density gradient the enhanced diffusivity increased linearly as the vertical density gradient decreased. Above the critical density gradient the enhanced diffusivity was zero, indicating no convection (Equation 5 - 4).

$$D = \begin{cases} 0 \text{ for } \Delta\rho > \Delta\rho_c \\ D_0\left(1 - \dfrac{\Delta\rho}{\Delta\rho_c}\right) \text{ for } \Delta\rho < \Delta\rho_c \end{cases} \qquad \textbf{Equation 5 - 4}$$

Where the variables were as in Equation 5 - 3.

III. A smooth scheme where the enhanced diffusivity was a smooth function of the vertical density gradient. For this study a decaying exponential function was used as it provided a reasonable fit to the OGCM data (Figure 5 - 2).

$$D = D_0 . e^{-\frac{\Delta\rho}{\Delta\rho_c}} \qquad \textbf{Equation 5 - 5}$$

Where the variables were as in Equation 5 - 3.

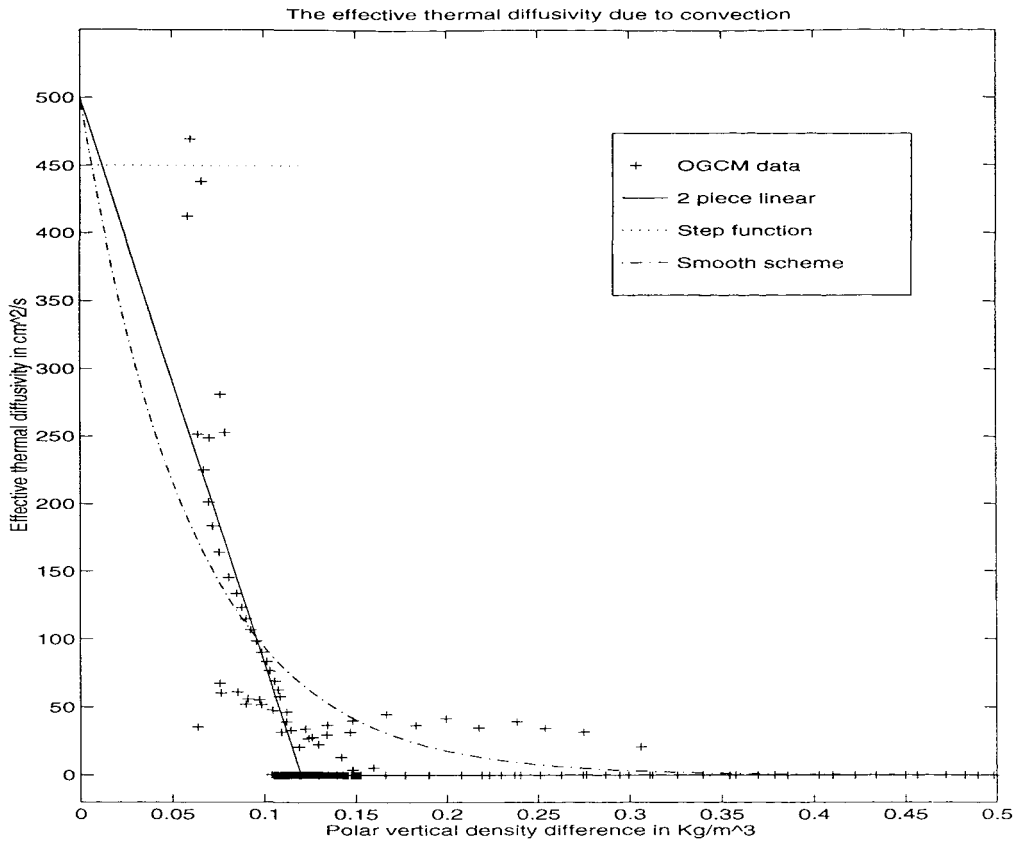

Figure 5 - 2: The enhanced diffusivity as a function of the vertical polar density difference for the 3 enhanced diffusion convection schemes (Equation 5 - 3 to Equation 5 - 5). The maximum diffusivity (D_0) and critical density difference ($\Delta\rho_c$) were chosen individually for each scheme to fit each scheme to the OGCM results.

5.2.1 Non dimensionalisation of the equations.

In non dimensionalising the equations for the reduced box model with an enhanced diffusion scheme there were 3 scales that could be chosen, a temperature, a salinity and a time scale. The reference temperature was picked as the weighted average of the effective atmospheric temperature ($\dot{T}$) and the temperature of the sub tropical surface box (T_1). A reference salinity was chosen as the weighted average of the sub tropical surface salinity (S_1) and the surface salt flux ($\dot{Q}_S$). Both averages were weighted by the time scales associated with the surface forcing (α) and horizontal diffusion (k^T_s and k^S_s scaled by the relevant length scales). To complete the non dimensionalisation a time scale was chosen such that the combination of the surface temperature forcing and horizontal diffusion of heat acting on the active surface box had a non dimensional e-folding time equal to 1. This set of scalings was chosen as it reduced the model equations to a simple form with a minimum number of free parameters. Defining a time scale τ, reference temperature T_0 and reference salinity S_0 (Equation 5 - 6):

$$\tau = \frac{1}{\frac{K_s^T}{Y_0 \cdot y} + \alpha}$$

Equation 5 - 6

$$T_0 = \frac{\frac{K_s^T . T_1}{Y_0 \cdot y} + \alpha . T^*}{\tau}$$

$$S_0 = \frac{\frac{K_s^S}{Y_0 \cdot y} . S_1 + q_*^S}{\frac{K_s^S}{Y_0 \cdot y}}$$

All variables have dimensions and are the same as in the previous equations.

The non dimensional parameters derived from these scalings are given in Table 5 - 1.

Using this non dimensionalisation the equations for the reduced box model with an enhanced diffusion convection scheme became (Equation 5 - 7):

$$\frac{dT_2}{dt} = 1 - T_2 + \left(\Gamma_0^T \Gamma + k_v^T\right)(T_4 - T_2) + m(T_1 - T_4)$$

Equation 5 - 7

$$\frac{dT_4}{dt} = \gamma\left\{k_d^T (T_3 - T_4) + \left(\Gamma_0^T \Gamma + k_v^T\right)(T_2 - T_4) + m(T_2 - T_3)\right\}$$

$$\frac{dS_2}{dt} = k_s^S (1 - S_2) + \left(\Gamma_0^S \Gamma + k_v^S\right)(S_4 - S_2) + m(S_1 - S_4)$$

$$\frac{dS_2}{dt} = \gamma\left\{k_d^S (S_3 - S_4) + \left(\Gamma_0^S \Gamma + k_v^S\right)(S_2 - S_4) + m(S_2 - S_3)\right\}$$

Where

$$\Gamma = \Gamma(\Delta\rho) = \Gamma\left(-(T_4 - T_2) + r(S_4 - S_2)\right)$$

Where all variables were non dimensional counterparts of their dimensional namesakes. The diffusivities included the appropriate spatial dimensions thus becoming time scales that were then non dimensionalised. Similarly the advective flux m was converted to a time scale and non dimensionalised. Γ^T_0 *and* Γ^S_0 *were the thermal and haline enhanced diffusivities for the convection scheme and* $\Gamma(\Delta\rho)$ *was the dependence of the convection scheme on the non dimensional vertical density difference.*

Definition of non dimensional parameter	Physical interpretation
$m' = \frac{m\tau}{2xyh_2}$	Non dimensionalised volume flux making this a measure of the strength of the meridional overturning cell.
$\gamma = \frac{h_2}{h_4}$	Ratio of the depths of the 2 boxes.
$k_s^{T'} = \frac{k_s^T \tau}{Y_0 \cdot y}$	The surface thermal diffusivity non dimensionalised in terms of the defined time scale and the meridional length scales.
$k_d^{T'} = \frac{k_d^T \tau}{\gamma Y_0 \cdot y}$	The non dimensional deep water thermal diffusivity.
$k_s^{S'} = \frac{k_s^S \tau}{Y_0 \cdot y}$	The surface haline diffusivity non dimensionalised in terms of the defined time scale and the meridional length scales.
$k_d^{S'} = \frac{k_d^S \tau}{\gamma Y_0 \cdot y}$	The non dimensional deep water haline diffusivity.
$k_v^{T'} = \frac{k_v^T \tau}{Z_0 h_2}$	A suitably scaled vertical diffusivity for temperature.
$k_v^{S'} = \frac{k_v^S \tau}{Z_0 h_2}$	The non dimensionalised vertical diffusivity of salt.
$T_n' = \frac{T_n}{T_0}$	The temperature of a given box scaled by the reference temperature.
$S_n' = \frac{S_n}{S_0}$	The salinity of a given box scaled by the reference salinity.
$\Gamma_0^{T'} = \frac{\Gamma_0^T \tau}{Z_0 h_2}$	The effective thermal diffusivity due to convection.
$\Gamma_0^{S'} = \frac{\Gamma_0^S \tau}{Z_0 h_2}$	The effective diffusivity of salt due to convection.
$r' = \frac{\beta S_0}{\alpha T_0}$	The ratio of the reference salinity and temperature. α and β are the thermal and haline expansion coefficients.

Table 5 - 1: The relationship between the dimensional and non dimensional variables. The non dimensional variables are denoted with a prime. All dimensional variables are as defined previously in this chapter unless otherwise stated.

Following a similar method to Welander (1986) the steady state values of T_2, T_4, S_2 and S_4 were found from Equation 5 - 7 as functions of $\Gamma(\Delta\rho)$. Using these values for the temperatures and salinities of the 2 polar boxes the implied vertical density difference ($\Delta\rho_{implied}$) was calculated. For a given set of parameters this gave $\Delta\rho_{implied}$ as a function of $\Gamma(\Delta\rho)$. A steady state was possible when the value of Γ imposed was equal to the strength of convection given by the convection scheme for the implied density difference ($\Gamma(\Delta\rho_{implied})$). The crossing points of these 2 curves (and so the steady states of the system) were determined numerically using a zero crossing algorithm and then refined using a modified bisection technique. The refining of the solutions was required to ensure that the density differences and strengths of convection matched to sufficient accuracy that they could be used as initial conditions for the reduced box model. The stability of the equilibria to infinitesimal perturbations was determined using linear stability analysis and checked by running the model.

The model was verified by checking the results against the analytic solutions for special cases. In particular: No overturning cell (m=0), very strong overturning cell ($m >> \Gamma$), no Convection and vertical diffusion (Γ=0, $k_v^T = k_v^S = 0$).

5.2.2 The possible equilibria of the reduced box model.

The reduced box model was found to have 2 possible equilibrium states using the step convection scheme, one with and one without convection. Using the piece wise linear convection scheme the model had 3 possible steady states, no convection, weak convection and strong convection. For the smooth convection scheme there were 3 possible steady states, very weak convection, weak convection and strong convection. The linear stability analysis showed all the states to be stable to infinitesimal perturbations though numerical experiments indicated that the weakly convecting state had a very small region of attraction. The small region of attraction made the weakly convecting state unlikely to be seen in model runs unless the initial conditions were specifically chosen to be very close to this equilibrium. The existence of these equilibria was dependent on the parameters of the model. It was possible for 1, 2 or 3 (in the piece wise linear and smooth case) equilibria to exist for a given set of parameters. At least one equilibrium state existed for any choice of parameters within a physically justifiable range.

In the reduced box model the surface forcing and horizontal diffusion were driving the surface box to a temperature and salinity of 1 (non dimensional units) and the deep box to a temperature of T_3 and a salinity of S_3. The advection tries to balance the heat and salt flow into and out of both boxes so forcing the deep box towards a temperature and salinity equal to T_1 and S_1 respectively. Similarly the advection pushed the temperature and salinity of box 2 towards that of box 3. This behaviour of the advection was caused by the use of a centred differencing scheme. The centred scheme implies that the temperature (or salinity) of the water being advected into or out of a box is equal to the mean of the temperatures (or salinities) of the 2

boxes involved. One interpretation of the centred scheme is that the temperature (or salinity) in a box is not homogenous. In the reduced box model the advection scheme was acting to match the tracer gradients into and out of both of the boxes.

Parameter	Range (non dimensional)	Physical meaning
Γ^T_0	13	Thermal enhanced diffusivity
Γ^S_0	528	Haline enhanced diffusivity
T_1	0.70 to 0.97	Temperature of box 1
T_3	0.28 to 1.32	Temperature of box 2
S_1	1.063 to 1.065	Salinity of box 1
S_3	1.030 to 1.090	Salinity of box 3
m	0 to 16	Strength of meridional overturning
k^T_d	1.61	Deep thermal horizontal diffusivity
k^S_d	1.70	Deep haline horizontal diffusivity
k^S_s	0.67	Surface haline horizontal diffusivity
k^T_v	0.018	Thermal vertical diffusivity
k^S_v	0.013	Haline vertical diffusivity
γ	0.5723	The ratio of the depth of box 2 to that of box 4
$\Delta\rho_{critical}$	0.126 to 0.195	The critical density difference
r	21.9 to 34.9	Ratio of haline to thermal density forcing for box 2.

Table 5 - 2: The parameters used in the reduced box model. The values for each parameter are calculated from the parameterisations developed in chapter IV. See table 5 - 1 for the relationship between the non dimensional (given above) and dimensional (in chapter IV) parameters.

Depending on the values of the model parameters the effects of advection and the combined effects of the horizontal diffusion and surface boundary conditions could either be acting together or in opposition. In either case the vertical density gradient was being forced towards a set value. The possible equilibria were determined by the combination of the model parameters but in general if the forced density difference was small compared to the critical density gradient then only the strongly convecting equilibrium was possible. When the forced density difference was comparable to but larger than the critical density difference all 3 steady states could be possible. When the density difference was much larger than the critical density difference only the non convecting equilibrium was possible.

In considering the affect of each parameter individually on the possible equilibria all the other parameters were held at their default values unless stated otherwise. The default values for the parameters were taken as the lower value given in Table 5 - 2. If the value of a parameter is not explicitly stated in the following discussion then it can be assumed to have the default value.

5.2.3 Response to the strength of the meridional overturning cell (*m*).

There were 4 responses depending on the strength of the advective overturning (Figure 5 - 3):

I. For negative m ($m<-2$), where the surface velocity was from pole to tropics, both the strongly convecting and no convection equilibria were possible for the step and piece wise linear schemes. The smooth convection scheme did not have a no convection state and so only the fully convecting equilibrium was possible. In this case the surface forcing and horizontal diffusion were driving the system towards warm fresh over cold salty water, while the advection was pushing the system to cold fresh over warm salty. Neither of the forcings was strong enough to dominate so the presence of convective mixing could alter the density gradient enough to make the convecting state possible. Without the additional mixing provided by convection the density difference was sufficiently high to inhibit convection.

II. When m was small ($-2<m<2$) all 3 steady states were possible for the smooth and piece wise linear schemes, both states were possible for the step scheme. The surface forcing and horizontal diffusion were driving the system to the hydrostatically stable state described in 1 but the convective mixing was sufficiently strong to dominate the density difference. As the convective mixing was competing against the other forcings to reduce the density difference there was a minimum density difference that could be achieved. Thus the maximum amount of convection was limited.

III. For medium m ($2<m<11$), only the strongly convecting equilibrium was possible for all 3 convection schemes. The advection was forcing the temperature gradient in the opposite direction to the surface boundary conditions and horizontal diffusion. This gave a weak vertical density difference thus only allowing a strongly convecting state.

IV. Strong m ($m>11$). All 3 equilibria were possible for the piece wise linear scheme and both equilibria were possible for the step convection scheme. Only the strongly convecting steady state was possible using the smooth parameterisation of convection. The advection dominated the system and was forcing the model to a state with cold fresh over warm salty water. Convective mixing of temperature was much weaker than that for salinity and the thermal convective mixing was of a similar magnitude to the advection. Thus the convection could mix away the stabilising salinity gradient without removing the temperature gradient. Hence making both the weak and strongly convecting states possible. The non convecting state was possible for the step and piece wise linear schemes as the underlying density difference was greater than the critical density difference.

Varying the other parameters in the reduced box model altered the forced density difference and the number and type of steady states accordingly.

5.2.4 Sensitivity to the temperature and salinity of the sub tropical surface box (box 1).

In the weak and medium advection cases the temperature and salinity of box 1 had a very small affect on the possible equilibria. Varying either T_1 or S_1 over the ranges in Table 5 - 2 did not change the number of, or strength of convection in, the equilibria for all 3 convection schemes.

For strong advection the state of box 1 did affect the possible equilibria, if the temperature was increased sufficiently the weak and no convection states were no longer possible. Increasing the salinity of box 1 in the strong advection case lead to the weakly convecting equilibria being possible for a lower strength of the advective overturning (for the piece wise linear scheme).

5.2.5 The affect of the temperature and salinity of the sub tropical deep box (box 3).

For weak advection the temperature and salinity of box 3 affected the possible equilibria for the piece wise linear and smooth convection schemes but not the step scheme. Increasing the temperature increased the strength of convection in the strongly convecting steady state while decreasing the strength of convection in the weakly convecting state. For the smooth scheme increasing the temperature beyond a critical limit made the non and weakly convecting states impossible to obtain. The salinity had the opposite affect in that increasing S_3 made the strength of convection decrease for the strongly convecting state and increased the strength of the weakly convecting state, for the piece wise linear scheme.

For medium and strong advection increasing the temperature of the subtropical deep water (T_3) increased the strength of convection for the weakly convecting state and decreased the strength of convection in the strongly convecting equilibria. Above a critical temperature the non convecting state became possible for all 3 convection schemes (Figure 5 - 4).

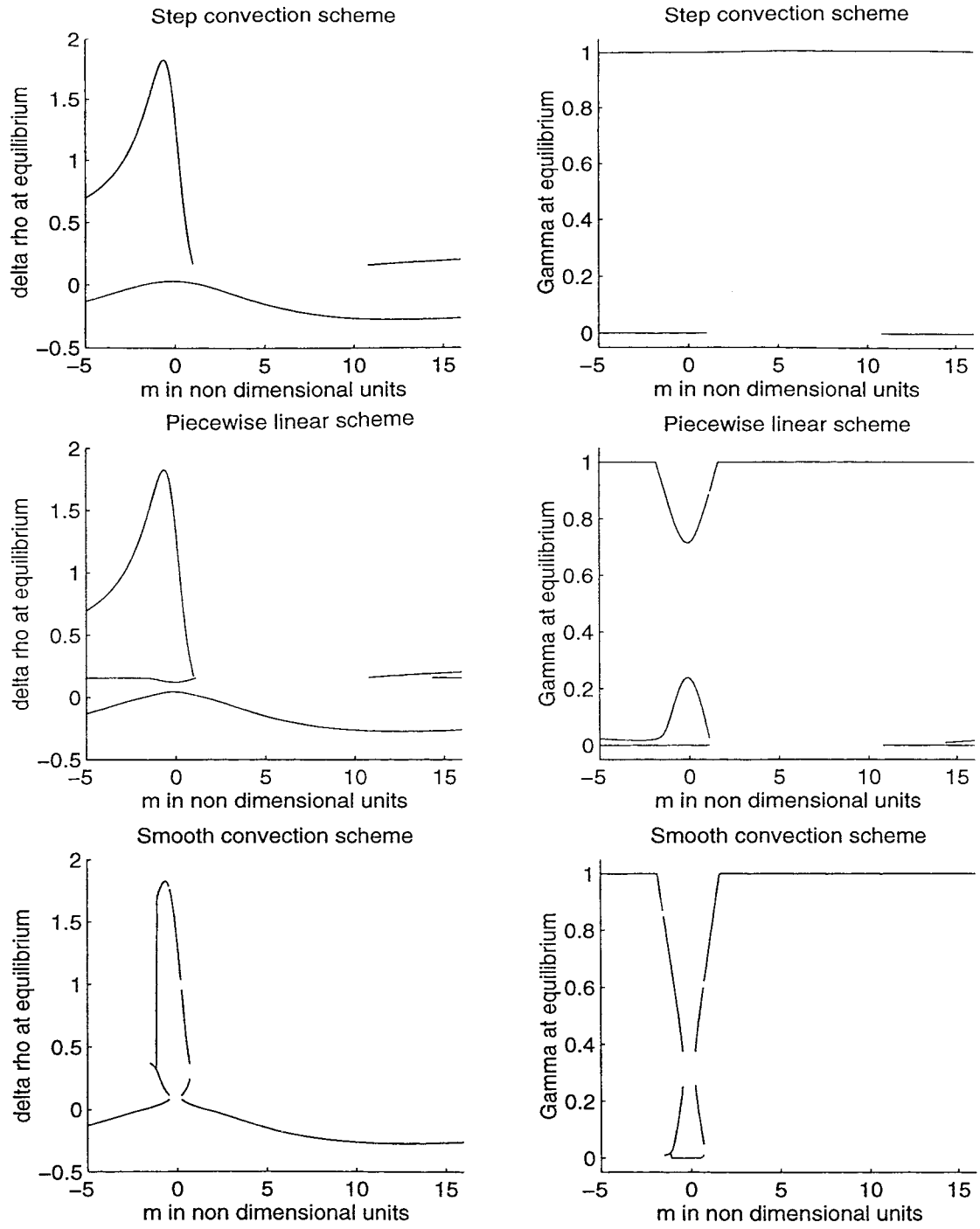

Figure 5 - 3: The vertical density difference ($\Delta\rho$) and the strength of convection ($\Gamma(\Delta\rho)$) for the equilibrium states of the reduced box model as a function of the advective volume flux (*m*). The results are shown for each of the 3 enhanced diffusion convection schemes with all other parameters held at their default values. Note that the gaps are an artefact of the numerical procedures used and not part of the real solution of the equations.

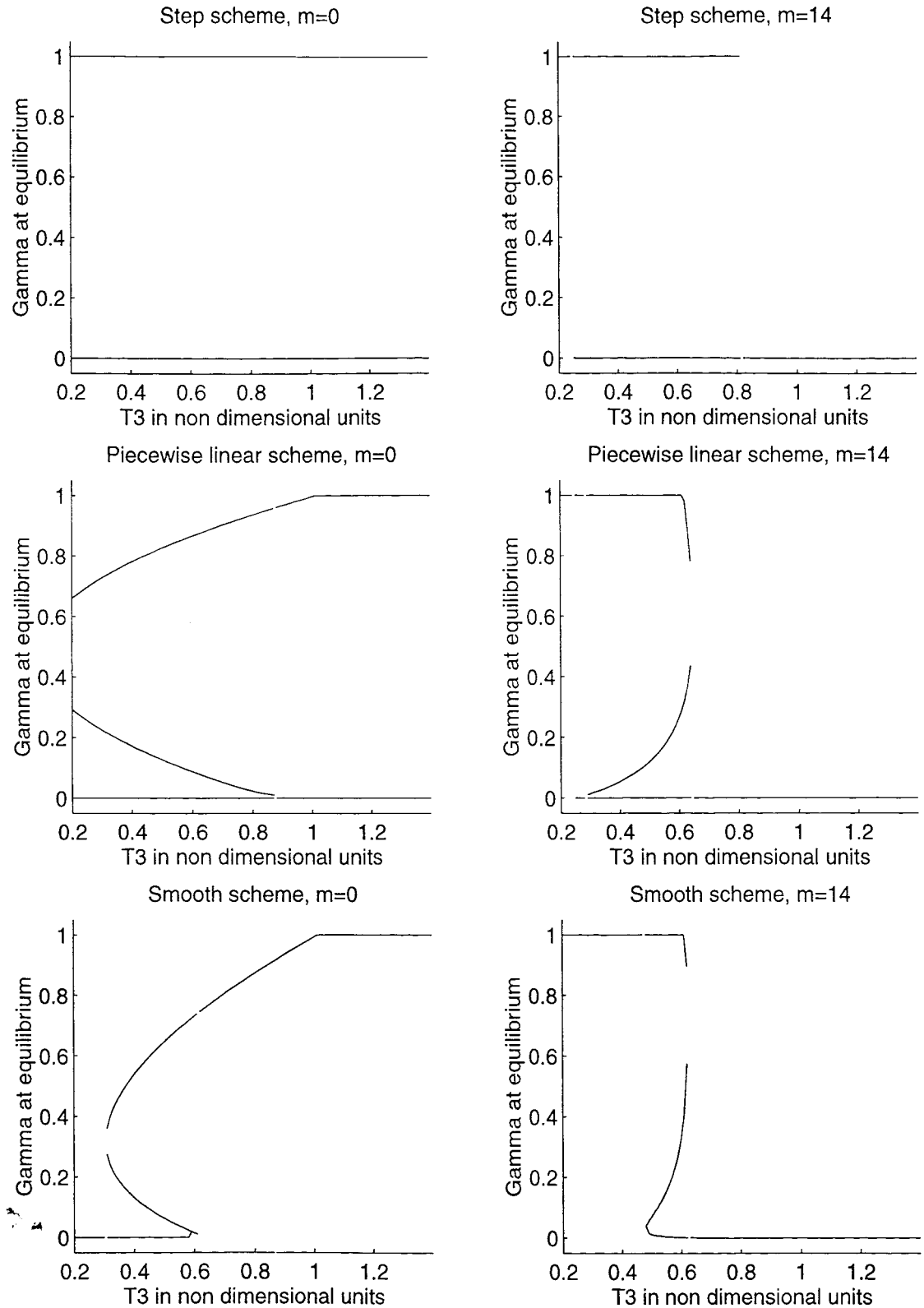

Figure 5 - 4: The strength of convection ($\Gamma(\Delta\rho)$) for the equilibrium solutions of the reduced box model for each of the 3 convection schemes as a function of the temperature of the deep sub tropical box (T_3). The graphs are shown for the cases with no and a strong meridional overturning cell (m).

5.2.6 The affect of the ratio of the haline to thermal density forcing for box 2 (r).

The haline to thermal density forcing ratio (r) included the effects of both the surface horizontal diffusion and the surface boundary conditions. For weak advection increasing the value of r had little affect on the states of the model apart from increasing the strength of convection in the weakly convecting state for the piece wise linear scheme. As the strength of the overturning cell was increased so was the sensitivity to the value of r. When overturning was of medium strength the value of r determined the possible equilibria for the step and piece wise linear schemes. For $r<32$ only the strongly convecting equilibrium was possible but for $r>32$ both the convecting and non convecting equilibria were obtained. The response of the smooth scheme was different in that the convecting equilibria was always possible.

For a strong overturning cell the density forcing ratio (r) had little effect on the possible equilibria for the step and piece wise linear cases. With the smooth scheme only the strongly convecting state was possible for $r<30$ but for $r>30$ the weakly convecting and non convecting equilibria also became achievable.

5.2.7 Sensitivity to the vertical diffusivities of salt and heat (k^S_v and k^T_v).

The reduced model was very insensitive to the values of the vertical diffusivities. Varying both of the non dimensional diffusivities over a large range had no affect on the number, type or stability of the equilibria for any of the 3 convection schemes. The non dimensional diffusivities were varied over the range 0 to 5. The maximum of this range was over 3 times the default value for the non dimension diffusivities.

5.2.8 The response to changes in the horizontal diffusivities of heat and salt (k^T_d, k^S_d and k^S_s).

With no meridional overturning the strength of the deep water thermal diffusivity (k^T_d) did not change the number or type of equilibria for any of the 3 convection schemes. The value of k^T_d did have some affect on the strength of convection in the strongly and weakly convecting equilibria for the piece wise linear and smooth schemes. Increasing the strength of the deep water diffusivity of heat caused the strength of convection in the weakly convecting mode to increase and the strength of convection in the strongly convecting mode to decrease.

In the weakly overturning case the value of k^T_d altered the number of possible equilibria. For $k^T_d<2.8$ (the default value of k^T_d was 1.61) only the strongly convecting equilibrium was possible for all 3 convection schemes. For $k^T_d>2.8$ the non convecting equilibrium was also possible for the step and piece wise linear schemes. Above $k^T_d=4$ the weakly convecting equilibria became possible for the piece wise linear scheme and the strength of the strongly convecting equilibrium decreased for both the piece wise linear and smooth schemes (Figure 5 - 5). The response above $k^T_d=5$ was not investigated as this was outside the physically justifiable range.

The response to changes in k^T_d for a strong meridional overturning cell (m=14) was very similar to that for the weakly overturning cell (m=4). For k^T_d<0.8 only the strongly convecting equilibrium was possible. Above this the non convecting equilibrium became possible for the step and piece wise linear schemes. When k^T_d>2.5 the weakly convecting state was seen for the piece wise linear convection scheme (Figure 5 - 5).

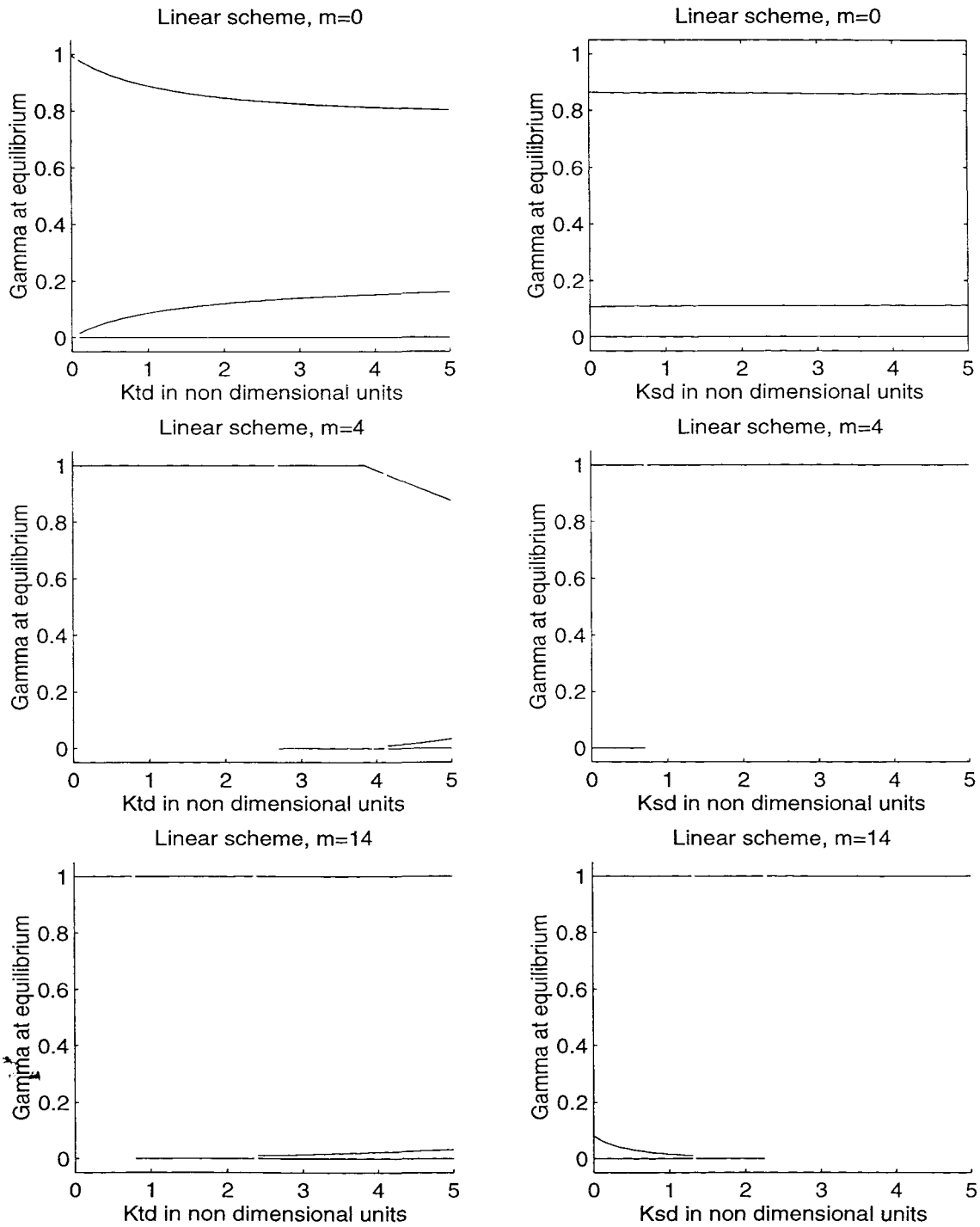

Figure 5 - 5: The strength of convection at equilibrium ($\Gamma(\Delta\rho)$) as a function of the deep water thermal (k^T_d) or haline (k^S_d) diffusivities for 3 strengths of meridional overturning (m).

The strength of the deep water horizontal diffusivity of salt (k^S_d) had no affect on the type or stability of the equilibria for no overturning cell.

For the weak and strong overturning cells the value of k^S_d did affect the response for the piece wise linear and step convection schemes. With a large k^S_d only the strongly convecting steady state was observed. As the value of k^S_d decreased the non convecting equilibria became possible (k^S_d<2.8 for strong overturning and k^S_d<0.8 for weak overturning). With the piece wise linear scheme a weakly convecting state was also possible for k^S_d<1.2 (Figure 5 - 5).

The relative strength of the surface diffusivity of salt (k^S_s) had little influence on the number, type or stability of the possible equilibria for all 3 schemes for no or weak overturning (m=0 or m=4). For a strong meridional overturning cell only the strongly convecting state was possible for k^S_s>1.5. Below k^S_s=1.5 the non convecting state was possible for the step and linear convection schemes. With k^S_s<0.2 the weakly convecting equilibrium was also possible for the piece wise linear scheme.

5.2.9 The affect of the strength of the convective mixing (Γ^T_0 and Γ^S_0).

The strength of the convective mixing for temperature (Γ^T_0) and salinity (Γ^S_0) had little influence on the equilibrium states of the reduced box model as long as the parameters remained large. If either Γ^T_0 or Γ^S_0 were made small (Γ^T_0<12, where the default value was 22.9 or Γ^S_0<50, where the default value was 923) the strength of convection in the weakly convecting mode increased and strongly convecting mode decreased (for the linear and smooth schemes with no overturning cell). If Γ^T_0 was less than 8 the weakly and strongly convecting states were not possible for the linear or smooth schemes.

5.3 The reduced box model with the coupled surface boundary conditions and convection scheme.

Coupling surface boundary conditions and the parameterisation of convection using the schemes derived in chapter IV increased the complexity and number of variable parameters in the reduced model. The differences in the results when using the 2 alternative convection schemes were:

- That over most of the parameter ranges the equilibria of the coupled scheme had a positive vertical density difference. Whereas the strongly convecting equilibria of the enhanced diffusion case had a hydrostatically unstable (negative) vertical density difference.
- For medium strength advection there were regions in parameter space where the coupled scheme exhibited periodic oscillations, unlike the enhanced diffuison case that always had at least one stable equilibrium. The possibility of oscillations brought the results more in line with those from the OGCM.

The physical interpretation of the coupled scheme results is similar that of the enhanced diffusion case. As before the surface boundary conditions, horizontal diffusion and advection were trying to impose a given density difference on the system. If this imposed density difference was sufficiently large then convection was inhibited. If the density difference was close to the critical density difference then multiple equilibria were possible and when the imposed density difference was small convection was encouraged. The feedback between the convection and surface boundary conditions, and that the surface forcing was applied to both boxes made more specific interpretation difficult.

5.3.1 Non dimensionalisation of the reduced box model with coupled scheme equations.

The non dimensionalised equations for the reduced box model using the coupled scheme were similar to those given in Equation 5 - 7 but included extra terms to represent the coupling of the surface boundary conditions and convection. The non dimensionalisation was chosen so that the variables and parameters in the 2 sets of equations (Equation 5 - 7 and Equation 5 - 8) represented the same processes and had similar magnitudes. In keeping the number of variable parameters to a minimum the exact definitions of some of the parameters changed slightly between the 2 sets of equations. Hence the parameters had different numeric values in the 2 cases. Though the exact definitions changed the general interpretations remained the same.

The values and interpretation of the non dimensional parameters used in the coupled version of the reduced box model described by Equation 5 - 8 are given in Table 5 - 3.

Equation 5 - 8

$$\frac{dT_2}{dt} = 1 - T_2 + \left(\Gamma_0^T \Gamma + k_v^T\right)(T_4 - T_2) + m(T_1 - T_4) +$$

$$\gamma^2 \xi q_T^* + \alpha_1 \left\{\left(\alpha\Gamma_2(1 - \ ) - 1\right)\left(T_1^* + T_2^* \ - T_2\right) + T_2^*\right\}$$

$$\frac{dT_4}{dt} = \gamma\left\{\begin{array}{l} k_d^T (T_3 - T_4) + \left(\Gamma_0^T \Gamma + k_v^T\right)(T_2 - T_4) + m(T_2 - T_3) \\ + \Gamma \xi q_T^* \end{array}\right\}$$

$$\frac{dS_2}{dt} = k_s^S (1 - S_2) + \left(\Gamma_0^S \Gamma + k_v^S\right)(S_4 - S_2) + m(S_1 - S_4)$$

$$\Gamma - \gamma^2 \ \xi q_S^*$$

$$\frac{dS_2}{dt} = \gamma\left\{\begin{array}{l} k_d^S (S_3 - S_4) + \left(\Gamma_0^S \Gamma + k_v^S\right)(S_2 - S_4) + m(S_2 - S_3) \\ + \Gamma \xi q_S^* \end{array}\right\}$$

Where

$$\Gamma = \Gamma(\Delta\rho) = \Gamma\left(-(T_4 - T_2) + r(S_4 - S_2)\right)$$

In the same manner as the enhanced diffusion case the effect of each parameter on the number and type of equilibria was investigated. Unless specifically stated all parameters had their default value that was the lowest value given in Table 5 - 3. A formal stability analysis was not performed as the enhanced diffusion case indicated that even if an equilibrium was stable to

infinitesimal perturbations this did not imply that it would be seen in model runs. The stability of the equilibria was determined by integrating the model forward in time using a 4-5th order Runge-Kutta method starting from the equilibrium solution plus a finite perturbation (Press et al 1992).

Table 5 - 3: The parameters used in the reduced box model with the coupled surface buoyancy forcing and convection scheme.

Parameter	Range (non dimensional)	Physical meaning
Γ^T_0	28.8	Thermal enhanced diffusivity
Γ^S_0	1164	Haline enhanced diffusivity
T_1	1.13 to 1.15	Temperature of box 1
T_3	0.33 to 2.2	Temperature of box 2
S_1	1.06 to 1.07	Salinity of box 1
S_3	1.03 to 1.09	Salinity of box 3
m	0 to 20.6	Strength of meridional overturning
k^T_d	2.03	Deep thermal horizontal diffusivity
k^S_d	2.15	Deep haline horizontal diffusivity
k^S_s	0.84	Surface haline horizontal diffusivity
k^T_v	0.039	Thermal vertical diffusivity
k^S_v	0.028	Haline vertical diffusivity
γ	0.5723	The ratio of the depth of box 2 to that of box 4
$\Delta\rho_{critical}$	0.15 to 0.31	The critical density difference
r	25.8 to 69	Ratio of haline to thermal density forcing for box 2.
α_1	0.117	The relaxation time of the thermal forcing
α_2	200	The ratio of the variable to fixed thermal forcing
T^*_1	0	The atmospheric reference temperature
T^*_{24}	0.41 to 0.88	The variability of the atmospheric temperature
ξ	0.111	A factor derived from the depths of boxes 2 and 4
q^*_S	-0.055 to -0.053	The surface fresh water flux for the convecting area
q^*_T	-11.5 to -5.4	The surface heat flux for the convecting area

5.3.2 The sensitivity to the strength of the meridional overturning cell.

For comparison with the enhanced diffusion case the affect of the strength of the meridional overturning (m) on the equilibria of the reduced model using the coupled scheme was examined for all 3 versions of convection scheme, step convection, piece wise linear and the smooth scheme (Though the parameterisations derived from the OGCM were only strictly valid for the piece wise linear scheme). Using the step convection scheme there were only 2 possible equilibria, one strongly convecting and the other with no convection. Weak and negative advection gave both these equilibria. As the strength of the overturning cell was increased both the equilibria became impossible to obtain, giving a band where the system had no steady state solutions. If the strength of the advection was increased further the convecting equilibrium became tenable (Figure 5 - 6). The fully convecting and non convecting equilibria were stable and acted as attractors as in the enhanced diffusion case.

The results for the piece wise linear scheme were similar to those of the step scheme. For negative overturning both the fully convecting and non convecting states were possible. With weak advection multiple states were obtained, fully convecting, strongly convecting, 2 weakly convecting and a non convecting equilibrium. Increasing the strength of the overturning further only the weakly convecting state was possible. The strength of the convection in this state increased as the strength of the meridional overturning increased until the maximum was reached. Similar to the previous results the weakly convecting equilibrium was unstable and therefore not seen in the model runs. For this partially convecting equilibrium to be stable over 0.35 (determined empirically) of the box had to be convecting. The results for the smooth convection scheme were the same as those for the piece wise linear scheme apart from the fact that non convecting state was never realised.

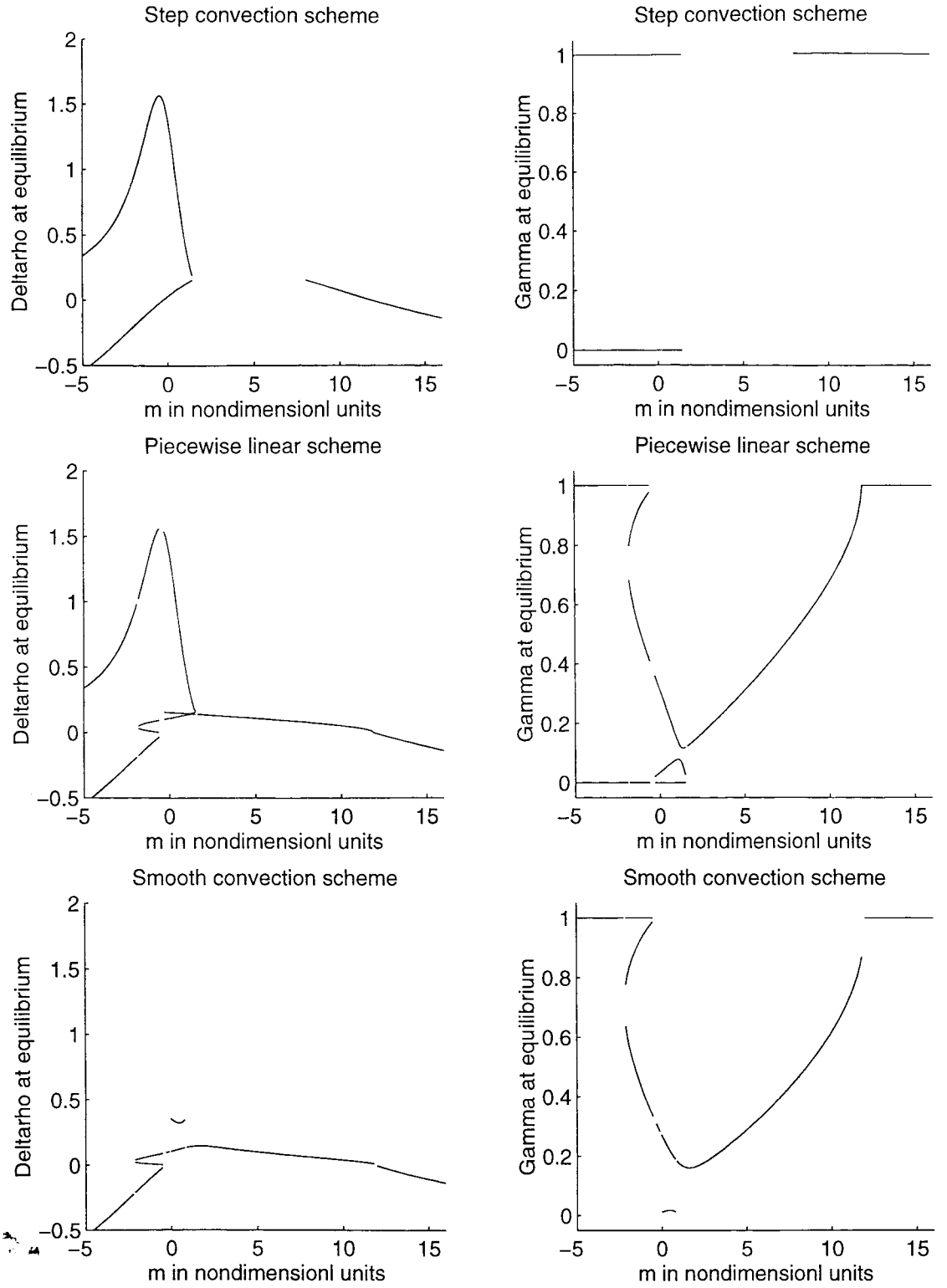

Figure 5 - 6: The vertical density difference ($\Delta\rho$) and the strength of convection ($\Gamma(\Delta\rho)$) for the equilibrium states of the reduced box model as a function of the advective volume flux (*m*). The results are shown for each of the 3 coupled surface boundary conditions and convection schemes with all other parameters held at their default values.

5.3.3 Periodic oscillations of the reduced coupled model.

Using the piece wise linear scheme there were no stable equilibria for $1.5 < m < 5.9$. In this region the model underwent periodic oscillations. The oscillations were similar to the deep decoupled oscillations seen in the OGCM in that they consisted of periods of weak or no convection terminated by a short bursts of strong convection. Both the amplitude and the period of the oscillation was affected by the strength of the advective overturning, especially near the limits of the range where oscillations occurred (Figure 5 - 7). For *m* close to 1.5 the oscillations had a period of approximately 280 years and the non convecting state lasted 4 times longer than the convecting state. Throughout the cycle the vertical density gradient remained positive. As the strength of the meridional overturning (*m*) increased the period of oscillation decreased and the range of the vertical density gradient increased. The fraction of the cycle that the model was convecting for increased as the period of oscillation got shorter. For sufficiently large *m* the density difference at the beginning of the convecting phase became negative, though the density difference was only negative for a small proportion of the convecting phase (Figure 5 - 8). For *m* above 5, increasing *m* further lengthened the period of oscillation especially as the value of *m* approached the limit of 5.9. The amplitude of the oscillations continued to increase with the strength of the meridional overturning (*m*). Above *m*=5.7 the amplitude of the oscillations became noticeably uneven and short period fluctuations were found in the non convecting stage (Figure 5 - 8). In this strong meridional overturning case the model could take multiple oscillation periods to settle into the periodic oscillations when started from random initial conditions. In the case with weak meridional overturning the model reached the periodic oscillation state within 2 oscillation periods (see section 5.4).

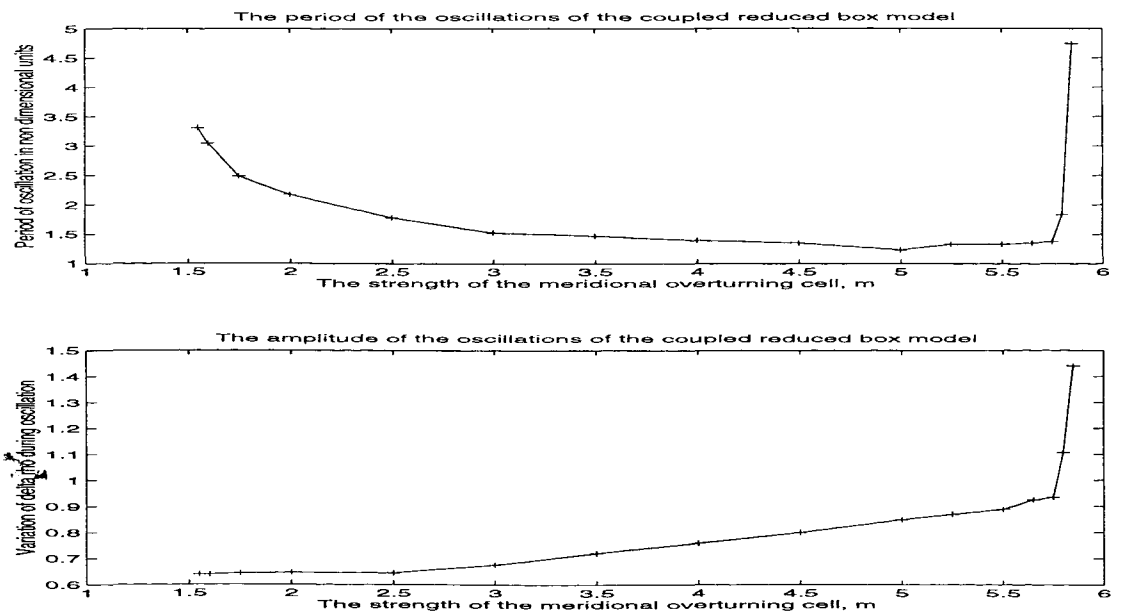

Figure 5 - 7: The period and amplitude of the oscillations of the reduced box model using the coupled surface boundary conditions and convection scheme as a function of the strength of the meridional overturning (*m*).

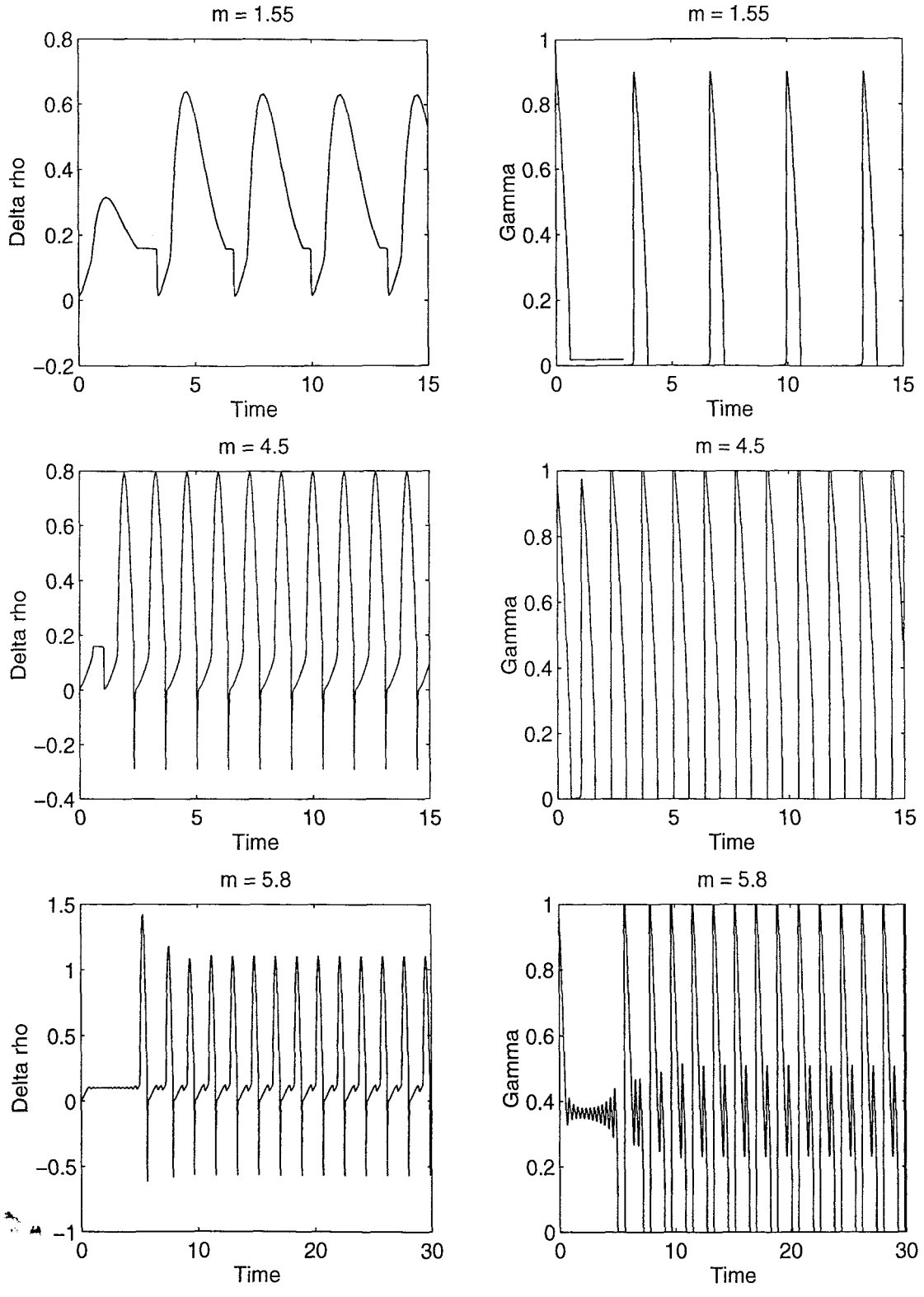

Figure 5 - 8: Oscillations of the reduced box model using the coupled surface boundary conditions and convection scheme for various strengths of meridional overturning (*m*). The vertical density difference and strength of convection ($\Gamma(\Delta\rho)$) are shown for each strength of meridional overturning.

5.3.4 The effect of the temperature and salinity of the surface sub tropical box (box 1).

Like the enhanced diffusion case the temperature (T_1) or salinity (S_1) of box 1 did not affect the possible equilibria of the reduced box model when the temperature or salinity were varied over the ranges given in Table 5 - 3. Though the temperature and salinity of box 1 had no noticeable affect on the possible equilibria they may affect the time evolution of the model.

5.3.5 Sensitivity to the temperature and salinity of the deep sub tropical box (box 3).

Varying the salinity of box 3 (S_3) had a very weak affect on the possible steady states for all strengths of meridional overturning (m). Increasing S_3 increased the strength of the weakly convecting equilibria for all cases but strong overturning. The increase in the strength of convection was not enough to make this weakly convecting state stable. For the strongly overturning case only the strongly convecting state was possible and this was not affected by the value of S_3.

The temperature of box 3 had a marked affect on the possible steady states of the model. For weak or no advection (m<1.5) increasing T_3 increased the strength of convection for the weakly convecting state. For T_3 <1.6 the non convecting and weakly convecting equilibria were possible but for T_3>1.6 only the strongly convecting and weakly convecting states were possible. If T_3 was sufficiently large (T_3>2.1) 3 different strongly convecting equilibria were obtainable. The opposite was true in the case of medium strength overturning, increasing the temperature of box 3 caused the non convecting equilibria to become possible and decreased the strength of the weakly convecting state. When the overturning was strong, a low temperature (T_3<0.5) made only the strongly convecting equilibrium obtainable but for a higher temperature only the non convecting steady state existed. In the transition region from convecting to non convecting equilibrium the weakly convecting state was possible. The strength of this state decreased as the temperature was increased.

5.3.6 The density forcing ratio for box 2's (r) affect on the possible equilibria.

As with the enhanced diffusion case the density forcing ratio (r) had little affect on the system for a weak overturning cell (m<1.5). If the haline forcing was sufficiently strong compared to the thermal forcing (r>60) then the non convecting state became possible for a medium strength overturning cell. The presence of the non convecting state replaced the periodic oscillations as the state acted as an attractor. For a strong overturning cell only the convecting equilibrium was possible for small r. As r was increased the non convecting equilibrium became possible as did a weakly convecting state.

5.3.7 Sensitivity to the surface boundary conditions.

Besides the density forcing ratio (r) the surface boundary conditions in the coupled scheme included the parameters that determined how the surface forcing responded to the strength of convection. The steady states of the model were insensitive to both the variability of the atmospheric temperature (T^*_2) and the strength of the freshwater flux into the convecting area

($\dot{q}_S$) when they were varied over the ranges given in Table 5 - 3. The possible equilibria of the model were sensitive to the value of the heat flux out of the convecting region ($\dot{q}_T$).

For all strengths of meridional overturning increasing the strength of the cooling to the convecting region ($\dot{q}_T$) decreased the strength of convection for all the convecting equilibria. In the case of a strong overturning cell increasing the cooling ($\dot{q}_T$) caused the fully convecting state to become partially convecting and for the strength of this convection to decrease as the strength of the cooling was increased. For a weak overturning cell increasing $\dot{q}_T$>10 made the partially convecting states unobtainable leaving only the non convecting equilibrium.

5.3.8 The affect of the vertical diffusivities (k^T_v and k^S_v).

As with the enhanced diffusion convection scheme, varying the vertical diffusivities of heat and salt did not alter the number, type or character of the equilibria of the reduced box model with the coupled surface boundary conditions and convection scheme.

5.3.9 Sensitivity to the horizontal diffusivities (k^T_d, k^S_d and k^S_s).

In agreement with the results from using the enhanced diffusion convection scheme, k^S_s had negligible affect on the steady state solutions.

k^S_d had no affect on the number of equilibria of the reduced coupled model. For very small k^S_d (k^S_d<0.4 where the default value was k^S_d=2.15) the strength of convection for the convecting states decreased as k^S_d decreased.

The horizontal diffusivity of heat k^T_d had an influence on the number and type of equilibria of the reduced coupled model. Similar to the enhanced diffusion case which was sensitive to the value of k^T_d. However the response of the 2 models to k^T_d was not the same. For a strong overturning cell only the strongly convecting state was possible. The strength of convection in this state was reduced for high values of k^T_d (Figure 5 - 9).

With a weak meridional overturning cell a weakly convecting state was possible for low values of k^T_d. As k^T_d increased a non convecting equilibrium became possible. Over a small range 3 equilibria existed, 1 non and 2 weakly convecting. For large k^T_d only the non convecting state was observed.

The response to k^T_d in the absence of advection was complex (Figure 5 - 9). Strongly convecting states were seen for high k^T_d and only a non convecting state existed for low k^T_d. For mid strength diffusion 1 non convecting and 2 weakly convecting states were possible. The strength of convection in the weakly convecting states increased with increasing k^T_d.

5.3.10 Response to the strength of the convective mixing (Γ^T_0 and Γ^S_0).

As with the enhanced diffusion case Γ^S_0 had very little influence on the equilibrium solutions to the reduced coupled model.

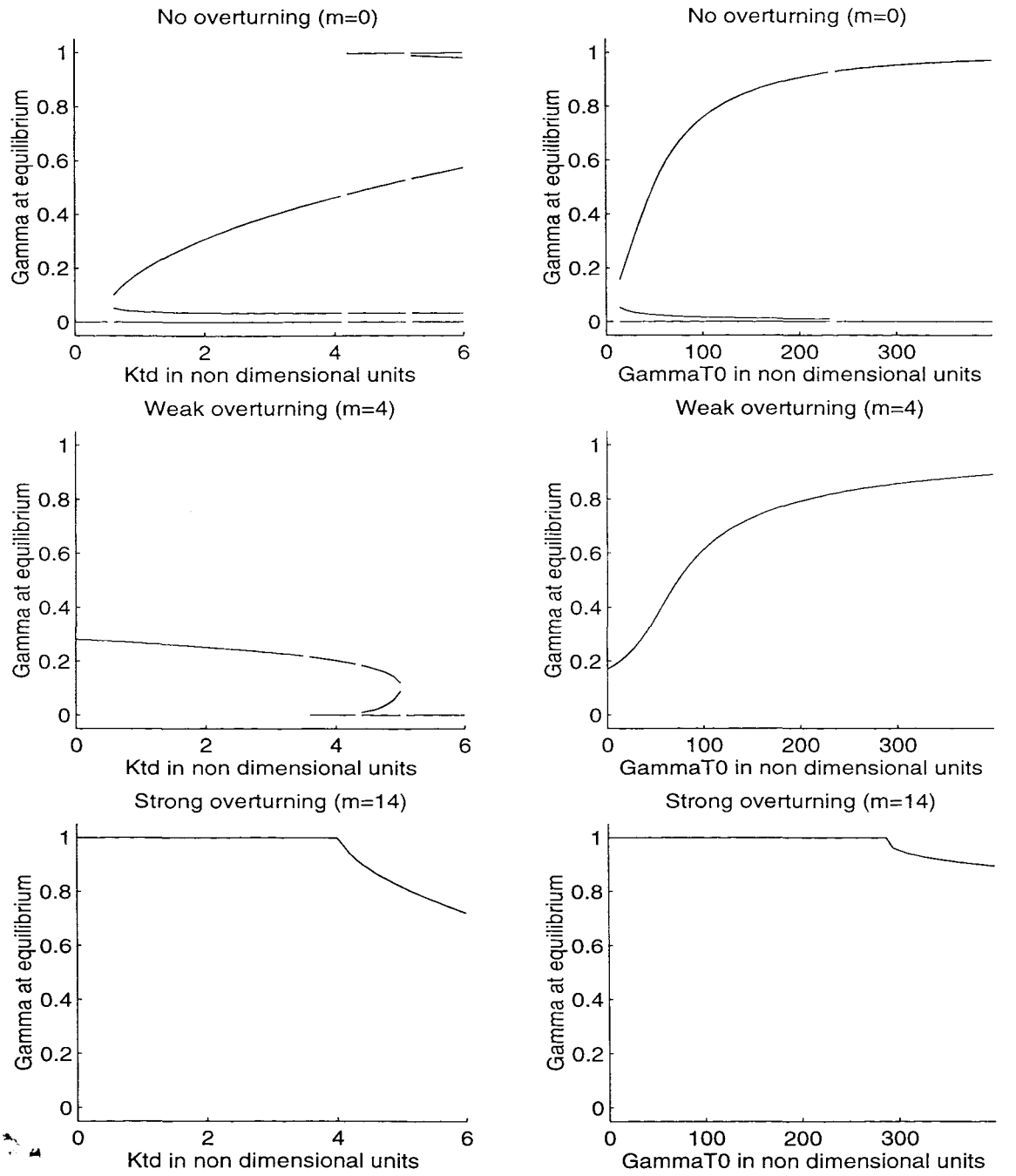

Figure 5 - 9: The strength of convection ($\Gamma(\Delta\rho)$) for the equilibrium states of the reduced coupled model as a function of k^T_d or Γ^T_0 for the strong, weak and no overturning cases.

The strength of the convective mixing for temperature (Γ^T_0) affected the steady state solutions of the reduced coupled model for weak and no overturning (Figure 5 - 9). For a weak meridional overturning cell there was only a weakly convecting equilibrium. The strength of convection for this equilibrium increased as Γ^T_0 was increased. With no meridional overturning there was a

non convecting state for small Γ^T_0 (Γ^T_0<20). Above this there were 2 extra weakly convecting states. The strength of one of these states increased as Γ^T_0 was increased. For large Γ^T_0 only the non convecting and a strongly convecting equilibria existed (Figure 5 - 9).

5.4 Summary of the results from the reduced box model.

With both the enhanced diffusion and the coupled schemes the reduced model exhibited a number of different equilibria. These equilibria were distinguished by the strength of the convective mixing associated with them. The nature of the equilibria that existed was strongly dependent on the strength of the meridional overturning, the deep water heating, the convection scheme, the horizontal deep water diffusivity of heat, the strength of convective mixing for temperature and the surface buoyancy flux. Using the enhanced diffusion scheme the reduced box model had multiple steady states but always had at least one stable equilibrium. This stable equilibrium was a sufficiently strong attractor to exclude oscillatory solutions. The equilibria found in the enhanced diffusion case fell into 4 categories, non convecting, weakly convecting that was unstable, strongly convecting that was stable and had a positive density difference and fully convecting which had a negative density difference. The equilibria for the reduced model using the coupled scheme fell into the same categories as those for the enhanced diffusion scheme and the affect of the parameters on the possible equilibria was also similar to the enhanced diffusion case. Adding the extra feedback between the surface boundary conditions and the strength of convection (as in the coupled scheme) altered the strength and occurrence of the strongly and fully convecting equilibria enough that for a range of parameter sets there were no stable steady states. This extra feedback also made the fully convecting equilibrium with an unphysical negative density gradient occur over a smaller portion of the parameter space.

When no stable steady states existed the model underwent periodic oscillations. These oscillations consisted of a period of weak or no convection followed by a shorter period of strong convection (similar to deep decoupled oscillations seen in the OGCM). The period and amplitude of these oscillations was sensitive to the strength of the meridional overturning and the strength of the deep water warming. The oscillations obtained using this coupled surface boundary condition and convection scheme occurred without the need for the density difference to become negative. To obtain similar oscillations using a convection scheme that completely mixed the 2 polar boxes when the density difference fell below a critical value (or an enhanced diffusion scheme) the value of the critical density difference had to be negative. The mechanism driving the oscillations in both cases was the same: The convection mixed away the density gradient that caused the convection. The density gradient was then re-established by the external forcing. By applying the surface boundary conditions to both polar boxes (as with the coupled scheme) the density gradient was forced back to a positive value by the convection scheme rather than driven back to a neutrally stable zero gradient.

Chapter VI

The full box model

6.0 Description of the full box model.

The full box model (FBM) developed in chapter IV divided a single hemisphere, single ocean basin both horizontally and vertically (Figure 6 - 1). The heat and salt fluxes between the boxes were given by the parameterisations obtained from the OGCM in chapter IV. The advective fluxes were given by a centred scheme where the strength of the meridional overturning cell was proportional to the meridional deep water density gradient. Fluxes due to diffusion were proportional to the relevant tracer gradient. The surface boundary conditions for the sub polar box and the convective fluxes were modelled using the coupled scheme discussed in chapter V and section 4.6. For the sub tropical surface box the surface buoyancy flux was driven by mixed boundary conditions, a Haney term for temperature and a fixed salt flux for salinity. Combining these processes the time evolution equations for the temperatures of the 4 boxes in the FBM were given by Equation 6 - 1.

$$\frac{dT_1}{dt} = \frac{1}{c_p \rho_0 vol_1}\left(Q_1^{surf} + Q_1^{adv} - Q_2^{adv} + Q_1^{diff} - Q_2^{diff}\right) \qquad \textbf{Equation 6 - 1}$$

$$\frac{dT_2}{dt} = \frac{1}{c_p \rho_0 vol_2}\left(Q_2^{coupled} + Q_2^{adv} - Q_3^{adv} + Q_2^{diff} - Q_3^{diff}\right)$$

$$\frac{dT_3}{dt} = \frac{1}{c_p \rho_0 vol_3}\left(Q_4^{adv} - Q_1^{adv} + Q_4^{diff} - Q_1^{diff}\right)$$

$$\frac{dT_4}{dt} = \frac{1}{c_p \rho_0 vol_4}\left(Q_4^{coupled} + Q_3^{adv} - Q_4^{adv} + Q_3^{diff} - Q_4^{diff}\right)$$

Where T_n was the temperature of box n (see Figure 6 - 1), t was time, c_p the specific heat capacity of sea water, ρ_0 the reference density, vol_n the volume of box n and Q_j^i the heat flux across face j due to the process denoted by i. The values of i were "surf" for a surface flux, "adv" for advective fluxes and "diff" for diffusive fluxes. $Q_n^{coupled}$ was the flux into box n due to the coupled surface boundary conditions and convection scheme.

The individual heat fluxes were modelled using Equation 6 - 2:

$$Q_1^{surf} = \alpha_{ref}\left(T^* - T_1\right) \qquad \textbf{Equation 6 - 2}$$

$$Q_1^{adv} = c_p \cdot \rho_0 \cdot \nu \frac{\left(T_3 + T_1\right)}{2}$$

$$Q_2^{adv} = c_p \cdot \rho_0 \cdot \nu \frac{\left(T_1 + T_2\right)}{2}$$

$$Q_3^{adv} = c_p \cdot \rho_0 v \frac{(T_2 + T_4)}{2}$$

$$Q_4^{adv} = c_p \cdot \rho_0 v \frac{(T_4 + T_3)}{2}$$

$$Q_1^{diff} = \frac{area_1 \cdot c_p \cdot \rho_0 \cdot \kappa^T_{v\,equator}}{dz}(T_3 - T_1)$$

$$Q_2^{diff} = \frac{area_2 \cdot c_p \cdot \rho_0 \cdot \kappa^T_{h\,surface}}{dy}(T_1 - T_2)$$

$$Q_3^{diff} = \frac{area_3 \cdot c_p \cdot \rho_0 \cdot \kappa^T_{v\,pole}}{dz}(T_2 - T_4)$$

$$Q_4^{diff} = \frac{area_4 \cdot c_p \cdot \rho_0 \cdot \kappa^T_{h\,deep}}{dy}(T_4 - T_3)$$

$$Q_2^{coupled} = Q_c + Q_a + \frac{h_2}{h_2 + h_4} Q_b$$

$$Q_4^{coupled} = -Q_c + \frac{h_4}{h_2 + h_4} Q_b$$

Where all the variables retain their definitions from Equation 6 - 1. α_{ref} *and* $\dot{T}$ *were the Haney coefficient and effective atmospheric temperature used in the surface boundary condition for the temperature of box 1,* $area_n$ *was the area of face n,* v *was the volume flux of the meridional overturning cell,* κ^T_h *and* κ^T_v *were the horizontal and vertical thermal diffusivities, dz was the vertical separation of the boxes and dy was the meridional separation of the boxes,* h_n *was the depth of box n and* $Q_{a,\,b\,and\,c}$ *were the heat fluxes due to the coupled surface boundary conditions and convection scheme (see section 4.6)*

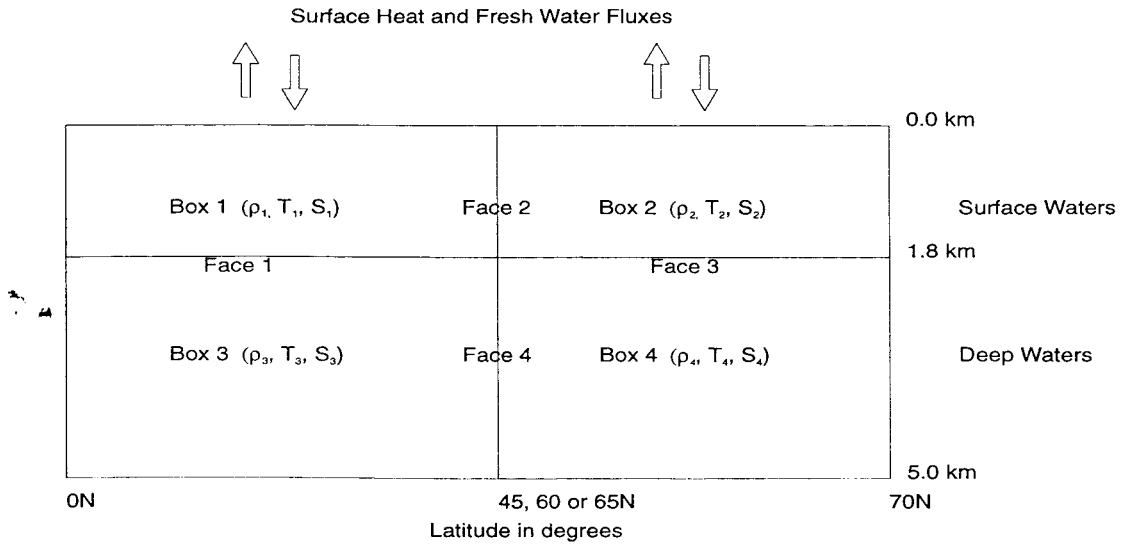

Figure 6 - 1: The layout of the boxes in the full box model (FBM).

The time evolution equations for the salinity of the boxes were very similar to those for temperature (Equation 6 - 3):

$$\frac{dS_1}{dt} = \frac{1000}{\rho_0 vol_1}\left(q_1^{surf} + q_1^{adv} - q_2^{adv} + q_1^{diff} - q_2^{diff}\right)$$

$$\frac{dS_2}{dt} = \frac{1000}{\rho_0 vol_2}\left(q_2^{coupled} + q_2^{adv} - q_3^{adv} + q_2^{diff} - q_3^{diff}\right)$$

$$\frac{dS_3}{dt} = \frac{1000}{\rho_0 vol_3}\left(q_4^{adv} - q_1^{adv} + q_4^{diff} - q_1^{diff}\right)$$

$$\frac{dS_4}{dt} = \frac{1000}{\rho_0 vol_4}\left(q_4^{coupled} + q_3^{adv} - q_4^{adv} + q_3^{diff} - q_4^{diff}\right)$$

Equation 6 - 3

Where S_n was the salinity of box n, and q_i^j the salt flux where the definition was the same as for the heat fluxes in Equation 6 - 1.

The salt fluxes between the boxes were given by Equation 6 - 4:

$$q_1^{surf} = \text{a constant salt flux}$$

$$q_1^{adv} = \frac{\rho_0 v}{1000}\frac{(S_3 + S_1)}{2}$$

$$q_2^{adv} = \frac{\rho_0 v}{1000}\frac{(S_1 + S_2)}{2}$$

$$q_3^{adv} = \frac{\rho_0 v}{1000}\frac{(S_2 + S_4)}{2}$$

$$q_4^{adv} = \frac{\rho_0 v}{1000}\frac{(S_4 + S_3)}{2}$$

$$q_1^{diff} = \frac{area_1 \cdot \rho_0 \cdot \kappa^S_{v\,equator}}{dz.1000}(S_3 - S_1)$$

$$q_2^{diff} = \frac{area_2 \cdot \rho_0 \cdot \kappa^S_{h\,surface}}{dy.1000}(S_1 - S_2)$$

$$q_3^{diff} = \frac{area_3 \cdot \rho_0 \cdot \kappa^S_{v\,pole}}{dz.1000}(S_2 - S_4)$$

$$q_4^{diff} = \frac{area_4 \cdot \rho_0 \cdot \kappa^S_{h\,deep}}{dy.1000}(S_4 - S_3)$$

$$q_2^{coupled} = q_c + q_a + \frac{h_2}{h_2 + h_4} q_b$$

$$q_4^{coupled} = -q_c + \frac{h_4}{h_2 + h_4} q_b$$

Equation 6 - 4

Where κ^S_v and κ^S_h were the vertical and horizontal diffusivities of salt.

The advective volume flux was parameterised using the scheme developed in chapter IV (Equation 6 - 5):

$$v = v_{offset} + v_0(\rho_4 - \rho_2) \qquad \textbf{Equation 6 - 5}$$

Where v_0 is the constant of proportionality, v_{offset} was the zero offset (with units of m^3/s) such that a zero density difference gave a positive overturning cell and ρ_n was the density of box n as calculated using the equation of state (Equation 6 - 10).

The heat and salt fluxes due to the coupled surface boundary conditions and convection scheme were modelled by Equation 6 - 6:

$$Q_a = c_p \cdot \rho_0 vol_2 . (1-\Gamma)\alpha(\Gamma)\left(T^*(\Gamma) - T_2\right) \qquad \textbf{Equation 6 - 6}$$

$$Q_b = \Gamma . Q_b^0$$

$$Q_c = \frac{c_p \cdot \rho_0 vol_2 . h_2}{(h_2 + h_4)\tau_T}(T_4 - T_2)$$

$$q_a = (1-\Gamma)q_{total}$$

$$q_b = \Gamma q_{total}$$

$$q_c = \frac{\rho_0 vol_2 . h_2}{1000(h_2 + h_4)\tau_S}(S_4 - S_2)$$

Where Γ was the proportion of the boxes convecting (Equation 6 - 9), $\alpha(\Gamma)$ and $T^*(\Gamma)$ were the Haney coefficient and effective atmospheric temperature for the surface temperature forcing of box 2, Q^0_b was the constant surface heat flux for the convecting region, q_{total} was the surface salt flux for box 2 and τ_T and τ_S were the time scales for the convective mixing of temperature and salinity (see chapter IV).

The Haney coefficient ($\alpha(\Gamma)$) and the effective atmospheric temperature ($T^*(\Gamma)$) were given by Equation 6 - 7 and Equation 6 - 8 respectively (see section 4.6).

$$\alpha(\Gamma) = \alpha_1(1 + \alpha_2\Gamma) \qquad \textbf{Equation 6 - 7}$$

$$T^*(\Gamma) = T_1^* + T_2^*\Gamma \qquad \textbf{Equation 6 - 8}$$

The proportion of boxes 2 and 4 that convected was parameterised using a piece wise linear function of the sub polar vertical density difference (Equation 6 - 9).

$$\Gamma = \begin{cases} 1 & \text{... for } \rho_4 - \rho_2 < 0 \\ 1 - \dfrac{\rho_4 - \rho_2}{\Delta\rho_{crit}} & \text{... for } 0 \le \rho_4 - \rho_2 \le \Delta\rho_{crit} \\ 0 & \text{... for } \rho_4 - \rho_2 > \Delta\rho_{crit} \end{cases} \qquad \textbf{Equation 6 - 9}$$

$\Delta\rho_{crit}$ was the critical density at which convection starts to occur.

The densities of the boxes were calculated using a linear equation of state (see section 4.7).

$$\rho_n = \rho_{ref} - \alpha T_n + \beta S_n \qquad \textbf{Equation 6 - 10}$$

Where ρ_{ref} was the reference density about which the equation of state was linearised, α and β were the thermal and haline expansion coefficients.

6.0.1 Values of the parameters used in the FBM.

The values of the parameters used in the FBM were those derived in chapter IV from the OGCM data. Table 6 - 1 lists the parameters used and their physical interpretations (see appendix F - The parameters used in the full box model).

Parameter	Value and units	Interpretation
α_{ref}	1.55×10^{-10} J/s.°C	Scaled Haney coefficient for box 1 surface forcing
T^*_1	19.9 °C	Effective atmospheric temperature for box 1
$k^T_{v\ equator}$	0.64×10^{-4} m^2/s	Vertical thermal diffusivity between boxes 1 and 3
$k^T_{v\ pole}$	0.70×10^{-4} m^2/s	Vertical thermal diffusivity between boxes 2 and 4
$k^T_{h\ surface}$	2.7×10^{3} m^2/s	Horizontal thermal diffusivity between boxes 1 and 2
$k^T_{h\ deep}$	3.6×10^{3} m^2/s	Horizontal thermal diffusivity between boxes 3 and 4
$k^S_{v\ equator}$	0.39×10^{-4} m^2/s	Vertical haline diffusivity between boxes 1 and 3
$k^S_{v\ pole}$	0.45×10^{-4} m^2/s	Vertical haline diffusivity between boxes 2 and 4
$k^S_{h\ surface}$	2.6×10^{3} m^2/s	Horizontal haline diffusivity between boxes 1 and 2
$k^S_{h\ deep}$	3.8×10^{3} m^2/s	Horizontal haline diffusivity between boxes 3 and 4
q_1^{surf}	1.1196×10^{7} Kg/s	Surface salt flux into box 1
q_{total}	-1.0324×10^{7} Kg/s	Surface salt flux into box 2
ν_{offset}	3.5×10^{6} m^3/s	Offset of the strength of the meridional overturning cell
ν_0	3.1918×10^{8} m^3/s.kg	Constant of proportionality between the deep water density difference and the strength of the meridional overturning cell
ρ_{ref}	1004.463 Kg/m^3	Reference density for the linear equation of state
α	0.1766 Kg/m^3.°C	Thermal expansion coefficient
β	0.6918 Kg/m^3.psu	Haline expansion coefficient
$\Delta\rho_{crit}$	0.16 Kg/m^3	Critical density difference for convection to occur

Parameter	Value and units	Interpretation
α_1	4.64×10^{-11} W/°C	Scaled Haney coefficient for box 2
α_2	200 no units	Ratio of variable to fixed Haney coefficient for box 2
T_1^*	0.0 °C	Fixed effective atmospheric temperature for box 2
T_2^*	7.0 °C	Variable effective atmospheric temperature for box 2
Q_b^0	-2.0470×10^{15} W	Surface heat flux for convecting area of box 2
τ_T	7.5894×10^{7} s	Time scale for convective mixing of temperature
τ_S	1.9036×10^{6} s	Time scale for convective mixing of salinity

Table 6 - 1: Some of the parameters used in the full box model.

6.1 Description of the numerics.

The equations of the FBM were integrated forward in time using a Runge-Kutta 4th order scheme with an adaptive time step (Press et al. 1992). The use of an adaptive time step allowed the model to resolve the sharp changes during the thermal flushes without requiring an inefficiently short time step for the long periods of inactivity in the haline driven mode. This scheme had 2 draw backs when applied to this model:

- In a few regions of parameter space the model could enter a rapidly oscillating state where convection was switching on and off. This caused the time step to shrink faster than the model evolved, such that the model never reached the prescribed end time. The oscillation was due to the numerical scheme overshooting either side of the correct value and not a real solution of the model. To overcome this instability a lower limit of 1 day was placed on the time step and the results flagged if this limit was encountered.

- The maximum size of the time step was limited by the formal accuracy of the scheme especially near some steady state solutions. The scheme caused the temperatures and salinities to oscillate either side of the steady state solution by an amount comparable to the accuracy limit chosen for determining the size of the time step (in all the model runs presented the accuracy was 1×10^{-6} or better). These small inaccuracies in the temperatures and salinities caused errors in the strength of the meridional overturning. The strength of meridional overturning was proportional to the differences in temperature and salinity between boxes. Errors in the temperature and salinity caused errors in the strength of meridional overturning that were larger than the formal accuracy of the scheme (by 1 or 2 orders of magnitude), though these errors remained small. As the model did not reach the

steady state solution the time step remained limited. Theoretically in a steady state the time step should have grown to become arbitrarily large but these oscillations precluded this, reducing the efficiency of the scheme.

6.2 Comparison to the OGCM results.

The FBM was integrated forwards in time from the same initial conditions as the OGCM. The parameters were fixed to the values given in Table 6 - 1 to match the corresponding parameters in the OGCM. For the total salt content of the FBM to match that of the OGCM the imbalance in the surface salt fluxes into boxes 1 and 2 was included (see chapter III). The salt flux into box 1 was 1.1196×10^{7} Kg/s of salt and into box 2 -1.03237×10^{7} Kg/s of salt (giving am increase in the average salinity of the ocean basin of 0.7 psu in 10000 years). This imbalance in surface salt fluxes was included to match the total salt content of the FBM to the OGCM. In the sensitivity studies the net surface salt flux was completely balanced (section 6.3).

Using these default values for the parameters the FBM correctly predicted that there was a rapid initial adjustment followed by ≅8000 years of a weak, non convecting circulation during which the ocean gained heat. This weak mode of circulation was terminated by a strong flushing event where heat was lost to the atmosphere. After the strong flush the FBM settled into a limit cycle of weak circulation followed by a thermal flush. The period of this limit cycle was 4 times longer than that of the oscillations seen in the OGCM. In general the FBM captured the weak circulation mode and the onset of the thermal flush but underestimated the length of the flushing events. Underestimating the length of the convecting modes meant that the FBM did not lose as much heat as the OGCM did in these convecting states. The difference in total heat content between the 2 models at the end of a flush caused the time evolution of the 2 models to diverge from this point. The model was sufficiently sensitive to some of the parameters that it was possible (with some trial and error) to tune the temperature or salinity of given boxes to evolve similarly to those of the OGCM for the initial weak circulation mode and subsequent thermal flush. The response of the FBM to variations in parameters is discussed in section 6.3.

To compare between the FBM and OGCM without engaging in the time consuming process of altering every parameter to provide the best fit to the OGCM results the FBM was run with the parameters described above except that the horizontal surface diffusivity of salinity which was increased to 1×10^{4} m^2/s. This increase was partly motivated by the change in the surface salinities of the FBM it caused. The increase was entirely valid as the horizontal diffusivities derived from the OGCM data did not have a high degree of accuracy.

As with the OGCM results the FBM results fell into 4 sections, the initial adjustment phase (0 to 200 years), the weak non convecting mode (approx. 200 to 7900 years), the strong flushing event and the final limit cycles. Taking each section in turn:

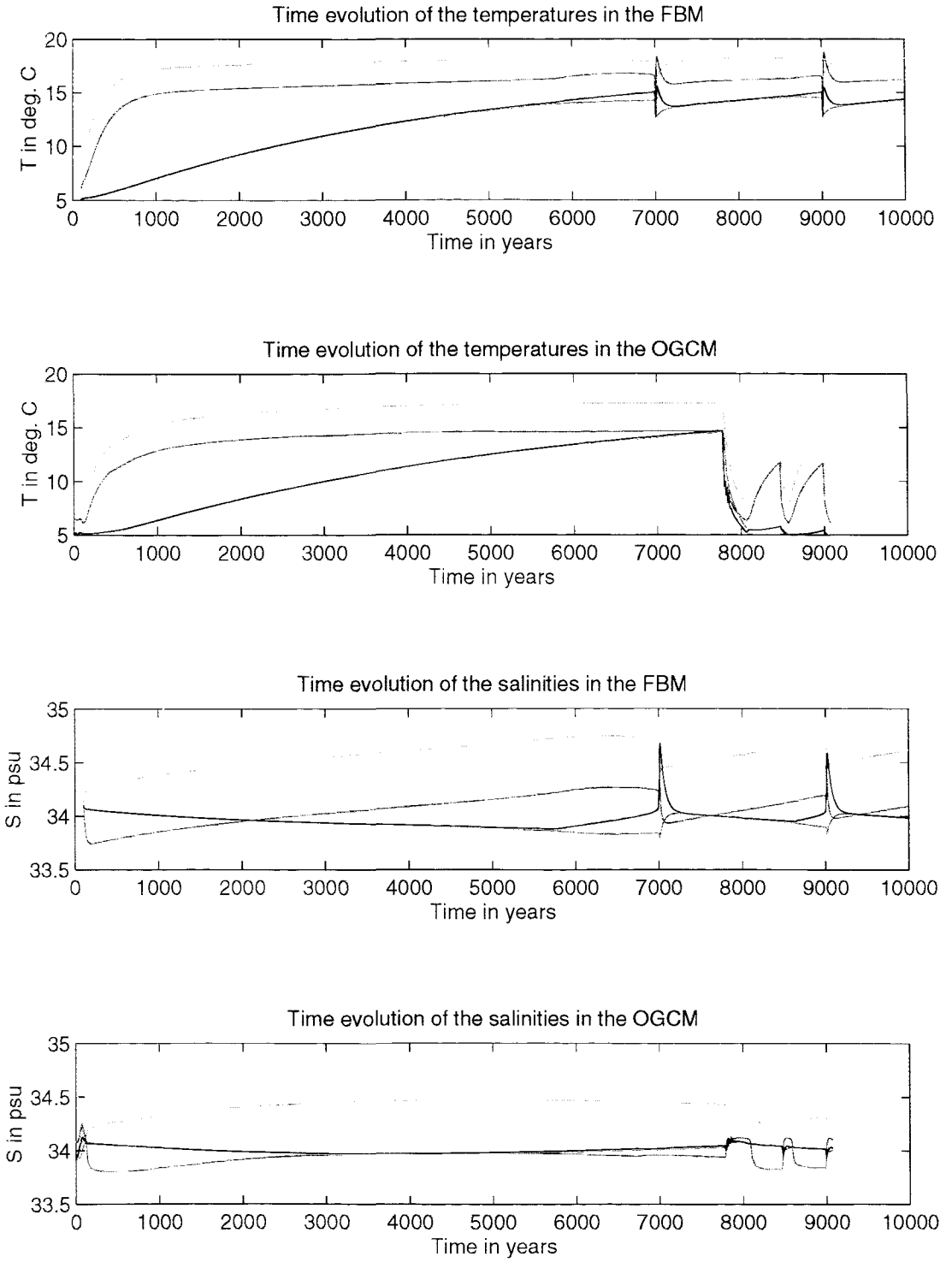

Figure 6 - 2: A comparison of the time evolution of the FBM and OGCM. The FBM was started with initial conditions representing the state of the OGCM after 100 years of integration and the FBM used the default values for all the parameters except the horizontal surface diffusivity of salt which was increased to 10^4 m^2/s. The linear trend in the salinities caused by the imbalance in the surface fluxes was removed for both sets of results. Red indicates the values for box 1, blue for box 2, green box 3 and black for box 4.

6.2.1 The initial adjustment phase (the first 200 years).

When the FBM was started from the same initial conditions as the OGCM, the FBM had an initial adjustment phase with strong convection and a positive meridional overturning cell. Unlike the OGCM this circulation only lasted for 20 years (compared to ≅200 years for the OGCM). Under estimating the length of time the convective adjustment lasted caused the FBM to over estimate the surface temperatures of both boxes 1 and 2 by up to 4°C and over estimate the temperature of the deep water by 0.25°C. However the surface (boxes 1 and 2) and deep (boxes 3 and 4) temperature differences in the FBM were very similar to those in the OGCM. This lack of convective and advective mixing caused the FBM to exaggerate the salinity differences when compared to the OGCM results. The surface tropical box (1) was too salty by 0.4 psu while the polar surface (box 2) salinity was 0.1 psu too fresh. The FBM under estimated the deep water salinity by 0.2 psu for both boxes 3 and 4.

Noting that the FBM did not resolve the effects of the initial adjustment phase particularly well the FBM was reinitialised with initial values corresponding to the state of the OGCM at 100 years into the run. By starting 100 years into the run the discrepancies between the 2 models total heat contents were avoided as the OGCM had almost completed the initial adjustment phase (Figure 6 - 2).

6.2.2 The weak non convecting mode.

Like the OGCM the FBM had a long period where there was no convection and a weak meridional overturning cell. During this period the ocean gained heat. In the FBM the temperature of all the boxes rose more rapidly and reached higher values than in the OGCM (Figure 6 - 2). Although the FBM over estimated the temperatures, the shape of, and the differences between the temperature curves was close to those given by the OGCM. However the difference between the temperatures of the tropical and polar deep waters (boxes 3 and 4) was larger in the FBM than the OGCM in the short period just before the thermal flush.

Due to the slight imbalance in the surface salt fluxes the total salt content of the ocean basin steadily increased with time. Like the OGCM the FBM maintained a constant difference between the salinities of the 2 surface boxes, though the FBM exaggerated the increase in the salinity of both surface boxes. Correspondingly the salinity increase of the deep water was smaller in the FBM than OGCM. In the short period before the thermal flush the salinity difference between boxes 3 and 4 increased in the FBM offsetting the temperature difference and making the density differences in both models similar.

6.2.3 The strong thermal flush.

The 7000 year long haline mode was terminated abruptly by a strongly convecting, strongly overturning thermal flush. In the OGCM the ocean basin cooled by 8°C and the salinity became more uniform during the strong thermal flush. The FBM followed these trends but the flush only lasted for 20 years whereas the flush in the OGCM lasted for ≅100 years. As the flush in the

FBM was much shorter than the OGCM the ocean basin (in the FBM) did not cool by the same amount (2°C compared to 8°C). Similarly the salinity was homogenised to a lesser extent in the FBM than the OGCM. This had the effect of leaving the FBM in a state that was warmer than the OGCM and where the salinity differences between boxes were greater than in the OGCM.

6.2.4 The limit cycles (deep decoupled oscillations).

After the strong thermal flush both the OGCM and FBM progressed in series of limit cycles. These limit cycles consisted of long periods with no convection and weak overturning interrupted by flushing events (deep decoupled oscillations). In the OGCM the DDOs had a period of ≅600 years compared to ≅2000 years in the FBM. The character of the DDOs was different for the 2 models as they had different initial conditions but both had a similar cycle of events. During the haline mode the temperatures of all the boxes increased, the OGCM more so than the FBM as the OGCM started from a cooler state. The surface salinities also increased while the salinity of the deep water remains roughly constant (Figure 6 - 2). This mode of circulation was terminated by a thermal flush where heat was lost from the basin. As with the strong thermal flush the FBM under estimated the time the flush lasted for compared to the OGCM and so did not lose as much heat as the OGCM. In both models the flushing event decreased the surface salinity and increased the salinity of the deep water.

When the FBM was initialised with a state corresponding to a point in the weak circulation of the DDOs or the flushing part of the DDO, the agreement between the FBM and OGCM was no better. In this case the FBM took a few thousand years (dependent on the exact starting conditions) to adjust and then settled into the same limit cycle as described above. During the adjustment period the FBM typically had an initial small amount of convection. This was followed by a longer period with no convection and weak meridional overturning where the ocean basin gained heat.

6.2.5 Comparison of the FBM and OGCM density gradients.

In both the FBM and the OGCM the dynamics were driven by the density gradients. The convection was driven by the vertical polar density gradient and the meridional overturning cell by the horizontal deep water density gradient. A comparison of the density gradients (or density differences) gives a measure of the FBM's ability to reproduce the dynamics seen in the OGCM.

The inclusion of the coupled convection and surface boundary conditions scheme ensured that the polar vertical density difference ($\rho_4 - \rho_2$) was always hydrostatically stable (positive). The sub tropical vertical density difference ($\rho_3 - \rho_1$) also remained hydrostatically stable throughout the model run. This was a marked improvement over the enhanced diffusion schemes where the vertical density differences could become negative, giving the physically unrealisable state of large portions of the ocean being hydrostatically unstable. The vertical polar density difference in the FBM followed a similar evolution to that in the OGCM and had a similar magnitude for WC1 (Figure 6 - 3). There was a sharp rise in the density difference after the initial adjustment phase and then a slow decay towards zero in both the FBM and OGCM. From the start of TF1

onwards the density gradients in the 2 models evolve differently. The character of the DDOs differed between the OGCM and the FBM. In the OGCM the polar vertical density difference increased during the weak circulation phase and then was rapidly reduced during the flush, where as the flushes increased the density difference in the FBM. Although both models showed DDOs with similar characteristics in the temperature and salinity the dynamics behind both models was subtly different. The dynamics were dependent on the temperature and salinity differences and so on the relative rates of change of these quantities and not the values themselves. The horizontal deep water density gradient was small for the non convecting circulation modes for both the OGCM and FBM. For both the OGCM and FBM the deep water density difference increased rapidly during a thermal flush but fell too rapidly in the FBM (Figure 6 - 3). The FBM did not model the limit cycles accurately as it could not resolve the local processes that triggered the convective flush in the OGCM.

6.2.6 The FBM as a possible climate model?

The validation of the FBM results against those of the OGCM highlights the processes that the FBM captured adequately and those it did not. The parameterisations employed in the FBM gave the heat and salt fluxes between the boxes to a reasonable degree of accuracy (see chapter IV). It was the combination of the parameterisations and the inherent non linearity of the system that caused the discrepancies between the 2 models. The FBM was able to predict the length and dynamics of the weak non convecting mode with a reasonable degree of accuracy and correctly models the rapid on set of the thermal strong flush. Although the FBM predicted the strength of convection and meridional overturning cell correctly it did not sustain this state for long enough. As the length of the flushes was too short in the FBM the heat loss from the basin was under estimated. Thus if the FBM were used as part of a simple climate prediction model it would be at this point that the prediction would have become invalid.

The FBM does not reproduce the DDOs exactly, and so could not be used as a predictive model. However the FBM did model the temperatures, salinities, heat and salt fluxes to a reasonable degree of accuracy and in a physically justifiable way. Thus the FBM could be used to examine the response of the thermohaline circulation to changes in the parameterisations and forcing in qualitative terms if not quantitative.

The FBM produced results that were physically consistent with the assumptions used to obtain the parameterisations of heat and salt fluxes between the boxes. The strength of the meridional overturning cell was driven by the deep water density gradient which was closely linked to the rate of deep water formation. The convection scheme allowed for the formation of cold, fresh deep water in the polar regions without large portions of the ocean becoming hydrostatically unstable. Using the coupled surface boundary conditions and convection scheme provided a direct connection between the surface cooling and the deep waters which gave the bottom water (formed by convection) reasonable characteristics without strongly altering the surface waters.

In these respects the FBM was able to reproduce the OGCM results by giving the correct dynamics and reasonable water mass characteristics. On a more detailed level the FBM fell short of being a predictive ocean climate model (see above).

The FBM showed similar characteristics to the 3 and 4 box models in chapter II. In that the FBM had both the Haline and Thermally dominated modes which were strongly controlled by the relative strengths of the surface buoyancy forcing. These results are somewhat unusual for a box model as the FBM has a long period before settling into DDOs. In my opinion the coupled surface boundary conditions and convection schemes influence on the polar vertical density gradient is a significant improvement over previous box models.

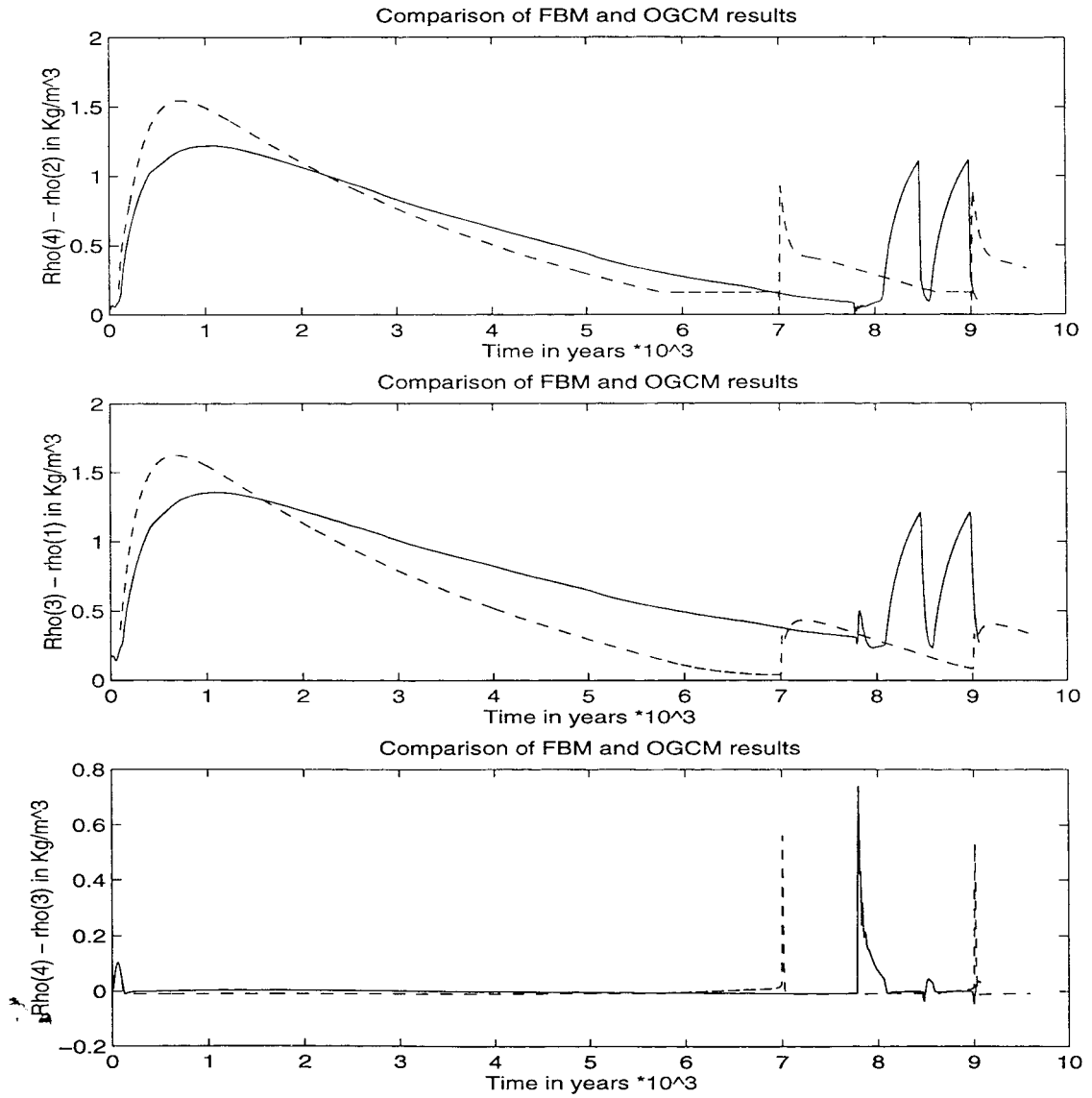

Figure 6 - 3: A comparison of the density differences between the various boxes in the OGCM and the FBM. The dashed line indicates the FBM results and the solid line the OGCM results. The FBM was started from initial conditions corresponding to the state of the OGCM at 100 years and all the parameters were set to the default values excepting the surface horizontal diffusivity of salt which was set to 10^4 m^2/s.

6.3 Response of the FBM to changes in parameters and the surface forcing.

The reduced box model (chapter V) was sensitive to the strength of the meridional overturning, the size of the diffusivities, the relative strengths of the thermal and haline surface buoyancy forcing and to the strength of surface cooling of the convecting area. Results from the reduced model were not sensitive to the other parameters. The FBM contained a large number of parameters so the results from the reduced box model were used as a guide to which parameters the FBM was likely to be most sensitive to. In these sensitivity studies all parameters were fixed at their default values given in Table 6 - 1 unless otherwise stated. The surface fresh water fluxes were set to be balanced so that the total salt content of the model was a conserved quantity. To conduct the sensitivity study the FBM was integrated forward in time for a large number of parameter sets. Since it was not possible to cover all possible initial conditions the results from the sensitivity study were based on a large collection of model runs where 6 different sets of initial conditions were used. These initial conditions were chosen to represent the state of the OGCM when starting (year 0), weakly overturning and no convection (year 100), weakly convecting and no convection with a well developed fresh water cap (year 6000), strong thermal flush (year 7910), weakly overturning no convection portion of the DDOs (year 8100), thermal flush during DDO (year 8500). The choice of initial conditions did not affect the finial state of the model be it a steady state or a limit cycle. This suggested that unlike the reduced model the FBM did not have multiple stable equilibria.

6.3.1 Sensitivity to the parameterisation of the meridional overturning.

The strength of the meridional overturning cell was controlled by 2 parameters, the constant of proportionality to the horizontal deep water density difference (ν_0) and the zero off set (ν_{offset}). From the OGCM data 1 standard deviation in ν_0 was 2 Sv.m^3/Kg and in ν_{offset} was 5 Sv.

Varying ν_{offset} over the range -2 to 14 Sv affects the existence and the period of the DDOs. For ν_{offset} less than 3 Sv the FBM did not oscillate when run for in excess of 80,000 years. Above 3 Sv, increasing ν_{offset} decreased the period of the DDOs and decreased the length of the adjustment phase before the DDOs were seen (Though the length of the adjustment phase was dependent on the initial conditions used) (Figure 6 - 4). Small variations in ν_{offset} had a substantial impact on the period of the DDOs and could cause the FBM to go from a regime where DDOs were possible to one where they were not and there was a steady state solution. These results were similar to those of the reduced box model (chapter V) where, for moderate strengths of meridional overturning cell, increasing the strength of the meridional overturning cell decreased the period of the DDOs. Beyond a critical value (over 3 standard deviations from the estimated value of ν_{offset}) the period of the DDOs increased as ν_{offset} was increased. I can find no direct physical explanation for ν_{offset} despite the models sensitivity to this parameter.

The constant of proportionality between the strength of the meridional overturning and the horizontal deep water density difference (ν_0) had a weak effect on the results of the FBM. Varying ν_0 over the range 300 to 340 Sv.m^3/Kg (10 standard deviations either side of the estimated value) only changed the period of the DDOs by 22%. Increasing ν_0 lengthened the period of the DDOs (Figure 6 - 4).

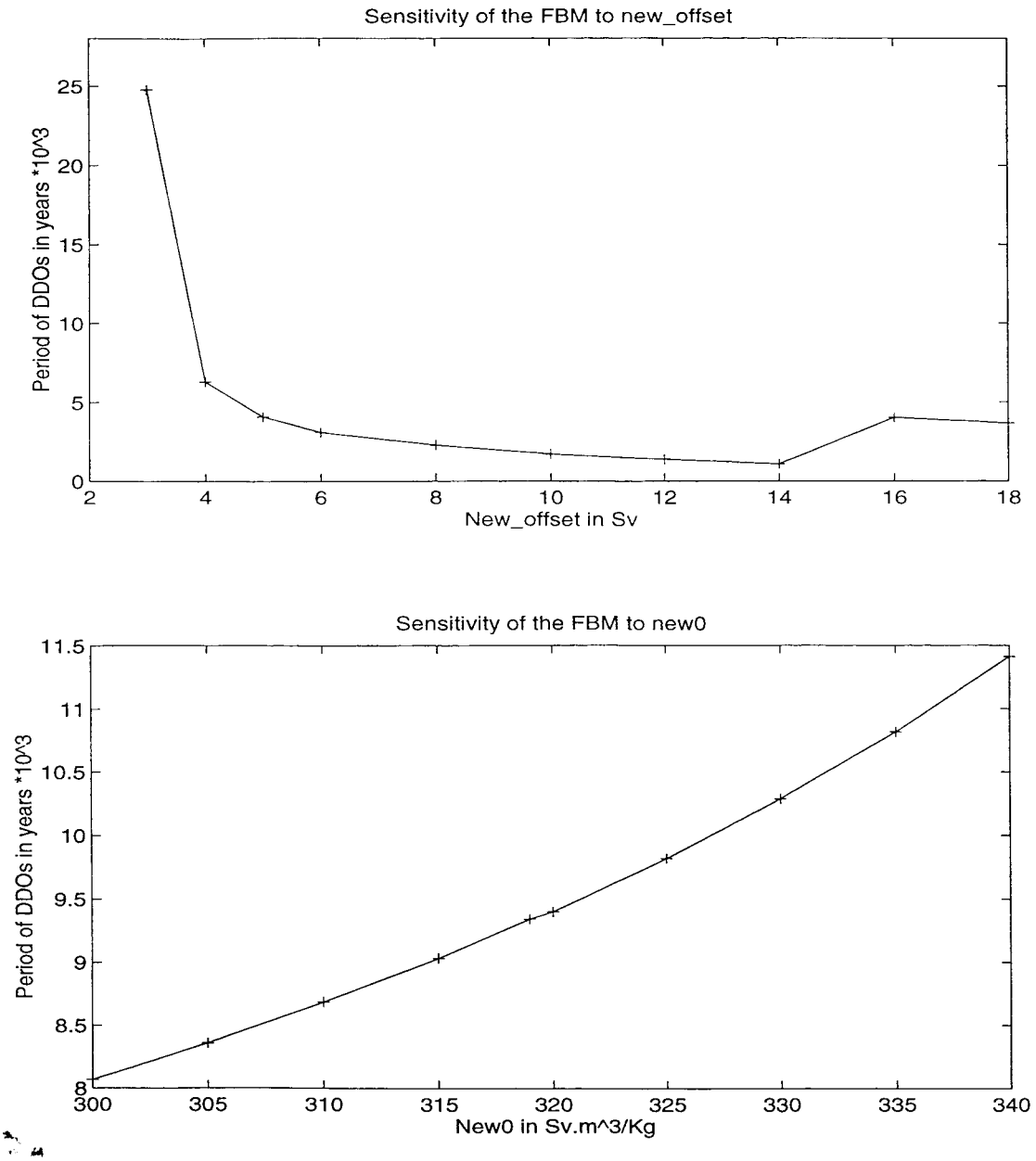

Figure 6 - 4: The variation in the period of the DDOs in the FBM due to differing values of the constant of proportionality between the strength of the meridional overturning cell and the horizontal deep water density difference (ν_0) and the zero off set (ν_{offset}). All other parameters were fixed at their default values.

6.3.2 Response to differing strengths of surface fresh water forcing (q_{total}).

The extra physical processes in the full box model made it much more sensitive to the strength of the fresh water forcing (q_{total}) than the reduced box model. The period of oscillation of the DDOs exhibited by the FBM was strongly dependent on the strength of the surface fresh water forcing, when the strength of the fresh water forcing was close to the default value used in the OGCM (1×10^7 Kg/s of salt). If the surface salt flux was increased beyond 1.1×10^7 Kg/s then the FBM had only a steady state with weak overturning and no convection. For weak haline surface forcing (below 0.8×10^7 Kg/s of salt) the oscillation period of the DDOs was insensitive to the strength of the haline forcing. Even with the thermal and haline surface forcing acting together to drive a positive overturning cell the FBM did not have a stable, convecting, strongly overturning circulation. The FBM was much more sensitive to the surface fresh water forcing than the reduced box model. The region of parameter space in which DDOs were possible was larger in the FBM than the reduced box model.

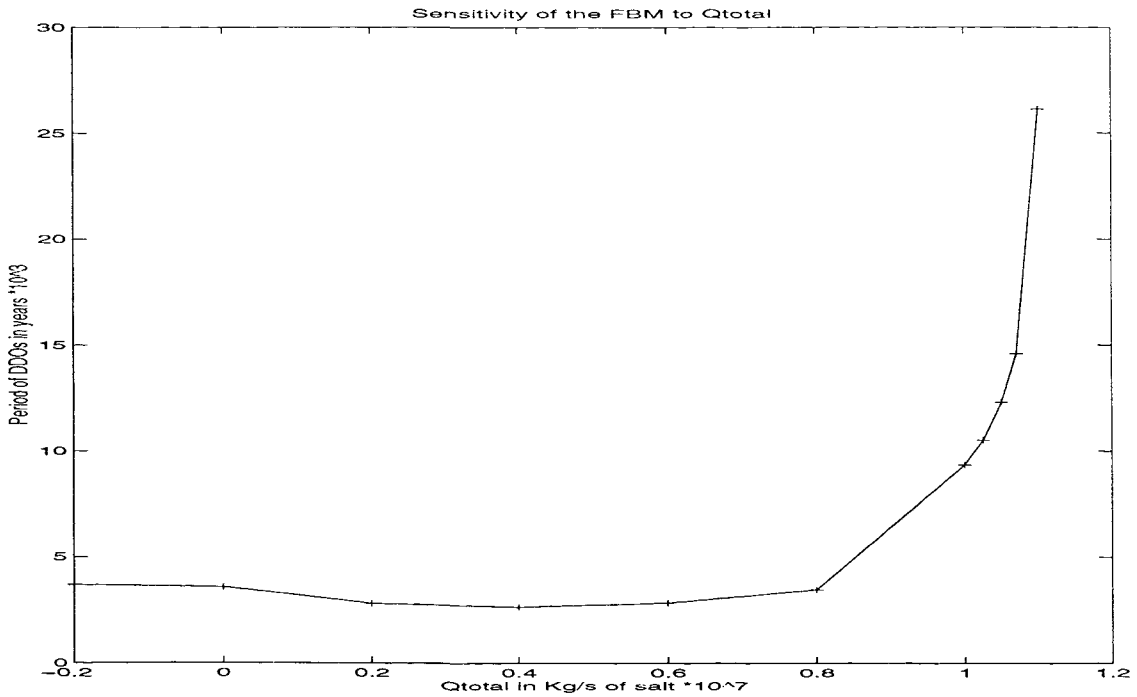

Figure 6 - 5 The dependence of the period of oscillation for the DDOs in the FBM on the strength of the surface haline forcing. The strength of the surface haline forcing is measured as the mass of salt added to box 1 per unit time.

6.3.3 The effects of varying the strength of the surface cooling over the convecting region (Q^0_b).

The FBM was reasonably insensitive to the strength of surface cooling for the convecting region. Varying Q^0_b between 100 and 1000 Watts/m^2 (The value obtained from the OGCM results was 238 Watts/m^2) only altered the period of oscillation of the DDOs by 24%. Both increasing and decreasing the strength of the cooling from 238 Watts/m^2 increased the oscillation period.

6.3.4 The sensitivity of the FBM to the vertical diffusivities of salt and heat.

Unlike the reduced box model the existence of and the period of oscillation of the DDOs seen in the FBM was strongly influenced by the sizes of all 4 vertical diffusivities ($k^T_{v\ pole}$, $k^T_{v\ equator}$, $k^S_{v\ pole}$ and $k^S_{v\ equator}$). The response of the model to varying the vertical diffusivities of heat was similar for both $k^T_{v\ pole}$ and $k^T_{v\ equator}$. Increasing the thermal diffusivities decreased the period of oscillation while reducing the vertical diffusivities of heat had the opposite effect. Reducing $k^T_{v\ pole}$ or $k^T_{v\ equator}$ too far ($k^T_{v\ equator} < 0.45\times10^{-4}$ m^2/s or $k^T_{v\ pole} < 0.30\times10^{-4}$ m^2/s) gave the FBM a steady state with weak overturning and no convection and DDOs were not observed. The period of the DDOs was much more sensitive to changes in the thermal diffusivities at small diffusivities than large diffusivities.

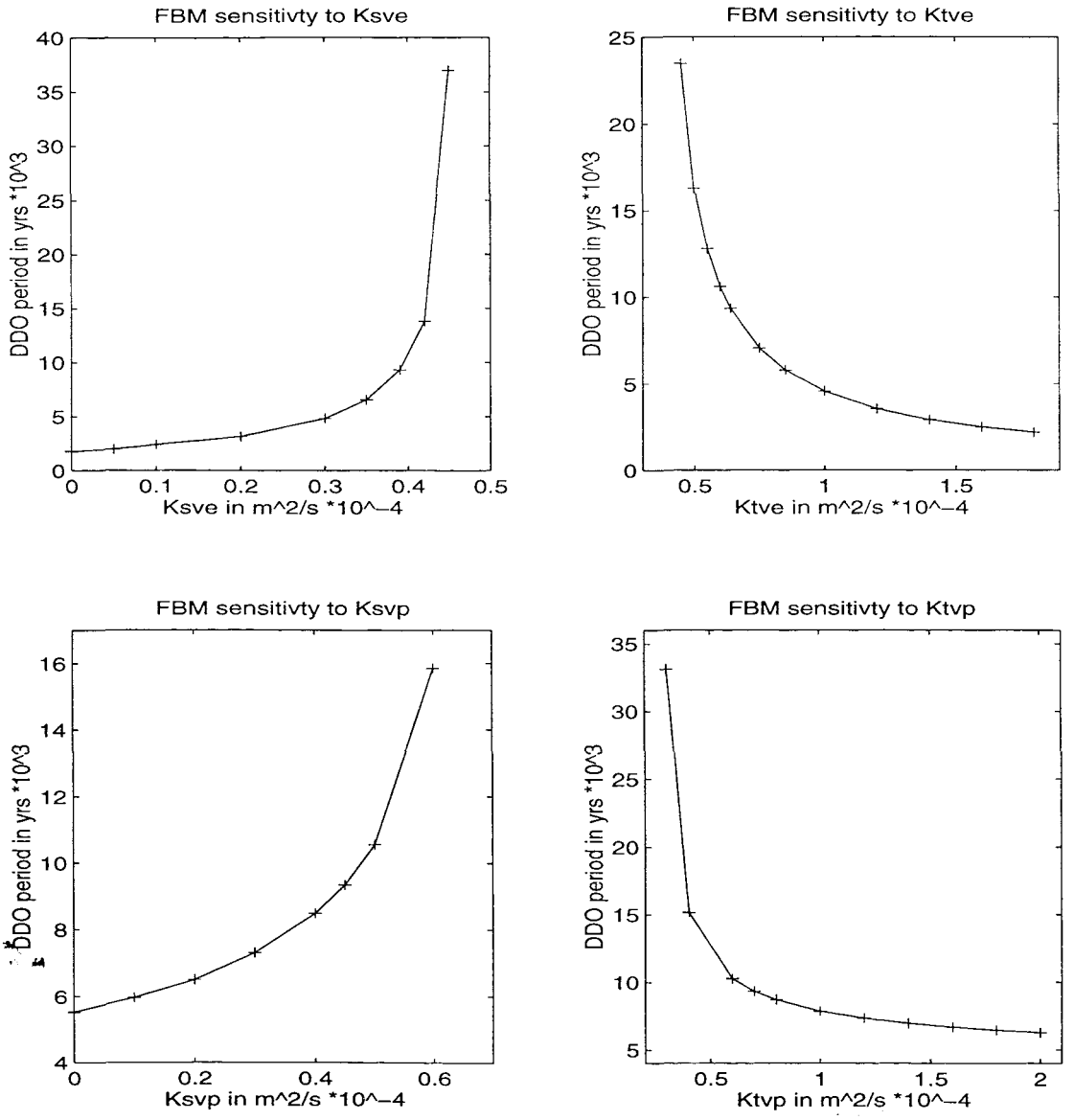

Figure 6 - 6: The effect of the vertical diffusivities on the period of oscillation of the DDOs in the FBM. The 4 diffusivities are indicated by Ktvp for $k^T_{v\ pole}$, Ktve for $k^T_{v\ equator}$, Ksvp for $k^S_{v\ pole}$ and Ksve for $k^S_{v\ equator}$.

The FBM behaved similarly to variations in the vertical diffusivity of salt for the polar and equatorial boxes, $k^S_{v\ pole}$ and $k^S_{v\ equator}$ respectively. High diffusivities gave long periods of oscillation while low diffusivities gave shorter periods of oscillation. In both cases there was a maximum diffusivity at which DDOs were still observed ($k^S_{v\ pole} > 0.60$ or $k^S_{v\ equator} > 0.45$). Beyond this the FBM had a weakly overturning, non convecting steady state. The period of oscillation was much more sensitive to increases in the diffusivities from the default value than decreases from the default value ($k^S_{v\ pole} = 0.39\times10^{-4}$ m^2/s and $k^S_{v\ equator} = 0.45\times10^{-4}$ m^2/s).

6.3.5 Sensitivity of the FBM to changes in the horizontal diffusivities of heat and salt.

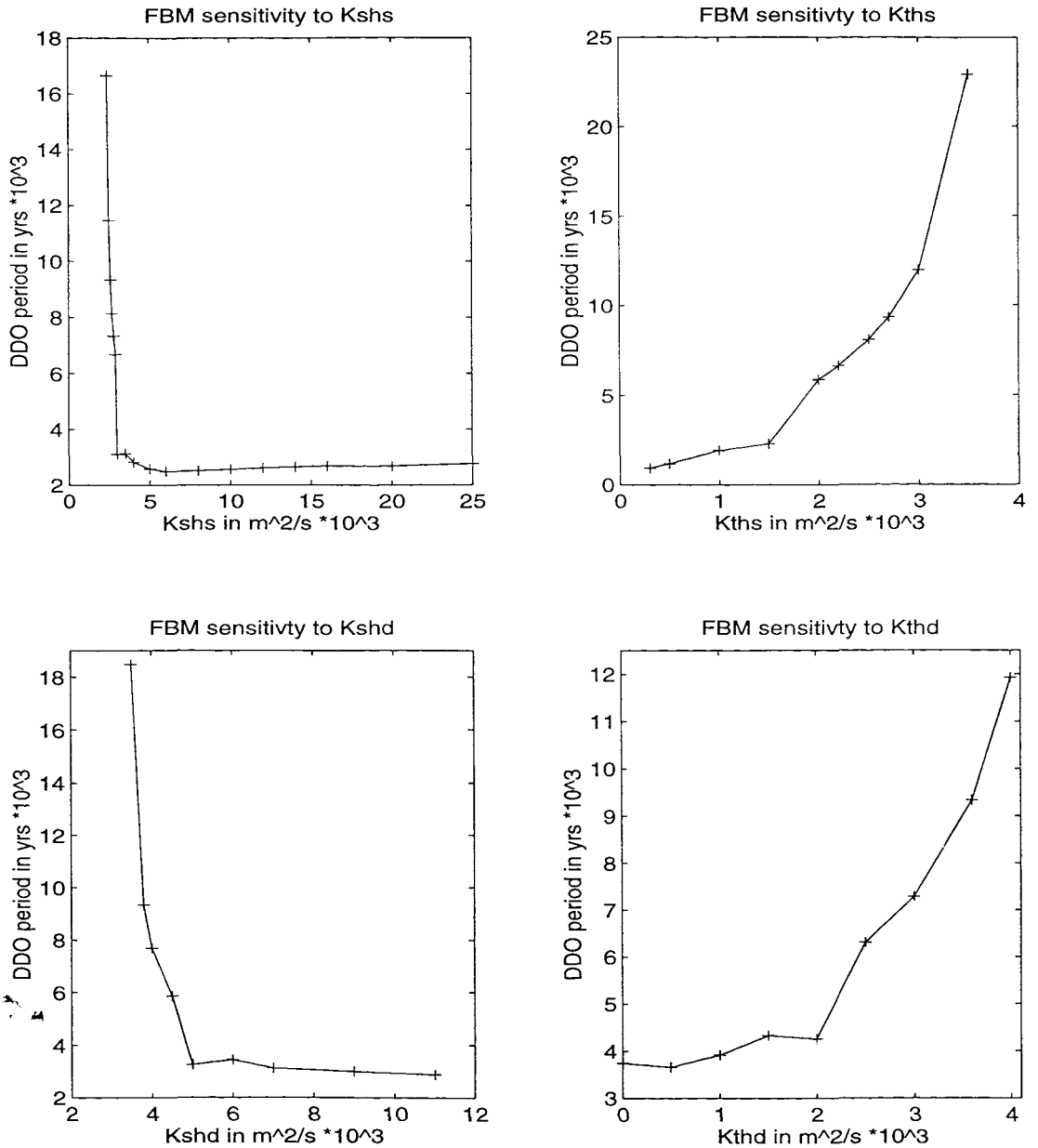

Figure 6 - 7: The effect of varying the horizontal diffusivities of temperature and salt on the period of oscillation of the DDO observed in the FBM. The diffusivities are indicated by Kshs for $k^S_{h\ surface}$, Kshd for $k^S_{h\ deep}$, Kths for $k^T_{h\ surface}$ and Kthd for $k^T_{h\ deep}$.

The FBM was as responsive to changes in the horizontal diffusivities as it was to variations in the vertical diffusivities (section 6.3.4). As with the vertical diffusivities responses to changes in both the thermal and both the haline diffusivities were qualitatively similar, though the magnitudes of the responses differed.

The period of oscillation of the DDOs was very sensitive to the value of the haline horizontal diffusivity close to the default values. For small haline horizontal diffusivities there was a long period of oscillation. Below a critical value ($k^S_{h\ surface} < 2.4\times10^3$ m^2/s or $k^S_{h\ deep} < 2.5\times10^3$ m^2/s) DDOs were no longer observed and the FBM had a steady state. For large horizontal diffusivities of salt the period of oscillation was short and independent of the value of diffusivity. Similarly close to the default value of the thermal diffusivities the period of oscillation was sensitive to the size of diffusivity and for small diffusivities the period of oscillation became insensitive. For large values of the horizontal thermal diffusivities ($k^T_{h\ surface} > 3.5\times10^3$ m^2/s or $k^T_{h\ deep} > 4.0\times10^3$ m^2/s) the FBM had a steady state and DDOs were not observed.

6.3.6 The affect of the convective time scales (τ_S and τ_T) on the evolution of the FBM.

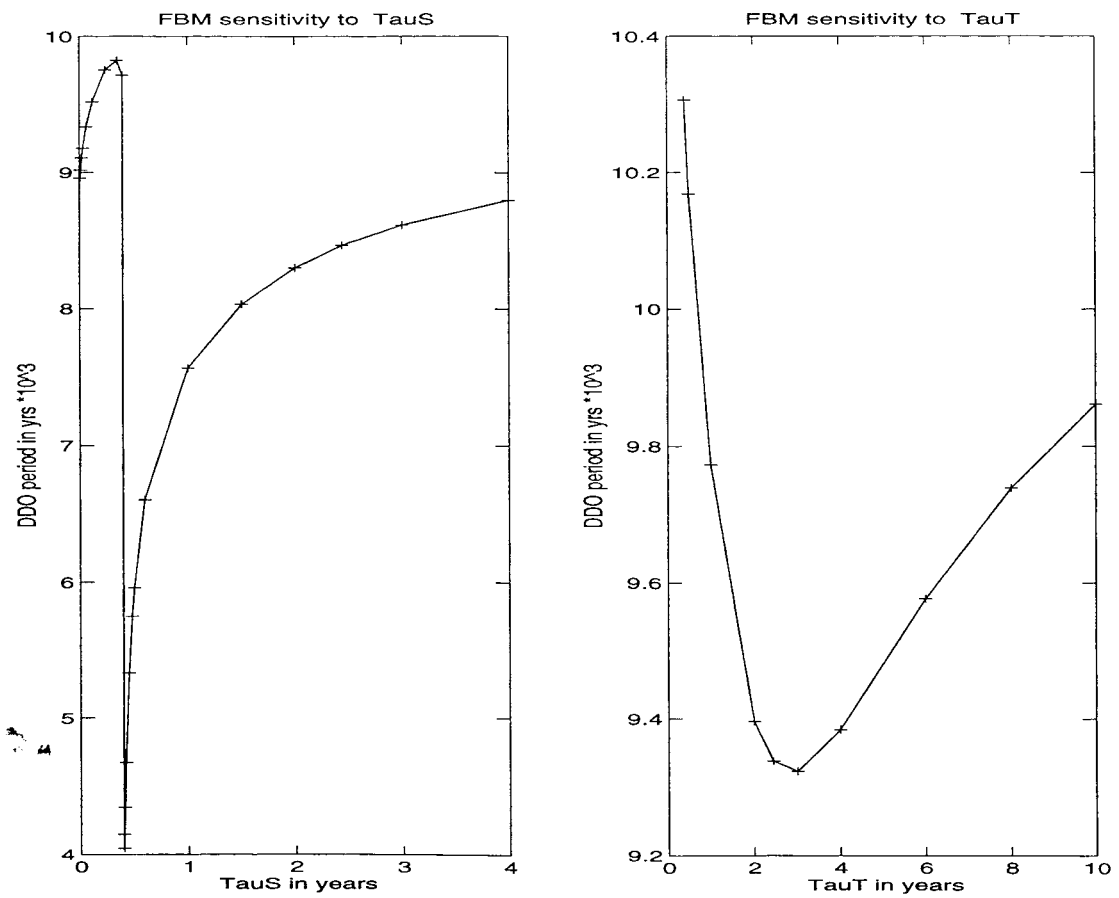

Figure 6 - 8: The variation of the period of oscillation during the DDOs of the FBM as affected by the thermal and haline convective time scales. The convective time scales are indicated by TauS for τ_S and TauT for τ_T.

Close to the default values the FBM results were insensitive to the convective time scales for both salinity and temperature. The period of oscillation of the DDO varied very little with changes in the thermal convective time scale, but if this time scale was reduced below a critical value (τ_T < 0.4 years) the FBM had a steady state (weak overturning and no convection) and DDOs were not observed. The FBM results were also insensitive to the value of τ_S in the range given by the OGCM results. If τ_S was increased to a similar value to τ_T the sensitivity increased, especially near τ_S = 0.4 years where there was a sharp jump in the DDO period (The period jumps from 9720 years for τ_S = 0.4 years to 4150 years for τ_S = 0.4001 years).

6.3.7 Interpretation of the sensitivity of the FBM to the model parameters.

The sensitivity study presented above was by no means comprehensive as only a limited number of parameter values were tested for each of the model parameters. For each of those values only a small set of initial conditions were used. The use of a small set of initial conditions was to some extent justified by the reduced box model results that showed that when multiple stable (to finite perturbations) equilibria existed both equilibria had large regions of attraction. In all cases the FBM results were independent of the choice of initial conditions suggesting that the final state of the model (be it a limit cycle or a steady state) was the only possible long time solution for all initial conditions.

An intercomparison of the sensitivity of the FBM to the model parameters is summarised in Table 6 - 2. The table lists the percentage change in the period of oscillation for the observed DDOs from the default value (that obtained using the default values for all the parameters) for 0.1, 0.9, 1.1 and 2.0 times the default value for the given parameter (0.1×θ, 0.9×θ, 1.1×θ and 2.0×θ). Also listed are the percentage changes in oscillation period of 1 standard deviation either side of the default value for the parameter (+σ or -σ). The standard deviations were obtained from the least squares fits that derived the default parameter values from the OGCM data and as such were not available for all the parameters. In my opinion the standard deviations obtained from the fits to the OGCM data for the diffusivities, especially of salinity, grossly under estimated the uncertainty in the parameters. I feel that the changes in oscillation period due to altering the parameter by 1 standard deviation should be used as a guide to relative sensitivity of the FBM to the parameters and not as estimates of the errors in the predictions made using the FBM.

As with the box models reviewed in chapter IV the DDOs in the FBM were driven by the competing affects of the meridional temperature and salinity gradients set up by the surface buoyancy forcing. During the long uncoupled phase the salinity gradient was dominant while the temperature gradient prevailed in the shorter thermal flushes. As the uncoupled phase lasted many times longer than the coupled flushing circulation the period of oscillation was controlled by the length of the uncoupled phase and not the thermal flush.

Enhancing the salinity gradient relative to the temperature gradient, by decreasing the horizontal diffusivities of salt, increasing the horizontal thermal diffusivities or increasing the surface fresh

water flux, lengthened the period of oscillation. If the meridional salinity gradient was increased sufficiently the haline driven mode became a stable state and the thermal flushes were inhibited.

Parameter	$0.1 \times \theta$	$0.9 \times \theta$	$1.1 \times \theta$	$2.0 \times \theta$	$+\sigma$	$-\sigma$
$k^T_{v\ equator}$	no oscil.	+25%	-14%	-65%	-0.9%	+1.3%
$k^T_{v\ pole}$	no oscil.	+7%	-5%	-26%	-0.3%	+0.4%
$k^T_{h\ surface}$	-91%	-17%	+25%	no oscil.	+2.0%	-1.4%
$k^T_{h\ deep}$	-61%	-13%	+25%	no oscil.	+1.5%	-0.8%
$k^S_{v\ equator}$	-79%	-29%	+122%	no oscil.	+3.7%	-1.7%
$k^S_{v\ pole}$	-39%	-8%	+12%	no oscil.	+11.7%	-8.3%
$k^S_{h\ surface}$	no oscil.	no oscil.	-26%	-73%	-2.0%	+3.5%
$k^S_{h\ deep}$	no oscil.	no oscil.	-25%	-67%	-2.0%	+7.4%
q_{total}	-66%	-28%	no oscil.	no oscil.	n/a	n/a
ν_{offset}	no oscil.	+116%	-23%	-73%	-77.0%	n/a
ν_0	-76%	-21%	+40%	no oscil.	1.4%	-1.6%
Q_b^0	+47%	+0.2%	+0.2%	+8%	-0.005%	+0.01%
τ_T	no oscil.	+0.3%	-0.1%	+1.4%	n/a	n/a
τ_S	-4%	-0.3%	+0.2%	+2%	n/a	n/a

Table 6 - 2: Sensitivity of the period of the DDOs to changes in the model parameters (see text for more detail).

Increasing the equatorial vertical diffusivity of heat transferred heat from the surface to the deep water faster. As there was a strong coupling between the 2 deep boxes this warming was transferred to the polar box. The more rapid warming of the deep polar box hastened the thermal flush as it decreased the polar vertical density difference. Thus the equatorial vertical diffusivity of heat affected the period of oscillation by controlling the rate of heat transfer to the deep polar box and so the density of the deep polar box. Similarly the equatorial vertical diffusivity of salt controlled the rate of salt transfer from the equatorial surface box to the deep water. Increasing the equatorial vertical diffusivity of salt increased the salt transfer to the deep water making the deep polar box saltier and so increasing the vertical polar density difference. The increased density difference inhibited the thermal flush and so lengthened the period of the DDOs.

The mechanism that controlled the response of the FBM to the polar vertical diffusivities was not clear. Altering the polar vertical diffusivities changed the deep water density gradient and so the strength of the meridional overturning. Although the meridional overturning was weak (less than

3 Sv) the small change in the advective fluxes dominated the initial changes in diffusivity. Increasing the thermal diffusivity (or decreasing the haline diffusivity) strengthened the meridional overturning cell and enhanced the advective mixing. The extra mixing reduced the vertical polar salinity and density gradient, thus promoting convection and the associated thermal flush. This shortened the period of oscillation. Changing the polar vertical diffusivities in the opposite direction had the opposite effect of lengthening the DDO period.

There was no obvious mechanism that governs the response of the FBM to changes in the coupling between the deep water density gradient and the strength of the meridional overturning cell. When ν_{offset} was increased it did not result in a stronger meridional overturning cell, rather the overturning strength decreased and the deep water became cooler and the oscillation period shorter. The reverse was true for a decrease in ν_{offset}. Conversely increasing ν_0 did increase the strength of the overturning cell but resulted in longer oscillation periods.

6.4 Response of the FBM to time dependent forcing.

In all the previous model runs there was no intrinsic time dependence in any of the forcing parameters. To assess the response of the model to time dependent forcing a stochastic component was added to the freshwater flux. To maintain the total salt content of the ocean the surface salt flux in to box 1 and out of box 2 remained equal but the magnitude was altered with time. The stochastic forcing was implemented by multiplying *qtotal* (Equation 6 - 6) by a time dependent constant. The time dependent constant varied with a uniform distribution over a set range with a prescribed time scale. Thus the time dependent constant would remain fixed for a given period of time and then have a new value chosen from a uniform distribution. This caused the value of *qtotal* to have a constant value (picked at random from a specified range with a uniform probability distribution) for a set period of time. The a new value was chosen for *qtotal* (from the same uniform distribution) and the model run continued for the same set period of time.

The FBM was run with the size of the perturbations in the surface salt flux varying from 1% to 90% of the default value (default value was qtotal=1×10^7 Kg/s of salt) and with the time scale varying from 1 day to 10 years. In all cases DDOs were observed that had the same circulation modes as described in section 6.2.4. The perturbations to the surface fresh water flux caused fluctuations in the surface salinities and to a lesser degree fluctuations in the salinity of the deep water. These fluctuations lead to oscillations in the strength of the meridional overturning cell. In all cases the FBM was run for 4 oscillations of the DDOs and the mean and sample standard deviation of the periods of oscillation calculated.

Adding a stochastic component to the surface forcing tended to increase the oscillation period (Figure 6 - 9). There was a weak dependence between the size of the perturbation and the increase in the period of oscillation, the larger the perturbation, the longer the period of oscillation. The period that the perturbation was applied for had no relation to the change in the mean period of the DDOs (Figure 6 - 9). As anticipated the larger the fluctuation in the fresh

water flux the higher the variability of the oscillation period. The time that the perturbation was applied for had some affect on the variability in the period of the DDOs. The variability was high when the perturbation had a time scale of 7 to 30 days. When the period was lengthened to between 6 months and 5 years the variability dropped. Lengthening the time period further increased the variability in the period of the DDOs.

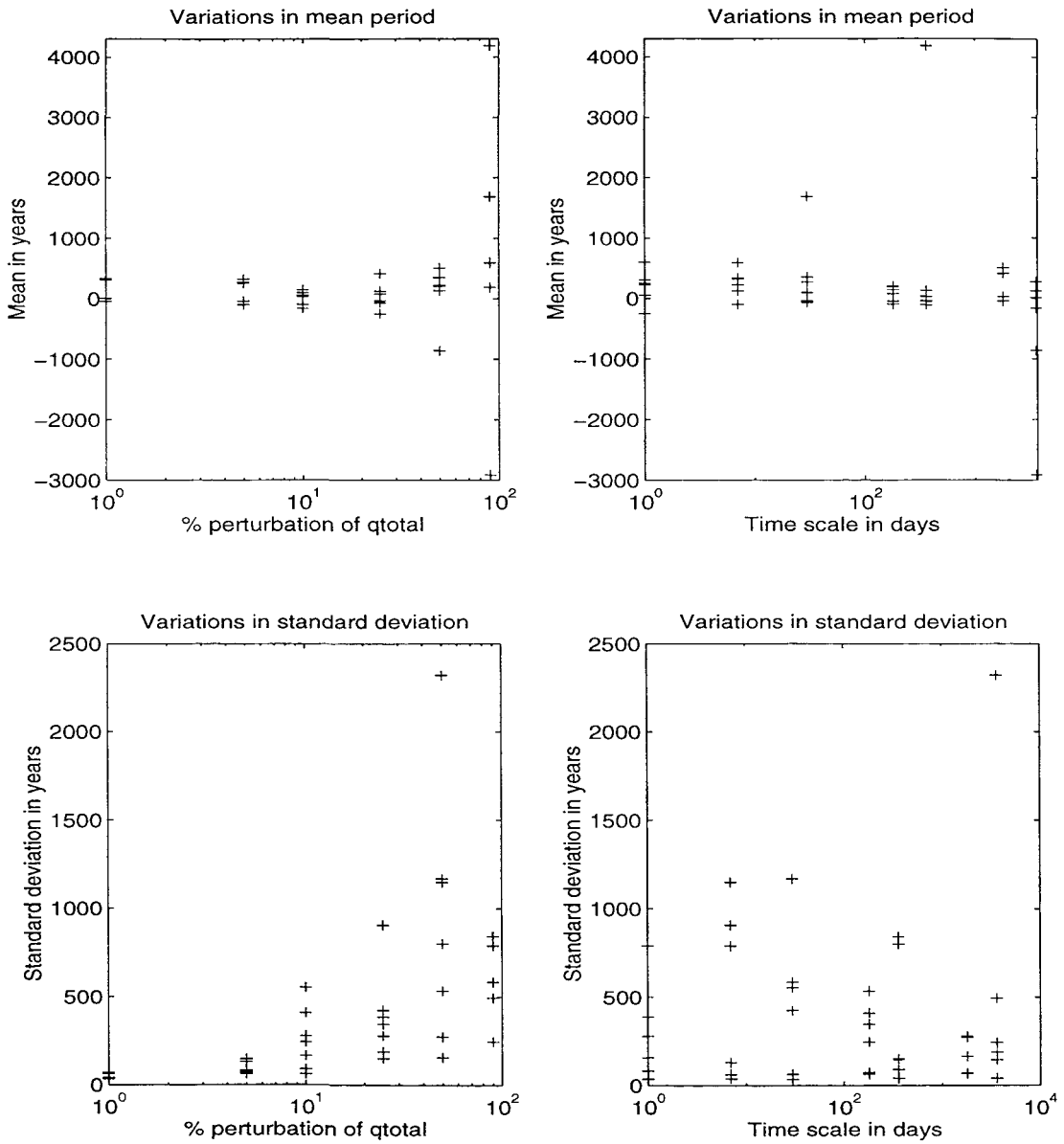

Figure 6 - 9: Variations in the mean and standard deviation of the oscillation period of the DDOs in response to fluctuations in the surface salt flux (*qtotal*). The random fluctuations to the surface salt flux were controlled by 2 parameters, the magnitude of the fluctuation (expressed as a percentage of the default value of *qtotal*) and the period for which the perturbation was applied before changing magnitude. The variation in the mean has been plotted with the zero line being equivalent to the mean oscillation period of the FBM without stochastic random forcing.

Chapter VII

Discussion and future work

7.0 Summary.

A coarse resolution single hemisphere, single basin, OGCM was run for just over 9000 years. The OGCM results showed multiple modes of thermohaline circulation that included an initial adjustment phase, 2 different haline dominated modes, 2 strengths of thermal flushes, deep decoupled oscillations and salt loop oscillations (chapter III). These circulation modes were examined in some detail and the dominant mechanisms for heat and salt transport identified. The stability and longevity of the modes of the thermohaline circulation were related to the strengths of the stabilising and destabilising feedbacks controlling each circulation mode.

The OGCM domain was divided into 4 boxes, the surface and deep waters of the sub polar and sub tropical gyres. For each box the mean temperature and salinity was calculated along with the heat and salt fluxes between the boxes. The heat and salt fluxes between the 4 boxes were calculated separately for diffusion, advection, convection and the surface forcing (chapter IV). Taking each process separately the heat and salt transport was parameterised in terms of the mean temperatures and salinities of the boxes. The parameterisations developed were able to estimate the tracer fluxes found in the OGCM from the mean temperatures and salinities with a reasonable degree of accuracy. To model the effects of bottom water formation by deep convection at high latitudes it was necessary to couple the effects of the high latitude surface forcing and convective mixing. This coupled surface forcing and convection scheme provided a direct connection between the surface buoyancy forcing and the deep waters (section 4.6). The strength of the meridional overturning cell was related to the deep water density gradient. Results from the OGCM suggested a linear relationship between the strength of overturning and the deep water density gradient, though there was a zero offset. The box model was very sensitive to the size of this zero offset.

The consequences of using the coupled surface boundary conditions and convection scheme were investigated using a reduced box model (chapter V). This reduced box model had 2 active boxes representing the surface and deep waters of the sub polar gyre. Heat and salt fluxes between the 2 active boxes were modelled using the parameterisations developed from the OGCM data while all other forcings were treated as variable parameters of the model. The reduced box model was constructed such that analytic solutions for the steady states were possible. This enabled a thorough study of the model's parameter space. Multiple stable equilibria were found for both an enhanced diffusion convection scheme and the coupled scheme developed from the OGCM data (chapter V). Deep decoupled oscillations were not possible in the reduced box model when an enhanced diffusion convection scheme was used though they were feasible when the coupled scheme was employed. The number type and stability of the possible equilibria of the reduced box model were determined over a large region

of parameter space for both types of convection scheme. Where oscillations were observed the influence of the model parameters on their strength and period of oscillation was determined.

Using the parameterisations developed from the OGCM data (chapter IV) a 'full box model' was developed. This full box model (FBM) consisted of 4 boxes that represented the surface and deep waters of the sub polar and sub tropical gyres making it directly comparable to the binned OGCM results. Integrating the full box model forwards in time from initial conditions equivalent to the initial conditions used for the OGCM the FBM was able to reproduce the main elements of the OGCM run. When compared to the OGCM the FBM was capable of making quantitative predictions of the circulation and length of the haline driven, weak circulation modes. However the FBM consistently under estimated the life time of the thermal flushes observed in the OGCM. The FBM did not exhibit multiple equilibria and only haline dominated weak circulations were found as steady states. Deep decoupled oscillations were seen over a large region of the parameter space. Guided by the results from the reduced box model a sensitivity study of the FBM was performed. The period and strength of the DDOs was highly sensitive to a number of the model parameters, with the period of oscillation changing by over 70% when the zero offset in the parameterisation of the strength of the meridional overturning cell was altered by 1 standard deviation (section 6.3).

The response of the FBM to time varying surface forcing was investigated by adding a stochastic component to the surface fresh water flux. This extra surface forcing altered the period and variability of the DDOs.

7.1 Discussion of the OGCM.

After spinning up the OGCM using restoring boundary conditions for both temperature and salinity the surface salt flux for the equilibrium state was diagnosed. On swapping to mixed boundary conditions using this diagnosed salt flux the equilibrium state was non longer stable and the OGCM had a strongly convecting, strongly overturning adjustment phase that lasted for ≈100 years (chapter III). This instability of the equilibrium state on switching to mixed boundary conditions is characteristic of OGCMs that use a diagnosed salt flux for the surface salinity forcing (section 2.1.2). Switching from restoring boundary conditions to mixed boundary conditions strengthened the effect of the haline advective feedback which destabilised the thermohaline circulation.

7.1.1 The haline dominated weak circulation modes of the OGCM.

Following the initial adjustment phase the OGCM had a long period when the thermohaline circulation was in a haline dominated mode (section 3.4). The circulation during this mode was very similar to the circulations during the haline dominated, weak circulations of the DDOs found later in the OGCM run. In these circulation modes the deep water was decoupled form the surface waters by a weak pycnocline. Deep water formation by convection was inhibited by a fresh water cap that covered the surface of the sub polar gyre. Warm salty intermediate water was formed by convection that penetrated down to the top of the pycnocline between the 2

surface gyres on the eastern boundary. Throughout these haline dominated modes the deep water gained heat. The heat was transported from the surface down to the pycnocline mainly by advection. Particle tracking showed that the warm waters of the sub tropical gyre spiralled downwards to the pycnocline and slightly cooler waters spiralled upwards in the sub polar gyre (section 3.4.2). Heat was transported across the pycnocline in to the deep waters mainly by diffusion.

Similar modes of weak circulation have been observed in OGCMs using mixed boundary conditions or restoring boundary conditions with long relaxation times for the sea surface salinity forcing (chapter II). In all cases these haline dominated modes were dependent on the convective feedback mechanism (section 1.3.3) being strong enough that a polar halocline catastrophe occurred. Results from coupled O-AGCMs and OGCMs with other types of more realistic forcing (EBMs or the modified Haney condition of Rahmstorf (1994)) indicate that mixed boundary conditions over emphasise the convective feedback mechanism (section 2.1.1). The short relaxation time used in the Haney boundary condition in the OGCM eliminated the stabilising effect of the thermal advective feedback (section 1.3.2). Thus the OGCM was overly biased towards the haline dominated modes of circulation as the stability of thermally dominated modes was under estimated.

The life time of the weak circulation modes during the DDOs was ≈10 times shorter than the life time of the initial haline dominated mode. The difference in life times was caused by variations in the sub surface salinity fields of the sub polar gyre. In all 3 cases the weak circulation was broken by the on-set of deep convection. This deep convection first occurred in the region of weakest vertical stratification. For all 3 cases the surface salinity perturbation required to trigger the deep convection was ≈0.1 psu (section 3.6).

If the surface buoyancy forcing had contained a time dependent component (to represent the high frequency noise present in the atmosphere) the life time of the initial haline dominated mode would have been shorter, though the period of the DDO would have increased (section 2.1.2 and section 6.4). The extra variability in the sea surface temperature and salinity would probably have created anomalously dense water triggering convection earlier. In addition to a bias towards the haline dominated modes the OGCM probably over estimated the life times of these modes.

7.1.2 The thermally dominated flushes of the OGCM.

The haline dominated modes of the OGCM were terminated by thermal flushes. During these flushes there was a strong meridional overturning cell driven by the formation of cold, fresh, dense bottom water by deep convection. Throughout the thermal modes the ocean rapidly lost heat to the 'atmosphere'. The circulation in all 3 flushes was similar though much stronger in the first flush. Differences in the strengths of the 3 thermal flushes were caused by variations in the length of the preceding haline dominated mode. Before the initial thermal flush the haline dominated mode lasted for ≈10 times longer than the other 2 cases. Thus the total heat content

and potential energy of the ocean before the first flush was much higher than for the other 2. As the thermal flushes were reliant on the stored potential energy to drive the strong overturning cells, the initial flush was stronger and lasted longer than the following 2.

In these thermally dominated modes deep convection occurred along the polar boundary of the model domain. The distance that this region of deep water formation extended towards the equator was controlled by the temperature of the deep water (section 3.5.3). There were strong temperature, salinity and density fronts along the interface (that ran zonally) between the convecting and non convecting regions. Along this front were strong geostrohpic currents that formed a zonal overturning cell (section 3.5.2). The meridional overturning cell was an extension of this zonal cell with most of the meridional circulation being concentrated in western boundary currents. The strength of the meridional over turning was a constant $^2/_3$ of the zonal overturning cell (section 3.5.4 and appendix E - Relation between the strength of the meridional overturning cell and the deep water density gradient).

The very high rates of meridional overturning (>250 Sv) in the OGCM were caused by the large amount of potential energy gained by the ocean during the haline dominated modes. As the OGCM over estimated the life time of the initial haline dominated mode it also over estimated the strength of the first thermal flush. The 60 Sv overturning cells found in the DDOs were of similar magnitude to those found in other OGCMs (chapter II) and probably a more realistic estimate of the strength of a possible thermal flush.

7.1.3 OGCM resolution and the convection scheme.

The coarse resolution of the OGCM was required so that the model could be run for a long time period (requiring a large number of time steps) in a reasonable amount of computer time. Using this low resolution reduced the speed of fast propagating waves along the western boundary (section 2.3). This probably caused the OGCM to over estimate the time lag in the response of the thermohaline circulation to changes in the high latitude surface forcing and tracer fields. As the influence of the stabilising (negative) feedbacks on the thermohaline circulation was small compared to the strength of the destabilising (positive) feedbacks the increase in the time lag was unlikely to destabilise the thermohaline circulation further (introducing a time lag into a negative feedback can cause the feedback to become destabilising rather than stabilising).

Using the NCON convection scheme rather than a complete mixing scheme altered the life time of the haline driven modes. The results from the FBM indicate that the surface forcing was not near the critical limit where the thermal mode may have become stable so the choice of convection did not strongly influence the stability of the thermohaline circulation (section 2.2.2).

7.2 The parameterisation of the heat and salt fluxes.

The OGCM results were binned into 4 boxes that corresponded to the 4 boxes used in the FBM. The mean temperature and salinity for each box was calculated along with the heat and salt fluxes into each of the boxes. By obtaining relationships between the heat and salt fluxes into the boxes and the mean temperatures and salinities of the boxes it was hoped to develop a set of parameterisations for use in the FBM. By comparing the predictions for the tracer fluxes made by the parameterisations and the binned OGCM data the accuracy of the parameterisations was estimated (chapter IV).

7.2.1 The advective fluxes.

The advective fluxes between the boxes were parameterised using a centred differencing scheme (section 4.2). The approximation that the advective flux between 2 boxes was proportional to the strength of the meridional overturning cell multiplied by the mean value of the temperatures or salinities of the 2 boxes had a very high correlation to the OGCM data. The strength of the meridional overturning cell was linearly related to the density difference between the 2 deep water boxes. There was a small zero offset that gave a positive overturning cell for no meridional density gradient (section 4.2.1). The correlation between the parameterised fluxes and the actual fluxes in the OGCM was 0.8 and a typical discrepancy in the heat or salt flux between the parameterisation and the binned OGCM data was ±10%.

7.2.2 The diffusive fluxes.

Fluxes of heat and salt due to diffusion were parameterised as being proportional to the relevant tracer difference (section 4.3). This parameterisation gave the fluxes to the correct order of magnitude and ensured that the fluxes were always down gradient, though the correlation with the OGCM data was not high.

The effective diffusivities obtained for the parameterisations were within a factor of 2 of those used in the OGCM. Although the diffusivities for heat and salt were the same in the OGCM, they differed for the box model.

7.2.3 The surface boundary conditions for the sub tropical box (box 1).

The surface heat flux into the surface sub tropical box was modelled by a Haney term with an effective atmospheric temperature of 19.9±0.2°C and a relaxation time of 208±2 years. This parameterisation worked best for low sea surface temperature where the surface heat flux was high. The accuracy decreased as the surface heat flux decreased (section 4.5.1).

The surface fresh water (or salt flux) translated directly from the OGCM surface boundary conditions. So there were no discrepancies between the surface fresh water flux used in the FBM and the OGCM (section 4.5).

7.2.4 The coupled polar surface boundary conditions and convection scheme.

To correctly model the convective heat flux between the 2 sub polar boxes it was necessary to consider the effects of convective mixing and the surface boundary conditions together (section 4.6). The coupled convection scheme developed allowed for a variable proportion of the 2 polar boxes to convect. The surface heat and salt fluxes into the convecting region were applied to both the surface and the deep boxes. This formed a direct connection between the surface buoyancy forcing and the deep water. In parameterising the surface heat flux the size of the convecting region was taken into account thus approximating to the variation of the 'atmospheric' temperature with latitude (section 4.6.1). The proportion of the sub polar boxes that was convecting was related to the vertical density difference between these 2 boxes (section 4.4.1). This coupled scheme had 3 advantages over the more traditional complete mixing or enhanced diffusion schemes:

- The coupled scheme modelled the heat fluxes into the 2 polar boxes much more accurately than either the complete mixing or enhanced diffusion schemes (section 4.6.1).
- The coupled scheme produces cold, dense deep water by providing a direct connection between the surface boundary conditions and the deep water. Thus the coupled scheme does not have to mix the surface waters to form deep water and so is closer to the 'chimney' view of convection (Alves 1995). The complete mixing and enhanced diffusion schemes form bottom water by mixing the surface and deep boxes.
- The coupled scheme inhibits the polar vertical density gradient from becoming hydrostatically unstable by forcing the deep water box towards a higher density than the surface box. Both the complete mixing and enhanced diffusion schemes drive the vertical density gradient towards being neutrally stable which is unphysical for such large portions of the ocean.

7.3 The reduced box model.

The reduced box model examined the effects of using the coupled convection scheme rather than the enhanced diffusion convection scheme (chapter V). When the enhanced diffusion scheme was used the reduced box model had either 1,2 or 3 possible equilibria (assuming that a piece wise linear scheme was being used). These equilibria were characterised by the strength of convection i.e. no, weak or strong convection. The no and strong convection states were stable to finite perturbations while the weakly convecting equilibria were not (section 5.2.2). The number and type of equilibria was dependent on:

- The choice of convection scheme (step, piece wise linear or smooth);
- The strength of the meridional overturning cell;
- The temperature of the deep tropical waters;
- The relative strengths of the thermal and haline surface forcing into the surface sub polar box;

- The deep water horizontal diffusivities of heat and salt.

The results of the reduced box model with the enhanced diffusion convection scheme were insensitive to the other model parameters.

7.3.1 The reduced box model with the coupled convection scheme.

With the coupled convection scheme the reduced box model exhibited multiple equilibria as it did with the enhanced diffusion scheme. As in the enhanced diffusion case the strong and non convecting states were more stable than the weakly convecting states. Unlike the enhanced diffusion case the strongly convecting equilibria had positive (stable) vertical density gradients. For a weak meridional overturning cell it was possible for no stable equilibria to exist. In these cases the reduced coupled box model underwent oscillations between convecting and non convecting states. The period of these oscillations was strongly dependent on the strength of the meridional overturning cell (section 5.3.3). Similar to the enhanced diffusion case the results were sensitive to (section 5.3):

- The strength of the meridional overturning cell;
- The temperature of the sub tropical deep water;
- The relative strengths of the surface haline and thermal forcings;
- The deep water horizontal diffusivities;
- The strength of the thermal convective mixing.

7.4 The full box model.

The full box model employed the parameterisations developed form the OGCM results including the coupled surface boundary conditions and convection scheme. Although the FBM was unable to reproduce the thermal flushes seen in the OGCM quantitatively, it could predict the life time and general evolution of the haline dominated modes and the initial onset and strength of the thermal flushes. The FBM was not sufficiently accurate to be used as a predictive tool for the OGCM. However the FBM qualitatively reproduced most of the controlling processes seen in the OGCM (section 6.2).

As the FBM was based on parameterisations derived from the OGCM data the FBM shared the OGCMs tendency to under estimate the stability of the thermal mode of thermohaline circulation. With this in mind the FBM was used to examine the response of the thermohaline circulation to changes in the model parameters and surface forcing.

The FBM was very sensitive to the zero offset in the parameterisation of the strength of the meridional overturning cell (section 6.3.1). However the results were not very dependent on the constant of proportionality between the deep water density difference and the strength of the meridional overturning cell. The dependence of the results of the FBM on the model parameters was similar to that of the reduced box model though the FBM was also sensitive to the vertical diffusivities (section 6.3.7).

Adding a time varying stochastic component to the surface fresh water forcing of the FBM effected the period of the observed DDOs. The variability of the DDO period due the strength and intrinsic time scale of this stochastic forcing was investigated (section 6.4). Including the stochastic forcing tended to increase the mean period of oscillation. Variability of the DDO period was dependent on the time scale of the stochastic forcing. The standard deviation of the oscillation period was large when the forcing time scale was between 7 and 30 days and when the forcing time scale was greater than 5 years.

7.5 Implications for future models of the thermohaline circulation.

This thesis attempted to develop a simple box model that would reproduce the modes of thermohaline circulation found in an OGCM. The box model constructed fell some what short of being able to make quantitative predictions of the time evolution of the thermohaline circulation. However the FBM contained the processes identified as controlling the thermohaline circulation. Thus the FBM was a useful tool for investigating the interactions of the various feedback and controlling mechanisms of the thermohaline circulation in a qualitative manner.

The finite element and flux formulation of the FBM equations make it suitable for use as a simple ocean climate model as it stands or for coupling with atmosphere and cryosphere models to examine the interactions within the climate system. A 2 hemisphere or global ocean box model could be constructed using the parameterisations developed. In this case care would need to be taken over the exact choice of parameters as the parameters were derived from a single hemisphere, single ocean basin OGCM. Even if all the parameteristations used in the FBM are not included in future box models then I would advocate the use of the coupled surface buoyancy forcing and convection scheme for the reasons given in section 7.2.4. These extensions to the FBM would allow the qualitative investigation of the climate system. However the sensitivity of the FBM to some of the model parameters and its inability to reproduce the thermal flushes suggest that box models of this type are not capable of making quantitative predictions of the thermohaline circulation.

I feel that a more fruitful approach to producing simple models of the thermohaline circulation would be to concentrate on correctly modelling the important processes. The sensitivity of the FBM to ν_{offset} suggests that these models should pay particular attention to the dynamics of the deep and surface western boundary currents to correctly predict the strength of the meridional overturning cell. As the variation of the surface temperature forcing with latitude had a strong influence on the strength of the deep water formation it would seem necessary to include this effect in future models. The difference in the large scale vertical diffusivities of heat and salt may influence the thermohaline circulation especially when a non linear equation of state is considered. Coupled O-AGCM results indicate that mixed boundary conditions are an over simplification of the surface forcing. It would seem prudent for future simple ocean models to include some form reactive atmosphere model so that they do not over emphasise the instability of the thermohaline circulation.

7.6 Wider implications.

The approach adopted in this thesis of deriving a simple conceptual model from a more complex model could be applied to most sets of OGCM or local area model results. Developing a simpler model that attempts to mimic the more complex model in a statistical sense provides a good test of the understanding of the complex system. I feel that one of the strengths of this approach is that it highlights those processes that can be averaged over and those small scale events that need to be resolved. This draws attention to the mechanisms that have a highly non linear influence on the system. Hence this approach identifies the parts of the more complex model that probably have a large impact on the accuracy of that model. This study identified the western boundary currents and the sub surface water properties of the sub polar gyre as having a large influence on the evolution of the thermohaline circulation.

The coupled convection scheme developed in this study provides a much smoother response to surface forcing than the NCON or other step convection schemes. This convection scheme that allows for a fraction of a box to convect is physically more realistic than the step convection schemes and not difficult to implement. It would be reasonably straight forward to include this type of convection scheme in most finite element models (and possibly finite difference models). I feel that any model that does not resolve the convective chimneys could benefit from a convection scheme that allows for partial convection within a grid cell.

I think this study has indicated that the thermohaline circulation can be strongly influenced by small scale processes, specifically convection and the structure of the deep western boundary current. Unfortunately this rather limits the scope for large scale averaging models like box models. However I feel that box models still have a part to play in examining and aiding the understanding of a particular state of the thermohaline circulation. By tuning a simple model to a particular state (or small set of states) of an OGCM the box model can then be used to study the effects of perturbations to the system. Using this approach the box models results become less reliable the further from the initial state the box model gets.

Appendix A

The OGCM equations

A.0 The model equations.

Under the assumptions used in the model the equations of motion and the equation of continuity could be written (Equation A - 1):

$$\frac{\partial u}{\partial t} + \Gamma(u) - fv = -\frac{m}{a}\frac{\partial}{\partial \lambda}\left(\frac{p}{\rho_0}\right) + F^u \qquad \textbf{Equation A - 1}$$

$$\frac{\partial v}{\partial t} + \Gamma(v) + fu = -\frac{1}{a}\frac{\partial}{\partial \phi}\left(\frac{p}{\rho_0}\right) + F^v$$

$$\Gamma(1) = 0$$

$$m = \sec(\phi)$$

$$n = \sin(\phi)$$

$$f = 2\Omega\sin(\phi)$$

$$u = \frac{a}{m}\frac{d\lambda}{dt}$$

$$v = a\frac{d\phi}{dt}$$

Where t was time u and v horizontal velocities, the Coriolis parameter, p pressure, ρ_0 *the reference density of sea water,* φ *latitude,* λ *longitude, a the radius of the Earth,* $\Gamma()$ *the advective operator and F viscosity.*

The local pressure *p* was given by the hydrostatic relation (Equation A - 2):

$$p(z) = p^S + \int_z^0 g\rho . dz \qquad \textbf{Equation A - 2}$$

Where p^S *was the surface pressure from the rigid lid approximation.*

The advective operator was defined by (Equation A - 3):

$$\Gamma(\mu) = \frac{\sec(\varphi)}{a}\left[\frac{\partial}{\partial \lambda}(u\mu) + \frac{\partial}{\partial \phi}\left(\frac{v\mu}{\sec(\varphi)}\right)\right] + \frac{\partial}{\partial z}(w\mu) \qquad \textbf{Equation A - 3}$$

Where μ *was an arbitrary scalar field.*

The corresponding conservation equation for an arbitrary scalar tracer (*T*) was (Equation A - 4):

$$\frac{\partial T}{\partial t} + \Gamma(T) = F^T$$ **Equation A - 4**

Closure of these equations was obtained by adopting the turbulent viscosity hypothesis giving (Equation A - 5):

$$F^u = A_{MV}\frac{\partial^2 u}{\partial z^2} + \frac{A_{MH}}{a^2}\left[\nabla^2 u + (1 - m^2 n^2)u - 2nm^2\frac{\partial v}{\partial \lambda}\right]$$ **Equation A - 5**

$$F^v = A_{MV}\frac{\partial^2 v}{\partial z^2} + \frac{A_{MH}}{a^2}\left[\nabla^2 v + (1 - m^2 n^2)v - 2nm^2\frac{\partial u}{\partial \lambda}\right]$$

Where A_{MV} and A_{MH} were the vertical and horizontal viscosities respectively and F^T was given by (Equation A - 6):

$$F^T = \frac{\partial}{\partial z}\left[\frac{A_{TV}}{\delta}\frac{\partial T}{\partial z}\right] + \frac{A_{TH}}{a^2}\nabla^2 T$$ **Equation A - 6**

Where A_{TV} and A_{TH} were the vertical and horizontal diffusion coefficients respectively and δ was defined such that a column of statically unstable water underwent infinite mixing and a column of statically stable water underwent uniform mixing.

Where ρ_z^L was the local vertical density gradient (ignoring compression effects) then the "NCON" convection scheme was given by (Equation A - 7):

$$\delta = \begin{cases} 1 & for\ \rho_Z^L \le 0 \\ 0 & for\ \rho_Z^L > 0 \end{cases}$$ **Equation A - 7**

A.1 The Introduction of Distorted Physics.

The introduction of distorted physics modified the equations to give (Equation A - 8):

$$\frac{\partial u}{\partial t} + \frac{1}{\alpha}[\Gamma(u) - fv] = \frac{1}{\alpha}\left[-\frac{m}{a}\frac{\partial}{\partial \lambda}\left(\frac{p}{\rho_0}\right) + F^u\right]$$ **Equation A - 8**

$$\frac{\partial v}{\partial t} + \frac{1}{\alpha}[\Gamma(v) + fu] = \frac{1}{\alpha}\left[-\frac{1}{a}\frac{\partial}{\partial \phi}\left(\frac{p}{\rho_0}\right) + F^v\right]$$

Where α was a global constant.

and the conservation equation for an arbitrary scalar (μ) became(Equation A - 9):

$$\frac{\partial \mu}{\partial t} + \gamma\left[\Gamma(\mu)\right] = \gamma\left[F^\mu\right]$$ **Equation A - 9**

Where γ was a function of depth only.

The equation of state was a function of temperature, salinity and depth (Equation A - 10). The actual equation of state used was the Knudsen equation of state (Bryan 86). The coefficients were calculated using a best fit to the UNESCO equation of state over temperature, salinity and pressure ranges suitable for each model level.

$$\rho = \rho(T, S, z) \qquad \textbf{Equation A - 10}$$

Where T was the potential temperature, S the salinity and the pressure effect was represented through z the depth.

Appendix B

The Stommel box model

B.1 The model equations.

Stommel (1961) envisaged an idealised ocean model of a single hemisphere ocean basin (Figure B - 1). There were 2 well mixed boxes of equal volume: A polar box with temperature T_p and salinity S_p, and an equatorial box with temperature T_e and salinity S_e. The boxes were connected by two pipes of negligible volume representing the deep and surface water path ways. The strength of the advective exchange between the two boxes, *q*, was assumed to obey a linear friction law. The system was driven by a surface buoyancy flux represented by restoring boundary conditions on both the salinities and temperatures.

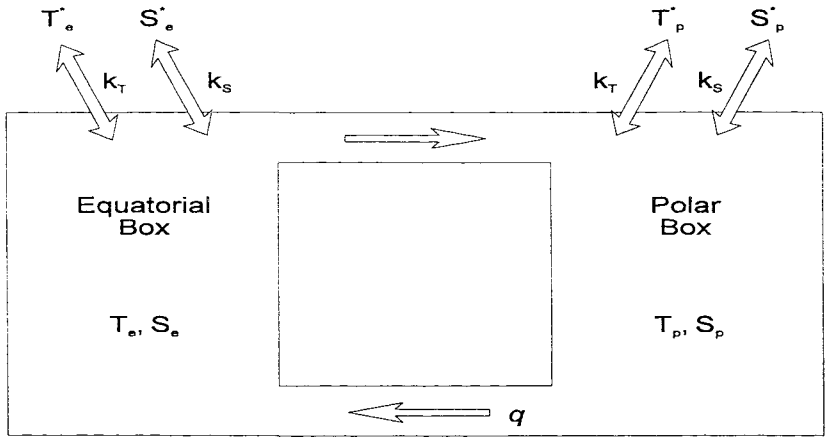

Figure B - 1: The 2 box Stommel model, where q is defined to be positive in the direction shown.

This model was governed by the equations (Equation B - 1):

$$\frac{dT_p}{dt} = k_T(T_p^* - T_p) + |q|(T_e - T_p) \qquad \textbf{Equation B - 1}$$

$$\frac{dT_e}{dt} = k_T(T_e^* - T_e) + |q|(T_p - T_e)$$

$$\frac{dS_p}{dt} = k_S(S_p^* - S_p) + |q|(S_e - S_p)$$

$$\frac{dS_e}{dt} = k_S(S_e^* - S_e) + |q|(S_p - S_e)$$

$$q = q_0\rho_0(\beta(S_p - S_e) - \alpha(T_p - T_e))$$

Where α *was the thermal expansion coefficient,* β *the haline contraction coefficient,* q_0 *was the constant of proportionality,* ρ_0 *the reference density for the linear equation of state and the other variables were as defined in Figure B - 1.*

B.1.1 Non dimensionalisation of the equations.

A suitable non dimensionalisation of the equations, that enabled investigation of mixed boundary conditions as a limiting case was (Equation B - 2):

$$\frac{dT}{d\tau} = 1 - T - |Q|T$$
$$\frac{dS}{d\tau} = R - \mu S - |Q|S$$
$$Q = \lambda(T - S)$$

Equation B - 2

Where these non dimensional variables were related to the dimensional variables by (Equation B - 3):

$$T = \frac{T_e - T_p}{T_e^* - T_p^*}$$
$$S = \frac{\beta(S_e - S_p)}{\alpha(T_e^* - T_p^*)}$$
$$R = \frac{\beta k_S(S_e^* - S_p^*)}{\alpha k_T(T_e^* - T_p^*)}$$
$$\mu = \frac{k_S}{k_T}$$
$$\lambda = \frac{2q_0\rho_0\alpha(T_e^* - T_p^*)}{k_T}$$

Equation B - 3

Thus the system was controlled by 3 non-dimensional parameters: *R* the ratio of the haline and thermal surface buoyancy fluxes, μ the ratio of the relaxation times for the temperature and salinity forcing, and λ the ratio of the relaxation time for temperature and the advective flushing time.

B.2 Steady states of the Stommel box model.

Assuming a steady state Equation B - 2 was rearranged to give *Q* as a function of *Q* and the non dimensional parameters of the system (Equation B - 4):

$$\frac{Q}{\lambda} = \Phi(|Q|) = \frac{1}{1+|Q|} - \frac{R}{\mu+|Q|}$$

Equation B - 4

Where $\Phi(|Q|)$ is defined by this equation.

The steady state solutions for the Stommel box model occurred when the 2 curves of Q/λ and $\Phi(|Q|)$ cross (Figure B - 2).

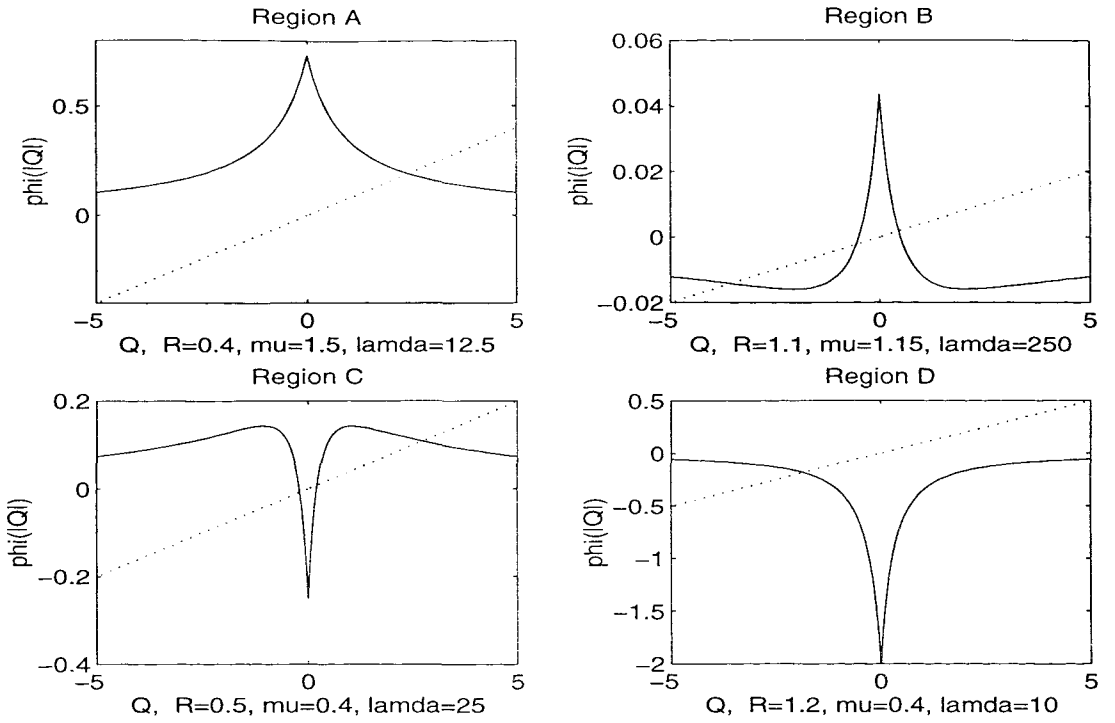

Figure B - 2: The characteristic shapes of Φ(|Q|) for the 4 regions shown in solid lines and Q/λ shown in dotted lines. The regions are defined as in Figure B - 3 and Table B - 1.

The number and type of solutions was dependent on the shape of Φ(|*Q*|) for a given position in *R*, μ parameter space. The equilibria were characterised by the sign of *Q*, if *Q* was positive then the equilibrium was dominated by the thermal forcing. For *Q* negative the equilibrium was dominated by the haline forcing. This report will not detail the linear stability analysis of the equilibrium states, merely quote the results of Zhang (1991) and Weaver and Hughes (1992). For μ>*R* a stable thermally dominant equilibrium existed and for μ<*R* there was a stable haline dominant equilibrium. The existence of these 2 equilibria was independent of the values of λ. For certain values of *R* it was possible for 2 extra equilibria to exist with the alternative surface forcing being dominant to that indicated by the μ, *R* relationship. However these equilibria could only exist if λ was sufficiently large.

B.2.1 Physical interpretation.

A more intuitive explanation required an alternative non dimensional parameter, the relative density ratio, *r* (Equation B - 5):

$$r = \frac{R}{\mu} = \frac{\beta(S_e^* - S_p^*)}{\alpha(T_e^* - T_p^*)} \qquad \textbf{Equation B - 5}$$

Then for the salinity driven, polar-equatorial, density gradient greater than the thermal density gradient (*r*>1) there was always a stable haline dominant equilibrium. If the haline buoyancy flux was less than the thermal buoyancy flux (*R*<1) and the advective flushing time was sufficiently

shorter than the relaxation time for the surface boundary condition on temperature (λ large) then 2 extra thermally dominated equilibria could exist. Similarly for the thermal density gradient greater than the haline density gradient (r<1) a thermally dominant equilibrium always existed. Two extra haline dominated equilibria were obtained if the haline buoyancy flux was greater than the thermal buoyancy flux (R>1) and the advective flushing time was sufficiently small (λ large).

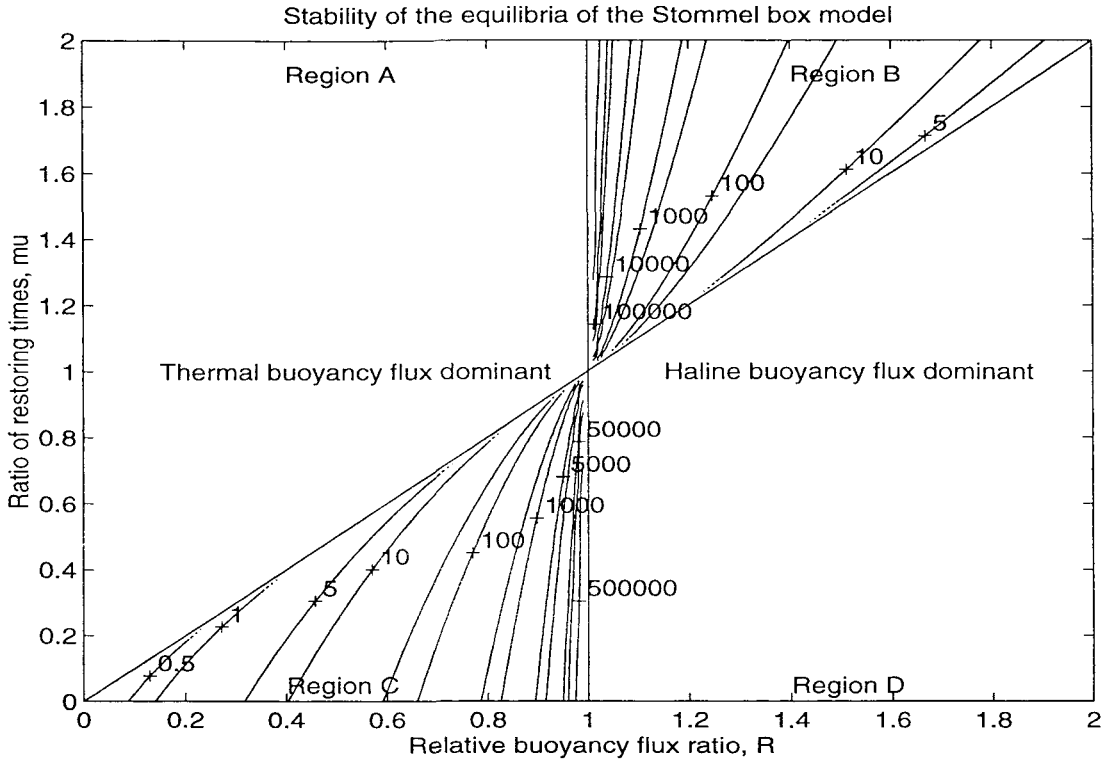

Figure B - 3: The contours indicate the minimum value of λ required for the extra 2 equilibria to exist in regions B and C. In regions A and D only one equilibrium could exist irrespective of the value of λ.

B.2.2 Mixed boundary conditions.

Mixed boundary conditions correspond to taking the limiting case when μ=0. Under mixed boundary conditions the state with a thermally dominant equilibrium and 2 haline dominant equilibria was not possible. A stable haline dominant equilibrium was always possible under mixed boundary conditions and 2 extra thermally dominant equilibria occurred if R was sufficiently small (R<1) and λ sufficiently large (Figure B - 4). See Marotzke (1990) for a discussion of the stability of the equilibria under mixed boundary conditions.

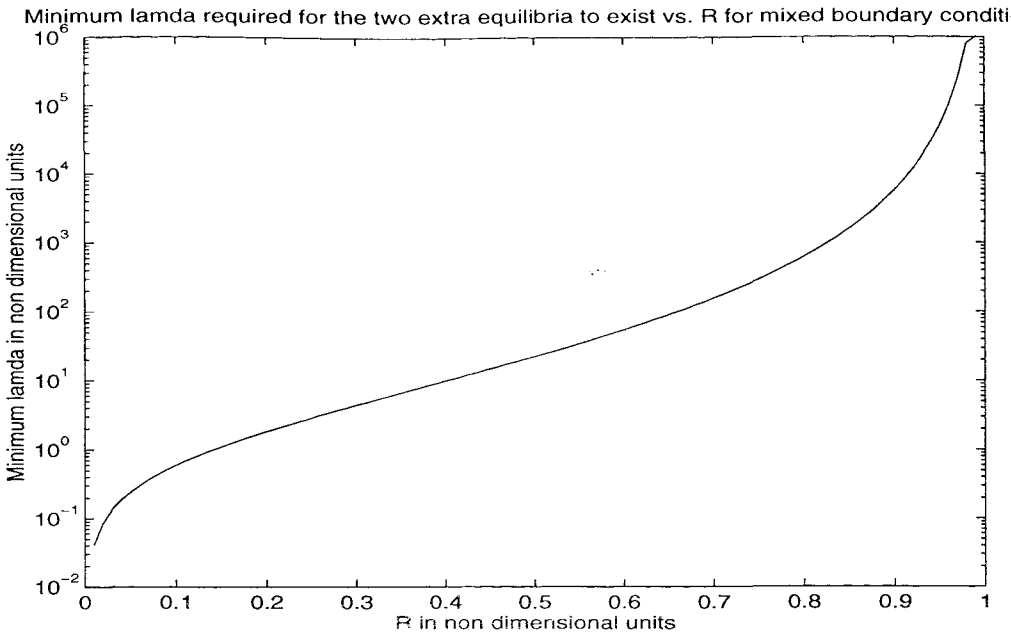

Figure B - 4: The minimum λ required for the two extra thermally dominant equilibria to exist as a function of R for the mixed boundary condition limit of the Stommel 2 box model.

B.3 Conclusions.

The Stommel 2 box model can have multiple equilibria depending on the relative strength of the thermal and haline surface buoyancy fluxes (*R*), the ratio of the restoring time for the temperatures and salinities (μ), and the relative strength of the advective flux to the surface forcing (λ) (Table B - 1). It was found that for weak advective coupling (small λ) the range of *R* that multiple equilibria could exist over was smaller than for strong advective coupling (large λ). The effect of small λ was most pronounced in the mixed boundary condition limit.

Region A	Region B	Region C	Region D
R<1 μ>R One stable thermally dominant equilibrium	R>1 μ>R One stable thermally dominant equilibrium and two possible haline dominant equilibria, one fast and stable, and one intermediate and unstable.	R<1 μ<R One stable haline dominant equilibrium and two possible thermally dominant equilibria, one fast and stable, and one intermediate and unstable.	R>1 μ<R One stable haline dominant equilibrium

Table B - 1: The steady state solutions of the Stommel 2 box model.

Appendix C

The OGCM parameters

Parameter or dimension	Value
Latitude spanned	0° to 70°
Longitude spanned	0° to 60°
Depth spanned	0m to 5000m
Resolution North - South	2.5°
Resolution East - West	3.75°
Number of grid boxes North - South	30
Number of grid boxes East - West	18
Number of grid boxes in the vertical	13
Total number of grid boxes	7020
Volume of ocean basin	1.997×10^{17} m^3
Surface area of ocean basin	3.994×10^{13} m^2
Horizontal eddy viscosity (A_{MH})	3×10^{9} cm^2/s
Vertical eddy viscosity (A_{MV})	1 cm^2/s
Horizontal diffusion coefficient (A_{HH})	2×10^{7} cm^2/s
Vertical diffusion coefficient (A_{HV})	0.5 cm^2/s

Level	Thickness in meters	Depth in meters of centre of box
1	50	25
2	52	76
3	63	133.5
4	78	204
5	116	301
6	176	447
7	263	666.5
8	395	999.5
9	616	1501
10	716	2167
11	780	2915
12	830	3720
13	865	4567.5

Appendix D

The stability criteria for the OGCM

D.0 Computational stability.

To maintain computational stability of the OGCM there were a number of constraints that were applied to the model parameters. The choice of the model parameters and their relation to these stability constraints is discussed below:

D.0.1 The time step for the tracer equations.

The evolution of the tracer fields was governed by (Equation D - 1):

$$\frac{\partial T}{\partial t} + \Gamma(T) = F^T \qquad \textbf{Equation D - 1}$$

See appendix A - The OGCM equations for further details and definitions of the variables used.

which was solved numerically using a finite difference scheme that was centred in both time and space. The use of this finite difference scheme gave rise to the following stability constraints on Δt_T (the time step used in the computations of the tracer fields (Bryan 1984)).

Criterion	Equation	Numeric Value
Horizontal diffusive criterion	$\Delta t_T < \frac{\Delta^2}{4A_{HH}}$	$\Delta t_T < 111\ days$
Courant - Friedrichs - Lewy (CFL) condition	$\Delta t_T < \frac{\Delta}{2u_{MAX}}$	$u_{MAX} < 128\ cm/s$ for Δt_T=1.25 days
Vertical diffusive criterion	$\Delta t_T < \frac{(\Delta z)^2}{4A_{HV}}$	$\Delta t_T < 145\ days$

Table D - 1: The stability constraints on the time step used for the tracer equations (taken from Mead 1989).

It can be seen that Δt_T=1.25 days (the time step used in the model runs) satisfied all of the above criterion.

D.0.2 The time step for the momentum equations.

Following Killworth (1984) the momentum equations used in the OGCM contained the distorted physics of Bryan (1984). The use of the distorted physics effectively reduced the phase speed of waves in the model. This allowed a larger time step for the momentum equations to be taken than would have otherwise been possible. The value of α was chosen such that the adjustment time scale due to the barotropic Rossby waves was comparable to the time scales associated

with the advective processes (Mead 1989). As in Semtner (1974) the OGCM used a semi-implicit treatment of the Coriolis term which placed a requirement for stability on α (Equation D - 2):

$$\alpha > \frac{4c^2(\Delta t_T)^2}{(\Delta x)^2} \qquad \textbf{Equation D - 2}$$

Where c was the phase speed of the first baroclinic mode and Δx was the horizontal grid spacing.

Given that:

c=300 m/s (Gill 1982)

Δt_T=108,000 s (1.25 days)

Δx=2.78×107 cm

implied that:

$\alpha > 5.4$

Which was obeyed for the value α=24 which was used in the model run. Using this value of α gave an effective time step for the momentum equations (Δt_V) of (Equation D - 3):

$$\Delta t_V = \frac{\Delta t_T}{\alpha} \qquad \textbf{Equation D - 3}$$
$$= 1.25 \; hours$$

The constraints on Δt_V were:

Criterion	Equation	Numeric Value
Horizontal diffusive criterion	$\Delta t_V < \frac{\Delta^2}{4A_{MH}}$	$\Delta t_V < 17.8 \; hours$
Courant - Friedrichs - Lewy (CFL) condition	$\Delta t_V < \frac{\Delta}{2u_{MAX}}$	$u_{MAX} < 30.9 \; m/s$ for Δt_V=1.25 hours
Vertical diffusive criterion	$\Delta t_V < \frac{(\Delta z)^2}{4A_{MV}}$	$\Delta t_V < 72.8 \; days$

Table D - 2: The constraints on the time step used in the momentum equations (taken from Mead 1989).

All of which were obeyed by the value of Δt_V used in the model.

D.0.3 Constraints on the viscosity.

In addition to the above constraints Bryan (1975) gives 2 constraints on the value of the horizontal viscosity (A_{MH}), the grid cell Reynolds number criterion (Equation D - 4) and the criterion for the resolution of the viscous boundary layer (Equation D - 5) (Munk 1950):

$$A_{MH} > \frac{1}{2} u_{\max} \Delta x \qquad \textbf{Equation D - 4}$$

$$A_{MH} > \beta \left(\frac{\sqrt{3}\Delta x}{\pi} \right)^3 \qquad \textbf{Equation D - 5}$$

Thompson et al. (1985) have suggested an alternative to the grid cell Reynolds number criterion (Equation D - 6):

$$\Delta t_V \leq \frac{2 A_{MH}}{u_{\max}^2} \qquad \textbf{Equation D - 6}$$

The model parameters given in appendix C - The OGCM parameters satisfy all of the above criterion.

D.1 The 2 grid point computational mode.

Weaver and Sarachik (1989) give a criterion for the vertical grid cell Reynolds number and the vertical Peclet number, that is sufficient but not necessary to ensure the elimination of the 2 grid point computational mode. The 2 grid point computational mode can become excited when using a centred finite difference scheme, introducing artificial oscillations into the velocity fields. The criterion for the vertical grid cell Reynolds number (Re_V) and the vertical Peclet number (Pe_v) are (Equation D - 7 and Equation D - 8):

$$\mathrm{Re}_V = \frac{w_{\max} \Delta z}{A_{MH}} < 2 \qquad \textbf{Equation D - 7}$$

$$Pe_V = \frac{w_{\max} \Delta z}{A_{TV}} < 2 \qquad \textbf{Equation D - 8}$$

The values used were:

Δz=50m at the surface and 800m at depth

A_{TV}=0.5 cm^2/s

Which gave the constraints on w of:

w<2×10-4 cm/s at the surface

w<6.3×10-6 cm/s at depth

These restrictions on w were not obeyed in the areas of strong downwelling observed during the model run. The power spectra of the velocity fields for these regions indicated that the 2 grid point computational mode was not excited to a significant amplitude and as such did not affect the results from the model.

D.2 Phantom warming.

A spatially centred finite difference scheme can contravene the 2nd law of thermodynamics in areas of constant downwelling. As the OGCM uses a spacially centred finite difference scheme for the tracer advection equation this "phantom warming" effect could occur. The magnitude of the phantom warming effect was estimated by comparing the advective heatfluxes calculated by the centred differencing scheme and the heatfluxes calculated using an upwind differencing scheme. The regions most prone to this phantom warming effect were the regions of strong downwelling. Calculations for these regions gave estimates for the magnitude of the phantom warming effect of 9.1×10^{10} Watts per grid point for the weak circulation mode and 4.6×10^{11} Watts per grid point for the thermal flushes. These values were 2 orders of magnitude smaller than the corresponding surface heatfluxes of 5.8×10^{12} and 1.5×10^{13} Watts per grid point respectively. Hence the phantom warming effect was negligible when compared to the dominant surface heat flux and so did not significantly affect the model results.

D.3 The Veronis effect.

The OGCM results are almost certainly influenced by the Veronis effect (Gough and Lin 1995). As the OGCM does not have an isopycnal diffusion there will diapycnal diffusion of heat and salt in regions with strongly sloping isopycnals. This effect will be most prevalent in during the thermal flushes when there are strong density fronts. The results of Gough and Lin (1995) suggest that this OGCM will tend to have warmer deep water, stronger upwelling on the western boundary and a stronger meridional overturning cell than an equivalent OGCM using isopyncal diffusion.

Appendix E

Relation between the strength of the meridional overturning cell and the deep water density gradient

E.0 A geostrophic model.

The ocean circulation in the TH mode away from the western boundary can be approximated using a model containing 2 boxes. The water within each box is assumed to be zonally uniform but the density is allowed to vary with depth. The interface between the 2 has a finite width of δ and each box has a surface pressure of p_{01} and p_{02} respectively (Figure E - 1).

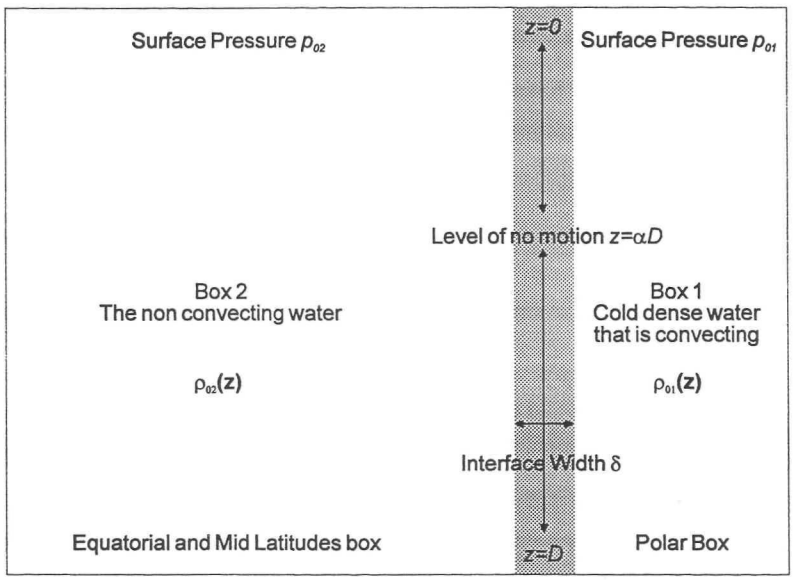

Figure E - 1: A simplified model of the ocean circulation in the TH mode.

Assuming that the velocity at the interface obeys geostrophy and that the hydrostatic assumption is valid then the interface velocity (u) is given by (Equation E - 1):

$$f.u(z) = -\frac{1}{\rho_0}.\frac{\partial p(z)}{\partial y} \qquad \textbf{Equation E - 1}$$

$$p(z) = p_0 - g\int_{s=0}^{s=z}\rho(s).ds$$

Defining a surface pressure difference Δp_0, the density difference $\Delta\rho$ and a density anomaly profile $\delta\rho(z)$ such that (Equation E - 2):

$$\Delta p_0 = p_{01} - p_{02}$$
$$\Delta\rho.\left(1+\delta\rho(z)\right) = \rho_1(z) - \rho_2(z) \qquad \textbf{Equation E - 2}$$
$$\int_{z=0}^{z=D} \delta\rho(z).dz = 0$$

Using Equation E - 2 the expression for *u* becomes (Equation E - 3):

$$u(z) = -\frac{1}{f.\rho_0.\delta}\left\{\Delta p_0 - g.\Delta\rho\left(z + D.S(z)\right)\right\} \qquad \textbf{Equation E - 3}$$
$$S(z) = \frac{1}{D}\int_{s=0}^{s=z} \delta\rho(s).ds$$

Where *S(z)* is a structure function that gives an indication of the skewness of the density anomaly function (δρ(z)). As all the zonal flow is confined to the interface region conservation of volume requires that the vertical integral of (*u(z)*) the zonal velocity is zero. This enables the surface pressure difference to be related to the structure function (Equation E - 4):

$$\Delta p_0 = g.\Delta\rho.D.\left(\frac{1}{2} + \overline{S(D)}\right) \qquad \textbf{Equation E - 4}$$
$$\overline{S(D)} = \frac{1}{D}\int_{z=0}^{z=D} S(z).dz$$

Assuming that there is a level of no motion as seen in the OGCM results for the TH mode then there exists an α such that $u(\alpha D)=0$. Substituting this into Equation E - 3 and Equation E - 4 gives (Equation E - 5):

$$Q = \frac{g.\Delta\rho.D^2.\alpha}{2.f.\rho_0}\left\{\alpha - 1 - 2\left(\overline{S(D)} - \overline{S(\alpha D)}\right)\right\} \qquad \textbf{Equation E - 5}$$
$$Q = \delta.\int_{z=0}^{z=\alpha D} u(z).dz$$

The zonal volume flux (*Q*) is proportional to the meridional density difference with the constant of proportionality being dependent on the depth of the ocean basin and the structure of the density profiles.

Appendix F

The parameters used in the full box model

Parameter	Value and units	Interpretation
c_p	3988 J/Kg.°C	Specific heat capacity of sea water
ρ_0	1026 Kg/m^3	Reference density for sea water
vol_1	5.6673*10^{16} m^3	Volume of box 1, the equatorial surface box
vol_2	1.5559*10^{16} m^3	Volume of box 2, the polar surface box
vol_3	9.9969*10^{16} m^3	Volume of box 3, the equatorial deep box
vol_4	2.7446*10^{16} m^3	Volume of box 4, the polar deep box
$area_1$	3.3128*10^{13} m^2	Area of surface 1, interface of boxes 1 and 3
$area_2$	7.6430*10^9 m^2	Area of surface 2, interface of boxes 1 and 2
$area_3$	8.6010*10^{12} m^2	Area of surface 3, interface of boxes 2 and 4
$area_4$	1.3482*10^{10} m^2	Area of surface 4, interface of boxes 3 and 4
dz	2500 m	Vertical separation of boxes
dy	3.8912*10^6 m	Horizontal separation of boxes
h_2	1820 m	Depth of surface boxes, boxes 1 and 2
h_4	3180 m	Depth of deep boxes, boxes 3 and 4
α_{ref}	1.55*10^{-10} J/s.°C	Scaled Haney coefficient for box 1 surface forcing
T^*_1	19.9 °C	Effective atmospheric temperature for box 1
$k^T_{v\ equator}$	0.64*10^{-4} m^2/s	Vertical thermal diffusivity between boxes 1 and 3
$k^T_{v\ pole}$	0.70*10^{-4} m^2/s	Vertical thermal diffusivity between boxes 2 and 4
$k^T_{h\ surface}$	2.7*10^3 m^2/s	Horizontal thermal diffusivity between boxes 1 and 2
$k^T_{h\ deep}$	3.6*10^3 m^2/s	Horizontal thermal diffusivity between boxes 3 and 4
$k^S_{v\ equator}$	0.39*10^{-4} m^2/s	Vertical haline diffusivity between boxes 1 and 3
$k^S_{v\ pole}$	0.45*10^{-4} m^2/s	Vertical haline diffusivity between boxes 2 and 4
$k^S_{h\ surface}$	2.6*10^3 m^2/s	Horizontal haline diffusivity between boxes 1 and 2
$k^S_{h\ deep}$	3.8*10^3 m^2/s	Horizontal haline diffusivity between boxes 3 and 4
q_1^{surf}	1.1196*10^7 Kg/s	Surface salt flux into box 1

Parameter	Value and units	Interpretation
q_{total}	$-1.0324*10^{7}$ Kg/s	Surface salt flux into box 2
v_{offset}	$3.5*10^{6}$ m^3/s	Offset of the strength of the meridional overturning cell
v_0	$3.1918*10^{8}$ $m^3/s.Kg$	Constant of proportionality between the deep water density difference and the strength of the meridional overturning cell
ρ_{ref}	1004.463 Kg/m^3	Reference density for the linear equation of state
α	0.1766 $Kg/m^3.°C$	Thermal expansion coefficient
β	0.6918 $Kg/m^3.psu$	Haline expansion coefficient
$\Delta\rho_{crit}$	0.16 Kg/m^3	Critical density difference for convection to occur
α_1	$4.64*10^{-11}$ W/°C	Scaled Haney coefficient for box 2
α_2	200 no units	Ratio of variable to fixed Haney coefficient for box 2
T_1^*	0.0 °C	Fixed effective atmospheric temperature for box 2
T_2^*	7.0 °C	Variable effective atmospheric temperature for box 2
Q_b^0	$-2.0470*10^{15}$ W	Surface heat flux for convecting area of box 2
τ_T	$7.5894*10^{7}$ s	Time scale for convective mixing of temperature
τ_S	$1.9036*10^{6}$ s	Time scale for convective mixing of salinity

References

Alves J.O.S. 1995: Open - ocean deep convection: Understanding and parameterisation. Thesis.

Bechmann A. et. al. 1994: Effects of increased horizontal resolution in a simulation of the North Atlantic. J.P.O., 24(2), 326 - 344.

Birchfield G.E. 1989: A coupled ocean - atmosphere climate model: temperature versus salinity effects on the thermohaline circulation. Climate Dynamics, 4, 57 - 71.

Birchfield G.E. et. al. 1990: A bimodal climate response controlled by water vapour transport in a coupled ocean - atmosphere box model. Paleoceanography, 5(3), 383 - 395.

Bond G. et. al. 1993: Correlations between climate records from North Atlantic sediments and Greenland ice. Nature, 365, 143 - 147.

Böning C.W. et. al. 1996: Deep-water formation and meridional overturning in a high-resolution model of the north-Atlantic. J.P.O., 26(7), 1142 - 1164.

Boyle E.A. & Keigwin L. 1987: North-Atlantic thermohaline circulation during the past 20,000 years linked to high-latitude surface-temperature. Nature, 330, 35 - 40.

Brass G.W. et. al. 1982: Warm saline bottom water in the ancient ocean. Nature, 296, 620 - 623.

Broecker W.S. 1987: Unpleasant surprises in the greenhouse. Nature, 328, 123 - 126.

Broecker W.S. 1991: Global change and oceanography programs. Nature, 254, 1566.

Bryan F. 1986: High - latitude salinity effects and inter hemispheric thermohaline circulaitons. Nature, 323, 301 - 304.

Bryan F. 1987: Parameter sensitivity of primitive equation ocean general-circulation models. J.P.O., 17, 970 - 985.

Bryan K. 1969: A numerical method for the study of the circulation of the world ocean. J. of Comp. Phys., 4, 347 - 376.

Bryan K. 1984: Accelerating the convergence to equilibrium of ocean - climate models. J.P.O., 14, 666 - 673.

Bryan K. & Cox M. 1972: An approximate equation of state for numerical models of ocean circulation. J.P.O., 2, 510 - 514.

Bryan K. et. al. 1975: A global ocean - atmosphere climate model. Part II. The oceanic circulation. J.P.O., 5, 30 - 46.

Cai W. 1996a: Surface thermohaline forcing conditions and the response of the present - day global ocean climate to global warming. J.G.R., C1, 1079 - 1093.

Cai W. 1996b: The stability of North Atlantic deep water formation under mixed boundary conditions with an imposed diagnostic fresh water flux. J.P.O., 26(6), 1081 - 1087.

Capotondi A. & Saravanan R. 1996: Sensitivity of the thermohaline circulation to surface buoyancy forcing in a 2D ocean model. J.P.O., 26(6), 1039 - 1058.

Carissimo A.H. et. al. 1985: Estimating the meridional energy transports in the atmosphere and ocean. J.P.O., 15(1), 82 - 91.

Cessi P. 1994: A simple box model of stochastically forced thermohaline flow. J.P.O., 24, 1911 - 1920.

Cox M.D. 1984: A numerical model of the ventilated - thermocline. Ocean Modelling, 49, 4 - 7.

Crowley T.J. 1983: The geological record of climate-change. Reviews of Geophysics, 21(4), 828 - 877.

Dansgaard W. et. al. 1993: Evidence for general instability of past climate from 250 - Kyr ice core record. Nature, 364, 218 - 220.

Dickson R.R. et. al. 1988: The "Great Salinity Anomaly" in the northern North Atlantic 1968 - 1982. Prog. Ocean., 20, 103 - 151.

Döscher R. et. al. 1994: Response of circulation and heat transport in the North Atlantic to changes in thermohaline forcing in northern latitudes: A model study. J.P.O., 24(11), 2306 - 2320.

Fannig A.F. & Weaver A.J. 1996: An atmospheric energy - moisture balance model: Climatology, inter pentadel climate change, and coupling to an OGCM. J.G.R., 101(D10), 15111 - 15128.

Figueroa H. & Olson D. 1994: Eddy resolution versus eddy diffusion in a double gyre GCM: Part II: The mixing of passive tracers. J.P.O., 24(2), 387 - 402.

Foldviik A. & Gammelsrøld T. 1988: Notes on southern-ocean hydrography, sea-ice and bottom water formation. Paleogeogr., Paleoclimatol., Paleoecol., 67(1-2), 3 - 17.

Gargett A.E. & Holloway G. 1992: Sensitivity of the GFDL ocean model to different diffusivities for heat and salt. J.P.O., 22, 1158 - 1177.

Gargett A.E. et. al. 1995: The effects of differential diffusion of T and S in a box model of thermohaline circulation. In press.

Gill A.E. 1982: Atmosphere - Ocean dynamics. Published by Academic Press. pp 662.

Gordon A.L. 1986: Is there a global scale ocean circulation? EOS, Transactions, Am. Geophys. Union, 67(9), 109 - 110.

Josey S.A. et. al. 1996: A new global air-sea heat and momentum flux climatology. International WOCE newsletter. No 24, 3 - 5.

Gough W.A. & Lin C.A. 1995: Isopycnal mixing and the Veronis effect in an ocean general circulation model. J.M.R., 53(2), 189 - 199.

Greatbatch R.J. 1994: A note on the representation of steric sea-level in models that conserve volume rather than mass. J.G.R.-Oceans, 99(C6), 12767 - 12771.

Greatbatch R.J. & Zhang S. 1995: An inter decadal oscillation in an idealised ocean-basin forced by constant heat-flux. J. of Climate, 8(1), 81 - 91.

Greatbatch R.J. et. al. 1994: *Inter decadal climate variability - a new perspective.* The Atlantic climate change program (Ed. Wilburn), 73 - 76.

Hall M.M. & Bryden H.L. 1982: Direct mechanisms of ocean heat-transport. Deep-sea Research A, 29(3), 339-359.

Haney R.L. 1971: Surface thermal boundary condition for ocean circulation models. J.P.O., 1(4), 241 - 248.

Hirst A. & Cai W. 1994: Sensitivity of a world ocean G.C.M. to changes in subsurface mixing parameterisation. J.P.O., 24(6), 1256 - 1279.

Huang R.X. 1993: Real fresh water flux as a natural boundary condition for the salinity balance and thermohaline circulation forced by evaporation and precipitation. J.P.O., 23(11), 2428 - 2446.

Huang R.X. 1994: Thermohaline circulation: Energetics and variability in a single - hemisphere basin. J. of Geophys. Res., 99(C6), 12471 - 12485.

Huang R.X. & Stommel H.M. 1992: Convection flow patterns in an eight - box cube driven by combined wind stress, thermal and saline forcing. J.G.R. 97(2), 2347 - 2364.

Huang R.X. et al. 1992: Multiple equilibrium states in combined thermal and saline circulation. J.P.O., 22, 231 - 246.

Hughes T.M.C. & Weaver A.J. 1996: Sea surface temperature - evaporation feedback and the ocean's thermohaline circulation. J.P.O., 26(4), 644 - 654.

Johnsen S.J. et. al. 1992: Irregular glacial interstadials recorded in a new Greenland ice core. Nature, 106, 285 - 292.

Keigwin L.D. et. al. 1991: Deglacial meltwater discharge, north-Atlantic deep circulation, and abrupt climate change. J.G.R.-Oceans, 96(C9), 16811 - 16826.

Killworth P.D. 1979: On "chimney" formations in the ocean. J.P.O., 2(3), 531 - 544.

Killworth P.D. 1983: Deep convection in the world ocean. Reviews of Geophysics, 21(1), 1 - 26.

Lenderink G. & Haarsma R.J. 1994: Variability and multiple equilibria of the thermohaline circulation associated with deep-water formation. J.P.O., 24(7), 1480 - 1493.

Levitus S. 1982: Climatological atlas of the world ocean. NOAA professional paper, 13, 173pp.

Lohmann G. et. al. 1995: A 1-D atmospheric energy-balance model developed for ocean modelling. Theoretical and Applied Climatology, 51(1-2), 25 - 38.

Lohmann G. et. al. 1995: Stability of the thermohaline circulation in an analytic investigation. Report 58.

Lohmann G. et. al. 1996: Sensitivity of the thermohaline circulation in coupled O/AGCM EBM experiments. Climate Dynamics, 12(6), 403 - 416.

Lohmann G. et. al. Pre-print: Stability of the thermohaline circulation in a simple coupled model.

Lorenz E.N. 1984: The local-structure of a chaotic attractor in 4 dimensions. Physica D, 13(1-2), 90 - 104.

Lorenz E.N. 1990: Can chaos and intransitivity lead to inter annual variability? Tellus, 42A(3), 378 - 389.

Maas L. 1994: A simple-model for the 3-dimensional, thermally and wind-driven ocean circulation. Tellus A, 46(5), 671 - 680.

Mantyla A.W. & Reid J.L. 1983: Abyssal characteristics of the world ocean waters. Deep-sea Research A, 30(8), 805.

Marotzke J. 1988: Instability and multiple steady states in a meridional - plane model of the thermohaline circulation. Tellus, 40A(2), 162 - 172.

Marotzke J. 1990: Instabilities and multiple equilibria of the thermohaline circulation. Thesis.

Marotzke J. 1991: Influence of convective adjustment on the stability of the thermohaline circulation. J.P.O., 21(6), 903 - 907.

McCartney M.S. & Talley L.P. 1984: Warm-to-cold water conversion in the northern north Atlantic. J.P.O., 14(5), 922 - 935.

McWilliams J. & Ghil M. 1994: Workshop tackles oceanic thermohaline circulation. EOS, 74(42), 493 & 498 - 499.

Mead C. 1988: Asymmetries of the oceanic thermohaline circulation and meridional heat transport. Thesis.

Milliff R.F. et. al. 1996: The general circulation responses of high-resolution North Atlantic models to synthetic scatterometer winds. J.P.O., 26(9), 1747 - 1768.

Munk W.H. 1950: On the wind - driven ocean circulation. J. of Meteorology, 7, 79 - 93.

Carmack E.C. & Foster T.D. 1975: On the flow of water out of the Weddell Sea. Deep Sea

Research, 22(11), 711 - 724.

Myers P.G. & Weaver A.J. 1992: Low frequency internal oceanic variability under seasonal forcing. J.G.R., 97, 9541 - 9563.

Oeschger H. et. al. 1984: Temporal variations in the BE-10 concentration levels found in the DYE-3 ice core, Greenland. Annals of Glaciology, 5, 16 - 17.

Oort A.H. & Haar T.H.V. 1973: New estimate of annual poleward energy transport by Northern hemisphere oceans. J.P.O., 3(2), 169 - 172.

Osborn T.J. 1996: Comment on "Climate drift in an OGCM" by S.B. Power. J.P.O., 26(8), 1661 - 1663.

Paillard D. & Labeyrie L. 1994: Role of the thermohaline circulation in the abrupt warming after Heinrich events. Nature, 372, 162 - 164.

Pierce D.W. et. al. 1996: Variability of the thermohaline circulation in an OGCM coupled to an atmospheric EBM. J.P.O., 26(5), 725 - 738.

Press et. al. 1992: Numerical recipes in C. Cambridge Press.

Rahmstorf S. 1994: Rapid climate transitions in a coupled ocean - atmosphere model. Nature, 327, 82 - 85.

Rahmstorf S. 1996: Comments on "Instability of the thermohaline circulation with respect to mixed boundary conditions: Is it really a problem, for realistic models" by Tzipierman E. J.P.O., 26(6), 1099 - 1105.

Roebber P.J. 1995: Climate variability in a low - order coupled atmosphere - ocean model. Tellus, 47(4)A, 473 - 494.

Rooth C. 1982: Hydrology and ocean circulation. Prog. in Ocean., 11(2), 131 - 149.

Ruddick B. & Zhang L.Q. 1989: The mythical thermohaline oscillator. J. of M. Reas., 47, 717 - 746.

Schiller et. al. 1996: The stability of the thermohaline circulation in a CO/AGCM. Report 188, 1 - 42.

Schmidt G.A. & Mysak L.A. 1996: The stability of a zonally averaged thermohaline circulation model. Tellus, 48(A)1, 158 - 178.

Semtner A.J. 1974: An oceanic general circulation model with bottom topography. University of California, Los Angeles, department of Meteorology, Numerical simulation of weather and climate, Technical report 9, 99pp.

Shaffer G. & Bendtsen J. 1994: Role of the Bering Strait in controlling North Atlantic ocean circulation and climate. Nature, 367, 354 - 357.

Stommel H. 1961: Thermohaline convection with two stable regimes of flow. Tellus, 13(2), 224 - 230.

Stommel H. 1986: A thermohaline oscillator. Ocean Modelling, 72, 5 - 6.

Thompson H.D. et.al. 1985: The cell Reynolds number myth. Internation J. for Numerical Methods in Fluids, 5, 305 - 310.

Thual O. & McWilliams J.C. 1992: The catastrophe structure of thermohaline convection in a two - dimensional fluid model and comparison with low - order box models. Geophysical & Astrophysical Fluid Dynamics, 64(1-4), 67 - 95.

Trenberth K.E. 1979: Mean annual poleward energy transport by the oceans in the southern hemisphere. Dynamics of Atmos. and Oceans, 4(1), 57 - 64.

Tziperman E. 1994: Instability of the thermohaline circulation with respect to mixed boundary conditions: Is it really a problem for realistic models? J.P.O., 24, 217 - 232.

Wadley M.R. et. al. 1996: Sensitivity of the North Atlantic to surface forcing in an OGCM. J.P.O., 26(7), 1129 - 1141.

Walin G. 1985: The thermohaline circulation and the control of ice ages. Paleogeogr., Paleoclimatol., Paleoecol., 50(2-3), 323 - 332.

Wang H. Birchfield G.E. 1992: An energy - salinity balance climate model: Water vapour transport as a cause of changes in the global thermohaline circulation. J. of Geophys. Reas., 97, 2335 - 2346.

Warren B.A. 1981: Deep circulaitons of the world ocean. Evolution of physical oceanography (Ed. Warren B.A. & Wunsch C.), 6 - 41.

Weaver A.J. 1990: Ocean currents and climate. Nature, 347, 432.

Weaver A.J. & Hughes T.M.C. 1992: Stability and variability of the thermohaline circulation and its link to climate. McGill centre for climate and global change research, report 92 - 5, 56pp.

Weaver A.J. & Hughes T.M.C. 1994: Rapid interglacial climate fluctuations driven by North Atlantic ocean circulation. Nature, 367, 447 - 450.

Weaver A.J. & Sarachik E.S. 1991a: The role of mixed boundary conditions in numerical models of the ocean's climate. J.P.O., 21(9), 1470 - 1493.

Weaver A.J. & Sarachik E.S. 1991b: Reply. J.P.O., 21, 17021.

Weaver A.J. et. al. 1991: Freshwater flux forcing of decadal and inter decadal oceanic variability. Nature, 353, 836 - 838.

Weaver A.J. et. al. 1993: Stability and variability of the thermohaline circulation. J.P.O., 23, 39 - 60.

Welander P. 1982: A simple heat oscillator. Dyn. Atmos & Ocean., 6, 233 - 242.

Welander P. 1986: Thermohaline effects in the ocean circulation and related simple models. Large - Scale transport processes in oceans & atmospheres. (Ed J. Willebrand).

Weppernig R. er al. 1996: Isotope data from Ice Station Weddell: Implications for the deep water formation in the Weddell Sea. J.G.R. 15, 25723 - 27740.

Winton M. 1993: Deep decoupling oscillations of the thermohaline circulation. Ice in the climate system (Ed. W.R. Peltier, NATO ASI series), 417 - 432.

Winton M. 1995: Energetics of deep-decoupling oscillations. J.P.O., 25(3), 420 - 427.

Winton M. 1996: The role of horizontal boundaries in parameter sensitivity and decadal - scale variability of coarse resolution OGCMs. J.P.O., 26(3), 289 - 304.

Winton M. & Sarachik E.S. 1993: Thermohaline oscillations induced by strong steady salinity forcing of ocean general-circulation models. J.P.O., 23(7), 1389 - 1410.

Yin F.L. 1995: A mechanistic model of ocean interdecadal thermohaline oscillations. J.P.O., 25, 3239 - 3246.

Zhang S. et. al. 1993: A re-examination of the polar halocline catastrophe and implications for coupled ocean - atmosphere modelling. J.P.O., 23(2), 287 - 299.